



Poznan University of Technology
Faculty of Mechanical Engineering



INVESTIGATION OF SUBSURFACE MICROCRACKS CAUSING PREMATURE FAILURE IN WIND TURBINE GEARBOX BEARINGS

By:

Tahseen Ali MANKHI

Student number: 3260

March 2023

Supervisor: Prof. dr hab. inż. Stanisław LEGUTKO

*Faculty of Mechanical Engineering / Poznan University of Technology
POLAND*

Co-Supervisor: Dr. Jasim H. AL-Bedhany

*Eng. College –Mechanical Eng. Dep./ University of Misan
IRAQ*

A thesis submitted to Poznan University of Technology for the degree of Doctor
of Philosophy in the Faculty of Mechanical Engineering

ABSTRACT

One reason behind the low rate of expansion of power production driven by wind is the premature failure of the Wind Turbine Gearbox Bearings (WTGBs). Unfortunately, the bearings fail within the first quarter of their designed life due to the unusual impacts they are subjected to in the production and operation processes. Despite the massive studies on fatigue damage in wind turbine gearbox bearings, their leading causes of failure remain unclear. The damage initiates as subsurface microcracks, then propagates to a macro scale and reaches the contact surface causing premature failure. Accordingly, by applying a set of experimental and simulation investigations, this research studies the microcracks in the early initiation stage (of lengths up to 15 μm) that significantly affect the bearing damage trigger.

The experimental investigations were performed on damaged samples referring to a failed inner race of a Double Roller Cylindrical Bearing (DRCB) taken from a planetary gearbox of a 2 MW wind turbine. The overall detected cracks (1,447) were classified based on their lengths, depths, inclinations, and whether or not they were associated with non-metallic inclusions (NMIs). To study the effect of the NMI's size on the occurrence of bearing damage, the aspect ratios of the cracked NMIs' were categorized into three levels: (1-2), (2-3), and greater than 3.

The behavior of NMIs regarding crack initiation has been studied in terms of the following indicators: subsurface stress distribution, the percentage of cracks associated with them, and the frequency of their aspect ratio. A Finite Element Analysis (FEA) was also conducted in this study to determine the stress concentration at the inclusion tips, which was found to be around 250 MPa, confirming that NMIs have a role in the bearings' damage. The statistical results showed that only about 15% of the overall investigated cracks were not associated with inclusions. As well, the most cracked inclusions were observed with low aspect ratios (1-2). The two later results underestimate the role of the NMIs and their sizes in crack initiation. The microscopic investigations showed that the bearing steel matrix was saturated with hard carbide particles, which may compress voids (as they are soft objects), especially the contiguous ones and lead to initiating microcracks. The absence of WEAs and WECs has been reported, which may suggest that the carbide dissolution follows crack initiation rather than precedes it. The following parameters: maximum shear stress

(τ_{\max}), Von-Mises stress (σ_{VM}), and traction force were evaluated using the profiles of cracks' inclinations and cracks' densities with increasing the depth below the contact surface. It has been observed that the subsurface small microcracks (1-15 μm) tend to have an inclination angle of 45° with the tangent to the contact surface. This indicates the impact of maximum shear stress in the crack initiation. In contrast, the observation of crack inclinations exceeding 90° may indicate the probability of torque reversal due to harsh operating conditions in their initiation. The Hertzian contact model was introduced to simulate the increase in the traction force caused by the effect of the operating conditions. The simulated coefficient of friction (μ) is assumed to be (0.15) instead of the standard value (0.05). The results demonstrate that the maximum shear stress becomes shallower ahead of the rolling direction (RD) with increasing the traction force. The similarity between presenting the two profiles (σ_{VM} vs. depths) and (number of cracks vs. depths) also confirms the effect of Von-Mises stresses on the cracks' initiation.

The premature bearing failure may be caused by the inappropriate bearing type selection used in the wind turbine gearbox (WTG). As a result, the multiple criteria decision-making approach was applied using the Analytical Hierarchy Process (AHP) tool - Expert Choice software (EC). The main differentiation criteria are cost, durability, reliability, feature design, and availability. It has been concluded that single-row tapered roller bearing is the superior option compared to single-row and double-row cylindrical bearings in wind turbine gearboxes.

In general, the obtained results provided several specific recommendations for improving the following processes associated with WTGBs: designing, manufacturing, operation, monitoring, and maintenance.

ACKNOWLEDGMENTS

First, I want to submit this humble effort to the savior of humanity, who will illuminate the globe and dispel the darkness. To the spirits of my mother, my father, all past, present, and future martyrs who sacrificed themselves to maintain our life and our future, especially those who defeated tyranny and anti-humanity forces. I also want to express my sincere thanks and gratitude to my supervisor, prof. dr hab. inż. Stanisław Legutko, for his valuable comments, encouragement, and support during the long period of this study. Without his attention, patience, and kind advices, time would have stretched forever for me. I extend my profound gratitude and sincere thanks to my co-supervisor, dr Jasim H. Al-Bedhany, for his valuable and encouraging comments, suggestions, recommendations, and for his review of all chapters of the dissertation. I will never forget the continuous support you gave me in my study. My thanks go to all my teachers at Poznan University of Technology, especially prof. dr hab. inż. Zbigniew Kłos (the Head of Doctoral Studies in the Faculty of Civil Engineering and Transport, PUT). Your support in guiding my ideas was instrumental in logically formulating my thesis. My special appreciation to whom assisted me in providing test samples for doing the required investigations. Sincere gratitude goes to the Iraqi Ministry of Electricity, the General Company of Electrical Energy Production - South Region, Engineering College – University of Misan - Iraq, the Iraqi Embassy in Warsaw, and the Iraqi Cultural Consulate in Bucharest. My final thanks and warm appreciation go to my family and friends for their unlimited support and patience while I studied abroad.

Tahseen Ali MANKHI

PUBLICATIONS AND CONFERENCES

1- “SELECTING THE MOST EFFICIENT MAINTENANCE APPROACH USING THE MOST EFFECTIVE MAINTENANCE STRATEGY AT THE HADITHA HYDROELECTRIC POWER PLANT USING MULTI-CRITERIA AHP DECISION SUPPORT”

By: Abdulmuttalib A. MUHSEN⁽¹⁾, Grzegorz M. SZYMAŃSKI⁽²⁾, Tahseen A. MANKHI⁽³⁾, and Bashar ATTIYA⁽⁴⁾

Journal: Scientific Papers of Poznan University of Technology / ORGANIZATION AND MANAGEMENT/ Faculty of Management Engineering, vol.78, **2018**.

ISSN: 0239-9415

<https://doi.org/10.21008/j.0239-9415.2018.078.09>

2- “SELECTING THE MOST EFFICIENT BEARING OF WIND TURBINE GEARBOX USING ANALYTICAL HIERARCHY PROCESS METHOD AHP”

By: Tahseen Ali Mankhi⁽¹⁾, Stanisław Legutko⁽²⁾, Jasim H Al-Bedhany⁽³⁾, and Abdulmuttalib A. Muhsen⁽⁴⁾

Journal: "IOP Conference Series, Materials Science and Engineering“, **June 2019**.

<https://iopscience.iop.org/article/10.1088/1757-899X/518/3/032050>

3- “INVESTIGATION OF SUBSURFACE MICROCRACKS CAUSING PREMATURE FAILURE IN WIND TURBINE GEARBOX BEARINGS”

By: Tahseen Ali MANKHI⁽¹⁾, Jasim H. AL-Bedhany⁽²⁾, and Stanisław Legutko⁽³⁾

Journal: (Results in Engineering - ScienceDirect), **Dec. 2022.**,

<https://doi.org/10.1016/j.rineng.2022.100667>

4- “A NEW METHOD OF FATIGUE LIFE PREDICTION AND DAMAGE ESTIMATION ”

By: Jasim H. AL-Bedhany⁽¹⁾, Stanisław Legutko⁽²⁾, Ali A. Resun⁽³⁾ and Tahseen Ali MANKHI⁽⁴⁾

Journal: Misan Journal of Engineering Sciences (MJES), **2023 (under evaluation)**

5. “A SURFACE STUDY OF FAILED PLANETARY WIND TURBINE GEARBOX BEARINGS TO INVESTIGATE THE CAUSES OF THE BEARING PREMATURE FAILURE ISSUE”

By: Jasim H. AL-Bedhany⁽¹⁾ Tahseen Ali MANKHI⁽²⁾, and Stanisław Legutko⁽³⁾

Journal: (Engineering Failure Analysis - ScienceDirect), March. **2023 (under evaluation)**.

NOMENCLATURES

σ_{VM}	Von-Mises stress (Pa)
τ_{max}	Maximum Shear Stress (Pa)
μ	Coefficient of Friction
L_{10}	Rated bearing life: number of loading cycles (in millions) to which 10% of the identical bearings are subjected to be failed. (cycles)
α	Angle of attack (degree)
$\alpha_{critical}$	Critical angle of attack (degree)
b	Half of the contact width (mm)
Q	The normal applied load to the contact surface (N)
R^*	Equivalent reduced radius (mm)
$R1$	Radius of the roller (mm)
$R2$	Radius of the raceway (mm)
E^*	Equivalent modulus of elasticity (GPa)
$E1$	Modulus of elasticity of the roller (GPa)
$E2$	Modulus of elasticity of the raceway (GPa)
ν_1	Poisson's Ratio of the roller
ν_2	Poisson's Ratio of the raceway
P_{max}	Maximum pressure distributed across the width of the contact (N/mm ²)
L	Contact length (mm)
$\sigma_x, \sigma_y \& \sigma_z$	Cartesian contact stresses (Pa)
S	Survivability probability
N	Number of enduring stress cycles (Cycles)
τ_o	Maximum shear stress in an orthogonal direction at the contact surface (Pa)
z_o	Maximum shear stress at the depth z_o (mm)
V	Hertzian stressed volume (mm ³)
$C_r \& C_a$	Radial and axial basic dynamic load ratings respectively (N)
$P_r \& P_a$	Radial and axial equivalent dynamic load ratings respectively (N)
n	The load life exponent, (n= 10/3 for roller bearings and n=3 for ball bearings)
a_{ISO}	Life correction coefficient
a_{nsk}	Life modification factor
L_{nmh}	Bearing life-based on the number of hours
a_1	The modification factor for reliability
N	Rotating speed (min-1)
e	Weibull exponent
$c \& h$	Experimental exponents
P	The actual bearing load (N)
P_u	The fatigue load limit (in which the bearing will last for more than 10 ¹¹ revolutions before failing) (N)
a_L	Lubricant parameter
a_c	The contamination factor
k	The lubricant viscosity ratio
ΔU	The differential of two contact surfaces' velocities
U_{av}	The average velocity of two contact surfaces

σ_w	Fatigue limit at the surface (Pa)
σ	Nominal stress at the surface (Pa)
Hv	Vickers hardness (Kgf/mm ²)
q	Friction force (N)
p_o	The maximum load on a roller (N)
$m\&n$	Constants which were calculated depending on the contact length and the coordinates (x and z) of the point at which the calculation was performed,
z	Depth from the contact surface (μm)
τ_{xz}	Cartesian shear stress (Pa)

ABBREVIATIONS

WTGBs	Wind Turbine Gearbox Bearings
DRCB	Double Roller Cylindrical Bearing
WT	Wind Turbine
NMIs	Non-Metallic Inclusions
WEAs	White Etching Areas
WECs	White Etching Cracks
AR	Aspect Ratio
RD	Rolling Direction
WTG	Wind Turbine Gearbox
SEM	Scanning Electron Microscope
LRM	Light Reflection Microscope
XRD	X-Ray Diffraction
AHP	Analytical Hierarchy Process
EC	Expert Choice
LCA	Life Cycle Assessment
IAEA	International Atomic Energy Agency
EROI	Energy Return on Investment
PV	Photo Voltage
CAGR	Compound Annual Growth Rate
RoR	Rate of Return
GL	Germanischer Lloyd
RCF	Rolling Contact Fatigue
NREL	National Renewable Energy Laboratory
PWTG	Planetary Wind Turbine Gearbox
FEA	Finite Element Analysis
MCDM	Multiple Criteria Decision-Making
WTG	Wind Turbine Gearbox
WEF	White Structural Flaking
DERs	Dark Etching Regions
CoE	Cost of Energy
O&M	Operation and Maintenance
HSS	High-Speed Shaft
LSS	Low-Speed Shaft
ISS	Intermediate-Speed Shaft
UW	Up Wind
DW	Down Wind
PF	Power Factor
SCIG	Squirrel-Cage Induction Generator
PMSG	Permanent Magnet Synchronous Generator
DFIG	Doubly Fed Induction Generator
EESG	Electrically Excited Synchronous Generator
WRIG	Wound Rotor Induction Generator
CRBs	Cylindrical Roller Bearings

TRB	Tapered Roller Bearings
CMS	Condition Monitoring System
SCADA	Supervisory Control And Data Acquisition
AISI	American Iron and Steel Institute
irWEAs	irregular White Etching Areas
BCC	Body-Centered-Cubic
FCC	Face-Centered-Cubic
BCT	Body-Centered Tetragonal
LABs	Low Angle Bands
HABs	High Angle Bands
EHD or EHL	Elastohydrodynamic
LP	Lundberg and Palmgren
SR	Slipping ratio
SRR	Slipping to roll ratio
FHA	Frictional Heat Accumulation
CTE	Coefficients of Thermal Expansion
WL	White Layer
DZ	Deformed Zone
ORD	Over-Rolling Direction
ASBs	Adiabatic Shear Bands
DERs	Dark Etching Regions
GSC	Geometric Stress Concentration
RBEs	Rolling Bearing Elements
LEDS	Low Energy Dislocation Structure
WS	Worn Surface
M	Bearing matrix
UTS	Ultimate Tensile Strength
CI	Consistency Index
DM	Decision Maker
COD	Crack Opening Displacement
SRTRB	Single-Row Tapered Roller Bearings
SRCRB	Single-Row Cylindrical Roller Bearing
DRCRB	Double-Row Cylindrical Roller Bearing
FMEA	Failure Mode and Effects Analysis

CONTENTS

ABSTRACT.....	I
ACKNOWLEDGMENTS.....	III
PUBLICATIONS AND CONFERENCES.....	IV
NOMENCLATURES.....	V
ABBREVIATIONS	VII
CONTENTS.....	IX
LIST OF FIGURES.....	XIII
LIST OF TABLES.....	XVI
1. CHAPTER ONE: INTRODUCTION.....	1
1.1 Justification of the research.....	2
1.1.1 Importance of renewable energy	2
1.1.2 Problem genesis.....	6
1.2 Aims and objectives of work.....	9
1.3 Scope of work.....	11
1.4 Thesis outline and layout.....	13
1.5 Key novelty and contributions to knowledge	16
2. CHAPTER TWO: LITERATURE REVIEW	17
2.1 History of wind energy.....	18
2.2 Main parts of wind turbine	19
2.2.1 Foundation (base).....	20
2.2.2 Tower	20
2.2.3 Rotor	20
2.2.4 Nacelle.....	23
2.3 Wind turbine’s power curve	28
2.4 Wind turbine gearbox bearings WTGBs.....	29
2.5 WT monitoring systems	32
2.5.1 Condition Monitoring Systems (CMS).....	32
2.5.2 SCADA monitoring system	32
2.6 Steel material of WTGBs	33
2.6.1 Oxides content influence	34

2.6.2	Titanium content influence.....	34
2.6.3	WTGBs material requirements	35
2.7	The manufacturing and heat treatment processes of WTGBs	37
2.7.1	The heat treatment process of WTGBs.....	37
2.7.2	Surface modification of 52100 steel	38
2.7.3	Grinding vs. turning.....	38
2.8	Rolling Contact Fatigue (RCF).....	39
2.8.1	Mechanism of RCF damage.....	40
2.8.2	Hertzian Contact Theory	41
2.8.3	Stress distribution	44
2.8.4	Lubrication effect in rolling contact	46
2.8.5	Slipping effect on bearing damage	48
2.9	Rating life prediction of bearing	50
2.9.1	Lundberg and Palmgren Method	51
3.	CHAPTER THREE: MICROSTRUCTURE ALTERATIONS AND FAILURE MODES.....	55
3.1	Non-metallic inclusions (NMIs).....	55
3.1.1	Stress concentration in NMIs.....	57
3.1.2	Voids formation	60
3.1.3	Types of non-metallic inclusions.....	61
3.1.4	Damage drivers in NMIs.....	63
3.1.5	Shape, size, and aspect ratio of NMIs.....	64
3.1.6	Steel cleanliness.....	64
3.2	Microstructural alterations.....	65
3.2.1	Phases of microstructural alterations.....	66
3.2.2	White Etching Areas (WEAs)	66
3.2.3	White Etching Cracks (WECs).....	67
3.2.4	Butterflies.....	68
3.2.5	Dark Etching Regions (DERs)	70
3.3	Failures modes and affecting factors in WTGBs	71
3.3.1	Factors affecting WTGB's failure.....	71
3.3.2	Failure modes of rolling element bearing.....	71
3.4	Hypotheses for interpreting the occurrence of microstructural alterations and failure modes	83
4.	CHAPTER FOUR: SUBSURFACE INVESTIGATION OF A PLANETARY WTGB	86

4.1	Methodology.....	87
4.2	Observed damage patterns	90
4.3	Analysis of contact stresses	94
4.4	Analysis of damaged inclusions	98
4.5	Crack density with depth	100
4.6	Analysis of crack inclination.....	103
4.7	Investigation of the microstructural alterations and their triggers.....	108
4.8	The surface investigation related to subsurface damage.....	111
5.	CHAPTER FIVE: SELECTING THE MOST EFFICIENT WTGB TYPE USING ANALYTICAL HIERARCHY PROCESS METHOD (AHP).....	113
5.1	Multiple Criteria Decision-Making (MCDM)	114
5.1.1	Analytic Hierarchy Process (AHP).....	114
5.1.2	Expert Choice (EC) software.....	115
5.2	Problem modelling.....	117
5.2.1	Variants (Alternatives)	117
5.2.2	Criteria (Objectives)	119
5.3	Pairwise comparison and synthesizing of analysis	121
5.4	Discussion of results.....	121
5.5	Chapter summary.....	132
6.	CHAPTER SIX: KEY FINDINGS, CONCLUSIONS, AND RECOMMENDATIONS FOR FUTURE WORK.....	133
6.1	Key findings and conclusions	133
6.2	Recommendations for future work	138
	REFERENCES.....	140
	APPENDICES	161
8.1	Appendix A1.....	161
8.2	Appendix A2.....	162
8.3	Appendix B1	163
8.4	Appendix C1	164
8.5	Appendix C2	165
8.6	Appendix D1.....	166
8.7	Appendix D2.....	167
8.8	Appendix E1	168
8.9	Appendix F1	169

8.10 Appendix F2 170
8.11 Appendix F3 171
8.12 Appendix F4 172
8.13 Appendix F5 173
8.14 Appendix F6 174
8.15 Appendix F7 175
8.16 Appendix F8 176
8.17 Appendix F9 177
8.18 Appendix F10 178
8.19 Appendix F11 179
8.20 Appendix F12 180
8.21 Appendix F13 181
8.22 Appendix F14 182
8.23 Appendix F15 183
8.24 Appendix F16 184

LIST OF FIGURES

Figure 1-1: CO ₂ emissions from renewable and nuclear electricity production systems	3
Figure 1-2: Energy Return on Investment (EROI) for various energy production technologies	4
Figure 1-3: Total installed wind turbine units (%) up to 2020 (a) for onshore, and (b) for offshore	4
Figure 1-4: New installed wind turbine units(%) in 2020 (a) for onshore, and (b) for offshore	5
Figure 1-5: New global wind power installations (GW)	6
Figure 1-6: Damage percentage of wind turbine gearbox components, according to NREL 2016	9
Figure 1-7: Theoretical and experimental works attaining the thesis objectives.....	11
Figure 1-8: Thesis structure of the main chapters	15
Figure 2-1: Main parts of a wind turbine unit.....	19
Figure 2-2: Pitch & yaw adjustment in WT unit.....	21
Figure 2-3: The angle of attack (α) and the critical angle of attack ($\alpha_{critical}$) in WT blade.....	22
Figure 2-4: Schematic of angular contact ball bearing	23
Figure 2-5: Schematic of a Planetary gearbox of 2MW wind turbine	24
Figure 2-6: Transient loading of operating events in a 750 kW - WT system	26
Figure 2-7: Loading and no loading zones in bearing	27
Figure 2-8: The power curve of Vestas V42 WT (600 kW)	28
Figure 2-9: A double spherical roller bearing of a wind turbine gearbox.....	29
Figure 2-10: (a) fully crowned roller bearing, (b) partially crowned roller bearing.....	30
Figure 2-11: The acting forces generated by a tapered roller bearing	31
Figure 2-12: Hardness vs. heat treatment for 100Cr6 steel	36
Figure 2-13: Retained austenite vs. heat treatment for 100Cr6 steel.....	36
Figure 2-14: Hertzian Contact Pressure Distribution for roller and inner raceway of a bearing.....	42
Figure 2-15: Cartesian stresses (normal and shear stresses) under RCF	44
Figure 2-16: Distribution of equivalent stress beneath the contact region	45
Figure 2-17: Normalized principal and equivalent stress beneath the contact area centre	46
Figure 2-18: (a) Elastohydrodynamic lubrication, (b) mixed friction, (c) wear, (d) particles between the contact surfaces	48
Figure 2-19: Different cases of bearing loading zones.....	50
Figure 2-20: Bearing life curves (a) for ball bearing, (b) for roller bearing	54
Figure 3-1: Subsurface butterfly in the inner raceway of a roller bearing	57
Figure 3-2: Damage propagation resulting from a NMI close to the contact surface	58
Figure 3-3: Location-based classification of inclusions.....	59
Figure 3-4: Voids formation in the material of bearing steel	61
Figure 3-5: (a) Cracks with and without inclusion, (b) cracks network, (c) high magnification for cracks and WEAs, and (d) WECs, cracks & micro-cracks.....	68
Figure 3-6: Butterfly microstructure feature (a) microscopic image, (b) Schematic	70
Figure 3-7: (a) early stage DER, (b) fully developed DERs and 30° bands, and (c) DERs, 30°, and 80° bands.....	70
Figure 3-8: Classification of failure modes in rolling bearings	72
Figure 3-9: Surface indentation and spalling at the inner raceway of a roller bearing	73

Figure 3-10: (a) subsurface RCF , and (b) surface initiated RCF resulting in surface spalling	74
Figure 3-11: Micropitting and Geometric Stress Concentration (GSC)for Cylindrical Roller Bearing (CRB) in WT	75
Figure 3-12: Creep of the inner ring on the shaft-seat	76
Figure 3-13: Abrasive wear on the inner raceway and roller of a Tapered Roller Bearing (TRB)	76
Figure 3-14: Adhesive wear at the inner raceway of a cylindrical roller bearing	77
Figure 3-15: (a) Moisture corrosion, (b) fretting corrosion on the inner race ball bearing, and (c) fretting and false brinelling (vibration corrosion) in the outer ring of a tapered roller bearing	79
Figure 3-16: Bearing damage due to electrical current (a)electrical pitting, (b)electrical fluting	80
Figure 3-17: Plastic deformation damage (a)TRB track spalling due to misalignment, (b) Loose mounting markings and discoloration.....	81
Figure 3-18: Plastic deformation at ball distance in the outer race of a ball bearing	81
Figure 3-19: (a) Forced fracture in the inner race shoulder of TRCB, (b)Thermal Cracks in the inner race of TRCB, and (c) Section of fatigue fracture of a cam / roller outer race contact	82
Figure 3-20: Cracks initiation and propagation throughout the bearing zones under the impact wear....	85
Figure 4-1: The sample preparation procedure for microscopic examination	87
Figure 4-2: Grinding and polishing machine with its used material	88
Figure 4-3: The characteristics data of the subsurface cracks.....	89
Figure 4-4: Subsurface damage types observed within the examined samples.....	90
Figure 4-5: Samples of damage patterns observed, (a) non-cracked and separated inclusion; (b) self-cracking inclusion; (c) double crack associated with inclusion; and (d) crack not associated with inclusion	91
Figure 4-6: Mixed damage type associated with an inclusion	92
Figure 4-7: The voids and carbides impeded in the bearing subsurface region	92
Figure 4-8: XRD analysis of separation area surround an inclusion.....	93
Figure 4-9: Cracks initiate close to the inclusion	93
Figure 4-10: pressure distribution based on Hertzian contact theory.....	94
Figure 4-11: Normalized contact stresses using Hertz contact theory, (a) maximum shear; (b) Cartesian shear, and (c) Von-Misses stress.....	97
Figure 4-12: Effect of traction on subsurface maximum shear stress distribution ($\mu=0.15$).....	98
Figure 4-13: Difference in stress distribution for the non-metallic inclusions.....	99
Figure 4-14: The percentages of the observed damaged inclusions and their Aspect Ratio	100
Figure 4-15: Distribution of the investigated small microcracks with depth.....	101
Figure 4-16: Crack density with depth of the examined samples.....	102
Figure 4-17: Simulating of Von-Mises stress with depth in terms of increasing the traction force].....	102
Figure 4-18: (a) Small straight cracks; (b)&(c) large kinked cracks	103
Figure 4-19 Characteristic of microcracks angles in shallow subsurface depths.....	105
Figure 4-20: Characteristic of microcracks angles at deeper subsurface depths	106
Figure 4-21: Correlation of cracks' inclination angles with depth for the investigated samples (top) and distribution of shear stress with depth (down)	107
Figure 4-22: Description of cracks based on their causative stress	108
Figure 4-23: The behaviour of carbides and voids as microstructural alteration triggers	109
Figure 4-24: Butterfly feature (a) with a central NMI, (b) with a dispersed nucleus.....	110
Figure 4-25: Surface damage analysing using Alicona analyser.....	111

Figure 4-26: Surface damage initiation pattern.....	112
Figure 5-1: Flowchart of the general decision-making process.....	114
Figure 5-2: AHP structure of selecting the most efficient wind turbine gearbox bearing.....	117
Figure 5-3: Tapered roller bearing, α : contact angle.....	118
Figure 5-4: (a) Single-row cylindrical roller bearing , (b) Double-row cylindrical roller bearings.....	119
Figure 5-5: Pairwise comparison of the main criteria with respect to the goal.....	122
Figure 5-6: Pairwise comparison of the cost sub-criteria with respect to the goal.....	123
Figure 5-7: Pairwise comparison of the feature design sub-criteria with respect to the goal.....	123
Figure 5-8: Pairwise comparison of the availability sub-criteria with respect to the goal.....	124
Figure 5-9: Pairwise comparison of the options with respect to the purchase cost.....	124
Figure 5-10: Pairwise comparison of the options with respect to consumable cost.....	125
Figure 5-11: Pairwise comparison of the options with respect to maintenance cost.....	125
Figure 5-12: Pairwise comparison of the options with respect to the durability.....	126
Figure 5-13: Pairwise comparison of the options with respect to the reliability.....	126
Figure 5-14: Pairwise comparison of the options with respect to assembly complexity.....	127
Figure 5-15: Pairwise comparison of the options with respect to the available space.....	127
Figure 5-16: Pairwise comparison of the options with respect to availability of standards.....	128
Figure 5-17: Pairwise comparison of the options with respect to bearing market share.....	128
Figure 5-18: Completion of pairwise comparison.....	129
Figure 5-19: Performance sensitivity -selecting the most efficient option.....	129
Figure 5-20: Dynamic sensitivity - selecting the most efficient option.....	130
Figure 5-21: Gradient sensitivity - selecting the most efficient option.....	130
Figure 5-22: (Head-to-head) - selecting the most efficient option.....	131
Figure 5-23: Two-dimensional sensitivity -selecting the most efficient option.....	131

LIST OF TABLES

Table 1-1: Yearly revenue of wind turbine power generation..... 7
Table 2-1: The rotor size of the largest commercial wind turbines nowadays..... 21
Table 2-2: Chemical compositions of 100 Cr6 & AISI 52100 bearing steel 33
Table 3-1: Influence of NMIs on mechanical properties..... 57
Table 3-2: Non-metallic inclusion types and morphology 61
Table 4-1: Grinding and polishing processes data 89
Table 5-1: Scale of Relative Importance 116

1

CHAPTER ONE: INTRODUCTION

Wind turbine energy is one of the essential renewable energies in terms of cost, cleanliness, reliability, security, and affordability. The Life Cycle Assessment (LCA) study of overall green energy generation confirms that CO₂ emissions are the lowest in wind turbines compared to other power generation technologies [1]. At the same time, the increasing growth of the global economy has led to an increase in demand for energy and more emissions of greenhouse gases, causing many climate changes [2]. On the other hand, wind turbine units produce almost 20 times the energy used to build them, which is the highest range among the different renewable energy systems [3][4]. This advantage puts wind turbine technology in a favorable energy source position and indicates that it can bring significant economic and environmental benefits relative to other power generation systems [3]. In recent years, the growth rate of wind turbine (WT) units has decreased because of its high maintenance cost [5]. The cost of installing a WT unit is about 1.3–2.2 million \$/MW for onshore and 4.0–4.5 million \$/MW for offshore [6]. The National Renewable Energy Laboratory (NREL) reported that 76% of the wind turbine gearboxes breakdowns refer to their bearings, as can be seen in [section 1.1.2](#). For more details, see (S. Sheng) Ref. No. [7]. Wind Turbine Gearbox Bearings (WTGBs) fail within 1–5 years instead of 20 years (according to the bearing rating life L_{10})[8][9][10]. There is no decisive theory that explains the reason/s behind the bearing premature failure by cracking and flaking (removing material from the contact surface). Various evidence supports the claim that the cracks initiate at the tips of non-

metallic inclusions in the subsurface of the bearing contact region[5][11][12][13]. Some failure modes also appear on the contact surface, such as pitting and indentations. However, other failure modes can be observed in the subsurface region, such as cracks and white etching areas. Bearing subsurface damage initiates as small microcracks, which propagate to a macro level, reaching the contact surface and causing flaking. During the crack propagation stage, the cracks change their direction. Consequently, studying the straight and small microcracks will give the crack initiation a clearer view. This study discussed the investigation results of simulation and experimental work of subsurface microcracks to indicate the most influential formations of the cracks and the effect of stresses that have the high probability of causing the premature failures in WTGBs.

1.1 Justification of the research

1.1.1 Importance of renewable energy

Since the first Arab oil embargo in 1973, there has been a significant focus on renewable energy. In 1997, the corporate world signed the Climate Agreement in Japan, according to which the major industrialized countries agreed to reduce greenhouse gas emissions and encourage various developments in the production of renewable energy. The gas crisis in Europe and the rise in energy prices worldwide resulting from the Russian war on Ukraine in 2022 could be an urgent motive for reviewing global policies supporting clean energy technology. For that, renewable energy could finally begin to gain ground in the electric power generation sector [14]. In addition to being nonrenewable, the prices of fossil fuels are highly volatile that press towards the expansion of renewable energy sources. Research priorities have shifted from conventional power sources to renewable ones considering rising modern concerns about the environment and climate. Many renewable technologies have been used in place of polluting fossil fuels for producing electricity, such as wind turbines, solar, geothermal, hydro, tidal, and biomass. The primary benefits of wind energy are its abundant supply and negligible impact on the environment [15]. Wind energy is less expensive and easier to build on a big scale than tidal and solar energy, which are both significantly more expensive [2]. According to the findings of a study conducted by the International Atomic Energy Agency (IAEA), the life cycle emissions of a wind turbine can range anywhere from 7 to 22 tons of CO₂ equivalent per gigawatt-hour (GWh) of electricity produced [1], as can be seen in [Figure 1-1](#). Based on Energy Return on Investment (EROI) tool, each wind turbine unit generates

roughly twenty times the amount of energy that was required to build it [3]. In 2010, researchers at the University of Vermont compiled data from 119 wind farms. They found that, on average, each farm generates about 20 times as much energy as was expended to construct it, making it twice as efficient as coal, as can be seen in [Figure 1-2](#). This gives wind technology an advantage over other energy sources and indicates that switching to wind energy could have significant financial and social benefits. Consistent improvements in wind energy technology will surely bring about additional decreases in the cost of producing energy [3]. The global wind power capacity reached 742.7 GW in 2020, with an additional 93 GW of newly installed units, as can be seen in [Figures \(1-3\) & 1-4](#).

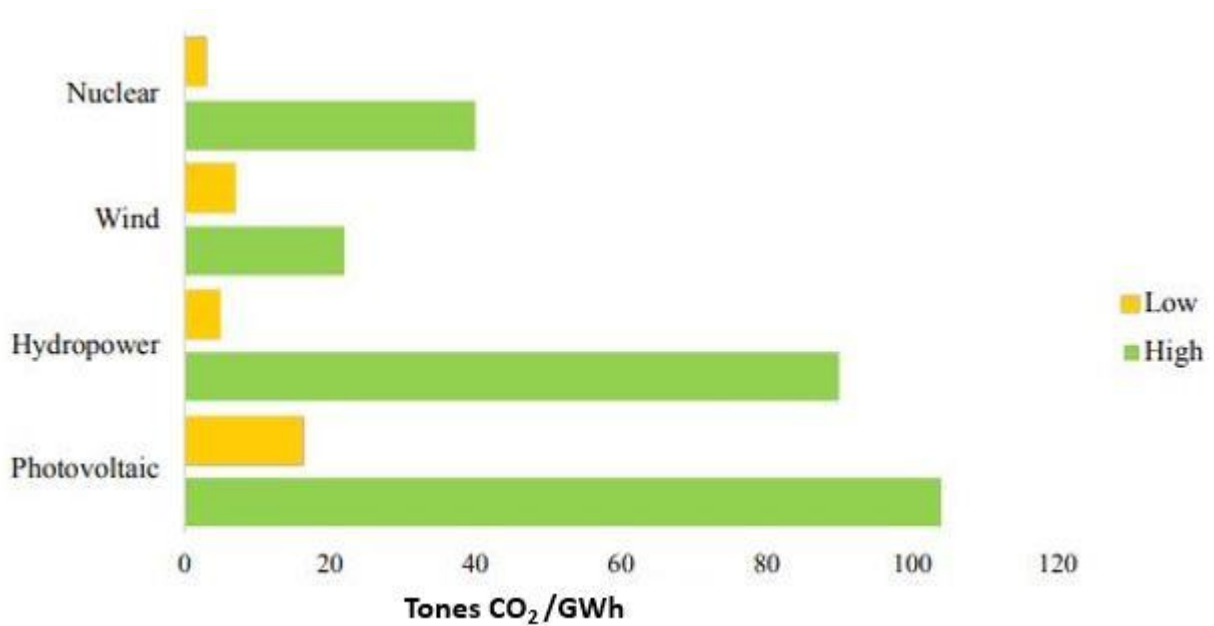


Figure 1-1: CO₂ emissions from renewable and nuclear electricity production systems [1]

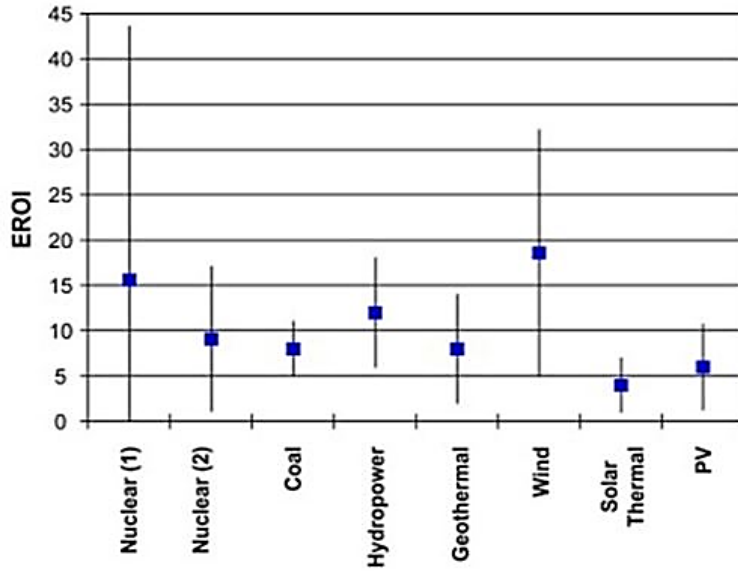


Figure 1-2: Energy Return on Investment (EROI) for various energy production technologies [3]

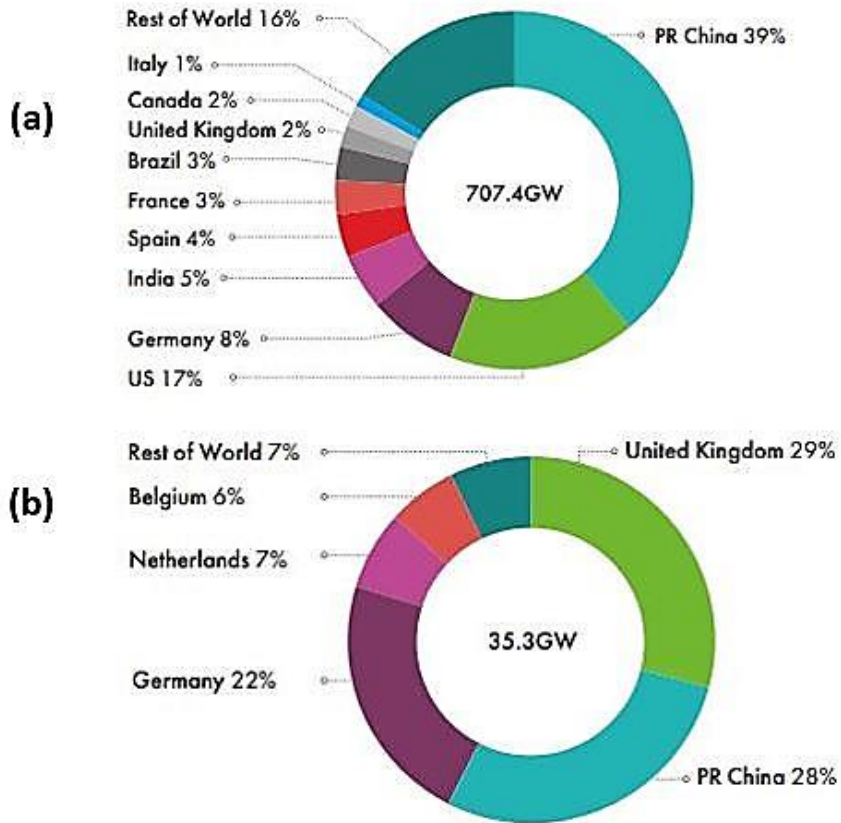


Figure 1-3: Total installed wind turbine units (%) up to 2020 (a) for onshore, and (b) for offshore [16]

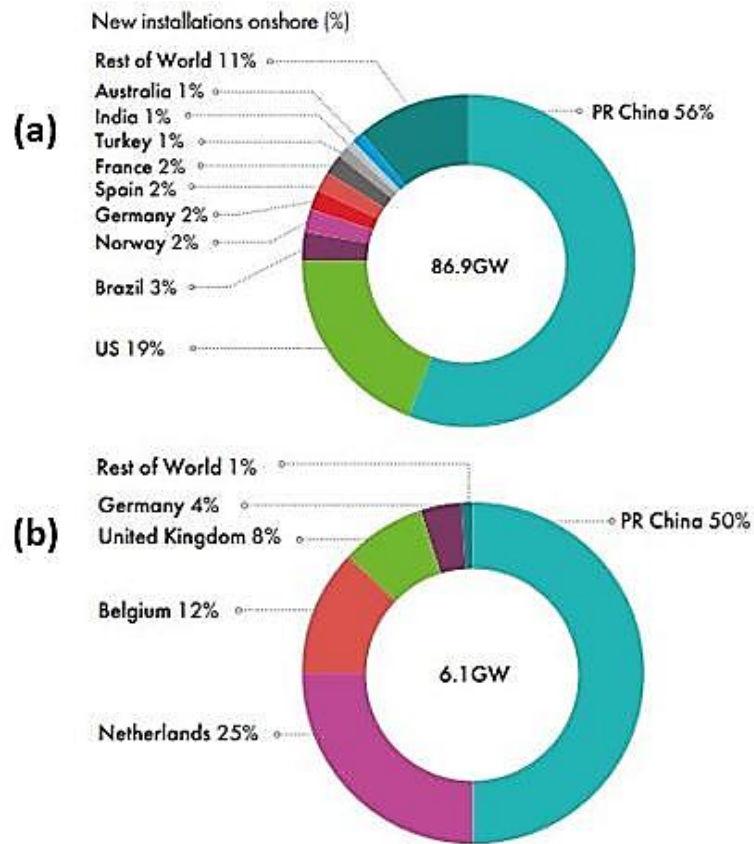


Figure 1-4: New installed wind turbine units(%) in 2020 (a) for onshore, and (b) for offshore [16]

The European Union Commission has announced the publication of the "Renewable Energy Road Map." It suggested "the Energy Roadmap 2050," which proposed that wind energy might provide (31.6- 48.7) % of Europe's electrical needs [17][18][19]. Wind energy capacity around the world has been growing steadily over the past few years and is anticipating to continue its expansion. It has been planned that the annual wind installations should increase dramatically to reach net zero by 2050 [16]. The Compound Annual Growth Rate (CAGR) is the Rate of Return (RoR) required to increase investment from its initial balance to its final balance, assuming profits are reinvested at the end of each period over the investment's lifetime, as can be seen in [Figure 1-5](#).



Figure 1-5: New global wind power installations (GW) [16]

1.1.2 Problem genesis

Wind turbines are subjected to severe surroundings conditions and operated under extreme variable loadings. Numerous wind turbine components are prone to breakdown and are both difficult and expensive to repair or replace. Turbines' tower heights, rotor diameters, and overall weights have nearly quadrupled in size and capacity. Newer, more powerful turbines with capacities of 8-12 MW are currently in the energy market [20][21]. Unfortunately, larger WT's are more prone to failures and need higher maintenance than smaller ones [22]. Larger turbines' costs can be reduced if condition monitoring is implemented and increase turbine reliability [23][24]. On the other hand, the constructional complexity of the overall farm site are substantially decreased when fewer and larger turbines are utilized [24]. Offshore wind farms prefer giant wind turbines because of the high costs associated with building the turbines and transferring their generating power. These farms also benefit from the view of higher efficiency of more consistent and substantial wind speeds. Moreover, installing a few large WT units requires fewer towers and ground anchoring systems, making the entire process simpler than constructing many small ones [24]. The yearly revenue of WT power generation is directly related to how much power the wind turbines generate as demonstrated in [Table 1-1](#). However, this is accompanied by an increase in

maintenance expenses, which raises the challenge of conducting the requisite research and technical work to reduce maintenance costs and boost returns.

Table 1-1: Yearly revenue of wind turbine power generation [382]

(A) Turbine size (MW)	⁽¹⁾ (B) Revenue (\$/hour)	⁽²⁾ (C) Yearly revenue For 100% capacity (\$)	For 65% Capacity (\$)	For 50% Capacity (\$)	For 35% Capacity (\$)
1	20	175,200	113,880	87,600	61,320
2.5	50	438,000	284,700	219,000	153,300
4	80	700,800	455,520	350,400	245,280
⁽¹⁾ (B)=The average price of electricity is 0.02 \$/kWh × (A) × 1000 (in Watt) ⁽²⁾ (C) Yearly revenue= (B)× (24) hour× (365) days × % capacity					

Bearings are crucial components of tribomachinery because they support loads and allow for rotation. They could need to keep running reliably under extreme conditions and massive static and cyclic loads. Bearings in large industrial gearboxes or drive train applications are often subjected to a wide range of operating conditions, such as those found in paper mill gearboxes, crusher mill gearboxes, lifting gear drives, and wind turbine gearboxes [8][25][26][27]. In WTs, the high cost of replacement, maintenance, and downtime makes caring for bearing reliability a higher priority than other parts. It means that more research on bearings failure is still required to reach a satisfactory operational life level.

Bearing failures in wind turbine gearboxes may occur earlier than expected. The failure starts on the contact surface of the bearing inner raceway. The surface initiation hypothesis states that cracks at the inner race surface might set in motion cracking that is later increased by external loading towards the subsurface. In comparison, the subsurface theory suggests that the damage may be caused by cracks introduced in the subsurface region from the weak locations, such as non-metallic inclusions and voids. There is not enough evidence to offer a definitive explanation for each hypothesis. When estimating the life of gearbox bearings, the manufacturers of WTGBs use the recommendations provided by Germanischer Lloyd (GL). The GL method estimates the bearing's remaining useful life based on the Rolling Contact Fatigue (RCF) analysis, which looked at the bearing's operation for 130,000 hours with a 10% chance of failure. Theoretically, the GL method postulated that WTGB will remain in operation for 20 years, however, it fails sooner (2–5) years during operating [28]. The premature failure of gearbox bearings results in a rise of the overall

energy costs due to the following indicators: turbine downtime, unscheduled maintenance, the replacement of the failed components, and the increase in warranty reserves. The average cost per failure in an offshore wind turbine gearbox as a significant replacement is about €230,000 (for materials only) [29]. The costs of operation and maintenance for wind turbines are expected to be more than twice as high as those for generating power using natural gas [30]. Even though the equipment's operation and maintenance costs are to some extent high, they are all considered long-term investments that should continue to generate a profit over time [24]. Many scientific collaborations have been established to assess the reasons behind WTGBs' failures such as the National Renewable Energy Laboratory (NREL). The latter reported that the most recent analysis of the distribution of damage reveals that WT bearings are responsible for 76% of the gearbox damage, gears are responsible for 17%, and the other systems are responsible for 7%, as can be seen in [Figure 1-6](#) [7][31]. Kotzalas and Doll [32] postulated that over 60% of gearbox failures might be traced to bearings. On the same conceptualization note, Feng et al. [33] demonstrated that WT gearbox breakdowns begin in the bearings rather than in the gears themselves.

The wind turbine gearbox (WTG) is a critical and expensive part of the drivetrain, accounting for 13% of the overall WT cost [34]. The inner race of the planetary roller bearing is a stationary (non-rotating) part. Hence, the applied radial load will concentrate only on one specific location and increase the damage occurrence likelihood [5]. As a result, the contact stress experienced by the inner ring increases for a given load. Inner rings are also typically installed on smaller shafts. The rings are heated to their expansion temperature during the construction and then slid onto the shafts. The rings' interference fit with the shaft is tightened as they cool, ensuring they will not come loose. A typical operation results in tensile hoop stress being superimposed on the contact stress in the bearing ring. When stress is applied, it works with the residual stress to accelerate fatigue damage [35]. WTGBs fail during one-fifth of their lifespan, however, the problem of WTGBs' premature failure remains unsolved in the literature review. From what has been mentioned, it is clear that new analytical studies are still required to mitigate the real emerging threats against the growth of green energy technology.

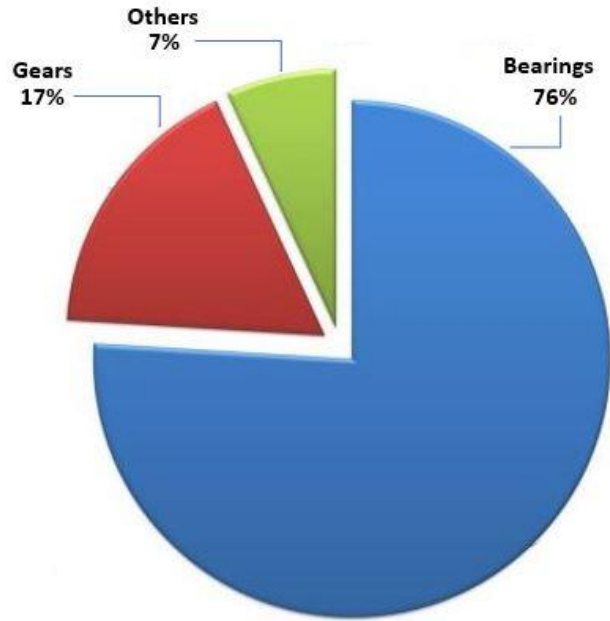


Figure 1-6: Damage percentage of wind turbine gearbox components, according to NREL 2016 [7]

1.2 Aims and objectives of work

This study aims to investigate the cracks' initiation in the subsurface region of the WTGBs in the context of studying their premature failure. Several factors are to be investigated regarding bearing damage, such as maximum shear stress, Von-Mises stress, and traction force. Furthermore, non-metallic inclusions, voids, and carbides are nonhomogeneous objects in the bearing steel matrix that need to reveal their roles in crack initiation. On the other hand, using the optimum bearing type in the Planetary Wind Turbine Gearbox (PWTG) may be a likely solution to mitigate the problem impact. [Figure 1-7](#) shows the thesis objectives and the experimental and simulation actions taken to meet them. The main objectives of this thesis can be summarized as follows: -

- 1- To determine the threshold of crack's length at which it starts to change direction using the experimental observations and the statistical work. Microcracks (less than the threshold) with fixed directions help to study the initiation cracking stage, while large ones (more than the threshold) with variable directions are concerning to the propagation stage.
- 2- To evaluate the role of non-metallic inclusions (NMIs) on crack initiation, the following indicators have been applied:

- a. Subsurface stress distribution using the Finite Element Analysis (FEA) model to detect the stress concentration of NMIs.
 - b. The percentage of cracks associated with inclusions to the total observed cracks of the investigated samples to evaluate the role of NMIs in the bearing premature failure.
 - c. The effect of NMI's Aspect Ratio ($AR = \text{length}/\text{width}$) on inducing cracks to evaluate the NMIs' sizes on the damage initiation.
- 3- To study the varying roles of maximum shear stress (τ_{\max}), traction force, and Von-Mises stress (σ_{VM}) on crack initiation and propagation, as follows: -
- 3.1 Maximum shear stress (τ_{\max}), using two indicators: -
 - a. The convergence degree of cracks' inclinations to τ_{\max} angle ($\pm 45^\circ$),
 - b. The distribution of shear stress vs. depth, based on Hertzian contact analysis.
 - c. Cracks' density (number of cracks) distributed for each 100 μm of depth (starting from the contact surface up to 1000 μm).
 - 3.2 Traction force, using four indicators: -
 - a. The convergence degree of the cracks' inclinations to the contact surface angle (0°) close to the contact surface with traction,
 - b. The distribution of shear stress vs. depth (based on Hertzian contact analysis),
 - c. The distribution of Von-Mises stress (σ_{VM}) vs. depth (with changing the traction force magnitudes),
 - d. Cracks' distribution (mentioned in the item 2.1 c)
 - 3.3 Von-Mises stress (σ_{VM}), using two indicators: -
 - a. The distribution of Von-Mises stress (σ_{VM}) vs. depth - with changing the traction force magnitudes (mentioned in the item 2.2 c),
 - b. Cracks' density vs. depth (mentioned in the item 2.2 d).
- 4- To clear up WEAs, WECs, voids, and carbides' roles in the crack initiation by analyzing the results of the microscopic investigation using optical and Scanning Electron Microscope (SEM).
- 5- To verify the effect of WT operating events on damage initiation by analyzing the microcracks' inclinations.

6- To select the most efficient WTGBs type by applying the Multiple Criteria Decision-Making (MCDM) approaches / (Analytical Hierarchy Process AHP) method / Expert Choice (EC) software tool.

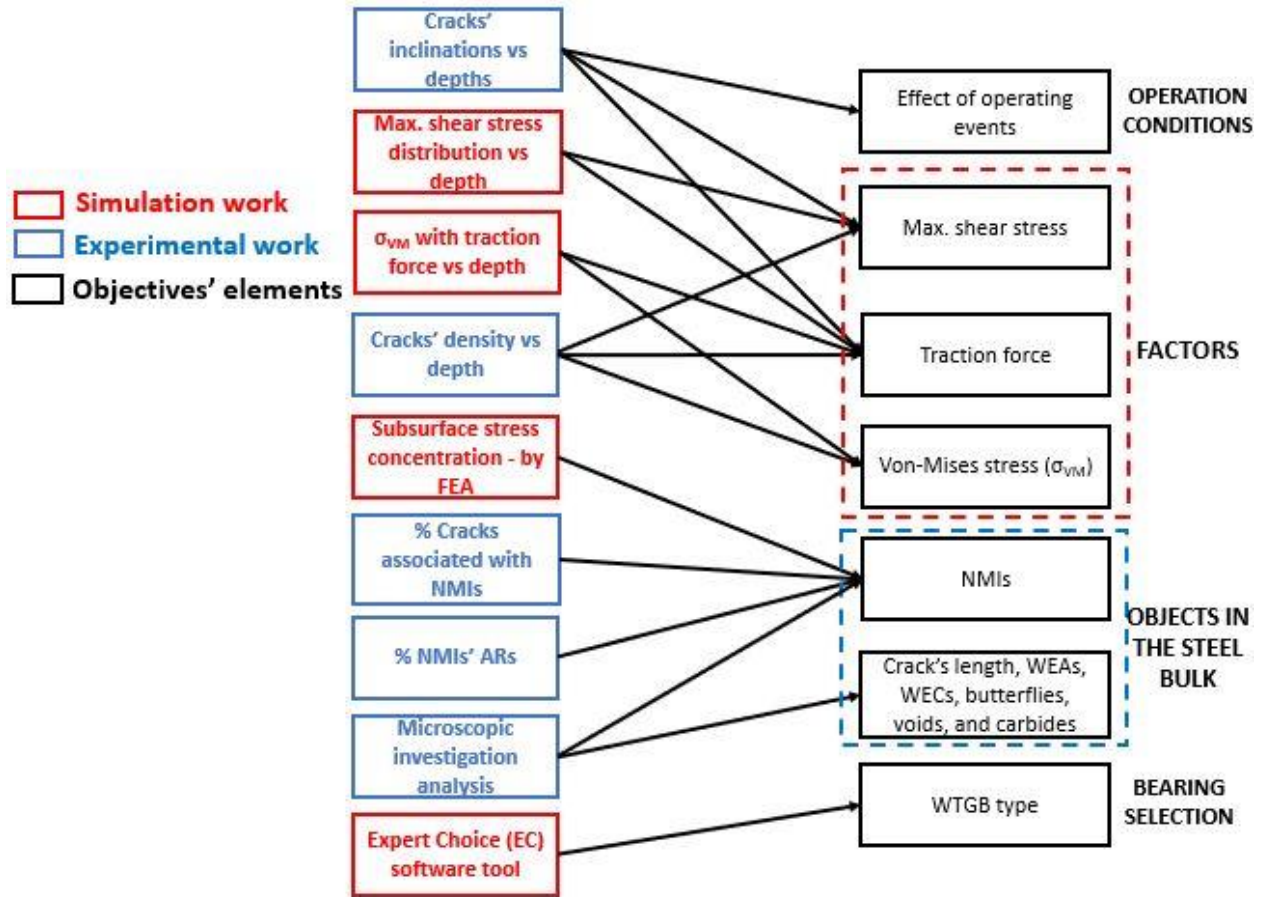


Figure 1-7: Theoretical and experimental works attaining the thesis objectives [the researcher]

1.3 Scope of work

The following subtitles describe the most important features regarding the scope of this study: -

Scientific Field of study: mechanical engineering, renewable energy, materials engineering, and production engineering.

Physical Part of Study:

- **System:** 2MW onshore WT,
- **Main part:** inner race of a planetary gearbox bearing (PGB),
- **Test samples:** The specimens were taken from the more severe damage region of the inner race of a Double Row Cylindrical Bearing (DRCB),
- **Investigated zone** – subsurface (mostly) and surface (rarely), as far as the subsurface layer analysis is concerned.

Investigation modes: simulation and experimental works, as follows:

1- Simulation Works: Several software applications have been used to make the required simulation and find the comparison results, as follows: -

- Finite Element Analysis (FEA) with (ABAQUS) to investigate the influence of stress distribution for the subsurface contact region and the stress concentration around NMIs.
- MATLAB programming to study the relationship of Von-Mises stress with depths, and maximum shear stress with the depth in case of exceeding the standard value of the coefficient of friction and contact stress.
- Multiple Criteria Decision-Making MCDM approach, using Analytical Hierarchy Process AHP- Expert Choice software to select the most efficient bearing type.

2- Experimental Works:

- **Apparatuses:** wire erosion, linear saw, and grinding - polishing machines were used to prepare samples. The microscopic investigation used a Light-Reflection Microscope (LRM) and a scanning electron microscope (SEM). An X-Ray Diffraction (XRD) analyzer has been applied to reveal the material components of the mysterious regions.
- **Interrelationships data:** The registered results were categorized statistically based on the following correlations: cracks' numbers vs. depths, cracks' inclinations vs. depths, cracks' lengths, and whether or not the investigated cracks were associated with the NMIs. The inclusions were classified into three levels based on their aspect ratio (AR). The other observations indicate the start point of cracks, the damage behavior of voids and carbides, and the presence or absence of WEAs with WECs.

Limitations:

- 1- Tapered type of WTGBs has been used recently in WT systems. Hence, the researcher could not provide a failed sample of that type to apply the study procedure and to compare the results due to confidentiality concerns.
- 2- Large cracks (with lengths $>15 \mu\text{m}$) are multidirectional at the propagation stage, so their inclinations were neglected.

1.4 Thesis outline and layout

The thesis chapters are structured in a flow chart, as can be seen in [Figure 1-8](#). Regardless of the introduction chapter that deals with the conceptual headlines of the research aims, its justification, problem genesis, aims, and objectives, the other chapters deal with many related theoretical, experimental, and deductive aspects of the research framework, as follows:

Chapter 2 presents three research axes related to the literature review of the thesis topic. The first one gives an overview of knowledge about WT (as an energy source, components, operations, and monitoring system). In addition, it highlights the types and designs of bearings utilized in the Wind Turbine Gearbox (WTG) with a recapitulation of the load distribution. The metallurgical and manufacturing requirements of WTGBs steel materials, the impact of incorporating different chemical compositions, their heat treatment process, and grinding with the turning process make up the second research axis. The last headline one describes the fundamental and analytical theories concerned with bearing damage, such as rolling contact fatigue, Hertzian contact theory, and rating life prediction methods.

Chapter 3 sheds light on the more specific topics regarding the microstructural alterations and failure modes of WTGBs. The most common surface and subsurface failure modes have been covered in the form of a (conditions-causes-solutions) triple review. Moreover, five patterns of damage features have been illustrated in this chapter as follows: White Etching Areas (WEAs), butterflies, White Etching Cracks (WECs), White Structural Flaking (WSF), and Dark Etching Regions (DERs). Nonmetallic inclusions and their surroundings in the bearing steel matrix were highlighted in terms of stress concentration, types, properties, and the related subject of steel cleanliness.

Chapter 4 displays the investigation work of this study. The simulation part reveals the stress distribution around non-metallic inclusions particles using ABAQUS and FEA. Samples of severely damaged bearings related to a 2MW wind turbine gearbox were investigated. The total observed (1,447) cracks were categorized based on lengths, numbers with depths, inclinations of the crack with the contact surface, and whether or not they were associated with NMIs. Another statistical work related to categorizing NMIs based on their Aspect Ratios (ARs). All experimental and simulation results have been analyzed and compared to each other to conclude several findings. The chapter focuses on the role of NMIs on crack damage initiation, voids, carbides, WEAs, WECs, Von-Mises stress, maximum shear stress, and traction force. Moreover, the presence of the cracks' inclinations has been discussed in correlation with the WT operating events.

Chapter 5 sets out the structure of selecting the most efficient WTGBs type using the Multiple Criteria Decision-Making (MCDM) approach. The combined specific outputs obtained from both chapter 1 (the specific information of WTGBs types) and chapter 4 (the sudden transient loading in WT) formulate the input parameters of MCDM. In other words, this chapter applies theoretical information and investigation results to produce a partial proposal for choosing the best bearing type for planetary stage in the WTG. It demonstrates the effectiveness of using “Expert Choice” EC software to implement the Analytical Hierarchy Process (AHP) to select the most compromised solution among several alternatives based on many criteria and sub-criteria. However, three types of bearings are compared with each other considering many criteria, especially durability and reliability that match the diagnosis of the premature failure of WTGBs.

Chapter 6 highlights the conclusions of the overall results and suggests several recommendations for future work. The propositions center on minimizing damage to WTGBs in the following bearings' phases: design, manufacturing, operation, and maintenance.

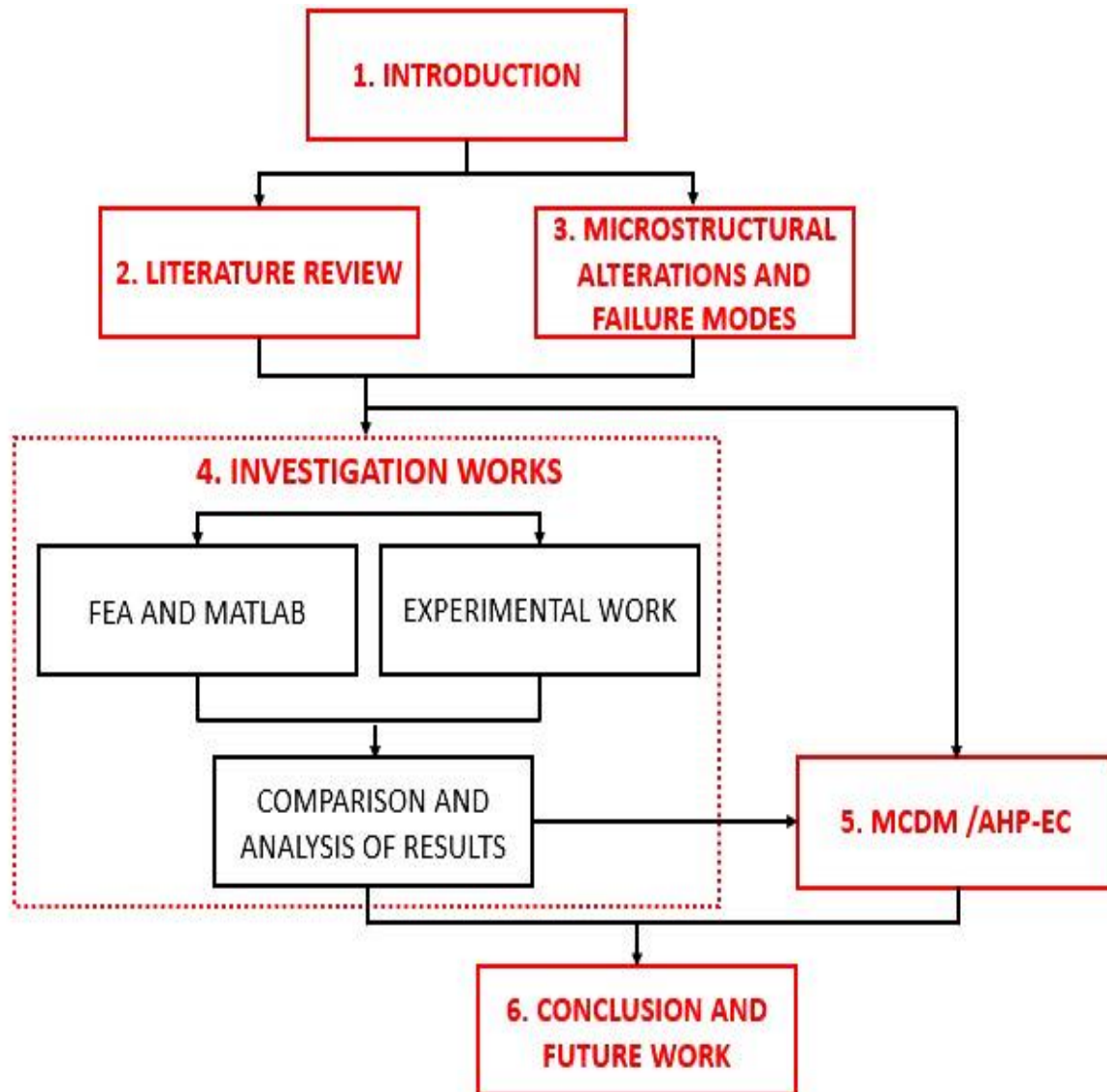


Figure 1-8: Thesis structure of the main chapters [the researcher]

1.5 Key novelty and contributions to knowledge

The key novelty items of this thesis are listed below: -

- 1- This is the first study to determine the threshold of crack length as 15 μm , after which the crack tends to change its orientation. Based on that, cracks can be categorized as small (microcracks) of lengths $<15 \mu\text{m}$ to study the initiation stage and large cracks of lengths $\geq 15 \mu\text{m}$ to study the propagation stage.
- 2- Contrary to many hypotheses, this study provided evidence that underestimated the consideration of non-metallic inclusions and their sizes as priority causes of crack initiation.
- 3- Highlighting other crack initiation triggers such as the soft area created by the contiguous voids and the hard carbides that compress these voids and non-metallic inclusions.
- 4- Conducting a combined investigation of (Von-Mises stress, maximum shear stress) and traction force to find their differential roles in crack initiation, in terms of the indication of both cracks' distribution and inclinations vs. depth.
- 5- Determining the single-row tapered roller bearing type as the most efficient compatible alternative for use in WTG in terms of several criteria, such as durability, reliability, cost, design features, and accessibility.

2

CHAPTER TWO: LITERATURE REVIEW

This chapter presents the knowledge base of this thesis. It outlines an overview of wind power energy history and identifies the main parts of the WT unit. More elaboration has been included regarding the gearbox system and the most common bearings types used in it. The severe operating events imposed additional challenges to the fatigue resistance of the WTGBs, which have been presented in this chapter as (torque–time) operating profile and (loading-no loading) bearing zones. As the monitoring process of WT operation is effective in failure predicting, this chapter highlights two monitoring systems: Condition Monitoring System (CMS) and Supervisory Control and Data Acquisition (SCADA). WTGBs’ material varies in their chemical composition, which affects fatigue endurance. For that, this part introduces the most common steel grades of WTGBs and their related requirements in the casting and heat treatment process. The plastic deformation at the bearing contact surface is an entrance to the occurrence of the failure stage. It has a correlation with stress distribution. Accordingly, Rolling Contact Fatigue (RCF) and Hertzian Contact Theory with other related subtitles (such as lubrication, slipping, and bearing life) are presented in this chapter.

2.1 History of wind energy

In 1887, the first significant power generation wind turbine of 12 kW was built in Cleveland, Ohio, and then by the end of World War I, Denmark had extensively used wind turbines of 25 kW. The creation of aircraft propellers and monoplane wings spurred American wind turbine development. Works in Denmark, France, Germany, and the United Kingdom (between 1935 and 1970) showed that large-scale WTs could be used. Europe recovered from the destruction of World War II and continued to thrive. The Danish Gedser mill's 200 kW three-bladed upwind rotor WT (the rotor in front of the tower) operated as early as the 1960s. In the 1970s, Germany was home to a proliferation of cutting-edge horizontal-axis designs, including variations on the helix and the ring. An important turning point in wind energy development occurred during the 1973 oil crisis when the US government began investing extensively in wind energy research and development. As a result, between 1973 and 1986, the commercial WT industry changed from small-scale applications in homes and farms (1-25 kW) to large-scale, utility-connected wind farms (50-600 kW). Incentives (such as federal investment and energy credits) granted by the United States government between 1981 and 1990 led to the construction of nearly 16,000 machines in California with outputs ranging from 20 to 350 kW (a total of 1.7 GW). Rising power prices and improved wind resource availability in the 1980s and 1990s created a small but constant market for wind farm developments in northern Europe. The first offshore wind farm with eleven 450 kW turbines was built off the coast of Denmark in 1991, launching the offshore wind industry. Europe is now the world's leader in offshore wind power since the industry has continued to develop this technology. Offshore wind farms may now use much larger turbines, ranging in size from 3.6 MW to 9.5 MW, with a 12 GW turbine just announced by General Electric. Initially, the cost of offshore wind production was prohibitive [36]. Nowadays, wind energy has shot to the forefront of international attention, attracting significant worldwide corporations [37]. Wind energy project success depends on the reliability of wind turbine systems. The low reliability reduces project income through increasing Operation and Maintenance (O&M) expenses and turbine downtime [38]. The Cost of Energy (CoE) is an essential indicator for evaluating energy projects. The O&M cost can make up 10–20 % of the total CoE related to a wind project [39].

2.2 Main parts of wind turbine

A wind turbine unit consists of four major parts: foundation or base, tower, rotor, and nacelle, as can be seen in Figure 2-2. The nacelle is mounted on a tower anchored to the ocean floor for offshore WT or to the earth for onshore WT by a (base) foundation. The typical WT has a rotor of three blades fixed onto a horizontal hub and connected to a planetary gearbox (GB) via a Low-Speed Shaft (LSS). The gearbox (GB) increases the rotational speed to be harmonic with the required frequency (50 or 60 Hz). A High-Speed Shaft (HSS) transmits the mechanical power from the gearbox to a generator that converts it into electrical energy.

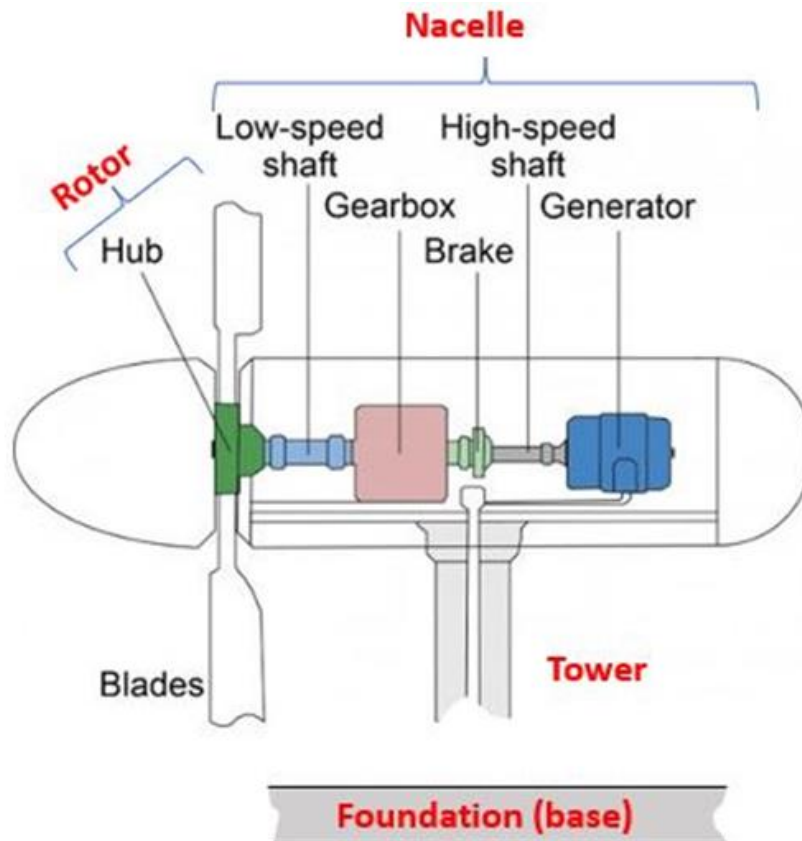


Figure 2-1: Main parts of a wind turbine unit- adapted from [40]

2.2.1 Foundation (base)

The onshore turbines' base is hidden by soil and cannot be seen from the air. It's a massive, concrete block that should support the entire turbine and all the forces acting on it. Offshore wind turbines have a base submerged in the sea and are invisible. The base of offshore turbines that extend far into the ocean is free-floating, but it has a substantial enough mass to support the turbine's weight and all the forces acting on it, keeping the turbine in a vertical position.

2.2.2 Tower

Most modern turbines have a steel tower ranging in height from 75–110 m, depending on the turbine's size and location. The tower's diameter is typically 3 to 4 m. In recent years, a large WT has rotor diameters of 129 m [24]. The general criterion regarding the height of a turbine's tower is to match the diameter of the circle the blades create when rotating. Most of the time, the taller a turbine is, the stronger and more frequent the winds it should withstand. It is because wind speeds increase at higher altitudes since the wind does not blow at the same rate at various distances from the ground.

2.2.3 Rotor

The rotor is the part of the turbine that starts rotating. It consists of two main parts: blades and a hub. The rotor typically has three blades and is made of lightweight glass fiber-reinforced plastic [41]. The blades have a hub in the middle that holds them together. A turbine can have two, four, or even number more than three blades. However, the three-blade rotor offers the highest efficiency. The blades aren't solid; they're constructed of a composite material that allows them to be both lightweight and robust. The current tendency is toward making them bigger (to accommodate more power), lighter (to save weight), and stronger. The blades take the shape of an airfoil to maximize airflow, just like the wings of a plane. They are not flat but feature a twist from base to tip. The blades can spin up to 90° on their axes. The term "blade pitch" describes this rotation. The hub holds the blades in place, allowing them to rotate independently of the rest of the turbine body. Increasing the blade diameter increases the output power, considering the influence of other vital WT parts on power output, such as the gearbox and generator, as illustrated in [Table 2-1](#) [42].

Table 2-1: The rotor size of the largest commercial wind turbines nowadays [37]

Company	WT	MW	Rotor (m)
<i>Gamesa</i>	G128	4.5	128
<i>Enercon</i>	E-126	7.5	127
<i>Repower</i>	6M	6.15	126
<i>Acciona</i>	AW-119/3000	3	119
<i>Sinovel</i>	SL3000/113	3	113
<i>Vestas</i>	V112	3	112
<i>Siemens</i>	SWT-3.6-107	3.6	107
<i>Nordex</i>	N100	2.5	100
<i>GE</i>	2.5xl	2.5	100
<i>Suzlon</i>	S88	2.1	88

The rate at which the wind blows can fluctuate at any time, even from one second to the next. Therefore, the output power of a turbine should be constantly changed to match the changing in wind conditions. Due to wind dying down and changing the wind directions, typical conversion rates are much lower, ranging from 30–40% for onshore wind turbines to 65–90% (or more significant in exceptional circumstances) for offshore wind turbines [24]. Pitch control involves changing the angle at which the blades spin, whereas yaw regulates the nacelle direction of the turbine to face the wind and getting more efficiency, as can be seen in [Figure 2-2](#).

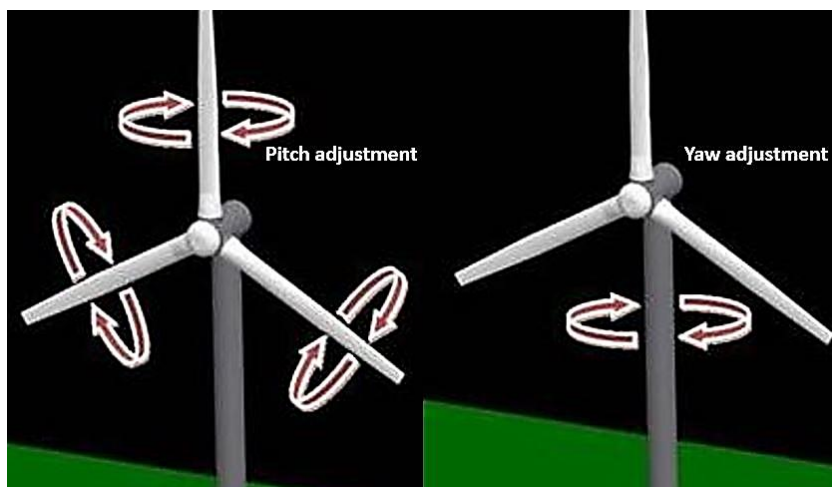


Figure 2-2: Pitch & yaw adjustment in WT unit [43]

Pitch control can keep WT blades at suitable angle for given maximum output power. The angle of attack (α) is determined by the blade's chord line and the wind's direction at which the blade is

set. While the critical angle of attack (α_{critical}), at which the air can no longer pass smoothly over the upper blade surface, as can be seen in [Figure 2-3](#). A wind turbine's angle of attack can be increased by stalling it, exposing more of the blade's flat side to the wind. In contrast, furling reduces the angle of attack by turning the blade's edge in the direction of the wind to produce what has been called an "aerodynamic brake," i.e., reduces the torque on the turbine blades. Because the aerodynamic force on the blade is altered by adjusting the pitch angle, the output power can be controlled [43].

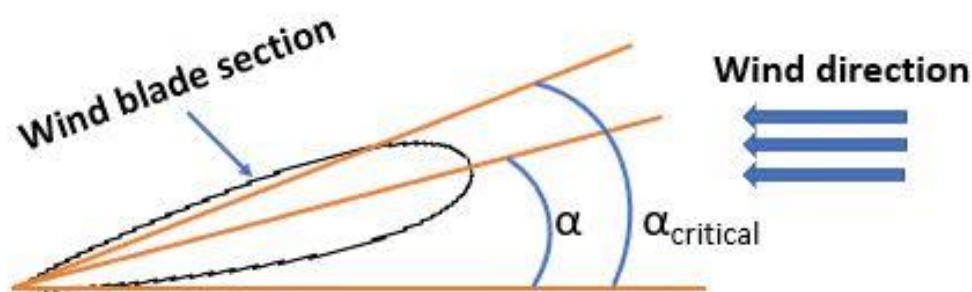


Figure 2-3: The angle of attack (α) and the critical angle of attack (α_{critical}) in WT blade [the researcher]

Yaw is the horizontal rotation of the whole wind turbine. It keeps the turbine pointed directly towards the wind to increase the area of the rotor rotating and, hence, the turbine's output. Because wind direction can change rapidly, the turbine's blades may not always face the wind direction, resulting in reduction of the produced power. The nacelle is supported by bearings, that permits it to rotate freely by a feature known as "Yaw Drive". These bearings can take on wind stresses in addition to those caused by the nacelle and the rotor weights. To turn the nacelle, a power should be supplied via a yaw drive mechanism. It has an electric motor and a gearbox to reduce the yawing speed [44]. The bearings in the yawing gearbox should be designed with a reduced profile and a higher degree of stiffness to handle the moment loads generated by the pinion. The yaw drive's main shaft rides on a specially designed angular contact ball bearing. Deeper grooves on the raceway surfaces of the inner and outer rings enable the bearing to support a higher axial load. A sectional illustration of this specific angular contact ball bearing can be seen in [Figure 2-4](#). This design can take on more axial load than standard angular contact ball bearings.

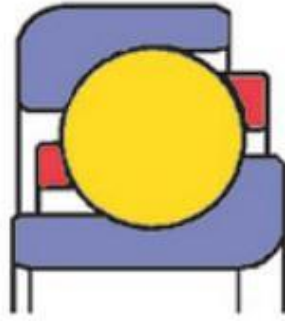


Figure 2-4: Schematic of angular contact ball bearing [44]

2.2.4 Nacelle

The nacelle is a housing located at the tower's top that holds all the necessary equipment for the turbine. It is a complex electromechanical system requiring a great deal of maintenance and care. In addition to the Low and High-Speed Shafts (LSS&HSS), the nacelle has two main parts: planetary gearbox, and generator.

2.2.4.1 Gearbox

The Wind Turbine Gearbox (WTGB) is an essential part of wind turbines since it is responsible for increasing the speed of the main shaft from its typical range of (15–35) rpm to (1500-1800) rpm with a total gear ratio of about 1:100, which is suitable for the generator [45]. The WTG works to increase the rotational speed at the tradeoff of torque. In contrast to many other applications, the WTG purpose is to reduce speed while increasing torque [46]. It has three stages: Low-Speed Stage (LSS), Intermediate-Speed Stage (ISS), and High-Speed Stage (HSS). The conventional WT gearbox has a planetary (epicyclical) gear in the input stage, as this type of gear can transmit high torques, large gear ratios can be achieved, and maintain a compact nacelle size [41]. In the planetary gearbox (PGB) type, the friction in the gear teeth and the roller bearings that normally used in this stage causes a portion of the transmitted power to be lost [47]. Three planets are typically used in the WTG planetary stage, but two planetary stages could be used in WT having capacities of greater than 3 MW [48]. The rotor's high input torque is split into three torques in the planetary stage, which builds up on the sun gear as the rotational speed increases [49]. Each planet gear is typically held in place by two planetary bearings. One of these bearings is known as the Up Wind (UW) bearing, and it is located on the side of the turbine hub. The other bearing, known as the Down Wind (DW) bearing locates next to the UW bearing and faces away from the

hub [49]. One planetary stage and two parallel stages make up the conventional gearbox configuration for a 2 MW unit. There are three shafts, each with one cylindrical roller bearing and two tapered roller bearings for shaft axial loads and guiding. Twenty bearings and nine gear wheels make up the gearbox, as can be seen in (Appendices A 1&A 2) [50]. The main low-speed rotor shaft connects to the planet carrier that holds all the planet gears. The mesh of these planetary gears with the fixed annulus (non-rotating ring gear) forces them to revolve, as can be seen in Figure 2-5 [41]. The turbine's gearbox has proven to be a problematic part of the WT unit. The wind's energy fluctuates over time, making it impractical to rely on for any appreciable period. Accordingly, overloading and underloading conditions in WT would be present during the oscillating operating loads. Premature failure of planet bearings can be caused by overloading and underloading [51]. Because of the unpredictable nature of wind, it is constantly changing. This results in fatigue and failure of the gear teeth due to overload and hammering stress. As well the planet bearings can become misaligned multiple times over the course of a single rotation [8].

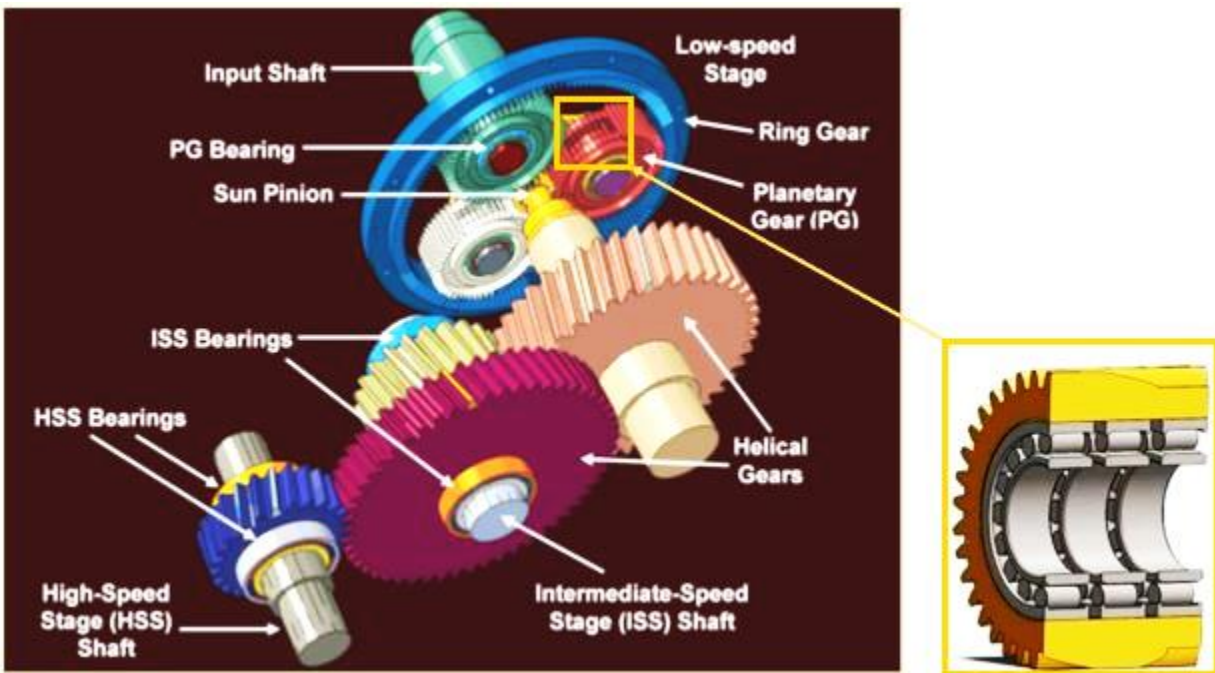


Figure 2-5: Schematic of a Planetary gearbox of 2MW wind turbine – adapted from [50][52]

Factors affecting Torque and load of WTGs

Even though WTGs use state-of-the-art design methods, they operate under more stress than expected. A steady start to WTG operation affects the torque and load by several variables, as follows:

- 1- Wind speed and direction (wind gust) [53][54],
- 2- Gearbox design (rotational speed and number of stages) [53][54],
- 3- Number of bearing rows [55],
- 4- Bearing tolerances [55],
- 5- Load differences between UW and DW [56][57],
- 6- The gearbox mounting system (two, three, or four points) [53][54].

In the case of a shutdown, the maximum torque exceeded the recommended threshold, although the torque was within the acceptable range in regular operation [53][58]. Wind gusts and other operating events, including start-up, shutdown, grid loss, generator engagement/disengagement, and braking subject the WTG to various loading conditions while the turbine is running, as can be seen in [Figure 2-6](#). After several braking cycles, it is possible to observe torque variations and torque reversal, which cause transient and impact loadings on the gearbox shafts and transmit to the gearbox bearings [59]. As torque and the rotating speed change, the bearing loading zone shifts, resulting in increasing the sliding during the over-loading cycle [8]. Accordingly, misalignment and impact loading can lead to excessive stress in gears and bearings contact areas [60]. Transient operating conditions and loading levels in WTGBs are unpredictable since the wind speed at which an event can take place considerably affects these loading levels. As a result, these loads are not considered by the designers during the bearing design and the bearing selection stage [60][61].

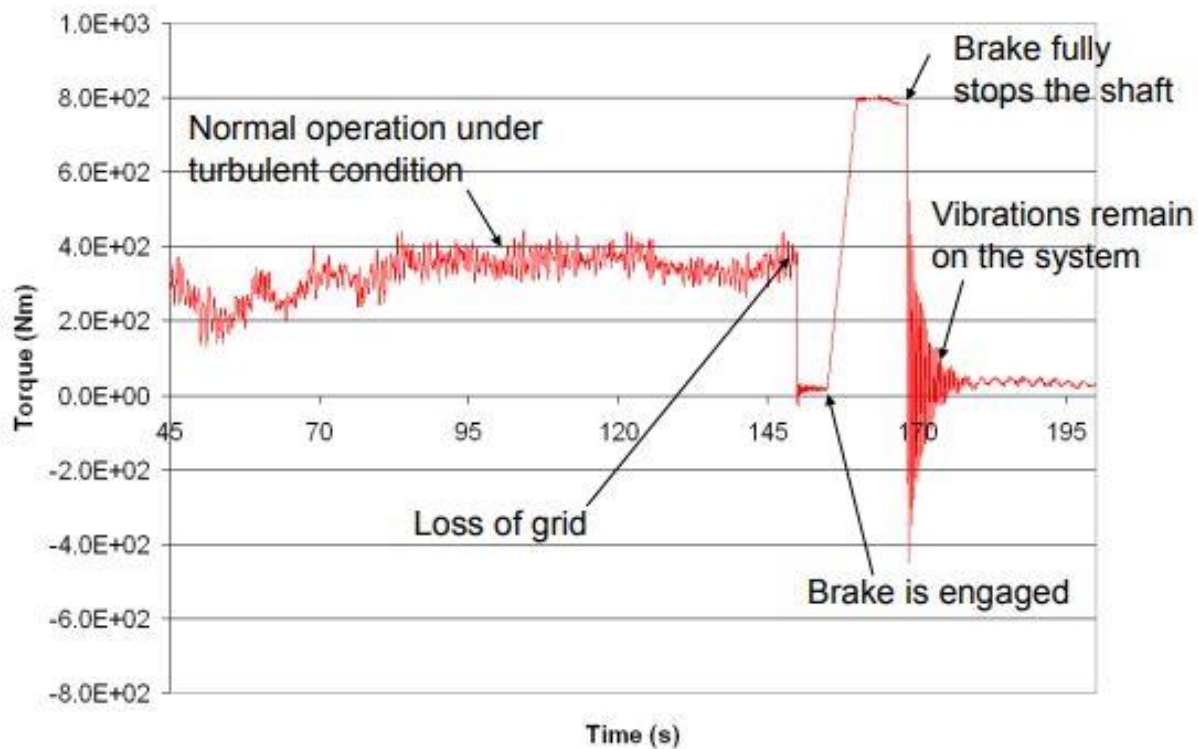


Figure 2-6: Transient loading of operating events in a 750 kW - WT system [62]

When a WT begins to rotate, the turbine generator is disconnected and remains so until the turbine reaches its steady state speed. This scenario is called a "no-loading" procedure [63]. The gravity of the drivetrain components, the rotational speed at start-up, and the gearbox's supporting structure are significantly impact the dynamic loadings that are applied to the wind turbines components [54]. An abrupt increase in loading occurs as the turbine generator is connected to the power grid. Because of this, a severe loading state can be produced for several transient loading cycles (impact). Eventually, the WT will resume its previous state of constant operation. The time is unknown for which the abrupt shift in the drivetrain loading level because it depends on the turbine's rotation and the wind speed [64]. On the bearing inner race, two distinct zones can be recognized depending on the direction of the loading bearing: loading and no loading zones, as can be seen in [Figure 2-7](#). When a roller enters the bearing loading zone, it is immediately subjected to a high-stress level due to the misalignment (skewing of the roller rotation axis). For example, misalignment in a 1.5 MW gearbox can result in a bearing contact pressure of more than 3 GPa which exceeds the yield stress of the bearing material [65].

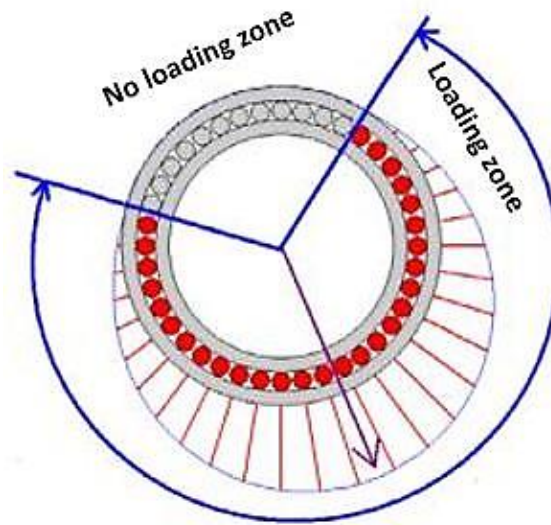


Figure 2-7: Loading and no loading zones in bearing [66]

2.2.4.2 Generator

The generator is responsible for transforming the mechanical energy of the rotor that has been harvested from the wind into electrical power. All power generation uses a three-phase alternate current at the commercial production level. Unlike the turbine rotor, the generator rotor should rotate at a higher speed to match the electrical network's frequency, often 50 or 60 Hz. The standard rotational speed for most generators is 1500 rpm (for 50 Hz) or 1800 rpm (for 60 Hz). The generator capacity is measured by the apparent power unit KVA, while the real power unit is kW. The ratio of real to apparent power is the so-called "Power Factor" (PF). Generators with higher power factors transfer more energy to the connected load. In contrast, the opposite is true for generators with lower power factors, which has higher power costs. The typical power factor of a three-phase generator is ~ 0.8 . The most common types of generators that have been used in WTs are as follows [65]: -

1. Squirrel-Cage Induction Generator (SCIG),
2. Permanent Magnet Synchronous Generator (PMSG),
3. Doubly Fed Induction Generator (DFIG),
4. Electrically Excited Synchronous Generator (EESG), and
5. Wound Rotor Induction Generator (WRIG).

The generator associated with wind turbines, thus far, is the induction generator because a synchronous generator should turn at a tightly controlled constant speed (to maintain a constant frequency). Each generator has a specific operating function, as how it is connected/disconnected will likely affect the gearbox load and its bearings.

2.3 Wind turbine's power curve

The wind turbine's power curve is displayed by its computer control system to adjust the produced power in terms of all the turbine unit components. The lift generated by the wind is sufficient to rotate the turbine blades once the wind speed reaches the cut-in wind speed (the minimum speed to produce power from the wind turbine, which is about 4.0 m/s). The turbine begins generating power, which grows in proportion to the wind's velocity. The turbine can reliably generate power (rated power) by maintaining a constant rotor speed. Hydraulic and aerodynamic brakes can prevent high winds from damaging WT components due to the cut-out wind speed (the maximum wind speed used to produce power, which is about 25 m/s), as seen in Figure 2-8. The rated wind speed at which the designed power of the WT can be achieved is called the "cut-off speed," which is about 16 m/s. Between the cut-off speed and the rated speed, the output power should be adjusted to the output power in a sufficient way.

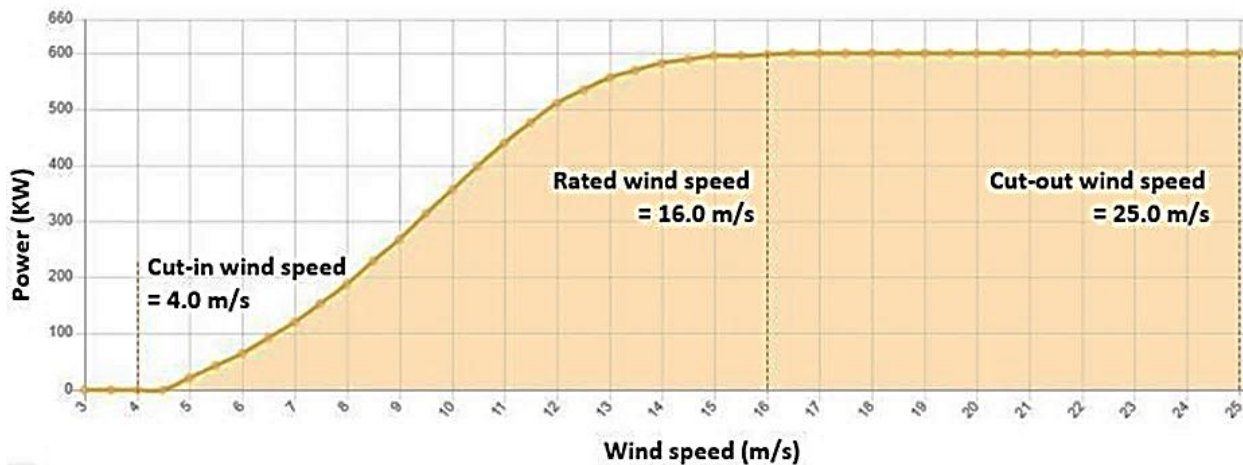


Figure 2-8: The power curve of Vestas V42 WT (600 kW) [67]

2.4 Wind turbine gearbox bearings WTGBs

Bearing is a mechanical component allows one component to rotate with another with minimal resistance. In other words, the bearing transmits the load while reducing friction between the moving parts of the loading machine [68]. Roller bearings have a higher loading capacity than ball bearings because of the greater contact area between the rolling element and the rings so it is utilized in WTGs. In general, two specific types of roller bearings are used WTGs, as follows: -

- 1- **Cylindrical Roller Bearings (CRBs):** They are used when a large radial load should be supported. High carbon alloy steel (EN31) is used for the inner and outer raceways and the rolling components. It is usually heat treated to have a hardness of ~ 700 HV, However, it is expected that the rollers should be harder than the other bearing parts due to concentrated loading on them. According to the number of rows of the rolling elements; CRBs also classified into a single row and double row bearings. The single row is the most common arrangement for a CRB, multiple-row arrangements are also possible and can significantly boost the bearing's capacity to support radial loads. Each bearing row consists of rollers spread around the bearing's circumference regularly by what called a cage. The cage, often made of brass or bronze, keeps the rollers from moving towards each other. In operation, one raceway is fixed, and the other is free to rotate (connected to the shaft) [41]. Four primary parts make up a roller bearing: the outer race, inner race, rolling elements (rollers), and cage, as can be seen in [Figure 2-9](#). The inner raceway is the driven part, typically connected to the shaft by an interference fit. All the elements and the inner and outer ring's contact surfaces have been precision polished to a relatively low grade of roughness.

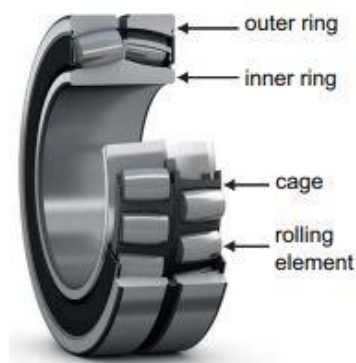


Figure 2-9: A double spherical roller bearing of a wind turbine gearbox [69]

With a little contact area at the bearing race, edge loading can significantly decrease the bearing's lifespan. Crowning the rollers is a standard procedure to avoid damage due to stress concentration at the roller edge and minimize the misalignment, as can be seen in [Figure 2-10](#) [70].

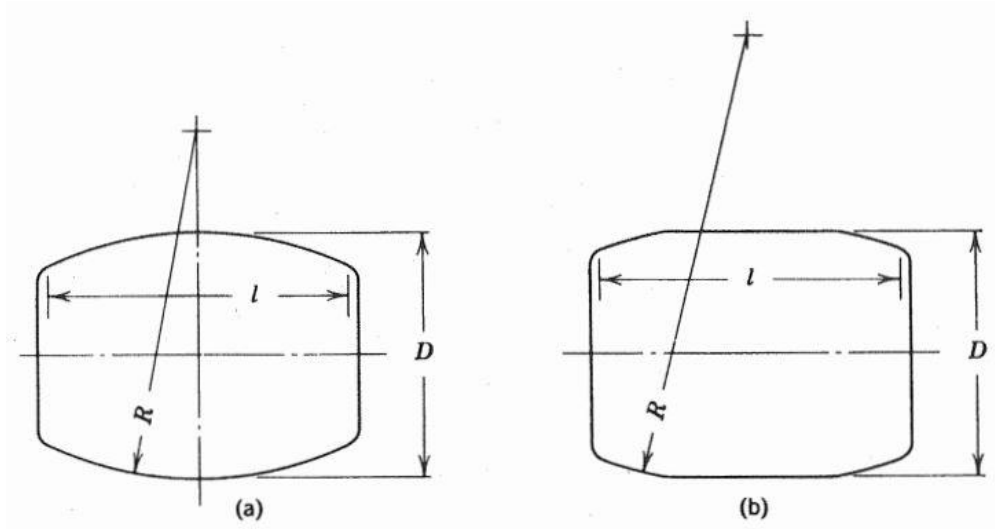


Figure 2-10: (a) fully crowned roller bearing, (b) partially crowned roller bearing [70]

- 2- **Tapered Roller Bearings (TRBs):** They can handle heavy loads in both directions (thrust and radial), in contrast to CRBs, which can only support moderate thrust loading, as can be seen in [Figure 2-11](#) [19]. The inner track is called the cone, and the outer track is called the cup. Because there is an angular gap between the cone and the cup, a force component is generated that compresses the tapered rollers [66]. In terms of clearance and play design, TRBs are entirely deficient. The maximum angle at which the cone or the cup can be positioned is based on the required thrust load support. It is possible to alter the degree of this angle. TRBs are often installed in pairs, with either the bearings facing away from each other (known as back-to-back) or toward each other (known as face-to-face). The TRB bearing cage is typically made of a single piece that cannot be disassembled.

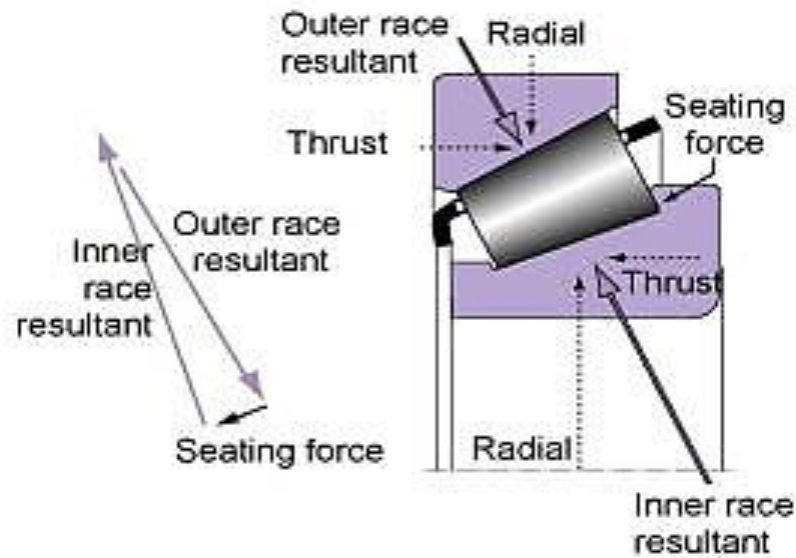


Figure 2-11: The acting forces generated by a tapered roller bearing [66]

The bearings are subjected to challenging conditions because of the many stresses imposed during operation, such as friction, surface deformation, and wear. High loads and debris entrainment can cause excessive clearances in the bearings [71]. One of the most significant problems with roller bearings is stress concentration, which can be caused by a misalignment, debris, roller profile, bending of the shafts carried by the bearings, or skewing of the rollers. This type of stress can be introduced into the contact surfaces of the inner race quite frequently (misalignment of the roller rotating axis from the bearing rotation axis) [46]. The maximum damage usually observed in the loaded zone of the raceway because of slipping occurrence [30][46]. Moreover, the hardness of the inner race is relatively lower than the other parts. This is an essential factor in the raceway surface's severe wear when subjected to abrasive wear on three bodies (roller, inner race, and metallic debris) [72]. As the roller element enters the bearing loading zone, it is subjected to skewing load (deviation of roller centerline from the bearing centerline). This causes a severe loading condition affecting the contact surface and subsurface stresses. Furthermore, inclusions, voids, and defects, which are disadvantages of the material casting process, can also generate a subsurface stress concentration below the contact surface zone [71]. A significant issue for wind turbines is that bearings often fail within 5–20% of their expected lifespans [25]. A more significant price tag for wind energy results from unexpected repairs and premature gearbox bearing replacements. Several factors have been related to bearing degradation, such as corrosion, hydrogen, tensile stress, lack of lubrication, excessive load, and stray currents [25].

2.5 WT monitoring systems

2.5.1 Condition Monitoring Systems (CMS)

Condition Monitoring Systems (CMS) have been introduced by many WT manufacturers. CMS analyzes many operational parameters of WT, such as wind speed, output power, the turbine rotational speed, vibration levels in the drive train, lubricant quality, and temperature [54]. The "add-ons," systems are optionally integrated into the basic WT installation [73]. However, this was done to protect the WT's drivetrain components from being severely damaged. WT monitoring is costly because of the high price of the necessary sensors and the large amount of data that should be acquired and processed [60][74][75]. Accordingly, CMS has not been widely implemented in wind turbines, despite the substantial losses caused by gearbox failures and the many works of literature showing bearing failure as the primary cause [41]. The feature information can be retrieved and uploaded to a cloud storage facility. When the feature data reaches the data center, it can be used to calculate and evaluate the dynamic reliability of wind turbines components in real-time. However, it can use engineering models, hardware, and software equipment, which will drastically cut down the maintenance costs and boost the efficiency of the wind turbine's functions.

2.5.2 SCADA monitoring system

Supervisory Control And Data Acquisition (SCADA) is a conventional condition monitoring system utilized in specific wind turbines [76]. It is the first extensively used monitoring system for wind turbines [41]. Typically, a wind farm's data from each turbine is transmitted to a control center for monitoring purposes. SCADA data can be processed to provide diagnostic and failure-predictive information [77]. The data recorded in the SCADA system performs the average calculations every 10 minutes to determine the wind speed, rotor, and generator speeds, as well as the generator's output power [73][78]. Most operating events take less time than the typical duration of SCADA, which is ten minutes. As a result, the data collected by SCADA are unaffected by of these events. On the other hand, the maximum, the minimum, and the standard deviation are frequently recorded. However, this data predicts when the bearings may fail. Thus, the gearbox maintenance can be scheduled. SCADA data quality is often compromised by lowering the number of parameters measured or the sample period due to the significant number of measurement channels and the resulting enormous data size [79]. Turbines may use different SCADA systems,

which could impede efforts to standardize data processing [80]. Despite these shortcomings, the SCADA system is an invaluable source of information regarding the operating and loading conditions of the drivetrain. Several methods can be used to utilize SCADA data for CMS of WTs, such as: trending, clustering, modeling normal behavior, modeling damage, assessing alarms and expert systems, and other applications [73]. Zhu and Li [15] illustrated that SCADA and CMS are separate systems but are not validated by each other. As a result, combining two test data sets based on SCADA and CMS is beneficial. With the same conceptual direction, Feng et al. [33] postulated that integrating the two systems is a future direction for the wind industry to monitor, diagnose, and forecast gearbox failure.

2.6 Steel material of WTGBs

Bearing steels require a good fatigue endurance against alternate shear stresses, resistance to wear, a high elastic limit to avoid excessive deformation during load, and adequate dimensional stability to withstand the thermomechanical loads subjected to in-service [8][19][81]. The most common steel grade used in manufacturing WTGBs is (100Cr6). It has the following equivalent grades referring to the American Iron and Steel Institute (AISI): 52100, EN31, & JIS-SUJ2). There are other grades that are used in the manufacturing of WTGBs, such as 100CrMo7 & 100CrMn6 [45][46][71]. Bearing raceway and rolling parts commonly use the same steel with a few changes in steel hardness. Recent research shows that rolling elements should be twice harder the other components to reduce rolling contact fatigue life [29][82][83]. Bhadeshia [45] showed the similarity in the composition of the two common bearing steel types, AISI52100 and 100CrMn6 with other more details about various bearing steel compositions as illustrated in [Table 2-2](#) and [Appendix B 1](#).

Table 2-2: Chemical compositions of 100 Cr6 & AISI 52100 bearing steel [% weight] [45]

Grade	C	Mn	Si	Cr	Ni	Cu	S	P
100 Cr6	0.90-1.05	0.25-0.45	0.15-0.35	1.40-1.65	≤0.30	≤0.30	≤0.025	0.03
AISI 52100	0.95-1.1	0.20-0.50	≤0.35	1.30-1.60	-	≤0.025	≤0.025	-

Bearing steel can be rendered martensitic by quenching in oil or salt at a temperature where most of the material is austenite. The martensite is then tempered at a low temperature to balance characteristics in conflict. Typically, small bearings are through-hardened. It means the steels have sufficient hardenability to become martensitic throughout the bearing material depth. In contrast, the surface layer of big bearings should be carburized to form a martensitic case. Alternately, big bearings can be through-hardened by increasing the hardenability of the steel by adding more alloying elements in higher concentrations [45]. Because through-hardened steels have a lower overall cost than other treatments of bearing materials, they are an excellent choice for most bearing applications. Carbo-nitride and case-carburized steels are normally more expensive than through-hardened steels, but they are utilized in situations when the former is not an acceptable alternative [71]. When through-hardened steels include more than 0.8% carbon by weight but less than 5% carbon by weight of total alloying elements, these steels are categorized as being of the (hyper) eutectoid-type. Carburized bearings have low carbon, high nickel, high compressive residual strains, and more retained austenite. Errichello et al. [84] demonstrated that through-hardened bearings are more likely to fail with axial cracks and WEA/WECs, but carburized bearings are not. However, they postulated that through-hardened bearings probably fail due to axial cracks, whereas carburized bearings fail due to macro-pitting. Eventually, they showed it is possible that carburized bearings with at least 20% residual austenite will be immune to irregular White Etching Areas (irWEAs) and will not have premature macro-pitting.

2.6.1 Oxides content influence

Oxides make up most of the oxygen in the solidified steel and are the primary cause of the damage-initiating processes when the steel is under fatigue loading. As a result, the oxygen concentration in current-bearing steels have to be controlled to less than 10 ppmw, unlike many other types of technology. In practice, the oxygen concentration can be measured with an accuracy of about ± 1.5 ppmw [45][85].

2.6.2 Titanium content influence

Titanium is not added to standard-bearing steel 52100. However, it exists in small amounts (about 0.0025 wt%), mostly from ferro-alloys (ferrochromium in particular) or scrap steel used in the steel-making process. It can be made when titanium oxide in the slag is broken down during making basic oxygen steel, especially when much aluminum is dissolved throughout the melting

process. In axially loaded or rotating-bending fatigue experiments, titanium carbides and carbonitrides have been recognized to initiate fatigue cracks. However, there is weak evidence in the context of rolling contact fatigue. LIU Yue et al. [86] postulated that nitrogen concentration should be kept below 10 ppmw to prevent the formation of titanium nitride. Moreover, the identical particle size and position of Ti(C, N) as oxides do not induce butterfly formation Justified by two possible reasons, as follows:

- 1- The strength of the interface between the carbonitride and the matrix, or
- 2- The particles are more resistant to fracture and, thus, are less effective at initiating cracks that propagate into the matrix.

2.6.3 WTGBs material requirements

Many requirements may be described in the WTGBs steel composition and their manufacturing process, as follows:

- 1- Strength and toughness properties:** When chromium steel hardened with martensite heat treatment, it can achieve various engineering qualities. The same hardness values can be achieved by varying the austenitizing and tempering temperatures. The contour chart's hardness lines are demonstrated in [Figure 2-12](#). Bearings with tiny, retained austenite content are required for dimensional stability, as can be seen in [Figure 2-13](#). They cannot be austenitized at temperatures higher than those required for their high-tempering temperatures. It is important to understand these interrelationships, some of which contradict one another so that bearing performance characteristics can be optimized. Hardness alone will not maximize a rolling bearing's fatigue life. Between 58 and 65 HRC, hardness has minimal impact on durability. Fatigue resistance is most vital in high plastic deformation resistance materials. An alternative to cyclic yield strength for high-strength steels is the micro-strain yield limit, often known as elasticity. During the initial stages of fatigue, plastic deformation can occur. However, this can be avoided if the material has a high cycle strength. Plastic deformability shows how well a material can bend and stretch without breaking. Optimizations of the raw material, the heat treatment parameters, and the final properties of the bearing material are complicated because fatigue processes may occur in a messy, homogeneous material matrix.

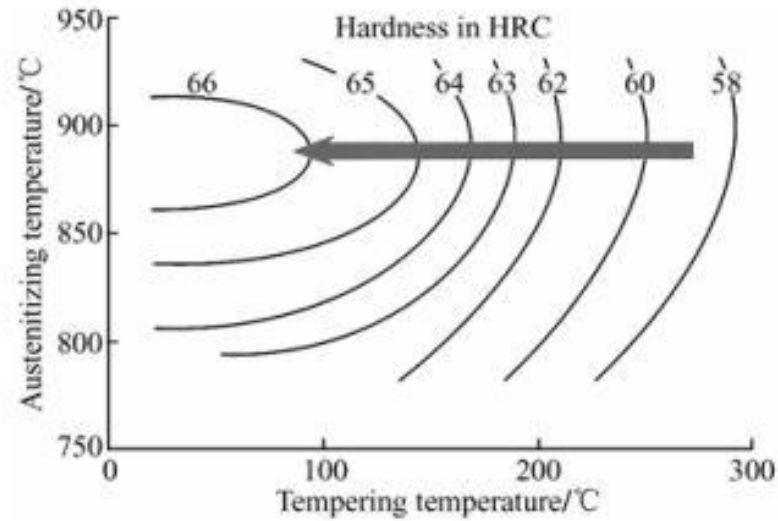


Figure 2-12: Hardness vs. heat treatment for 100Cr6 steel [87]

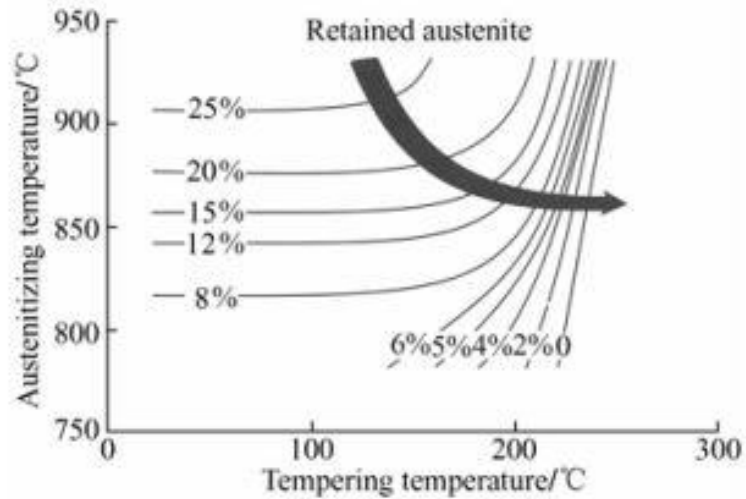


Figure 2-13: Retained austenite vs. heat treatment for 100Cr6 steel [87]

2- Residual stress: This factor has a favorable impact on the component's strength and life expectancy. Local structural transformation and residual-stress pattern alterations occur when steel is over-rolled under contact stresses [88][89]. Tensile residual stress promotes crack initiation and propagation in the rolling contact body subsurface, while compressive residual stress reduces it [89]. According to A. Olver [90], hoop and tensile stresses can

cause vertical crack growth, but compressive residual stresses in the zone between 0 and 0.5 mm below the contact surface could prevent crack propagation.

- 3- Rolling bearings' dimension stability:** If the components in rolling contact alter their dimensions while being used, any effort to reduce the amount of stress caused by the design or lubrication will be for naught. Numerous reasons, such as a weakened press fit, changed clearances or decreased preload, might lead to premature bearing failure. Because hardened rolling-bearing steel keeps both austenite and martensite, the change between the two phases can make the size of the material unstable. Because of temperature and time, volume growth is inhibited by increasing the martensite carbide precipitation and promoted by increased austenite retention. The combined result of these two operations completely changes the component's dimensions. Tensile stresses, which are produced, for instance, by a tight press fit on the shaft, help dimensions grow. In addition, compressive tensions force dimensional change in the direction of the absence of compressive stresses while stabilizing retained austenite.

2.7 The manufacturing and heat treatment processes of WTGBs

2.7.1 The heat treatment process of WTGBs

Austenitization, quenching, and tempering are the three processes should be applied throughout the manufacturing process for WTGBs steel as follows:

- 1- Austenitization process: the plain carbon steel is heated to around 850 °C for approximately 15 minutes. This causes the steel to transform from Body-Centered-Cubic (BCC) ferrite structure to a Face-Centered-Cubic (FCC) crystal structure in a solid solution, which results in the formation of austenite. Iron carbide (Fe_3C) so-called “cementite”. This is dissolved for low levels as the high percentage has a negative effect on the bearing fatigue life.
- 2- Quenching process: the material is rapidly quenched in water or oil baths to a temperature where martensite with a structure of Body-Centered Tetragonal (BCT), which forms in a supersaturated solid solution. At 723 °C, the carbon level is higher than the solubility limit in ferrite, which is 0.02 wt.%. In its current state, martensitic plain-carbon steel is extremely

hard, and brittle. Thus, its usefulness is constrained by its sensitivity toward minor material faults.

- 3- Tempering process: it gives the material the required hardness and decreases brittleness. The already-quenched martensite is heated to precise temperatures during the tempering process and kept for predetermined period of time. Although it is common practice to separate the process into distinct temperature stages, it is vital to keep in mind that there is an overlap between the sequential stages that are physically adjacent to reach others [81][91]. 100Cr6 steel's microstructure is hardened and toughened by tempering at 180 °C for 1-2 hours to has a hardness of (60 HRC). Through-hardened bearing steels like AISI 52100 are typically tempered between 160 °C and 200 °C. Considering the oil flash temperature is higher, it should be higher than the maximum operating temperature (90 °C) [8][45][46][71].

2.7.2 Surface modification of 52100 steel

Surface-modified bearings are frequently used in the automotive industry or for extremely large bearings having diameters greater than 3 meters when through-hardening is not an option [92]. 52100 steel undergoes laser treatment with a surface hardness of more than 1000 HV. When the laser conditions are applied, surface melting occurs, a mixture of ledeburite eutectic, significant amounts of retained austenite, and martensite are created. However, this mixture is not considered ideal in terms of rolling contact fatigue issue [93][94]. The addition of nitrogen to the surface of 52100 steel increases its hardness and introduces compressive residual stress, which penetrates several micrometers [92][95]. The resistant behavior of friction and wear is changed when titanium is implanted to a depth of about 0.1 μm. Carburizing introduces compressive residual stress of about 200-300 MPa on the surface, which improves fatigue performance [92]. Despite the need for extensive grinding on the bearing surface following heat treatment, the typical hardening depth is less than 1 mm.

2.7.3 Grinding vs. turning

Grinding is more efficient than hard turning in capital investment, output, and pollution reduction. It may create a wider variety of high-precision components with superior surface integrity, such as ball bearings and gears. Despite having many advantages over the more expensive grinding method, hard turning is still in its infancy in the industrial use. However, hard

turning has a downside of forming white layers in the finished product's and the surface's integrity [96]. Hard turning has been economically, environmentally, and technologically competitive since the late 1970s. Surface roughness, micro-hardness, microstructure, residual stresses, etc., characterize machining-induced surface integrity. At the same time, machined components' surface integrity affects fatigue life, especially in rolling contact. Hard turning can provide advantageous surface integrity, such as a deep "surface" compressive residual stress, which may extend a component's fatigue life [97]. AISI 52100 grade steel can be treated by plasma-immersion ion injection to harden its surface to a depth of around 40 μm . However, the steel should be heated to 500 °C for at least 3–5 hours to attain this hardness. Iron nitrides rather than chromium nitrides were found to be responsible for the increase in surface hardness [98].

2.8 Rolling Contact Fatigue (RCF)

Rolling Contact Fatigue (RCF) is a form of fatigue damage characterized by the initiation of surface and/or subsurface cracks under sliding and rolling contact conditions of two bodies. It occurs because of alternating localized contact stresses that induces a plastic deformation at the contact region. Components of tribo-machinery, such as rail-wheel contacts, gears, bearings, cam-followers, etc., frequently break due to rolling contact fatigue [5][99][100][101]. In bearings, the repeated stresses induced in the contacts between the rolling elements and the raceways are causing rolling contact fatigue. RCF differs from other forms of classical fatigue, for example unlike bending or uniaxial (tensile or compressive) wear, which can result from a considerable tensile stress component, RCF is produced by a complicated state of stresses. RCF initiates microcracks in or around the non-metallic inclusions of the bearing subsurface region, which then spread as flaking (removing of material pieces from the contact surface), leading to failure in WTGBs [102]. By introducing an appropriate amount of lubrication between the contact surfaces, spalling and pitting can be effectively reduced [103].

2.8.1 Mechanism of RCF damage

RCF damage was hypothesized to manifest in two categories: surface-originated pitting and subsurface-originated spalling [104].

- 1- Surface-originated pitting: This hypothesis suggests the cracks start at the contact surface, travel through the material, shift their orientation, and head back toward the contact surface. A piece of material may be removed from the surface that is in contact within the contact region [105][106]. In other words, micropitting and flaking can be formed on a surface due to asperity contact or surface defects [71]. Damage of contact surfaces probably occurs because of surface distresses on the surface of the contacting bodies, such as pits, fretting scars, etc. [104].
- 2- Subsurface-originated spalling: a subsurface fracture is induced because of shear stress. The crack propagates toward the contact surface in various directions, and the material may flake when the cracking reaches the contact surface [101][107]. It means that the subsurface shear stresses created by rolling contact probably lead to the development of cracks, which then propagated to the surface and caused spalling [71]. Rolling element bearings are thought to fail primarily due to subsurface material fatigue, such as cracks initiation, if the bearings are correctly loaded, lubricated, mounted, and aligned; otherwise, the surface initiation mechanism is the most likely to take place [100]. Furthermore, if the contact surfaces of the bodies are relatively smooth, subsurface-originated spalling is the primary contributor due to RCF [104]. RCF has six specific distinct manifestations [90]:

- 1- Subsurface initiation (spalling) [45][108],
- 2- Subcase fatigue (case crushing),
- 3- Surface initiation (pitting),
- 4- Localized stress concentration, such as (roller ends),
- 5- Micropitting (Peeling), and
- 6- Section fracture.

The term "debris" is significantly fragmented due to bearing flaking produced by micropitting or flaking. It can boost RCF and have a more detrimental effect on hastened development of severe damage. Large debris may cause localized severe stress levels, vibrations, and impact loading between the contact surfaces. This will eventually reduce bearing lifespan [109][110][111]. Jalalahmadi et al. [102] found that as the defect density and size of the inclusion increased, the

RCF life significantly decreased. On the other hand, location and orientation of the damage initiation are significant in fatigue life. E. Kerscher [112] suggested raising the bearing steel's static strength and hardness to increase the fatigue limit. He associated this idea with the microstructure of the bearing steel. Bearings with favorable clearance showed a gradual decrease in fatigue life when tested by Oswald et al. [113]. In contrast, bearings with negative clearance showed a potentially rapid decrease in bearing life.

2.8.2 Hertzian Contact Theory

In 1896, Hertz developed his theory to describe the form and size of the contact surface and the induced stresses distribution. He assumed that under the elastic loading condition, isotropic, homogenous and normal compressed bodies with no traction (perfect smooth contact) and a relatively small contact width, the contact pressure distribution seems elliptical, as can be seen in [Figure 2-14](#). Accordingly, it is possible by using Hertzian theory to calculate the following parameters: maximum shear, orthogonal shear, Von-Mises stress, and octahedral shear stress based on consideration. Hertzian contact generates cyclic stress when a curved or flat surface rolls over another curved or flat surface under an average load. The stress distribution due to Hertzian contact is distinct from structural fatigue of bending or torsion. Instead of a point or line of contact, Hertz reasoned, a limited contact area should form, spreading the load out over the surface and avoiding the infinite stress that would result from the point of contact [71]. Some significant characteristics governing RCF include geometry, contact pressure, and the material's mechanical properties, may be predicted by applying the Hertzian theory to the stresses encountered by the bearing during dry contact [114]. The Hertzian theory is relevant for somewhat accurate determination of contact pressure in bearings and subsurface stresses even when the contact surfaces of rolling element bearings are not perfectly smooth and lubricated [90]. Lai and Stadler [115] concluded that when a bearing's seat deviates from its ideal shape by more than a predetermined amount, it can weaken the material, leading to the initiation and rapid growth of cracks and, ultimately, the bearing's failure. They found that Hertzian contact and bulk tensile stress cause shear stress, which initiates cracks in an axial direction.

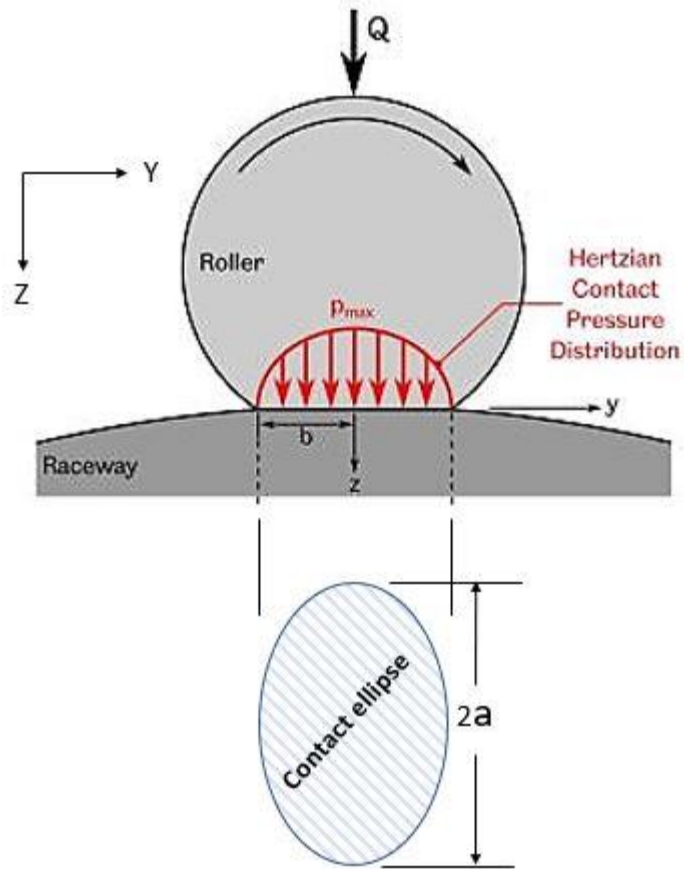


Figure 2-14: Hertzian Contact Pressure Distribution for roller and inner raceway of a bearing [the researcher]

The following equations are used to describe the Hertzian theory:

$$b = \sqrt{\frac{4QR^*}{L\pi E^*}} \quad (2-1)$$

$$\frac{1}{R^*} = \frac{1}{R_1} + \frac{1}{R_2} \quad (2-2)$$

$$\frac{1}{E^*} = \frac{1 - \nu_1^2}{E_1} + \frac{1 - \nu_2^2}{E_2} \quad (2-3)$$

$$p_{max} = \frac{2Q}{L\pi b} \quad (2-4)$$

where

b : half of the contact width,

Q : the normal applied load to the contact surface,

R^* : equivalent reduced radius,

R_1 : radius of the roller,

R_2 : radius of the raceway,

E^* : equivalent modulus of elasticity,

E_1 : modulus of elasticity of the roller,

E_2 : modulus of elasticity of the raceway,

ν_1 : Poisson's Ratio of the roller,

ν_2 : Poisson's Ratio of the raceway,

p_{max} : maximum pressure distributed across the width of the contact,

L : contact length.

Figure 2-15 depicts the cartesian stress and shear stress induced in the material's subsurface as the Hertzian loading travels over it. The following symbols σ_x , σ_y , σ_z , and τ_{xz} describe the cartesian normal contact and shear stresses respectively. Subsurface stress components are measured on a vertical axis normalized to maximum Hertzian pressure, while x shows the location of the center of Hertzian contact (in x -direction) relative to the point of contact pressure. The distance is measured at half of the contact width and then normalized. With little surface traction, the over-rolling direction moves to the direction of the traction. Shear stress is the only type of stress whose value goes from positive to negative and back again. Because of this, RCF is often called a shear-driven phenomenon. It is important to note that in RCF the heavily stressed area of the material is usually only a few hundred microns deep. For that, fatigue takes place on a scale like the size of the material's grains, and the way of the material wears down is very sensitive to material's microstructure [99].

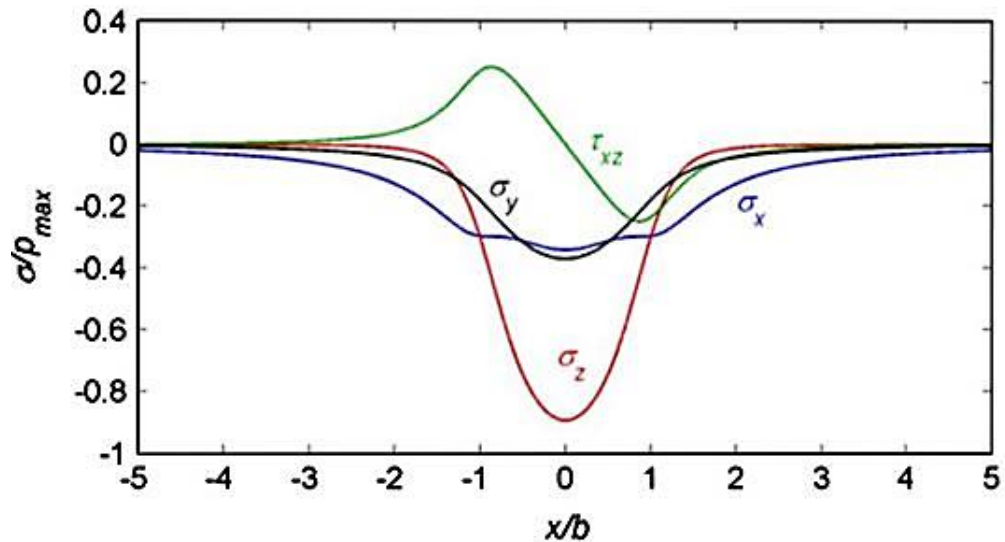


Figure 2-15: Cartesian stresses (normal and shear stresses) under RCF [99]

Stressed volume, alternating shear stress, and the number and depth of stress repeats and the residual stresses affect the bearing's life [116]. Von-Mises equivalent stress, which reflects the triaxial stress field during rolling contact, is locally more significant than the yield strength of the material, in addition, a micro deformation occurs. A common feature of bearing rolling contact fatigue (RCF) is a subsurface cracking, which can progress to spalling. There has been a correlation between RCF and the change from the austenitic phase to the martensitic phase. Microplastic deformation accumulates in the region of the highest shear stresses below the surface, where this transformation has been shown to reach its peak [100]. Under rolling contact, a Dark Etching Regions (DERs) have been observed with creating globular and elongated grains in the zone with the highest shear stresses. Low Angle Bands (LABs) and High Angle Bands (HABs) of ferrite were found in the martensitic matrix during the (RCF). An increase in rolling surface hardness and spalling is typically noticed in conjunction with developing these white bands on the rolling surface [286].

2.8.3 Stress distribution

The primary stressor in rolling contact is the Hertzian contact pressure distributed in a semi-elliptical at the elastic contact zone. For a rolling contact zone, the stress is a function of the direction and magnitude of the stresses underneath the contact areas. Figure 2-16 depicts Von-Mises stress as a three-dimensional diagram and a contour diagram. By using the small semi-axis

b of the contact area, $Y = y/b$ (horizontal normalized distance from contact center) and $Z = z/b$ (normalized depth below the contact surface). This graph shows the equivalent stress is a function of the contact pressure p_0 .

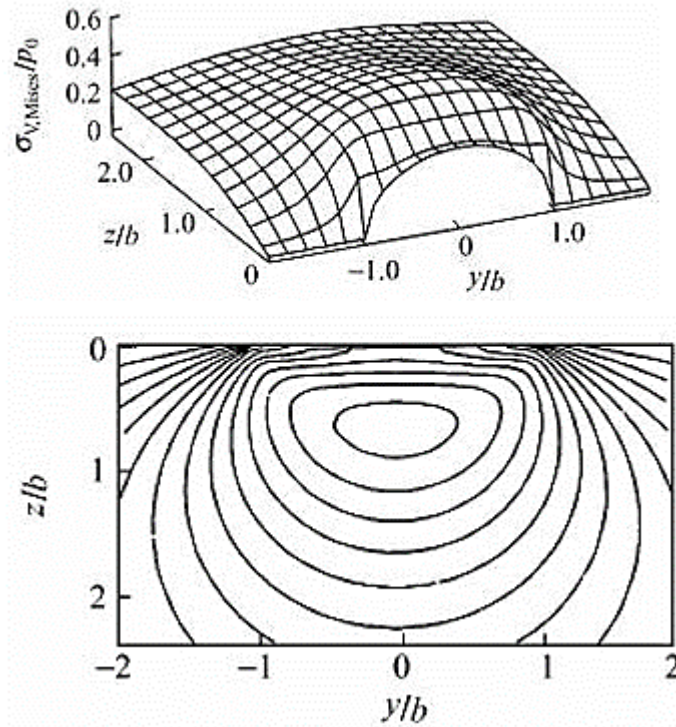


Figure 2-16: Distribution of equivalent stress beneath the contact region [87]

Starting from the contact area center ($y = 0$), the equivalent and principal stress in the material can be seen in [Figure 2-17](#). The equivalent stress is relatively low because two significant surface stresses have converged to the same magnitude. Wherever the gaps between the three principal stresses are the widest, that is where the equivalent stress is at its highest. Even when the bearings are operating under optimum Elastohydrodynamic EHD circumstances and, as a result, have a very low coefficient of friction within the rolling contact region, the damage will often begin close to or at the contact surface [87]. This will be discussed in more details in the following section

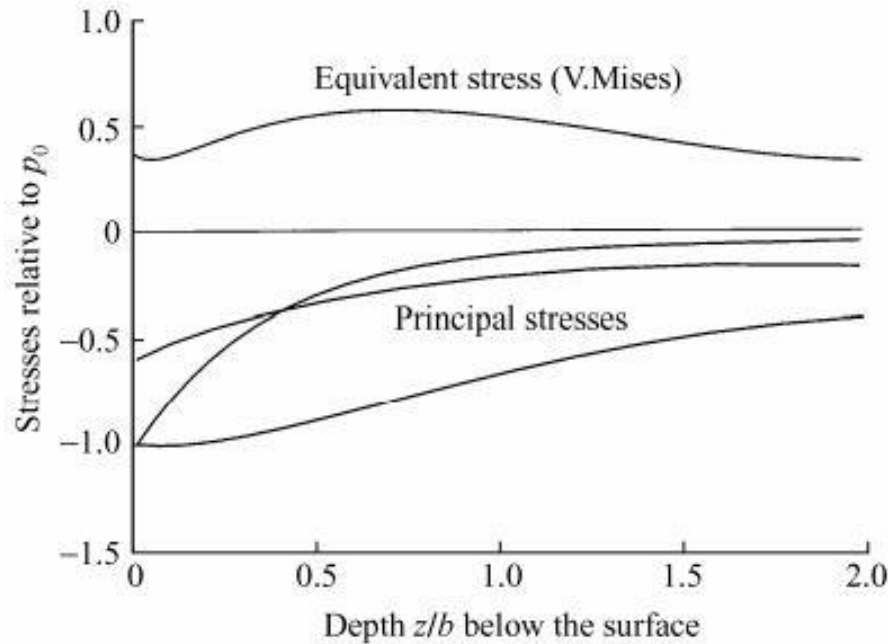


Figure 2-17: Normalized principal and equivalent stress beneath the contact area centre [87]

2.8.4 Lubrication effect in rolling contact

Lubrication is required for rolling element bearings to function properly so that the contact surfaces can remain separated while the bearing is in motion. Lubricating bearings and gears of a wind turbine unit require a recirculating system that controls lubricant temperature and removes debris. Lubricant quantity, type, and cleanliness are three crucial aspects that should be considered in the design of WT and the operation phases. Such lubricant films can be as thin as a few nanometers or as thick as hundreds of microns. One of the essential features of a lubricant is its viscosity, which shows how much it slows down motion. More remarkable load-carrying ability is achieved at greater viscosities. The viscosity of a fluid, on the other hand, varies not just with pressure but also with temperature. Various design and production options can be considered when introducing external loads into the rolling contact elements under different operating conditions of speed, kind of lubrication, and amount of lubricant to minimize the contact stresses. Wind turbine drivetrains should endure several harsh operating situations while functioning normally. These include high loads and unstable conditions like torque reversals and grid failure. However, this can lead to a breakdown in the lubricating layer, increasing the friction loss and the risks of bearing and gear failure. The same lubricant is used for gears and bearings of type ISO VG-320 [8]. The oil flash temperatures for wind turbine gearboxes ought to be much higher than the average

working temperatures, which are limited to a maximum of 90° [71]. Martins et al. [47] revealed that in the case of the thinner lubricating layer, the higher the coefficient of friction, the higher the lubricant temperature, and eventually, the frequent rolling pressure leads to surface failure. Furthermore, low operational loads, such as those experienced when wind turbines are idling, can cause slippage damage [61]. [Figure 2-18](#) shows four primary cases for the contact of rolling element in the following details [87].

- 1- Elastohydrodynamic lubrication (EHL or EHD):** it is a form of film lubrication in which the contacting surfaces undergo elastic deformations of at least the same magnitude as the film thickness separating them due to the extraordinarily high contact pressure. EHL ensures that there is no direct metal-on-metal contact [71]. Cams, gears, and bearings have elastohydrodynamic lubrication [97][117]. The appropriate coordination of bearing load, speed, lubricant viscosity, and surface quality of the contact areas produces a load-carrying lubricating film between rolling contact parts that are entirely separated. Normal loads are transferred under optimal elastohydrodynamic lubrication conditions that can achieve the longest possible lifespans [87]. Hanwei Fu et al. [118] postulated that EHD could theoretically remove the induced surface RCF and the adequately lubricated bearings while RCF caused by the subsurface region becomes the dominant.
- 2- Mixed friction:** if the load-carrying by the lubricating film is not built-up during operation, the roughness peaks in the contact areas will rub against each other's. There are many reasons behind the occurrence of the (mixed friction) case, such as the lubricant used in the stationary bearing isn't the suitable one or when the bearing starts and stops even if it's operating under EHD circumstances in a steady state.
- 3- Wear:** the lubricating conditions deteriorate, resulting in solid body friction in dry conditions. Rolling contact elements are damaged and rendered inoperative under these conditions, but they are unusual. Protective coatings or reaction layers created by additives and suitable lubricants are used when short lubrication breakdowns occur, even though this is an abnormal operating condition.
- 4- Particles in contact area:** dry friction is much less likely to happen than contaminants in the lubricating gap or foreign particles in the contact area. Mineral particles (such as mold sand or grit) or metal particles can contaminate the lubricant such as (chips, grinding dust, and abraded material). In the same way, their hardnesses range from (very soft) to

(extremely hard), just like the harnesses of the rolling elements. The particles also can be generated in many different sizes, shapes, and places. When foreign particles enter the contact area of a bearing, they leave marks (indentations) on the contact surfaces. The indentation's edge breaks the lubrication coating, causing a state of mixed friction, and the fabric around the indentation is plastically deformed and work hardened. Favorable residual stresses from heat treatment (and/or) machining are greatly disturbed. The bearing service life might be drastically reduced because of this surface damage. The more indentations in the rolling contact area are generated by bigger particles, the shorter the life expectancy. Cycled particles can act as a cutting tool and wear down the mating part if they embedded in the surface of the rolling contact components.

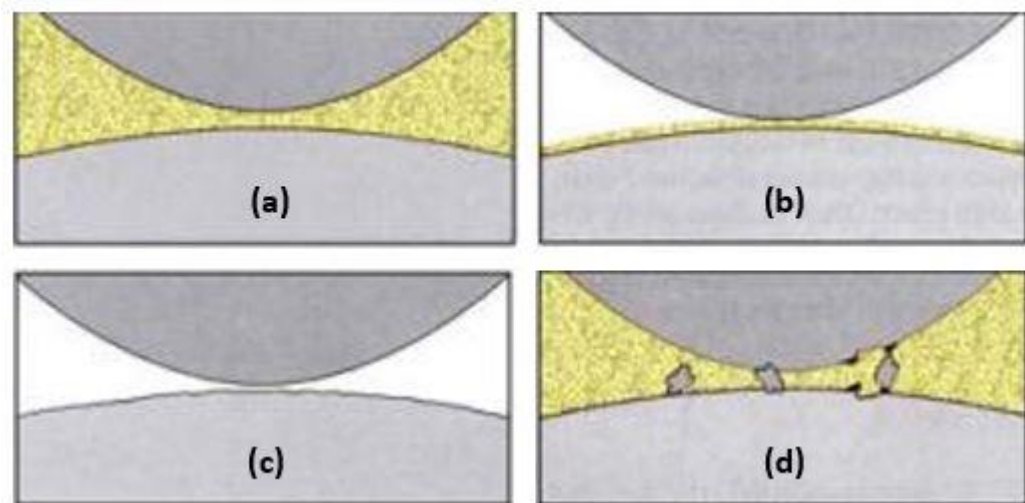


Figure 2-18: (a) Elastohydrodynamic lubrication, (b) mixed friction, (c) wear, (d) particles between the contact surfaces [87]

2.8.5 Slipping effect on bearing damage

Slipping occurs when there is a relative motion between two bodies in contact with each other. High speeds, torque reversals, drivetrain acceleration or deceleration, misalignment, transient loading, the differences in speeds between roller and raceway (low at the beginning of motion versus high in the final speed), etc., are all operational situations can lead to the bearing slipping. Slipping can cause damage to a material's features, leading to accelerating the fatigue failure process and reducing the material's fatigue life [51]. Slipping and rolling contact with the lubricant helps to open up the crack mouth i.e., increase the distance between the separated sides

of the crack, and making the penetration more effective. When a penetration occurs, the resulting periodic and large pressure pulses at the crack face play an essential role in fracture progression. The frequency of the pressure pulses, and the operating conditions, would directly affect the likelihood of failure [119]. On the other hand, the roller moves in the bearing loaded and unloaded zones, leading to changes the friction levels between the roller and its raceway, unbalancing, skewing, and slipping. The stress distribution on the contact surface and subsurface should be considered since the contact load increases the size of the loading zone. When rollers leave and enter the load zone at various rates, they accelerate and decelerate at different periods, leading to roller slipping [64]. If the bearing is still not preloaded, the load zone will have the shape of an ellipse, as can be seen in [Figure 2-19](#). When the torque is reversed, there is a shift in the load zone. Because of this change, the rollers may be subjected to more significant acceleration and deceleration, resulting in roller slipping. As a result, tapered roller bearings (as preloaded) are utilized in the design of today's wind turbine gearboxes [120]. This design intends for the loaded zone to be focused across the entire bearing's diameter, meaning that it will reach across all the rollers and take on a nearly circular form. However, if the loads are more than the preload during the torque reversal, then the load zone will revert to its more conventional circular shape. The rate of slippage in a roller bearing rises with torque reversal and transient loading because of the accelerating and decelerating of the rolling sections [121]. Helsén et al. [64] demonstrated that a tapered roller bearing's preloading could be exceeded during torque changes if the roller slips, which can happen under severe loading conditions. Typically, the slip characteristics affect topography, the initiation, and the propagation of the microcrack [122]. Slipping is always stated as a slipping ratio ($SR\%$), which is also called the “Slip to Roll Ratio” ($SRR\%$). It can be defined as the ratio of the difference in velocities between the two contact surfaces (ΔU) to the average velocity of them (U_{av}).

$$SR\% = \frac{\Delta U}{U_{av}} \quad (2-5)$$

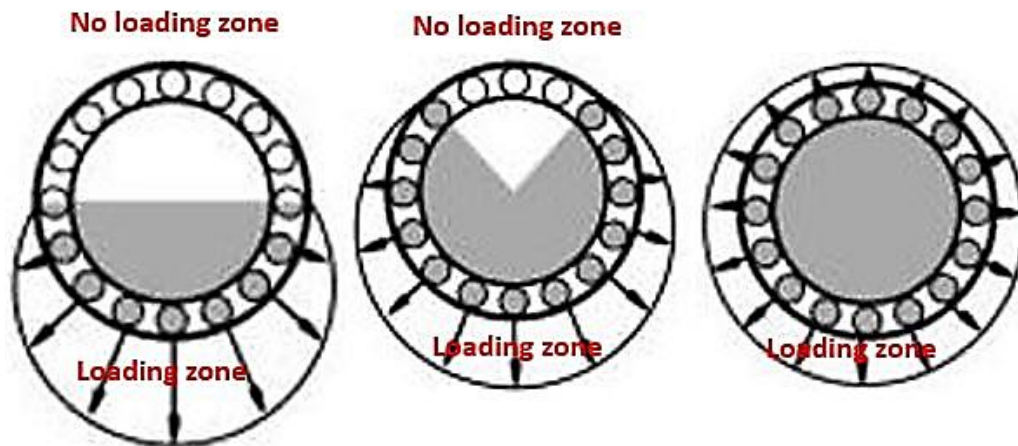


Figure 2-19: Different cases of bearing loading zones – adapted from [23]

Based on the slipping ratio formula, SR has a negative value when the traction force is in the opposite direction of the rolling direction; conversely, SR has a positive value [123]. Bearing SR is affected by a considerable number of variables, such as contact load, lubrication surface roughness, rotational speed, direction, and velocity of the contact surface [46]. Keller et al. [124] predicted the loading level, slipping ratio (SR), and the number of cycles are crucial to initiating WECs. They found that the loading level of 1.9 GPa or more with a high negative SR (-30 %) and at least 30 million cycles at a rolling velocity of 1 m/s are required to form these microstructural alterations. Furthermore, they postulated the Frictional Heat Accumulation (FHA) needed to produce WECs was about 6 MJ. The surface roughness is substantially vital to SR and can modify the contact loading level on the surface asperity, another effect of surface roughness on fatigue life [125][126].

2.9 Rating life prediction of bearing

The bearing's life is the number of revolutions or hours that a bearing is expected to last before the material of the rings or rolling parts shows signs of damage [127]. ISO 281:2007 [128] is the international standard for rating bearings and is usually considered throughout the industry. However, each manufacturer uses unique design life assessments, resulting in significant variations between the estimated and the actual bearing lives.

2.9.1 Lundberg and Palmgren Method

In 1947, Lundberg and Palmgren (LP) developed the first method for estimating bearing lifespan. However, the LP method can only applied to bearings made from AISI 52100 through-hardened steel. They postulated that the fatigue cracking begins at weak areas in the material underneath the rolling contact surfaces. Moreover, the fatigued life would be measured in terms of the number of stress cycles that had to be endured before the first spall, the applied contact stress, and the chance of surviving. The principal formula (2-6) expresses the LP method as follows: -

$$\ln\left(\frac{1}{S}\right) \propto \frac{N^e \tau_o^c V}{z_o^h} \quad (2-6)$$

where

S : survivability probability (usually used as 90%),

N : number of enduring stress cycles,

τ_o : maximum shear stress at the depth z_o ,

z_o : the depth below the surface to where τ_o is located,

V : Hertzian stressed volume,

e : Weibull exponent (a statistical indicator),

c & h : Experimental exponents.

The following primary equations (2-7)&(2-8) were developed from the LP theory and derived from the principal formula. This developing formula has been used as standard in the industry for the estimating of theoretical bearing rating life [49]. The rating life (L_{10}) can be defined as the number of million revolutions of the testing bearings at which 10% of these bearings showing up the first signs of surface spall as an indicator of failure. In other words, the LP method assumes 90% survivability under identical loading and operating conditions. Hertzian contact theory is usually used in calculating bearing life since the maximum orthogonal shear stress is induced in the bearing material. L_{10} relates the bearing fatigue life to the load that was applied to estimate the rating life of radial and axial bearings respectively as follows:

$$L_{10} = \left(\frac{C_r}{P_r} \right)^n 10^6 \quad (2-7)$$

$$L_{10} = \left(\frac{C_a}{P_a} \right)^n 10^6 \quad (2-8)$$

where

L_{10} : Bearing rating life (in millions of revolutions),

C_r & C_a : Radial and axial basic dynamic load ratings respectively (in Newtons),

P_r & P_a : Radial and axial equivalent dynamic load ratings respectively (in Newtons), and

n : The load life exponent, ($n= 10/3$ for roller bearings and $n=3$ for ball bearings).

The LP method depends on constant and radial loading, so adjustment factors have been introduced to make more accurate for diverse operating situations [129][130]. WTGBs fail in the first 20% of the theoretical L_{10} life. Accordingly, the LP method does not match the actual bearing life and requires more developments to estimate the bearing life accurately. In 2007, a revision was made to ISO 281, the worldwide standard using for calculating the bearing lifetime. The modification added a new coefficient, denoted by " a_{ISO} " which considers various factors affecting the bearing's life span, such as the fatigue limit load, the lubrication conditions, and the contaminants in the lubricating oil, as illustrated in equation (2-9) [44].

$$L_{nmh} = a_{ISO} \times \frac{10^6}{60N} \left(\frac{C}{P} \right)^n \quad (2-9)$$

where

L_{nmh} : Bearing life based on the number of hours

a_{ISO} : life correction coefficient

C : Basic load rating (N)

P : Dynamic equivalent load (N)

N : Rotating speed (min^{-1})

Specific software has considered a wide range of factors in the calculation of the bearing life, such as the shaft displacement and the rigidity of the housing, in addition to the bearing internal clearance and the fatigue limit of the shaft system [44]. Takemura et al. [131] developed another advanced bearing life equation (2-10), which incorporating a life modification factor a_{nsk} (based

on data from bearing life tests). By applying the equation, they showed that the theoretical bearing life was consistent with the empirical one.

$$L_{able} = a_1 a_{NSK} L_{10} \quad (2-10)$$

where

L_{able} : Advanced bearing life,

a_1 : The modification factor for reliability,

a_{NSK} : Life modification factor.

The life modification coefficient is a function of two factors: lubricant parameter (a_L) and the load factor $[(P-P_u)/C]$, as illustrated in the [formula \(2-11\)](#). Experimentally, [\(Appendices C 1&C 2\)](#) illustrate the lubricant viscosity ratio (k), since it usually considered as an important factor. Firstly, it has to calculate the value $(P-P_u)/C \times 1/a_c$, then using an appropriate life curve (ball/roller) bearing to find (a_{NSK}) and apply the advanced bearing life equation, as can be seen in [Figure 2-20](#).

$$a_{NSK} \propto F \left(a_L, \left(\frac{P - P_u}{C \cdot a_c} \right) \right) \quad (2-11)$$

where

P : The actual bearing load,

P_u : The fatigue load limit (in which the bearing will last for more than 10^{11} revolutions before failing),

a_L : Lubricant parameter,

a_c : The contamination factor, and

k : The lubricant viscosity ratio.

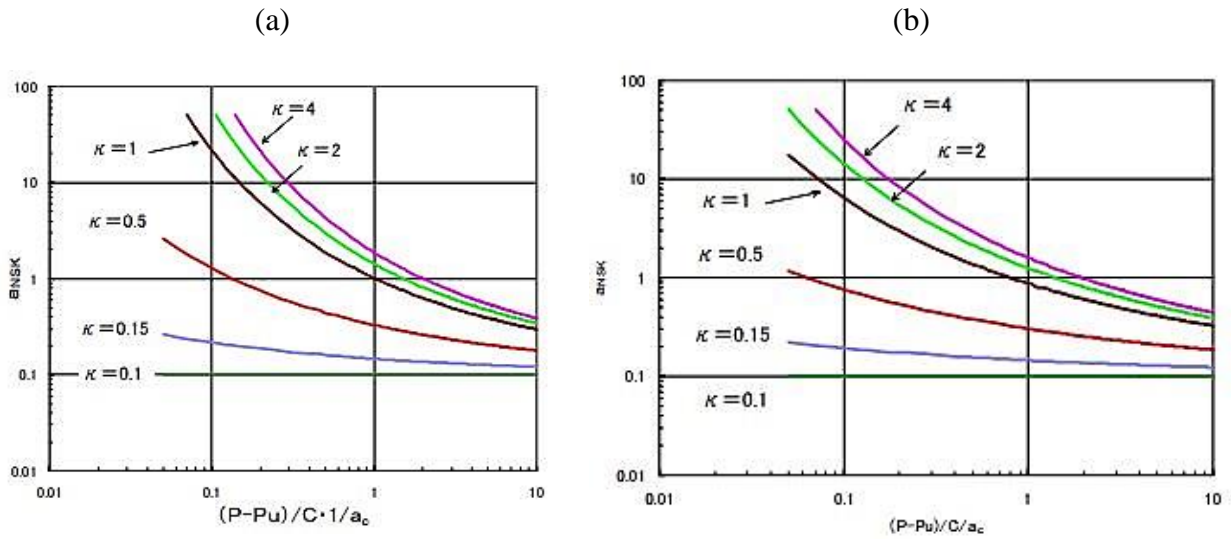


Figure 2-20: Bearing life curves (a) for ball bearing, (b) for roller bearing [131]

3

CHAPTER THREE: MICROSTRUCTURE ALTERATIONS AND FAILURE MODES

This Chapter discusses the more related topics of the study to be matched with the specific items of the experimental and simulation thesis works. It reveals the ambiguity and the overlapping of many scientific concepts and creates fundamental pillars of knowledge for analyzing the investigation results more accurately. Three subtitles are overviewed in this Chapter as follows: -

- 1- Non-metallic inclusions, their stresses, types, damage drivers, aspects, their relationship to the cleanliness of steel, and voids,
- 2- Microstructure alteration, and
- 3- The main related failure modes.

3.1 Non-metallic inclusions (NMIs)

Non-metallic inclusions (NMIs) are those compounds that form when metals combine with non-metals such as oxides, sulfides, and nitrides. However, there are other complicated species, such as oxysulphides and carbonitrides [132]. Many different components are utilized throughout the manufacturing process to facilitate the procedure and the subsequent machining process. These elements have the potential to form non-metallic inclusions (NMIs) in steel by combining with

other elements [71]. Depending on the manufacturing process, the NMIs may be separated into bands or sections within the steel or distributed through the material bulk. The heat treatment and manufacturing process can affect the inclusion's cohesion with the steel material [5]. Herring [133] reported that the admixture dissolubility of the steel matrix decreases during the cooling and the consolidation. Despite their modest volume proportion, NMIs have a significant impact on the characteristics of steels. Murakami [134] proposed that cracks initiate in rolling contact fatigue (RCF) from inclusions in the subsurface contact region. A critical role is played by NMIs in ductile fracture, fatigue, and corrosion processes. NMIs are oriented in a specific direction in the bearing bulk material during the steel casting process [135]. It is essential to control the NMIs in the matrix to improve the steel's cleanliness and quality. The steelmaking industry has made substantial process advances over the previous few decades, leading to better control percentage of the inclusion volume, size, and composition. Because NMIs have an influential role in engineering, the phrase “inclusion engineering” has been used extensively in scientific research since the 1980s [136][137][138][139].

The mechanical properties of steel are directly affected by the related properties of non-metallic inclusions, as illustrated in [Table 3-1](#) [140][141]. On the other hands, the brittle bodies in the steel bulk enhance the brittleness and hardness properties of bearing steel by about 30-50% [38][142][143]. Sometimes, WTGBs damage accompanies by microstructural alterations, in which the NMIs act as crack triggers. They have the potential to create another damage mode, called “butterfly,” as seen in [Figure 3-1](#) [99][144]. There are many inclusion standards that have been considered for the assessment requirements of NMIs, such as ASTM E2283, GOST 1778-70, IS4163:2004, ISO 4967:2013 (E), JIS G0555, DIN 50602, and ASTM E45 [145].

Table 3-1: Influence of NMIs on mechanical properties [141]

NMI's element	Existence form	Mechanical Properties
S, O	Sulfide and oxide inclusions	<ul style="list-style-type: none"> • Ductility, Charpy impact value, anisotropy • Formability (elongation, reduction of area and bendability) • Cold forgeability, drawability • Low temperature toughness • Fatigue strength
C, N	Solid solution	• Solid solubility (enhanced), hardenability
	Settled dislocation	• Strain aging (enhanced), ductility and toughness (lowered)
	Pearlite and cementite	• Dispersion (enhanced), ductility and toughness (lowered)
	Carbide and nitride precipitates	<ul style="list-style-type: none"> • Precipitation, grain refining (enhanced), toughness (enhanced) • Embrittlement by intergranular precipitation
P	Solid solution	<ul style="list-style-type: none"> • Solid solubility (enhanced), hardenability (enhanced) • Temper brittleness • Separation, secondary work embrittlement



Figure 3-1: Subsurface butterfly in the inner raceway of a roller bearing [the researcher]

3.1.1 Stress concentration in NMIs

The effects of NMIs on the fatigue life of bearing steel are still up for debate. However, it is undeniable that their size and quantity play a crucial role in how bearings perform under stress concentration. When stress concentration levels around inclusions reach their high values (mostly

at the NMIs' tips), cracks may initiate and propagate in multi-directions on the surface and the subsurface of the bearing contact region, as can be seen in [Figure 3-2](#) [87][135].

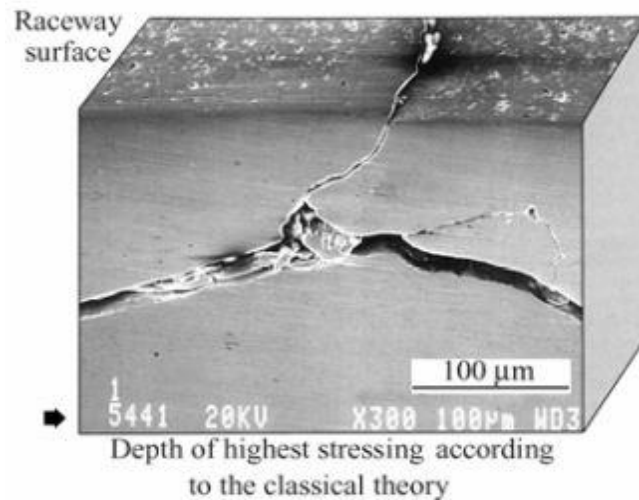


Figure 3-2: Damage propagation resulting from a NMI close to the contact surface [87]

Guan et al. [146] postulated that non-metallic inclusions increase the stress in the bearing steel, and the highest Von-Mises stress concentrates near the inclusion, which makes cracks more likely to be noticeable in the subsurface region. On the other hand, inadequate lubrication can enhance the stress concentrations at the inclusions [52]. The following factors that related to stress concentration should be considered in the analyzing process of the inclusions' effect on fatigue strength [126]:

- 1- Inclusion shape,
- 2- The adherence of inclusions to the matrix,
- 3- The elastic constants of both the inclusions and the matrix, and
- 4- The size of the inclusions.

The inclusion and steel matrix have different thermal expansion coefficients and mechanical properties, for this, the residual stress will be introduced at the interface between the inclusion and the bulk during the heat treatment of the material [12]. Murakami & Beretta [147] demonstrated by using an approach like fracture mechanics, that the fatigue life of a material is inversely proportional to the square root of the inclusion size. Solvano-Alvarez et al. [148] confirmed that the site of the most significant orthogonal shear stress is where the majority of the de-bonding damage (separating the inclusion's material from the bulk) is concentrated.

Ultimately, the de-bonding of NMIs causes bearing fatigue failure. Murakami [12] classified NMIs into three categories based on their location: internal inclusions, inclusions in contact with the surface, and surface inclusions, as depicted in Figure 3-3. An equation for each type has been formulated individually to calculate the fatigue limit at the contact surface, as illustrated in the equations (3-1), (3-2) & (3-3). The test results of the inclusion fatigue tests and their physical properties have been detailed in (Appendices D1&D2). Neishi et al. [149] hypothesized that the RCF life and the onset of shear cracking in the subsurface are directly proportional to the MnS inclusion length projected to the load axis. On the other side, Francesco Manieri et al. [150] implied that white etching cracks (WECs) are not to blame for premature bearing failures, but rather, WECs and bearing failures coincide due to "a specific temporal history of applied contact stress." They mentioned that it would be more practical to study the stress profile under which the affected applications run rather than WECs.

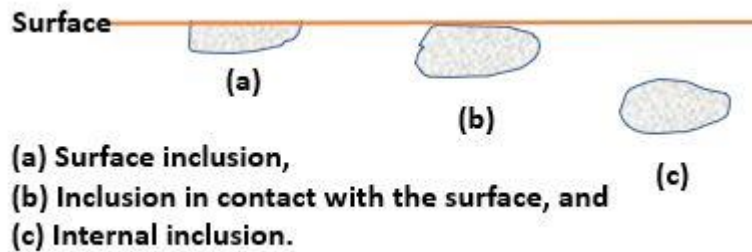


Figure 3-3: Location-based classification of inclusions - adapted from [12]

$$\sigma_w = \frac{1.43(H_V + 120)}{(\sqrt{\text{area}})^{1/6}} \quad (3-1)$$

$$\sigma_w = \frac{1.41(H_V + 120)}{(\sqrt{\text{area}})^{1/6}} \quad (3-2)$$

$$\sigma_w = \frac{1.56(H_V + 120)}{(\sqrt{\text{area}_i})^{1/6}} \quad (3-3)$$

where,

σ_w : Fatigue limit at the surface,

Hv: Vickers hardness,

$\sqrt{\text{area}}$: Inclusion length factor, and

$\sqrt{\text{area}_i}$: length of internal inclusion factor.

3.1.2 Voids formation

Voids are gaps, which appear in the steel bulk as black spots through the microscopic investigations. They formed as a result of heat treatment and manufacturing processes of bearing steel. NMIs may separate from the surrounding bulk material after quenching, providing a free surface at the subsurface inclusion due to their higher thermal contraction rates. Hence, the weak bond between NMIs and the steel matrix help to initiate these voids in the steel matrix, as seen in [Figure 3-4](#). The voids can be observed at the boundary between the steel matrix and the inclusion and in other locations in the subsurface region surrounded by carbide particles. Many researchers [142][143] proposed that extending the lifespan of Rolling Contact Fatigue (RCF) may be occurred by decreasing the oxide's size and voids. As the voids are the softer objects in the steel components, it confirms that damage causative is inherent in the steel material [12]. AL-Bedhany [5] considered these voids as one of the important crack initiation sources in addition to the crack initiation from the inclusions. Furthermore, when the bearing steel is deformed, strain incompatibilities may also cause cavities at the inclusion interface [151]. Many researchers [152][153][154][155][156] referred the formation of voids to the difference in Coefficients of Thermal Expansion (CTE) between the non-metallic inclusions and the other steel components. The CET variation causes residual tensile or compressive stresses in the steel matrix during the quenching, contracting, and solidification process. If the NMIs have larger CTEs than the steel, the contraction of inclusions would be faster; and the (inclusions-steel) bonds would become weaker. Accordingly, cavities and voids would be formed by the interference of these (inclusions/matrix). Eventually, inclusions would be detached from the matrix. [Appendix E 1](#) shows CTE values and other related physical parameters for various types of NMIs [157].

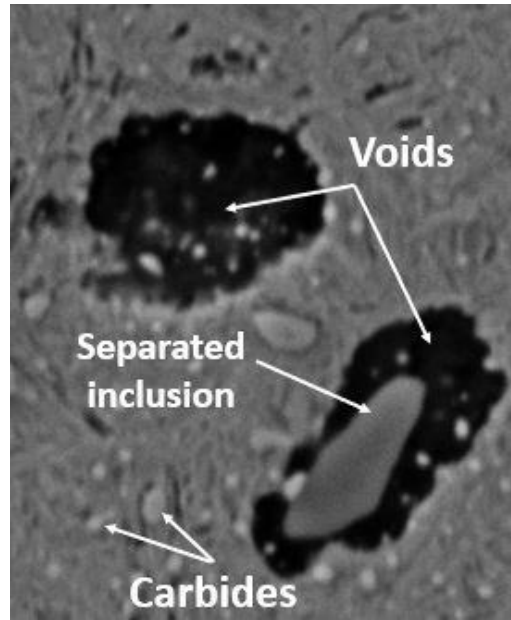


Figure 3-4: Voids formation in the material of bearing steel [the researcher]

3.1.3 Types of non-metallic inclusions

Typically, non-metallic inclusions can be classified into five groups based on their shape and distribution in the subsurface region, as illustrated in [Table 3-2](#) [35][117][45][158].

Table 3-2: Non-metallic inclusion types and morphology [158]

	Physical properties	Particles' color / direction	Particles' status (individual /combined)	Aspect ratio AR (length/width)	Shape
Sulfide group	Highly malleable	Grey	Individual	A wide range	Generally rounded ends
Aluminate group	Non-deformable	Bluish or black aligned with the direction of deformation	At least (3)	Low (Generally, <3)	Angular
Silicate group	Highly malleable	Dark grey or black	Individual	A wide range (Generally, >3)	Sharp ends
Globular oxide group	Non-deformable	Bluish or black,	randomly distributed	Low (Generally, <3)	Angular or circular
Single globular group	-	-	Single	-	Circular (or nearly circular), of diameter > 13 μm

Furthermore, there are other basic ways in which the non-metallic inclusions are classified as follows: -

1- Based on their chemical compositions:

1.1 Deoxidizers: Steelmaking elements have a high oxygen affinity and can be functioned as deoxidizers. When used on liquid steel, these non-metallic deoxidation chemicals are generated. Calcium additives are used in the steel casting process to filter out any remaining impurities, but these additives affect the RCF of the bearing steel [8]. Strong nucleation of tiny inclusions occurs when deoxidizing are introduced to the liquid steel. Inclusions continue to grow due to diffusion, coalescence, and collisions after this initial nucleation [140].

1.2 Sulfides: Elements that do not dissolve easily in iron, such as Ca and Mg have a strong enough affinity for sulfur to form non-metallic sulfides at the temperatures of liquid metals. Most sulfurs in steel should be taken out of the solution by refining the slag, and the rest should be taken out by precipitation reactions that happen mostly when the steel solidifies. The most common example of this NMI type is manganese sulfide (MnS).

Hashimoto [159] estimated that the inclusions' chemical composition is crucial in the rolling contact fatigue life. For example, steel with inclusions of $\text{SiO}_2\text{Al}_2\text{O}_3$ has a significantly longer RCF life than steel with Al_2O_3 or $\text{Al}_2\text{O}_3\text{CaO}$ inclusions. The corresponding characteristics of some types of non-metallic inclusions can be described as follows: -

- Manganese sulfides and silicates have deformation in a manner analogous to that of the steel matrix. These inclusions are ductile and have a significant amount of extension in the rolling direction.
- Alumina inclusions and clusters are hard and brittle inclusions and are shattered into stringers or separated shards due to the metal working.
- Complex inclusions with multiple phases have a rigid core encased in a more malleable surrounding phase. When subjected to moderate degrees of deformation, these inclusions often exhibit ductile behavior. However, they frequently exhibit a thick center and protracted ends when subjected to severe stresses.
- Inclusions of calcium aluminate undergo a very little or no deformation at all.

2- Based on the starting point of the solidification phase and process according to the following classification: -

2.1 Primary solidified inclusions: The inclusions, which can be formed before the starting of steel solidification. Theoretically, it is possible to remove primary NMIs from liquid steel.

2.2 Secondary solidified inclusions: The inclusions form after the start of steel solidification. They develop during the solidification process and are almost impossible to get rid of, and they can only be "engineered" to have a minimally negative impact on the final product.

2.3 Endogenous: They originate from the process of steelmaking, such as sulfides and oxides.

2.4 External: Inclusions that originate outside the metal, such as refractory particles, entrapped slag, covering the liquid metal, and sand in cast alloys, are known as exogenous inclusions. When compared to their endogenous counterparts, exogenous tend to be larger [160][161][162][163].

3- Based on their sizes as follows:

3.1 Macro level inclusions: Large enough to have a high probability to cause failure, and

3.2 Micro level inclusions: Small size, resulting low probability to cause failure [164].

3.1.4 Damage drivers in NMIs

The RCF life can be determined by either the matrix-inclusion interface state, the inclusion composition, their configuration, and distribution [165]. Evans [8] demonstrated that the level of damage caused by inclusion can be determined by several factors, such as coefficient of thermal expansion (CTE), elastic modulus, shape, size, and chemical composition [151]. For example, alumina and calcium aluminates inclusions have a higher yield strength than the steel matrix, making them more prone to void formation, however, brittle inclusions initiate cracks under high levels of loadings or during the manufacturing process. Oxides, carbides, slags, and refractories retain their formation original after the manufacturing process. It means they are even worse than MnS in rolling contact fatigue and help to induce cracks [32][33][61][72][279][318]. Maciejewski [32] revealed that the presence or absence of the more ductile manganese sulfide (MnS) inclusions and brittle oxides affect the fatigue endurance limit, crack propagation, and fracture toughness. Because of their high hardness and brittleness, oxide inclusions such as SiO₂, Al₂O₃, and Al₂O₃CaO have a more significant impact on the development of butterfly features failure than the other

varieties because of their high hardness and brittleness [32]. Moreover, the oxide NMIs create tensile residual stresses, induce cracking, and eventually cause fatigue damage. Hard inclusions with a lower CTE, such as Al_2O_3 , are more likely to cause tensile and compressive stresses than soft inclusions having higher CTE, such as MnS inclusions.

3.1.5 Shape, size, and aspect ratio of NMIs

When the steel undergoes a high deformation, such as when rolling it throughout manufacturing of bearing rings; the inclusions tend to lengthen in the plane parallel to rolling direction. Accordingly, NMIs can vary in aspect ratio (i.e., they can be globular or elongated), and their length has a wide range from 1 to 500 μm , depending on the inclusion composition [166]. The configuration of NMIs affects the probability of creating cracks; for example, thin-flattened NMIs can behave as virtual cracks and may propagate as real ones. Danielsen et al. [167] postulated that large MnS inclusions are non-associated with the crack network. During the hot formation of the bearings' manufacturing process, manganese sulfides MnS inclusions elongated in different aspect ratios because of their high deformability. The metal casting process indicates the value of the inclusion aspect ratio. There is a disparity in the many reviewed researches regarding the correlation of stress concentration in NMIs with their aspect ratio [32][54][63][207][208]. This study has discussed this matter in (section 4.4) based on the statistical analysis of the investigation results. The aspect ratio of the manganese sulfides (MnS) can be reduced by controlling the geometry of the inclusions using specific additives, which modifies the material's hot plasticity [32]. The bearing steel grade AISI 52100 has Al_2O_3 and TiN inclusions. Al_2O_3 inclusions appear with spherical or elliptical shapes [72], while TiN inclusions have smaller and cubical shapes. The sharp NMIs increase the stress concentrations; thus, the fatigue resistance will be less than the other rounded types [72][102].

3.1.6 Steel cleanliness

The term "steel cleanliness" refers to match all the NMIs requirements such as quantity, chemical composition, size, feature, and distribution style in terms of increasing the RCF resistance of the steel. Accordingly, "Inclusion Engineering" has been introduced as a specific subfield of ferrous process metallurgy that concerned with controlling the above-mentioned steel cleanliness elements of NMIs. All the controlling processes of materials are implementing through the refining and solidification processes of the liquid metal status [140]. Evans [71] postulated the

decreasing of oxygen level in steel from 30 ppm to 5 ppm, resulting in a life improvement of 10 times [71]. Producing soft inclusions will reduce the crack initiation even if the oxygen concentration is high. The intensity and size of inclusions can be expressed as material cleanliness. The NMIs are categorized based on their chemical compositions and dimensions, then indicating the cleanliness index by following the international standard ISO 4967-2013 [158][168]. Clustering and floating out can be used to remove the small inclusion units; for example, alumina inclusions have a higher tendency to form clusters than calcium aluminate inclusions. In the steelmaking process, inclusions cannot be prevented entirely; however, the amount that can be reduced has many technological and economic effects [17][169]. For bearing steel, the maximum allowable inclusion fraction is that the total oxygen ≤ 10 ppm, and the maximum NMI size $\sim 15\mu\text{m}$ [141].

3.2 Microstructural alterations

The term "microstructural alterations" refers to any damaged feature including a change in the material structure at the microscale level. When bearing steel is subjected to rolling contact fatigue (RCF), its internal composition could show microstructural changes that can be observed the microscopic investigation of the bearing in the sections. Alterations in the microstructure close to cracks (or at their tips) brought out by the movement of crack faces relative to each other, and this may cause a wear debris [170][171]. Microstructural alterations are represented by various features such as White Etching Areas (WEAs), White Etching Cracks (WECs), butterflies, and Dark Etching Regions (DERs) [71][84][99][103]. Holweger et al. [172] hypothesized that a plastic deformation, followed by an impact loading, can cause the internal contents of the steel to be disrupted as mechanical microscale waves in the impact region. They elucidated that these waves are probably the primary factor initiating microstructural alterations. Ooi et al. [173] observed that the microstructure alterations often occur after the formation of cracks. The microstructural alterations can be observed in many mechanical applications, such as: -

- bearings and main shafts of wind turbine gearboxes,
- marine pod drive bearings,
- hydrogen fuel system bearings,
- bearings of paper milling machine,

- electromagnetic clutches,
- automotive alternators,
- air conditioner compressors,
- aircraft turbine bearings,
- water pump and driveline transmission bearings,
- gears of stone crushers, and
- crane lifting devices. [26][32][39][174][175][176][177]

3.2.1 Phases of microstructural alterations

The cyclic stresses of rolling contact fatigue causing microstructural alterations in the bearing steel has the following phases: -

- 1- **Shakedown phase:** The steel material tends to be responded to contact stresses because of the work-hardening or the limited plastic micro-strain. The generation of defects within the crystal matrix structure, including dislocations and vacancies, occurs because of small-scale dislocation glide. However, the material strength increases due to the induced residual stress. This phase ends after ~1000 cycles when the plastic deformation does not occur quickly.
- 2- **Steady phase:** It starts directly after the end of the previous phase. It has been recognized in this phase that the steel material has an elastic response toward the RCF and the induced contact stresses. After around 10^9 cycles, the steady phase tends to reach its end. The phase duration depends on the amount of the contact pressure and the rotational speed.
- 3- **Unstable phase:** In this phase, an additional plastic deformation occurs, the yield strength decreases, and crack nucleation starts [45][46][71][178][179][180][181].

3.2.2 White Etching Areas (WEAs)

When a bearing of WECs is sectioned and etched with Nital (~ 1% nitric acid in ethanol), the response will appear in the white visual description of the microstructural alterations as white etching areas (WEAs) [30]. WEAs are microstructure changes that look white under optical microscopy of etched samples with 1% nital (1% nitride acid and 99% ethanol). The dissolution of hard and brittle spherical carbides may be the cause of their formation [14]. WEAs may surround the inclusions or voids. They were observed in tempered martensite and carbide-free nano-sized

bainite-bearing steels. Two inclination angles of WEA which are 30° and 80° related to rolling direction, despite the former being harder than the latter [116][182]. They consist of nanocrystalline ferrite grains with diameters ranging from 5 to 300 nm and a hardness of 10 to 50% greater than the matrix in which they are embedded and elongated. A considerable number of researchers postulated that the spherical carbides have broken up and dissolved, forming the WEAs [8] [11][27][30][71][129][152][155][172][183][184][185][186][187]. Šmeļova et al. [188] proposed that the main reason for WEAs formation may be the rearrangement of carbon and chromium inside the microstructural modification area. The grain boundaries of the material act as carbon traps, creating a weak zone prone to cracking. Remaining stress may play a significant role in the emergence of WEAs, as Voskamp et al. referred to [88]. On the other hand, the microstructural change resulting from the friction between the crack faces may lead to the formation of WEAs [115][152]. Impact loading probably has a significant role in generating of WEAs under high- stress concentration of the NMIs causing subsurface cracks [109][183][189].

3.2.3 White Etching Cracks (WECs)

White etching cracks (WECs) are broad branching crack networks that contain white local areas of microstructural alteration that ultimately lead to macro-pitting/spalling in bearings [71][174]. The cracks are fissures in the material's subsurface surrounded by white etching areas (WEAs) [190]. WECs are most often linked to failures in the high-speed shaft bearings of wind turbine gearboxes [191]. Evans et al. [11][107][183] postulated that inclusions with average lengths of 10 to 20 µm are more likely to trigger the formation of WECs depending on the inclusion type, orientation, and position (location below the contact surface). WEC formation can be attributed to the stress concentrations in the NMIs, crack face rubbing, and the impact loading that generates an Adiabatic Shear Bands (ASBs), that illustrated in (section 3.4) [11]. The impact loading, along with high surface traction and contact pressure, are critical contributors to the onset of micro-cracks and white etching areas (WEAs) at the non-metallic inclusions, which may ultimately result in the formation of WEC networks [189]. Evans [8] postulated that WECs usually spread irregularly as branching networks and have a metallic appearance similar to butterflies. The inner ring of the bearing is heated and then pressed onto the shaft before being shrunk and permanently fastened by cooling. The fitting process creates tensile stress in the ring; hence a possibility of WECs with a wide damaged WEA is considerable [28]. Šmeļova et al. [192] and Grabulov [193] observed that the dissolving of iron-chromium carbide could form carbon-

supersaturated ferritic grains as WECs of a White Layer (WL) and a Deformed Zone (DZ). A relatively small number of severe impacts could lead to form WL which represents the primary phase of WECs. [Figure 3-5](#) illustrates the presence of micro-cracks with and without inclusions, cracks network, WEAs, and WECs.

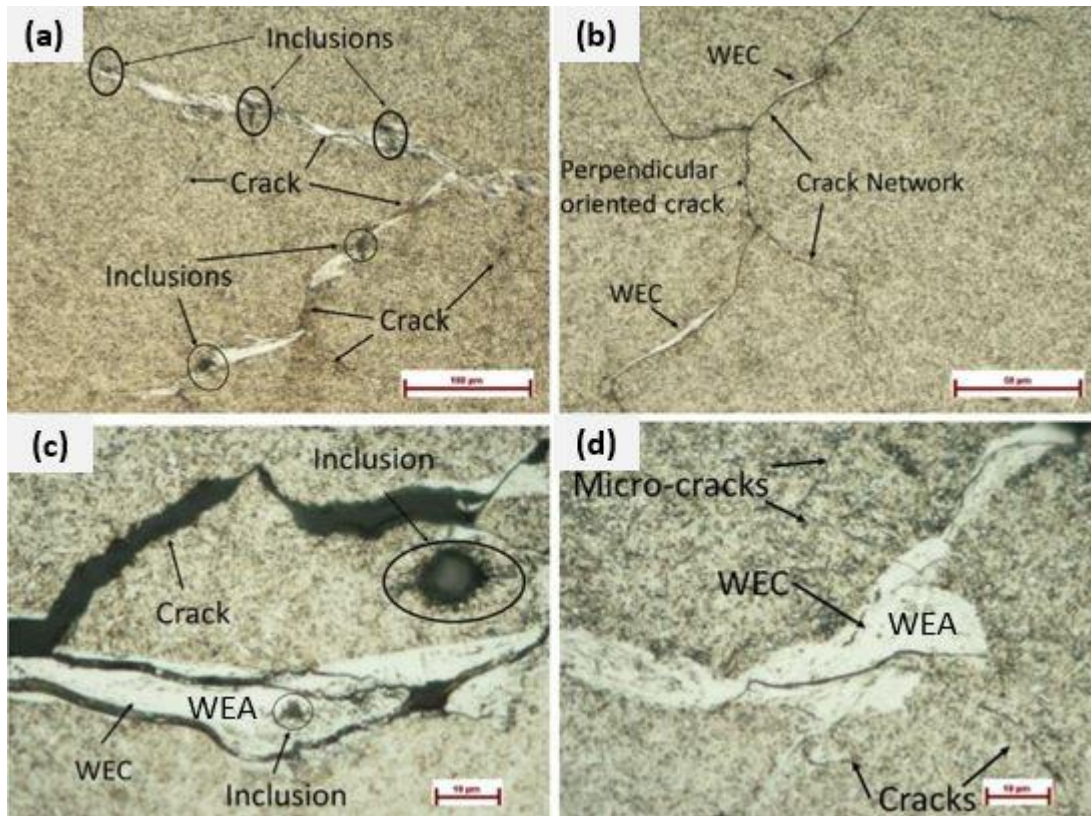


Figure 3-5: (a) Cracks with and without inclusion, (b) cracks network, (c) high magnification for cracks and WEAs, and (d) WECs, cracks & micro-cracks [144]

3.2.4 Butterflies

Butterfly feature is a specific type of microstructure alteration in which one or two wings connected to a central non-metallic inclusion in the configuration of a butterfly when subjected to highly localized subsurface stress, an example of this alteration feature can be seen in [Figure 3-6](#) [194]. The butterfly wing is a cracks that have fine and coarse ferritic grains (5-10) and (50-100) nm respectively [99][195]. These nano-ferrite grains are caused by the clustering of network dislocations [196]. The butterfly inclination is measured in the direction of the over-rolling direction (ORD), and its total length is termed “the wing span”. Guetard [197] demonstrated that butterfly angles are likely controlled by their depth beneath the contact surface. Furthermore, he

determined that butterflies can be formed in the subsurface region with an orthogonal shear stress of ~450 MPa. A study by Singh et al. [144] pointed out the maximum depth of orthogonal shear stress correlates to the distribution of butterfly wing depth. Butterfly wings have a maximum depth from the contact surface of about 1.5 mm with a range size of (10-100) μm and ranges of inclined angles with a rolling contact surface of (30°-50°) and (130°-150°) [142][196]. Nevertheless, the degree to which butterfly wings are oriented varies depending on the size and type of the inclusion represents the butterfly nucleus [144]. When bearing rotation is reversed, a second symmetrical pair of butterfly wings is formed [107]. The butterfly nucleus (NMI) tends to be debonded in their tips. For that, WEAs in butterfly wings are anchored to the debonding spaces at the NMI's tips as they have a high-stress concentration. [198][199]. The wings of butterflies' features may propagate on both sides in multi-directions and link to another crack network up to a specific length [71]. It has been determined by Grabulov [193] that butterflies can be formed at ~450 MPa of orthogonal shear stress in the subsurface region.

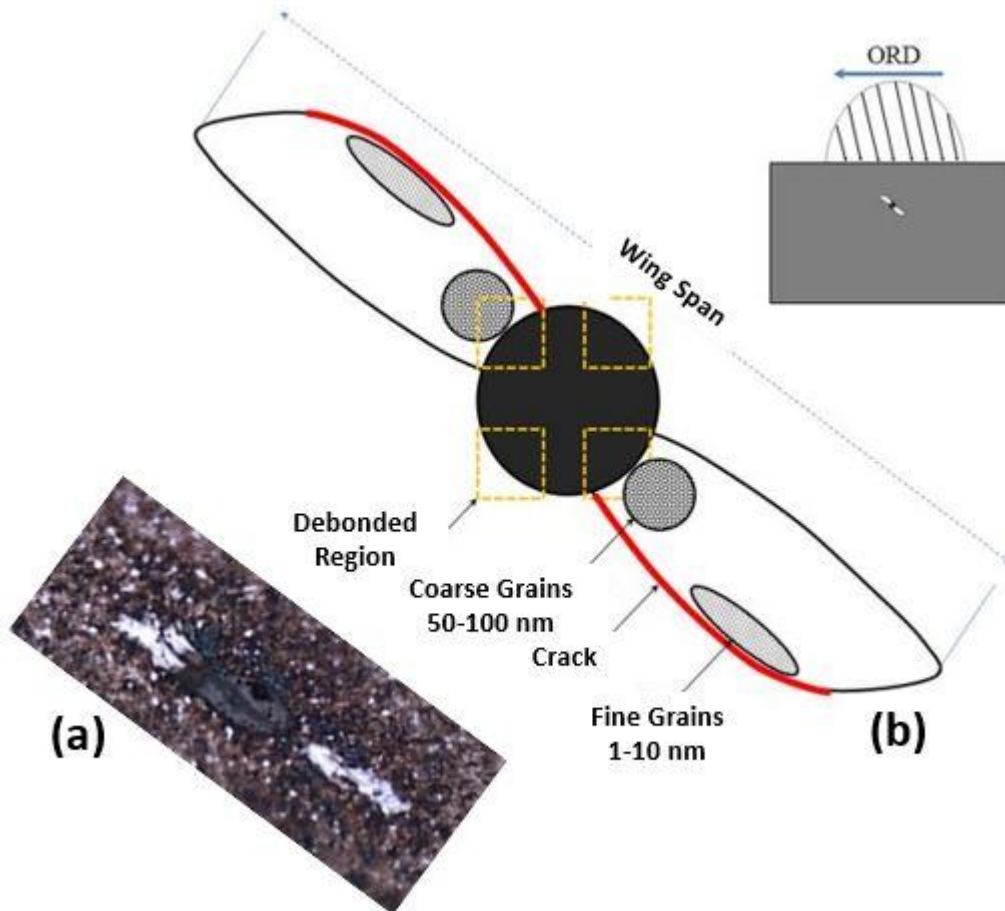


Figure 3-6: Butterfly microstructure feature (a) microscopic image, (b) Schematic— adapted from [195]

3.2.5 Dark Etching Regions (DERs)

Dark Etching Regions (DERs) are heterogeneous grains in the ferritic phase. DERs are observed as deformed dark bands at depth $\sim (100-600) \mu\text{m}$ beneath the contact surface of the inner races bearing using optical microscopes, as can be seen in Figure 3-7 [84][200][201]. Two significant factors may indicate the intensity of DERs: fatigue cycles' number, and Hertzian stresses' level [46][186]. H. Swahn et al. [200] reported that AISI 52100 steel required 5×10^6 and 5×10^7 cycles to form DERs under a maximum contact pressure of 3.72 GPa and 3.28 GPa, respectively. According to Gegner [143], WEC formation is preceded by the formation of DERs. Szost et al. [202] postulated that the microplastic deformation may induce the formation of DERs in the slip motion, which forces carbon particles to migrate to the more dislocated region [158][203]. A different hypothesis by Hirth [204], which states that the formation of DERs may refer to the martensite decay phase.

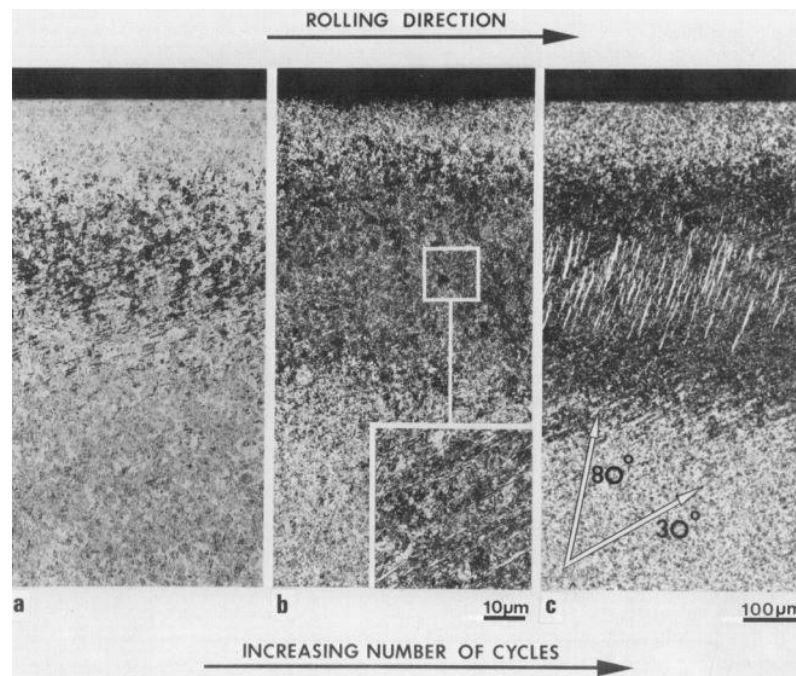


Figure 3-7: (a) early stage DER, (b) fully developed DERs and 30° bands, and (c) DERs, 30°, and 80° bands [200]

3.3 Failures modes and affecting factors in WTGBs

3.3.1 Factors affecting WTGB's failure

Bearing failure and microstructural changes in WTGBs are influenced by various factors, such as the followings: -

- 1- Mechanical factors: including high compressive loading, impact loading, vibration, slipping, and the materials mechanical properties,
- 2- Tribological factors: lubricant, surface roughness, contamination, temperature, and (load-speed) relation,
- 3- Microstructural factors: grain size and type, inclusions, voids, carbon content, and heat treatment.
- 4- Chemical factors: hydrogen embrittlement, electrical current, compositions of materials and inclusions, carbon diffusion, and phase transformation [5][205].

Oila and Bull [206] analyzed seven factors regarding the drivers of WTGBs failure: load, lubricant, temperature, surface roughness, material, slipping, and speed. They concluded the load and slipping are more influential than the other factors. Machining and heat treatment processes create residual stresses that might contribute the plastic deformation [207]. Errichello et al. [84] hypothesized that the high nickel content, a large amount of retained austenite, low carbon composition of the bearing core, and increasing the residual compressive stress could give higher fatigue damage resistance. The following configurational aspects related to turbine size (gearbox-bearing), manufacturing, and design, in addition to other factors related to specifications, such as lubrication and filtration, are also significant factors affecting the bearing fatigue life [51][57][182].

3.3.2 Failure modes of rolling element bearing

A component can be considered to have failed and is no longer functional when it cannot perform the design function. The failed bearing cannot conduct its function and there are many indicators for that, for example noise and vibration levels exceeding the predetermined threshold. In addition, inadequate (or non-filtered) lubricant and high cyclic load may cause dents on the

contact surfaces, and seizure and can be considered as failure modes. Furthermore, the buildup of induced stress enhances the plastic deformation by causing structural alterations. Failure modes describe the styles of rolling bearing damage, which have been classified to several types based on their characteristics, appearance, and the reasons of their occurrence: fatigue, wear, corrosion, electric erosion, plastic deformation, and cracking. [Figure 3-8](#) depicts a scheme of the bearings' failure modes. [Appendices \(F 1-F 16\)](#) describe various bearing failure modes, conditions, causes, and solutions in more detail.

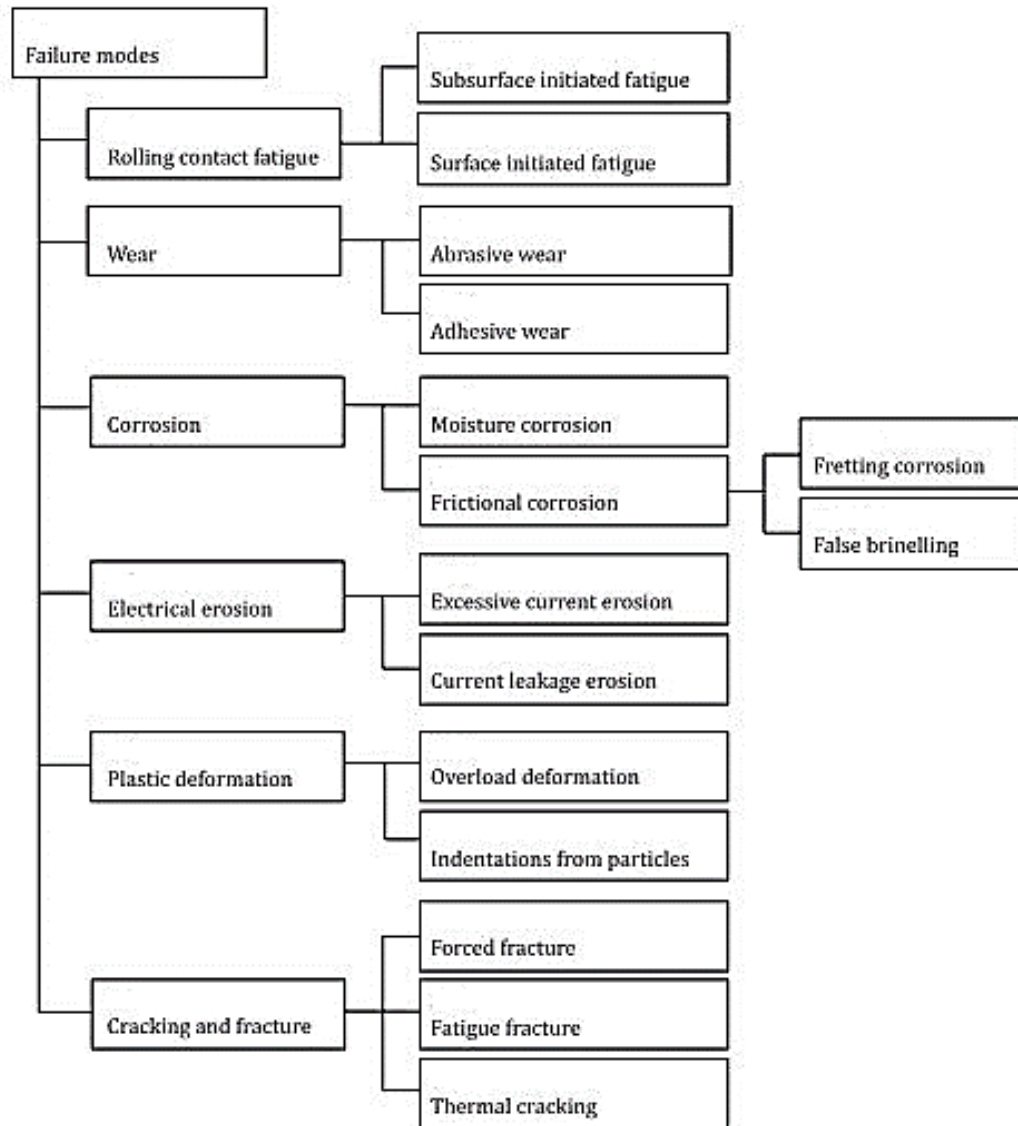


Figure 3-8: Classification of failure modes in rolling bearings [208]

There are some influential factors causing the bearing failure modes, as follows: -

- 1- Fatigue:** It occurs on the bearing's surface and/or subsurface because of the surface roughness that makes the rolling elements less significant with the lubricating film thickness. The subsurface-initiated fatigue, the microcracks initiate beneath the contact surface region as a result of the cyclic loading [234]. The subsurface failure propagates on the bearing raceway as flaking (spalling) and/or indentations, as can be seen in [Figure 3-9](#). Asperities on the rolling element can rub against the bearing raceway if the lubrication is inadequate, the improper lubricant is used, the operating temperature is too high, or the surface is too abrasive [208][209]. The plastic shear stress, as proposed by Lin and Ito [210], is thought to produce a slip between the layers of the material that leads to the initiation of the fatigue surface cracks. Nakai et al. [211] postulated that the bearing failure scenario started from the surface region. They also concluded that when the vertical crack got to a certain depth, a horizontal crack would be formed. The following modes can be recognized as examples of failure-initiated fatigue: -

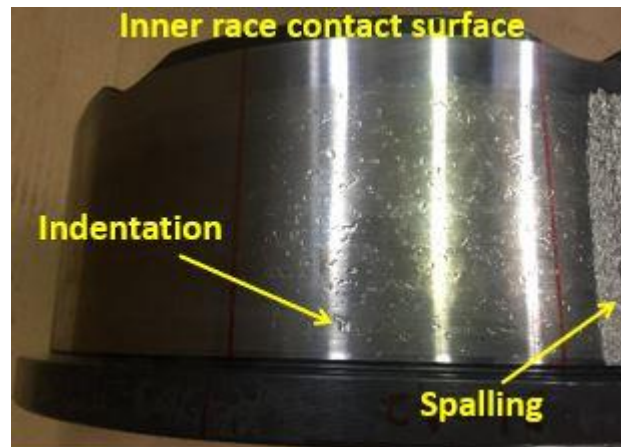


Figure 3-9: Surface indentation and spalling at the inner raceway of a roller bearing [the researcher]

- 1.1 Spalling (flaking):** It describes the material removal from the bearing contact surface, that develops from the subsurface loaded zone, as can be seen in [Figure 3-10](#) [8][27][72]-[108][166][202]. If such bearings stay in service, the forming debris may cause localized overloading and stress concentrations in the contact zones and severe surface deterioration. The contact surface may initiate damage because of insufficient bearing lubrication. In most situations, the spalling of material from the surface could result from the change in

the material microstructure and the microcracks spreading toward or from the deformation zone [183][208]. High-concentrated stresses from dents, nicks, debris, and the geometric stress concentration from deflection and misalignment of the bearing shaft can lead to spall the material from the raceways and rolling elements [212]. Morales et al. [111] postulated that a characteristic V-shaped spall might be seen developing at the trailing edge of a pre-indentation raceway. If this failure mode associated with WEA; it is known as White Structure Flaking (WSF) [5][32][216][26][130]. Other potential WSF drivers are the severe operating conditions of WT, corrosion, water pollution, electricity, tribo-chemistry, slip, vibration, and bending stress [72].

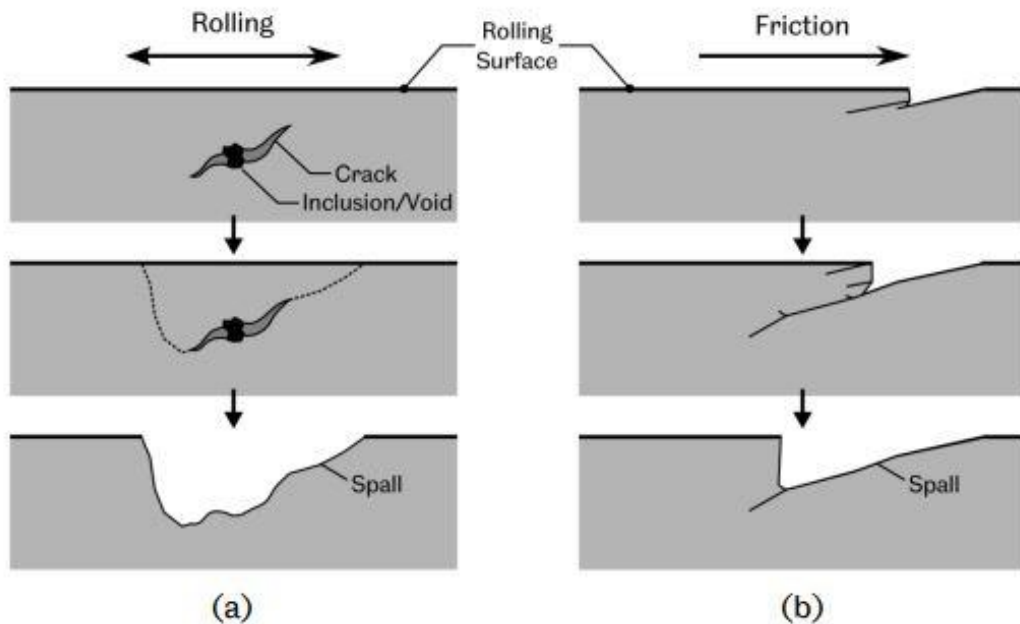


Figure 3-10: (a) subsurface RCF , and (b) surface initiated RCF resulting in surface spalling [213]

1.2 Micropitting: It is the scratching or removing of material from a metal-to-metal contact surface due to the tangential shear stress effect driven by the rolling and sliding motion. Micropitting reduces the tolerance in the rolling element bearings and gears, which are recognized via the bearing noise [30]. Many factors affect the manifestation of micropitting, such as speeds, loads, sliding and rolling velocities, and surface topography [5][206][214][215][216]. In general, the micropitting mechanism is linked to asperity contact, which causes the lubricant layer to be broken down [209]. A small amount of

roller/raceway slippage may cause micropitting, the breakdown of the oil coating, and the penetration of hard particles of contamination into the oil [71] . Micropitting might appear as debris dents in the roller bearings' ends, so-called "Geometric Stress Concentration (GSC) micropitting," as can be seen in [Figure 3-11](#).

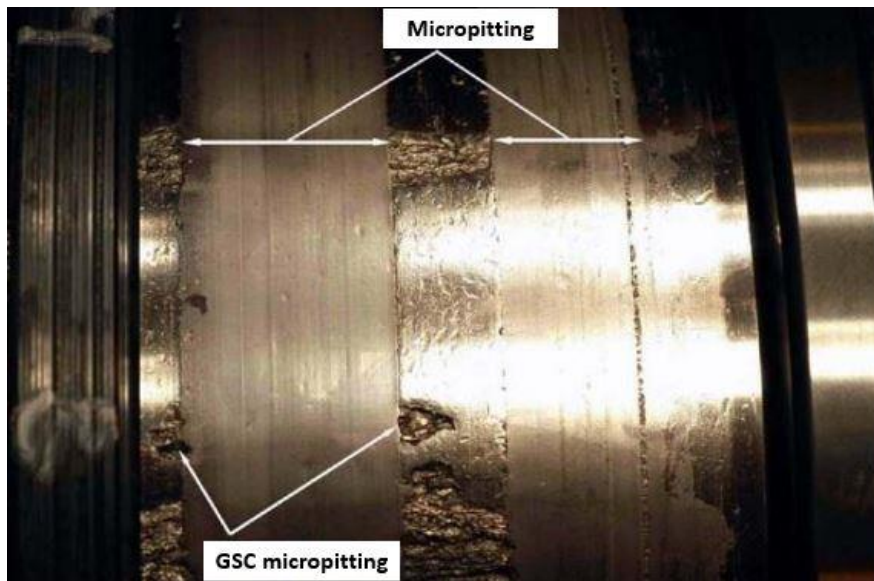


Figure 3-11: Micropitting and Geometric Stress Concentration (GSC)for Cylindrical Roller Bearing (CRB) in WT [216]

1.3 Creep: When the diameters of two objects are slightly different, the two components will rotate at slightly different speeds. In the bearings, creep occurs if the inner or outer race moves against its seat with a slight change in rotational speed. Creep is considered sliding contact damage that causes extreme surface plastic deformation [30]. Mostly, it results from localized frictional heating at the surface, specifically in areas with insufficient lubrication layer thickness. Moreover, a light load, rapid acceleration, and inadequate lubrication may cause creep. In the event of creep, the asperities may cause the ring/seat contact area to take on a glossy finish, as can be seen in [Figure 3-12](#). The combination of creep and sliding in the race/seat contact can cause further damage, such as score marks, fretting corrosion, and wear. The precautionary could include reducing acceleration, increasing load, applying surface coatings, and enhancing lubrication [208].



Figure 3-12: Creep of the inner ring on the shaft-seat [217]

2- Wear: The interaction of two sliding or rolling/sliding contacting surfaces results in the gradual erosion of material from a surface [208]. Because of contacting asperities created by removing particles from the raceway and the roller of the bearing; wear develops in Rolling Bearing Elements (RBEs). There are two types of wear in bearings: abrasive and adhesive wear.

2.1 The abrasive wear: It could occur either because of reduced lubrication or the contamination of the lubricant by other foreign small and hard particles. If the bearing contact surfaces become dull, friction will increase, and leading to the remove particles from the contact surfaces. Material loss take places when hard particles slide against each other so that a hard surface or particle slides across another surface and cuts or plows away some of the surface material, as can be seen in [Figure 3-13](#). As the running surfaces and possibly the cage gets worn down, more and more of these particles are made. The degree to which the surfaces become dull depends on how big and what kind of abrasive particles are. Eventually, the wear gets worse and worse, which causes the bearing failure. The polishing process can occur when the abrasive particles are very soft [208].



Figure 3-13: Abrasive wear on the inner raceway and roller of a Tapered Roller Bearing (TRB) [208]

2.2 The adhesive wear: It caused by the slipping of Rolling Bearing Elements (RBEs) on the raceways. The material moves from one surface to another because of the frictional heat and, in some cases, a re-hardening of the surface [212]. In operation, the adhesive wear may occur if the rolling elements are too lightly loaded and then subjected to a high acceleration due to the re-entry into the bearing loading zone, as can be seen in [Figure 3-14](#) [208].



Figure 3-14: Adhesive wear at the inner raceway of a cylindrical roller bearing [208]

2.3 Three-body abrasive wear: Three main stages can be recognized for the abrasive wear in case of inducing a third body (in addition to inner race and roller), which is a foreign particle such as debris. These stages can be explained, as follows: -

- **Stage 1 (indentation and macrocrack formation):** due to the compressive stress caused by a third body placed between the inner ring and the rollers, multiple millimeter-sized indentations, and macro fractures in lengths of several centimeters may be formed. The inner raceway hardness is lower than that of the roller, which makes the indentations and macro fractures larger and deeper (significantly more extensive than the particle sizes, i.e., less than 10 μm) [72].
- **Stage 2 (regional plastic deformation):** areas with indentations are more likely to become plastically deformed.
- **Stage 3 (wear out of the surface):** the wear-out surfaces of the two bodies grow broader and deeper as the base materials have been removed, causing a fracture. However, the amount of wear is directly proportional to the material's hardness [72].

3- Corrosion: It is a chemical reaction on metal surfaces. Two types of corrosion can be recognized in bearings, which are moisture and frictional corrosion.

3.1 Moisture corrosion: It occurs because of the contact between bearing metal with acid or moisture, storing practices, poor handling, and packaging [218]. One common misstep is touching the bearing surfaces with bare hands. Gradually, the bearing surfaces deteriorate as the material is turned into oxides, leaving behind various-sized and colored stains in shades of yellow, brown, and red. The abrasive paper with a fine grade would eliminate small amounts of rust, while highly rusted components require re-grinding and machining. Untreated rust will worsen and cause macro pitting [41]. The result is the formation of pits and then the flaking of their contact surface, as can be seen in [Figure 3-15 \(a\)](#).

3.2 Frictional corrosion “tribo-corrosion”: Under a high loading condition, the lubricant would be squeezed out of its surface contact zone. As a result, friction force increases in the contacting zone, removing the protective oxide layer and causing oxidation followed by material removal from the bearing contact surface [46]. There are two kinds of frictional corrosion: fretting and false brinelling (vibration corrosion).

- **Fretting corrosion:** It develops in load-transmitting surfaces with oscillating contact micro-movements. Asperities oxidize and are wiped off; powdery rust forms (fretting rust, iron oxide). The bearing surface turns reddish black. Loads and/or vibrations cause damage when the mounting fittings' radial clamping is overcome. Rough, wavy bearing, shaft, and housing surfaces can compromise mounting fit and cause fretting corrosion [208], as can be seen in [Figure 3-15 \(b\)](#).
- **False brinelling (vibration corrosion):** It occurs in the rolling element/raceway contact zones of non-rotating races due to micromovements and/or elastic contact resilience under cyclic vibrations. False brinelling in standby equipment can result in closely spaced flutes when long halted periods are alternated with brief running sessions. Electric current damage is distinguished by rolling components showing similar markings but at a less advanced stage. Bearings, blade pitch, gear components, and yaw, which experience only a limited range of motion or structural vibration, are prone to this failure mode. The lubricant is squeezed away from the contact zone, and the oxide layers protecting the area are stripped away. It causes faster wear on the raceway, which limits the positioning system's smooth performance [30], as can be seen in [Figure 3-15 \(c\)](#).

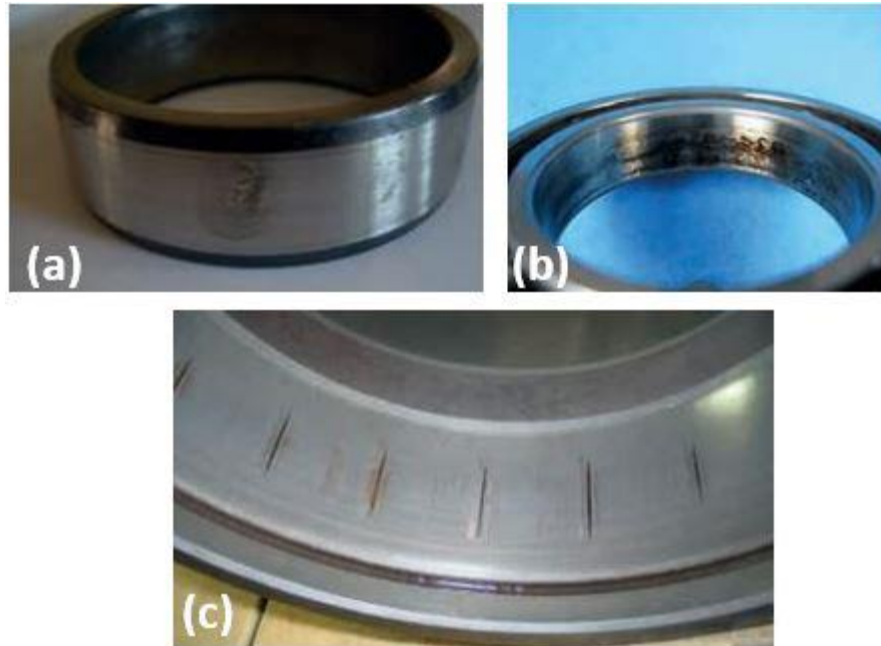


Figure 3-15: (a) Moisture corrosion, (b) fretting corrosion on the inner race ball bearing, and (c) fretting and false brinelling (vibration corrosion) in the outer ring of a tapered roller bearing [208]

4- Electrical erosion: Because of the high voltage created by the flow of electricity, sparks might flow between the bearing raceway and the roller. It would lead to welding, melting, and pitting of the bearing surface in the contact area [46]. Inadequate insulation, inductive effects, or improper grounding can contribute this failure mechanism by allowing electric current to flow through the bearing components. Electricity can be generated in several ways, including via lightning strikes, grid current leakage, and inadvertently charged components [219]. Intense heat can be produced by an electrical arc, the high temperature in the arc may be enough to melt the metal on bearings. The electrical erosion is either fluting or electrical pitting. The fluting leads to regular wear patterns, while electrical pitting leads to erratic ones, as can be seen in [Figure 3-16](#) [220][221].

4.1 Electrical pitting: It occurs when there are significant voltage differences between the bearing housing and the shaft. If they are not correctly grounded, current can pass through the lubricant layer that prevents direct contact between the rollers and raceways. The current produces sparks and arcs, leading to localized melting and welding of the roller and track surfaces. The welded areas are sheared off when the surfaces slide, leading to roughening and material loss. The material properties around the concentrated melting

zone are altered by electrical pitting, leading to a significant increase in the localized mechanical properties. The pitting serves as seeding locations for further cracking and micro-pitting.

4.2 Electrical fluting: Low-intensity direct or alternating current flows over the bearing roller and the raceway, causing electrical pitting and then electrical fluting. Most shutdowns occur because of a malfunctioning of the generator or an electrical grid breach. As a result, fluting can be considered as a common in generator bearings. As the rolling components traverse the craters created by the electrical pitting, and a mechanical resonance vibration can be produced. The result is a uniform band of brownish, axial, shallow ridges around the racetrack.

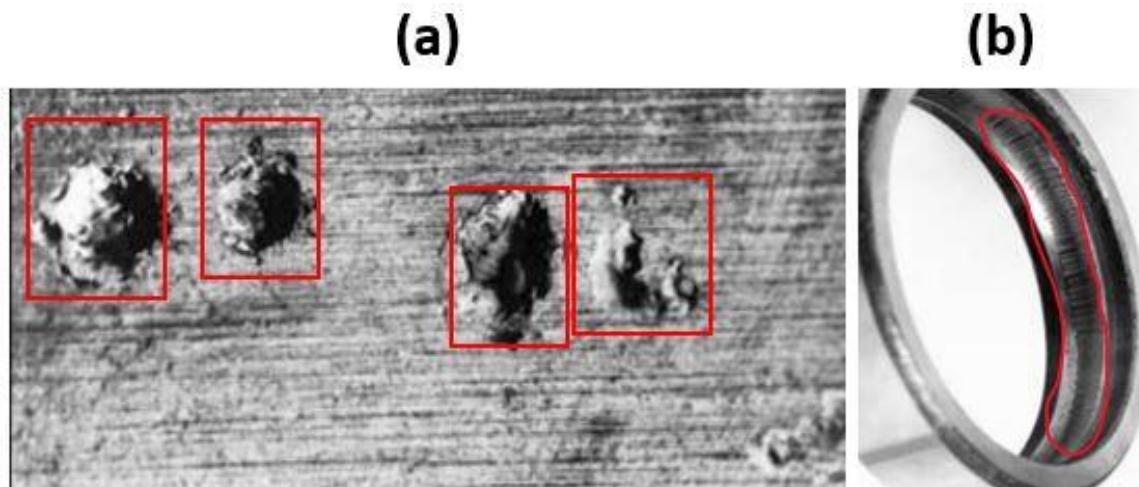


Figure 3-16: Bearing damage due to electrical current (a)electrical pitting, (b)electrical fluting [221]

5- Plastic deformation: If the bearing material is subjected to stresses that exceed its yield strength, permanent deformation of the metal will occur, so-called “plastic deformation.” At a microscale, the contact load between a rolling element and the raceway yields a large percentage of the contact footprint (the contact area) [142]. Misalignment and transient loading are the triggers of the plastic deformation, causing overheating, fretting corrosion, discoloration, and scored tracks, as can be seen in [Figure 3-17](#) [222][223]. Vibration might arise when the rollers are no longer move along their original design path due to a permanent change in the geometry of the rollers and/or the raceways [42]. Overload

deformation and particle indentations are two examples of plastic deformation, [Figure 3-18](#) shows examples of this damage.

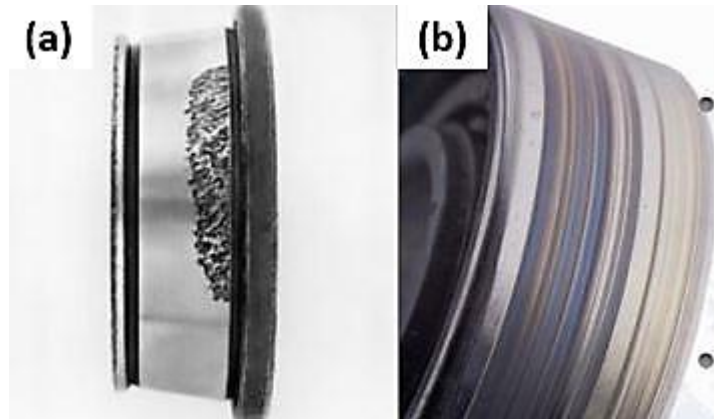


Figure 3-17: Plastic deformation damage (a)TRB track spalling due to misalignment, (b) Loose mounting markings and discoloration [128]

5.1 Overload deformation: It can occur in a stationary or spinning bearings (uncommon). Overloading a stationary bearing by static or shock load causes plastic deformation at the rolling element/raceway contacts, which form shallow depressions or flutes on the bearing raceways. Surface finishing or residual machining are markings at the bottom of the depression or the flute identify overload from the artificial brinelling or electrical fluting. Moreover, the excessive preloading or improper mounting can also cause overloading and then a deformation.

5.2 Indentations from particles: Indentations are created on the raceways of rings and rolling elements when particles are over-rolled multiple times. The characteristics of the particles can be presented by the dimensions and contours of the indentations left behind. Indentations occurs when debris from the system or foreign abrasive particles become trapped between the raceways and the rolling components, and the lubricant becomes polluted [212].



Figure 3-18: Plastic deformation at ball distance in the outer race of a ball bearing [208]

6- Cracking and fracture: If the stress of the contact surface in a bearing component is higher than its Ultimate Tensile Strength (UTS); cracking will occur. At an advanced stage, cracks can propagate and the material elements separate from the bearing surface and eventually lead to fracture. In inclusions and voids, the relatively low contact loads may exceed UTS and initiate microcracks in them [46][208]. The crack can cause a component to fracture when it spreads through a segment to the other side of it or to location where a portion becomes detached from the rest of the component [208]. There are three modes of cracking and fracture as follows: -

6.1 Forced fracture: Local over-stressing, such as from impact, or an excessive interference fit, such as excessive hoop stress induced throughout the bearings' assembly with their shafts. This can result in a forced fracture due to a resultant stress that exceeds the material's (tensile) strength, as can be seen in [Figure 3-19\(a\)](#).

6.2 Thermal cracking: High frictional heating from sliding may cause thermal cracking. Cracks appear perpendicular to sliding. Because of the local re-hardening and significant residual tensile stress, hardened steel is prone to thermal cracking, as can be seen in [Figure 3-19\(b\)](#).

6.3 Fatigue fracture: It occurs when the fatigue strength limit is repeatedly exceeded in bending, tension, or torsion. Once the initial crack has been initiated, it spreads across a portion of the cross-section, eventually causing a forced fracture. Rings are the most common site of fatigue fracture, as can be seen in [Figure 3-19\(c\)](#).

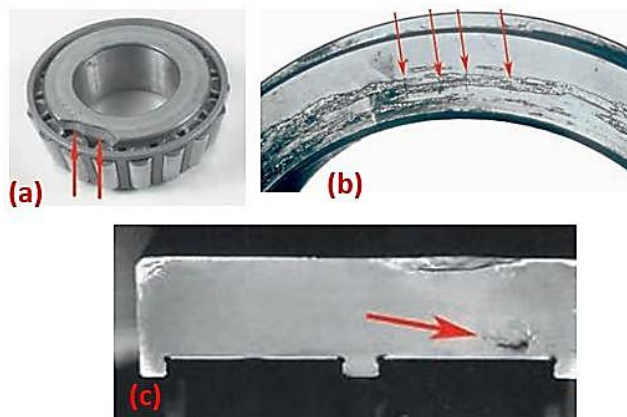


Figure 3-19: (a) Forced fracture in the inner race shoulder of TRCB, (b) Thermal Cracks in the inner race of TRCB, and (c) Section of fatigue fracture of a cam / roller outer race contact [208]

3.4 Hypotheses for interpreting the occurrence of microstructural alterations and failure modes

The following hypotheses illustrate the likely root causes of the microstructural alterations in the WTGBs' steel: -

- 1- Hydrogen diffusion: Many factors, such as lubricant, water contamination, transient operating conditions, and the steel manufacturing process, are responsible for producing hydrogen that diffuses into the bearing raceway. The degradation reaction generates lubricant fragments such as H_2^+ , CH_3^+ , $C_2H_3^+$, $C_2H_4^+$, and $C_3H_7^+$ [142][224][225][226]. Esters, ethers, and carboxylic acids are some of the additional oxidation reaction products that have been found in the lubricant and the metal oxide layer [227][228][229]. Uyama et al. [230] postulated that WECs initiation refers to the surface cracks due to a hydrogen effect generated from lubricant dissolving under high local compressive pressure at the surface crack when the roller travels over the surface crack tip. The hydrogen-induced speeds up WSF by boosting a local plasticity and increasing the grain slip deformation, which ultimately increases the crack density during the RCF [88][190][231][232]. During the bearing operation, an electrical current is induced, which may generate hydrogen from the lubricant and cause the lubricant chemical instability [154][173][177][233][234][235][236]. Ruellan et al. [121] tested pre-charged bearings with hydrogen. The results showed that these bearings had a more remarkable ability to induce microstructural alterations than those not charged with hydrogen. Other environmental factors such as water contamination, corrosion, severe contact conditions, and stray current promote the generation of atomic hydrogen. The penetration of the hydrogen into the bearing steel probably accelerates rolling contact fatigue and triggers cracks. During rolling contact, hydrogen could get into the bearing steel in the following two ways [27][52][143][237][238][239]: -
 - through surface cracks, where water contamination or lubricant can get in and cause hydrogen ions, which released locally by tribo-chemical reactions at the crack tip nascent surfaces; and

- through wear-induced nascent surfaces, hydrogen is made by the breakdown of lubricants through catalytic reactions and tribo-chemical reactions of water.
- 2- The Adiabatic Shear Bands (ASBs) are the regions induced due to impact loading of deformed and transformed regions caused by the stress concentration, leading to increasing temperatures and phase transformations. Cavitation creates pulses in the contact surface and may initiate WECs through a rapid process that results in the ASBs. Such pulses can be seen as a peak or much more as a ballistic impact, in the outlet region of a contact lubricated under Elastohydrodynamic lubrication conditions. The material grains would be disturbed by mechanical waves caused by the high impact loadings [172].
 - 3- Cyclic stresses of typical over-rolling may lead to an accumulation of the strain energy around the inhomogeneous objects (inclusions and voids); and causing plastic deformation, material deterioration, Dark Etching Regions (DERs), and cracking. As a result of this excess energy, nano-sized ferrite grains grow up within the steel, and the steel recrystallizes into WECs [240]. Energy dissipation is inadequate in the localized region of the bearing steel, as explained by Gould and Greco [241]. They hypothesized that the predicted Frictional Heat Accumulation (FHA) is proportional to the applied load, friction, the relative velocity of the contact bodies, and the time of the machine running [242]. Their findings indicated the required FHA to trigger microstructural alterations is about 6.26 MJ.
 - 4- The Low Energy Dislocation Structure (LEDS) theory, as modified by Kuhlmann and Wilsdorf [243], and states that, in a dislocation structure having a plastic deformation, the instant heat generation within the deformed particles is in equilibrium with the applied shear stress and the slip band. It was based on Taylor's work, which suggested that the microstructural grains be broken up into refined grains to maintain the structure's stability under high loads.
 - 5- Tensile frictional stresses from surface cleavage cracking would be receptors for aged and contaminated lubricants; hence, corrosion fatigue cracking leads to WECs. Gegner & Wolfgang [244] hypothesized that the brittle spontaneous tensile stress-induced cracks are typically responsible for forming preparatory fracture faces on the surface of a material. Branching of crack is afterward promoted by corrosion fatigue under the impact of the penetrating lubricant and breakdown of its layers.

- 6- Microcracks are created during the casting of the bearing steel as J. Campbell [245] proposed. The formation of relatively cold faces while pouring molten steel inside the casting process was to blame for the formation of microcracks and oxide defects.
- 7- Yang et al. [105] postulated that there are two distinct zones located underneath the Worn Surface (WS) that zones are subjected to (P) impact wear: the first is a White Layer (WL), and the second is a Deformation Zone (DZ) located above the other bearing matrix (denoted by M), as can be seen in Figure 3-20. The weakening of the border of the WL can be attributed to the disparity in deformation that occurs at the contact between the WL and DZ. Suh [246] confirmed that delamination occurs when microscopic cracks inside the WL spread along the WL's border or perpendicular to the worn surface path.

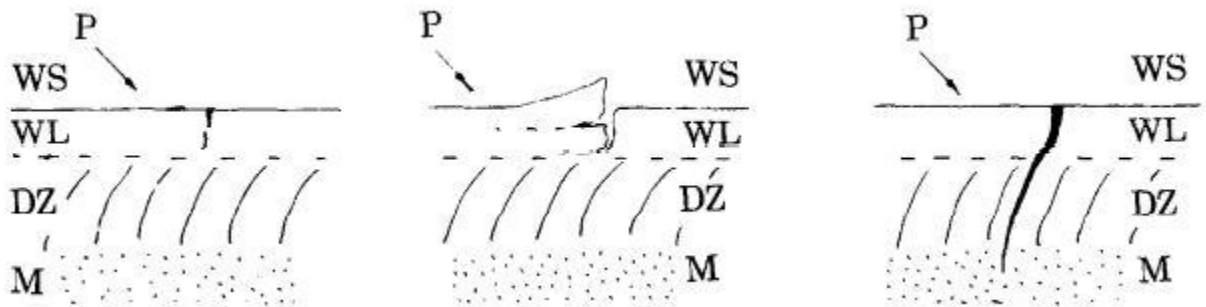


Figure 3-20: Cracks initiation and propagation throughout the bearing zones under the impact wear [109]

- 8- Solano-Alvarez and Bhadeshia [185] discussed the microcrack initiation and grain size control using Vickers hardness measurement equipment and heat treatment. They suggested three significant determinants in the initiation of cracks: the size of the austenite grains, the amount of stress that was transferred between the martensite and the austenite, and the carbon content of the martensite.

4

CHAPTER FOUR: SUBSURFACE INVESTIGATION OF A PLANETARY WTGB

In this chapter, the subsurface microcracks samples have been analysed. These samples were taken from the severely damaged inner race bearing of a planetary wind turbine gearbox. It was observed that these microcracks tend to change their directions at a length of about 15 μm . Hence, the cracks were classified as large and small based on the mentioned length limit. As the small cracks represent the primary stage of initiation, their analysis may give many indications in terms of inclinations, depths, lengths, and stress distribution. The correlation of microcracks distribution with subsurface contact stress indicates the role of Von-Mises, maximum shear stress (orthogonal shear), and traction force in the crack initiation. The investigation of this specific role represents a side of the study of the premature failure of WTGBs.

4.1 Methodology

The specimens from a failed planetary bearing of a 2 MW onshore wind turbine gearbox have been taken from the severely damaged region (not presented due to confidential policy). The specimens were carefully prepared and examined using different types of microscopes. The observed cracks were classified according to the following specifications: depths, densities, inclinations, and the inclusions' association. The severely damaged regions of the failed planetary WTGB were investigated by cutting, preparing, and examining the subsurface damaged areas. The data of microcracks' location, inclination angle with the rolling surface, and their relative location with non-metallic inclusions are analyzed to identify the possible cause of microcrack initiation leading to premature failure. The samples were cut by using a wire erosion machine and then by a linear saw machine at high speed (> 3000 rpm) and low cutting rate (0.3 mm/min) to reduce the possible damage due to sample cutting. The cutting can show the circumferential plane, i.e., the bearing rolling plane and the axial plane, as can be seen in [Figure 4-1](#). This figure also presents the mounting using a conductive resin to examine the samples by Scanning Electron Microscope (SEM) due to the resin's ability to absorb electrons.



Figure 4-1: The sample preparation procedure for microscopic examination [247]

An optical microscope - Light Reflection Microscope (LRM) is also used to scan the samples. After mounting, the samples were ground using coarse grinding paper (low grinding paper grade). The first grinding stage is to remove the unwanted impurities from the mounting process and make the metal sample completely flat to be ready for the other grinding and polishing processes. The materials used in the grinding and polishing process can be seen in Figure 4-2. The grinding papers and the polishing disc were fixed a rotating magnetic base of the grinding and polishing machine. At the same time, the samples were put in specific holes on a rotating disc connected to the rotating head with sample pressing rods to exert the grinding and polishing forces which fed on the data entry screen of the grinding and polishing machine.



Figure 4-2: Grinding and polishing machine with its used material [247]

Table 4-1 illustrates the details of the grinding and polishing processes with the rotational speeds and directions with the load of pressing the samples throughout each grinding and polishing step. The relatively small pressure throughout the last three sample polishing process is vital to reduce the possible damage due to the preparation process.

Table 4-1: Grinding and polishing processes data [247]

Process	Grinding			Polishing				
Step No.	1	2	3	1	2	3	4	5
Grade (par/in ²) and (μm)	240	600	1200	6	3	1	1	0.04
Force (N)	25	25	20	20	20	15	15	10
Time (s)	Until level	360	360	540	560	480	360	540
Base speed (rpm)	200	200	200	150	150	150	200	200
Head speed (rpm)	51	61	61	51	51	51	51	51
Rotational direction (base/head)	Same	Same	Same	Same	Same	Same	Opposite	Opposite

Nital (1% nitric acid in 99% ethanol) was used for the etching process. This etchant concentration helps to reveal the bearing material grain boundaries, carbides, and WEAs in the examined samples. The sufficient etching shows various light colors on the sample's surface. The samples were investigated using SEM and LRM. The cracks' depths (distances below the contact surface), cracks' angles (the inclination angle of the crack with the contact surface), and crack lengths, as can be seen in Figure 4-3 were recorded, classified, and analyzed for each investigated sample.

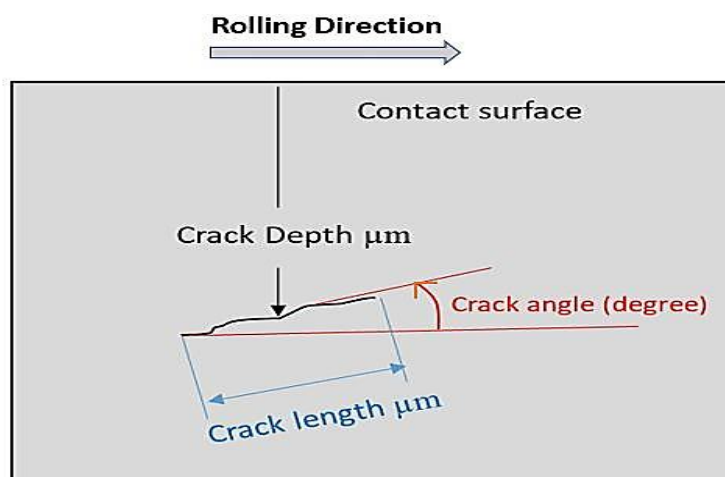


Figure 4-3: The characteristics data of the subsurface cracks [247]

4.2 Observed damage patterns

Different subsurface damage patterns have been observed throughout the microscopic examination of the samples, as illustrated in [Figure 4-4](#). One of the interesting observations is the separation of the inclusions from the material bulk, as can be seen in [Figure 4-5\(a\)](#). This separation (void) may be a damage mode produced throughout the sample preparation. However, this possibility has less opportunity due to the relatively low pressure on the samples throughout the grinding and polishing processes. The other option is that the separation is a type of damage that represents the primary crack initiation from the inclusions due to heat treatment of the bearing material or within the bearing service.

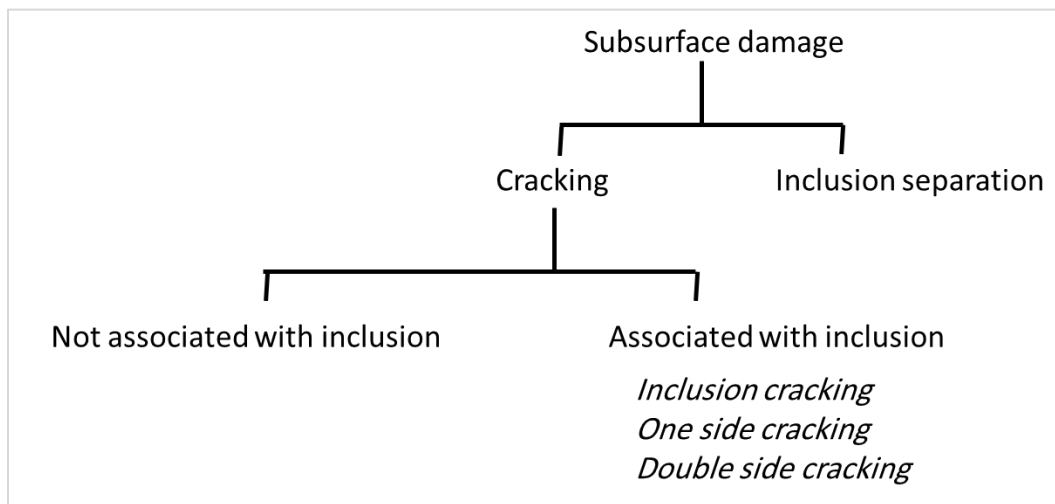


Figure 4-4: Subsurface damage types observed within the examined samples [247]

Cracks were observed as associated or non-associated with Non-Metallic Inclusions (NMIs). The cracked inclusions were also often separated from the material bulk and cracked either from the tip/s, or along its body (self-cracking). However, cracks that non-associated with inclusions were the most prevalent damage observed features—see [Figure 4-5](#). Mixed damage patterns of self-cracking, separation, and associated cracking were also observed in addition to undamaged inclusions in the vicinity of the severely damaged inclusion, as can be seen in [Figure 4-6](#). It may indicate the marginal role of NMIs in initiating the damage and that other factors are more influential. The white spots observed within the examined surface using SEM are carbides (iron saturated with carbon). These carbides are introduced through the heat treatment process and may represent a trigger of microcrack initiation [71]. Many carbides are associated with small black

spots, probably voids within the bearing material. Some researchers have considered these voids to be one of the sources of crack initiation [5]. Voids are mostly compressed and surrounded by high hardness-carbides [11][46]. Each contiguous group of voids makes it easy to connect with each other's to initiate a new crack that propagates through the nearest voids — see Figure 4-7. It is probably essential to reduce the number of carbides by improving the bearing material heat treatment and reducing the voids in the bearing bulk to prolong the bearing fatigue life.

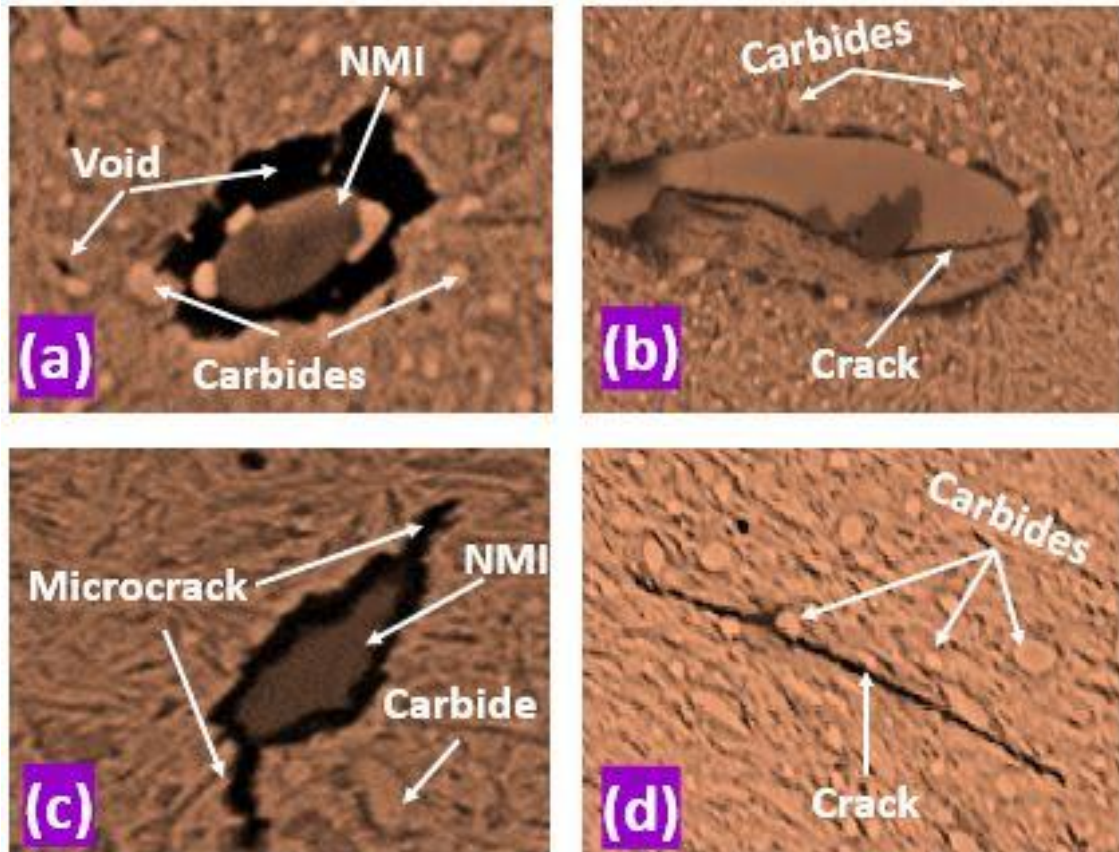


Figure 4-5: Samples of damage patterns observed, (a) non-cracked and separated inclusion; (b) self-cracking inclusion; (c) double crack associated with inclusion; and (d) crack not associated with inclusion [247]

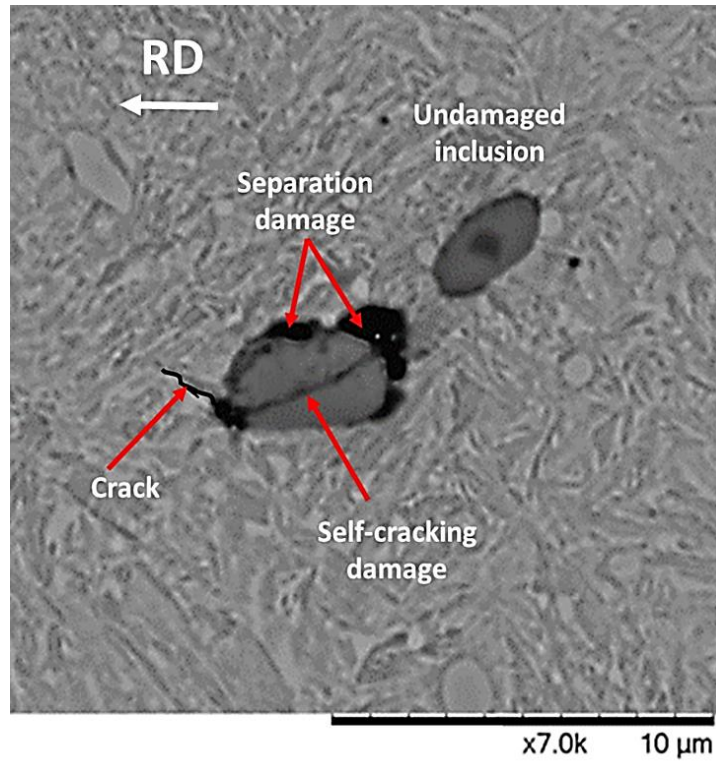


Figure 4-6: Mixed damage type associated with an inclusion [247]

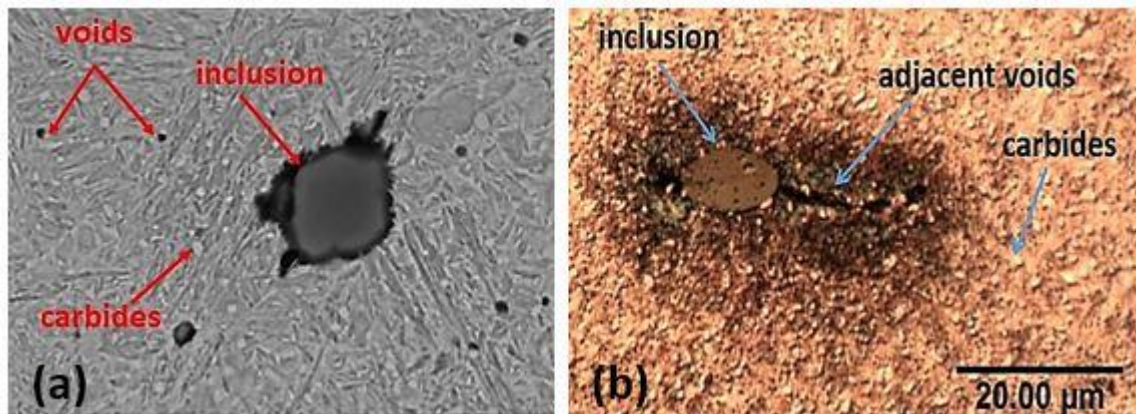


Figure 4-7: The voids and carbides impeded in the bearing subsurface region [247]

X-Ray Diffraction (XRD) is an available analysis tool in SEM to show the material components of an indicated region. This advantage has been used to analyze the misty black separated area around the inclusion, as illustrated in [Figure 4-8](#).

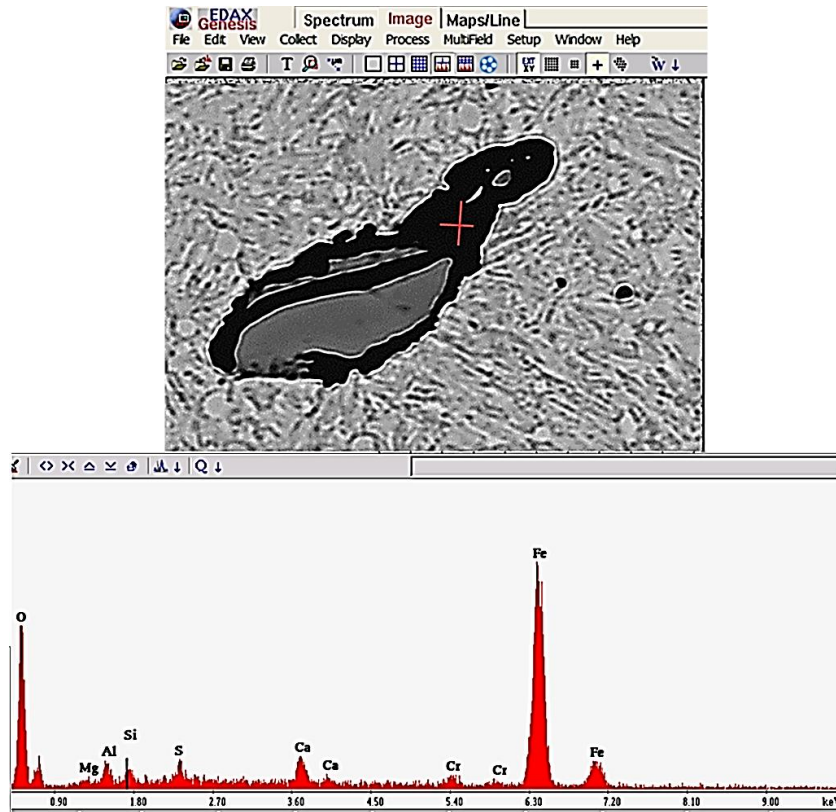


Figure 4-8: XRD analysis of separation area surround an inclusion [247]

Enlarging one inclusion ($\times 15000$) and focusing on the inclusion boundary shows that the small cracks originate very close to the inclusion boundaries and not from the inclusion body, as can be seen in Figure 4-9. There is substantial evidence that the leading initiation site of damage is not only the inclusion body itself but also the voids close to the inclusion boundaries.

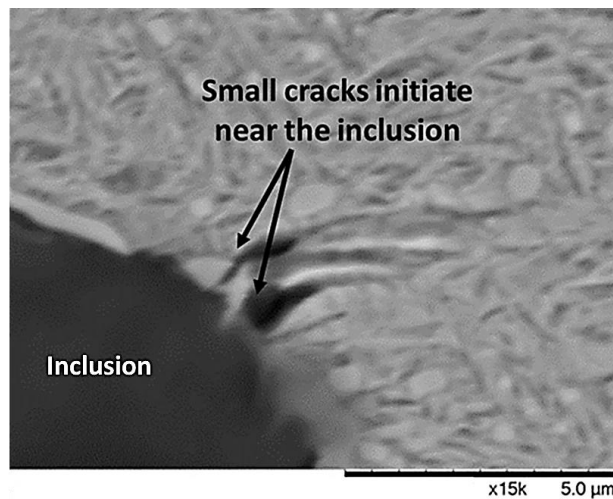


Figure 4-9: Cracks initiate close to the inclusion [247]

It was found that there were no white etching cracks (WECs) or white etching areas (WEAs) within the investigated regions. The interpretation of this result is that the formation of WECs and WEAs may follow the crack initiation. This finding refutes the hypothesis of damage initiation due to WEAs. It supports Stadler's research [248] which hypothesized that the WEAs and WECs are a consequence of the damaged region but not its cause.

4.3 Analysis of contact stresses

The contact of bodies is one of the most critical problems in mechanical engineering because the contact load produces contact stress; and leading to damage. Hertz analyzed the contact problem of two lenses under specific conditions, such as the perpendicular load between the two bodies, and there is no slipping. In addition, the dimensions of the contact region are minimal compared with the dimensions of the contact bodies [249]. Due to slight friction in the bearing (less than 5%) and the bearing radial load, Hertz's contact theory can be applied to bearings. Finite Element Analysis (FEA) revealed the stimulating effects of slipping and friction on the values and locations of the contact stresses and their distributions. This study has used this technique to predict the profile of maximum shear stress and Von-Mises stress, as illustrated in the equations (4-1) - (4-10). The subsurface damage distribution analyses were compared with the distributions of subsurface stresses. The stresses and constants were calculated according to Hertz contact theory, as can be seen in Figure 4-10, using the superposition technique to insert the effect of friction.

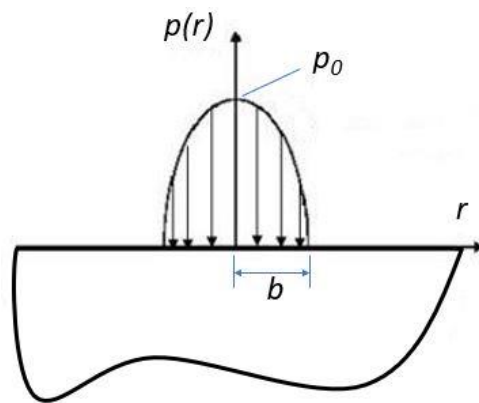


Figure 4-10: Pressure distribution based on Hertzian contact theory [the researcher]

$$p(r) = p_0 \sqrt{1 - (r/b)^2}, r < b \quad (4-1)$$

$$\delta = \frac{(1 - \nu^2)\pi}{2E} p_0 b \quad (4-2)$$

$$\mu = \frac{q(s)}{p(s)} = \frac{q_0(s)}{p_0(s)} \quad (4-3)$$

$$(\sigma_x)_q = \frac{q_0}{b} \left[n \left(2 - \frac{z^2 - m^2}{m^2 + n^2} \right) - 2x \right] \quad (4-4)$$

$$(\sigma_z)_q = -\frac{q_0}{b} n \left(\frac{m^2 - z^2}{m^2 + n^2} \right) \quad (4-5)$$

$$m^2 = \frac{1}{2} [\{(b^2 - x^2 + z^2)^2 + 4x^2 z^2\}^{0.5} + (b^2 - x^2 + z^2)] \quad (4-6)$$

$$n^2 = \frac{1}{2} [\{(b^2 - x^2 + z^2)^2 + 4x^2 z^2\}^{0.5} - (b^2 - x^2 + z^2)] \quad (4-7)$$

$$\tau_{xz} = -\frac{p_0 n}{b} \left(\frac{m^2 - z^2}{m^2 + n^2} \right) \quad (4-8)$$

$$\tau_{max} = \sqrt{\left(\frac{\sigma_x - \sigma_z}{2} \right)^2 + \tau_{xz}^2} \quad (4-9)$$

$$\sigma_{VM} = \sqrt{\frac{(\sigma_x - \sigma_y)^2 + (\sigma_y - \sigma_z)^2 + (\sigma_z - \sigma_x)^2 + 6(\tau_{xy}^2 + \tau_{yz}^2 + \tau_{zx}^2)}{2}} \quad (4-10)$$

where

r : Location in x -axis

δ : Depth at center

μ : Coefficient of friction,

q : Friction force,

p_0 : the maximum load on a roller,

m and n : Constants which were calculated depending on the contact length and the coordinates (x and z) of the point at which the calculation was performed,

z : The depth from the contact surface,

σ_x , σ_z , τ_{\max} , τ_{xz} , and σ_{VM} : The cartesian contact stresses, maximum shear, Cartesian shear stress, and Von-Mises stress, respectively.

b : Half of the Hertzian contact length.

Normalized analyses (dimensionless analyses) of stresses using Hertz contact theory represent a general case where the stress values are divided by the normal contact pressure on the contact surfaces, and the depths are divided by the contact region length. [Figure 4-11](#) presents the distribution of three stresses in the subsurface of two circular cross-sections in contact (identical to the rolling element and inner race of the bearing). The existence of traction force due to rolling element movement changes the shear stress distributions towards the rolling surface ahead of the rolling direction, as seen in [Figure 4-12](#). Only the shear stress was analyzed after introducing the traction force because the materials probably fail quickly under this type of stress. The traction force also increases the stress values in front of the vertical centerlines of the contact bodies (i.e., towards the rolling direction). However, the contact stress is reduced on the other side of the contact bodies centerlines. The traction also decreases the depth of the maximum stress, i.e., the location of the maximum stress is being nearer to the contact surface. This finding supports the results postulated in many other literatures [46][250][251][252][253]. The damage is produced due to stress; for that, stress distribution with depth can be compared with the subsurface damage distribution to predict which stress type is the leading cause of damage. The analysis of maximum stress distributions with depth under the action of contact and traction also helps in predicting the stress and traction levels at which damage may be produced, as explained in [section 4.5](#).

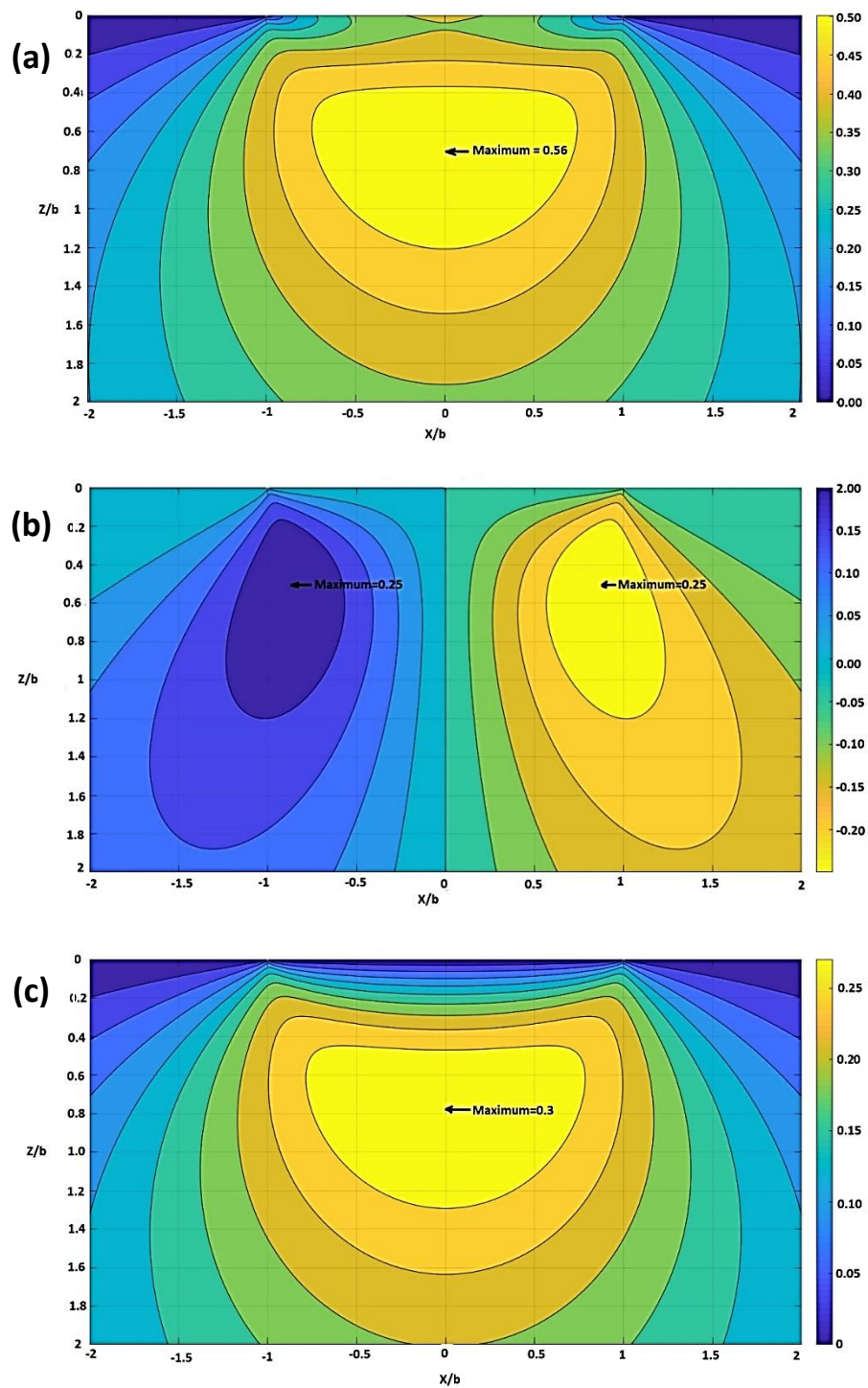


Figure 4-11: Normalized contact stresses using Hertz contact theory, (a) maximum shear; (b) Cartesian shear, and (c) Von-Mises stress [247]

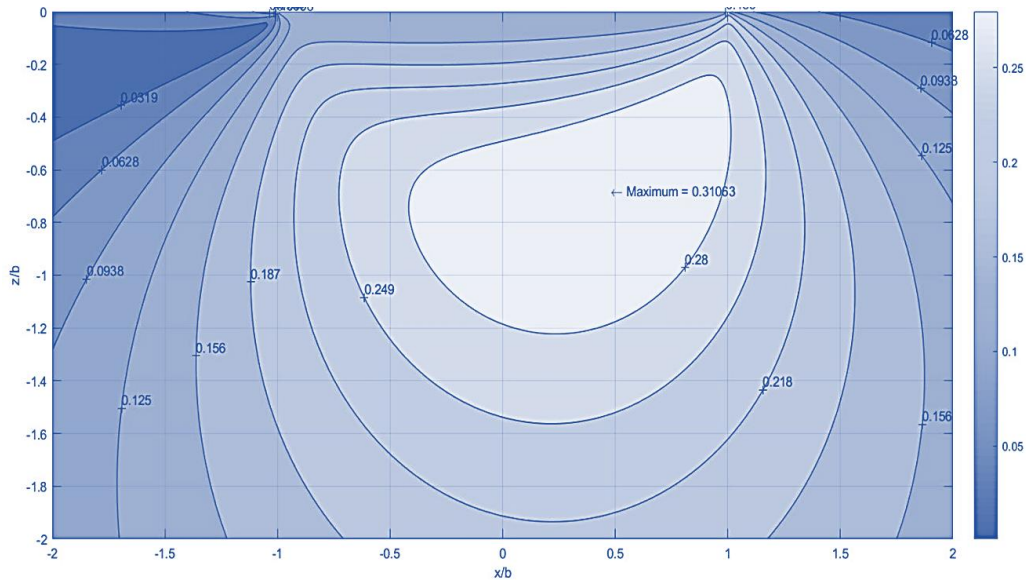


Figure 4-12: Effect of traction on subsurface maximum shear stress distribution ($\mu=0.15$) [247]

Different operating events were confirmed throughout the turbine operation, such as emergency braking, shutdown, grid connection/disconnection, and generator engagement/disengagement. In these events, the loading (torque) reverses its direction, and some severe transient loading occurs. The loading levels throughout these events depend on the turbine output power at which the event takes place. The extreme loading levels in the opposite direction may produce damage patterns that differ from the typical operating damage.

4.4 Analysis of damaged inclusions

Non-metallic inclusions are impurities in the bearing material embedded within the steel matrix throughout the manufacturing process. They were specified in much of the research as one of the most efficient sites of damage initiation in the subsurface of the bearing contact region [45][254][255]. ABAQUS software as a Finite Element Analysis (FEA) have been applied to study the stress distribution around a non-metallic inclusion region. The simulation results showed differences in stress concentration of about 250 MPa between the inclusions' bodies and their neighboring areas, as can be seen in Figure 4-13. This consequence opened the door to going in deep to investigate the role of inclusions in cracking initiation using an experimental and statistical scope of work.

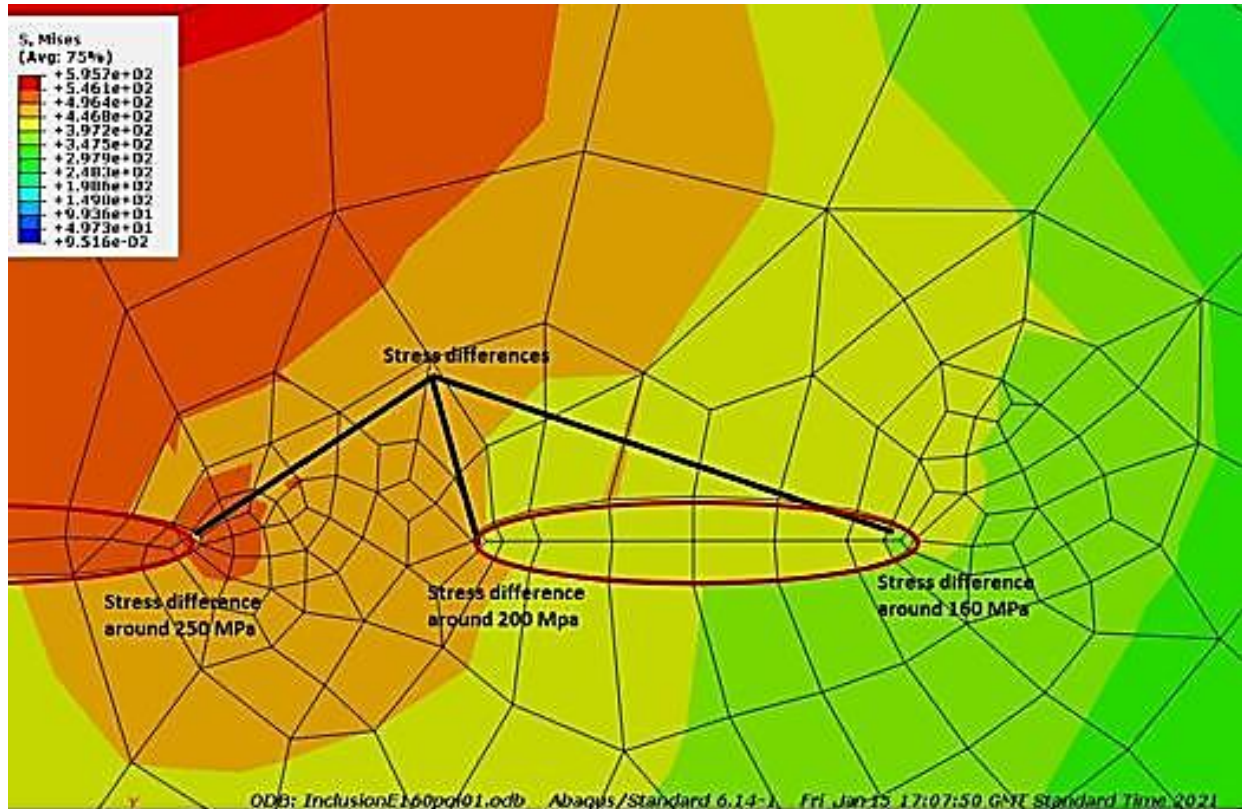


Figure 4-13: Difference in stress distribution for the non-metallic inclusions [247]

The values of inclusions' Aspect Ratios (ARs), i.e., length/width ratio, were categorized into three levels: (1-2), (2-3), and >3. It has been observed that 217 microcracks (each length < 15 μm) were associated with inclusions. That represents $\sim 15\%$ of the total 1,447 examined microcracks. The relatively low percentage of cracks associated with inclusions may indicate a more subordinate role of the non-metallic inclusions than the previous research about the cracking damage initiation. Most of the damaged inclusions were found to have an AR in the range of (1-2), as can be seen in Figure 4-14, which means that the inclusion length may not significantly affect the crack initiation.

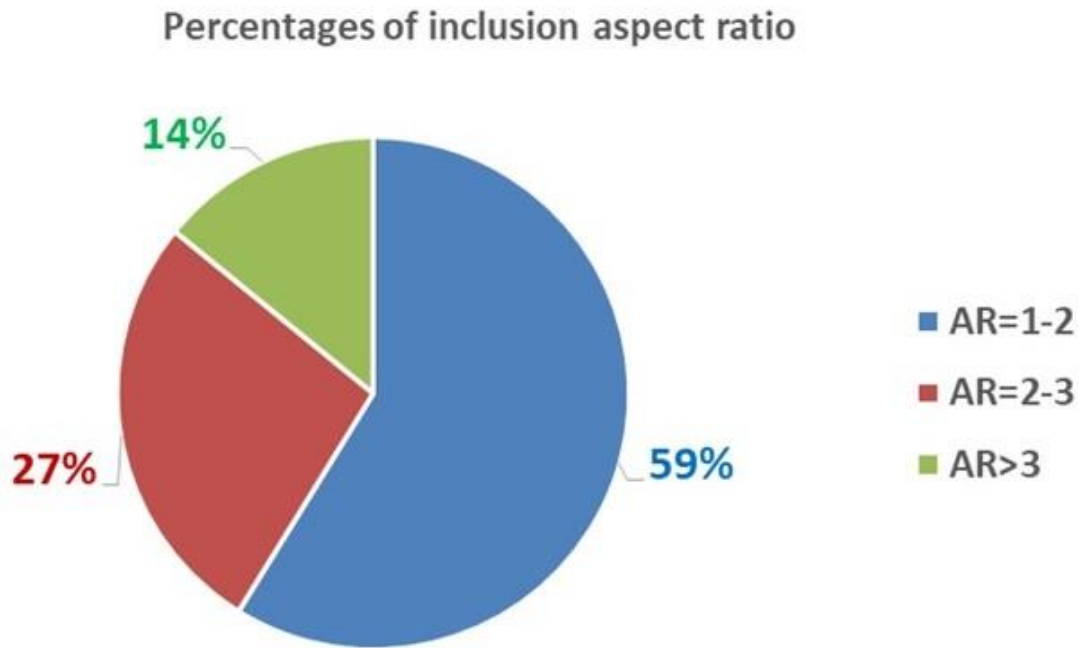


Figure 4-14: The percentages of the observed damaged inclusions and their Aspect Ratio [247]

4.5 Crack density with depth

The observed straight small microcracks (1,447 subsurface cracks) in the investigated samples were presented with their depths in [Figure 4-15](#). The same procedure of analysis has been conducted for each sample separately. The crack distribution (density) for the samples (S1 - S5) showed similar distribution patterns for the total investigated cracks, as can be seen in [Figure 4-16](#). The distribution of Von-Mises stress with depth has been calculated and presented using MATLAB software, considering the effects of increasing coefficient of friction and traction force. The maximum subsurface Von-Mises stress is located below the contact surface; however, the maximum density of small microcracks is also very close to the contact surface. The graphical profile of the cracks' density with depth ([Figure 4-16](#)) is identical to the Von-Mises stress distribution ([Figure 4-17](#)), which probably refers to the considerable role of Von-Mises stress in crack initiation. It has been concluded that the crack distribution refers to a traction force relatively higher than that presented in the previous studies [46].

The microcrack densities in shallow regions for all the investigated samples pointed out the possibility of higher contact stresses than the bearing design (and/or) a traction force more remarkable than that considered throughout the bearing design process. Re-evaluating the contact stress standard for WTGBs should match the severe operational conditions. These high contact stress levels are probably produced throughout the transient loading of the turbine operating events (braking, grid-loss, generator connection/disconnection, etc.), which should be considered throughout the bearing selection process.

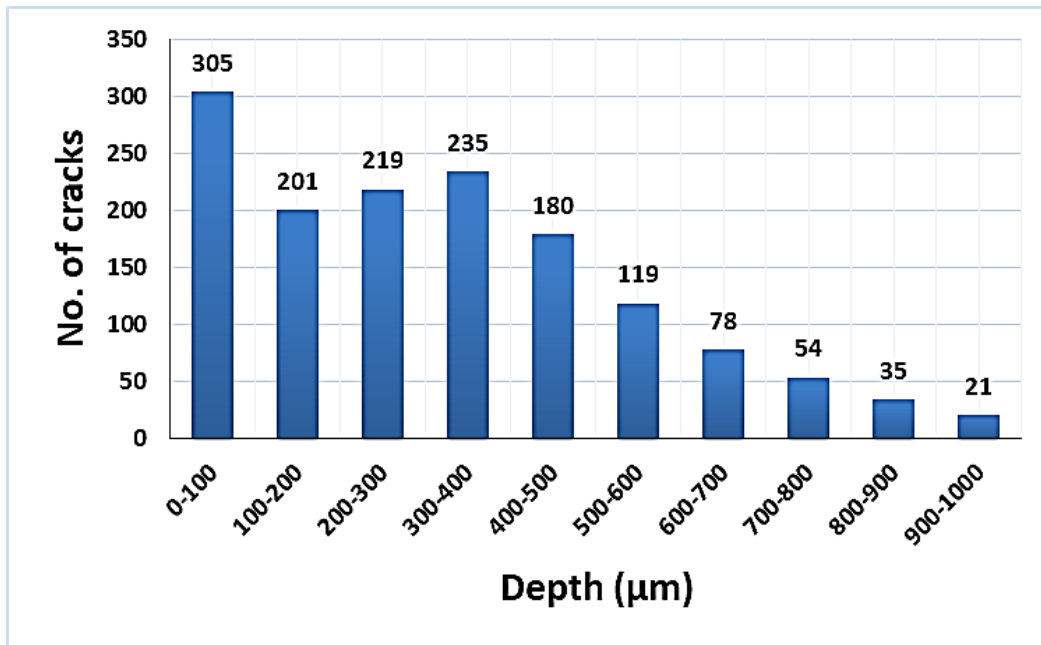


Figure 4-15: Distribution of the investigated small microcracks with depth [247]

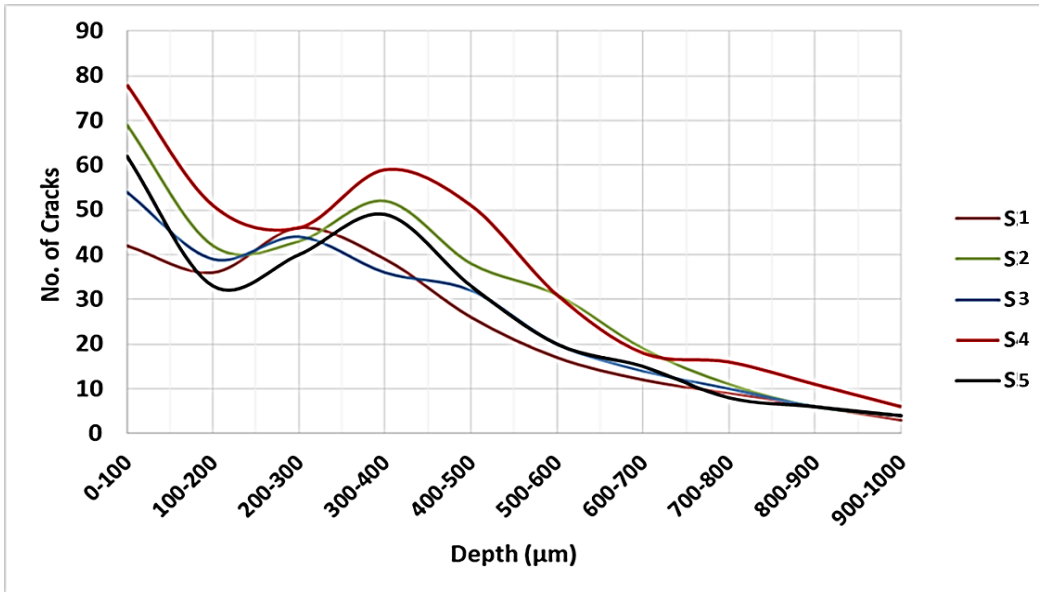


Figure 4-16: Crack density with depth of the examined samples [247]

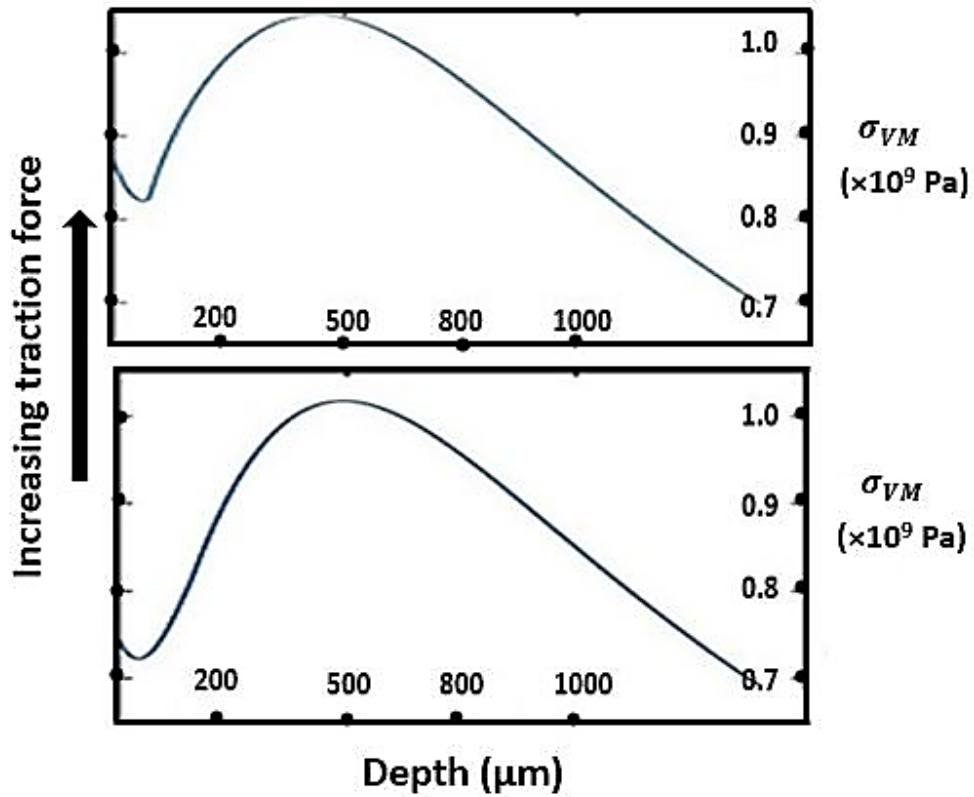


Figure 4-17: Simulating of Von-Mises stress with depth in terms of increasing the traction force [247]

4.6 Analysis of crack inclination

According to the failure theories, Von-Mises stress (σ_{VM}) or maximum principal stress (σ_1) are the possible causes of crack initiation under tensile stress [88][190]. However, under compression and shear action, maximum shear stress (τ_{max}) is also a possible cause of bearing failure and damage [182][256]. The inclination angle of a crack is not easily specified due to the change in the crack direction throughout the propagation process. Cracks of lengths smaller than 15 μm were observed to have unchangeable directions, while those longer than 15 μm propagated in many variable directions. For that, 15 μm has been considered as the limit for distinguishing large and small cracks, as can be seen in Figure 4-18. Solano-Alvarez and Bhadeshia [186] also concluded that shear stress and rolling direction affect the orientation of cracks beneath the surface.

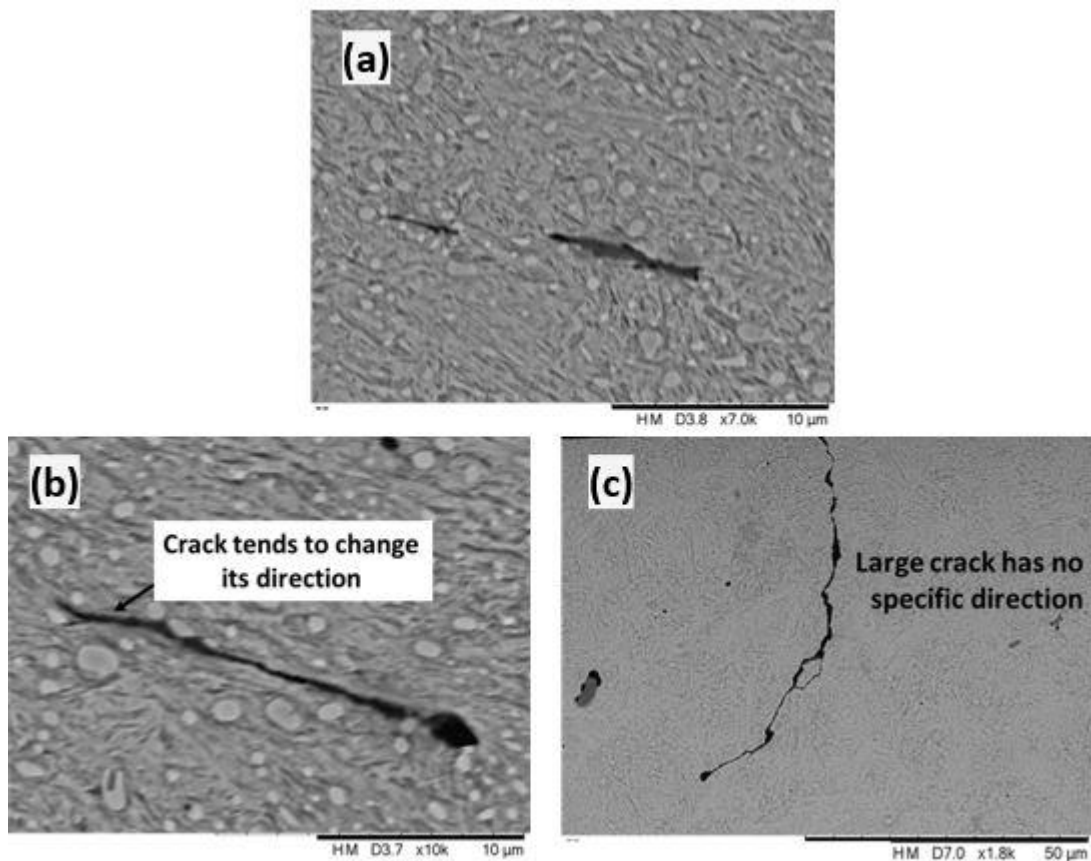


Figure 4-18: (a) Small straight cracks; (b)&(c) large kinked cracks [247]

Von-Mises stress is a resultant stress and hasn't a specific direction, while the maximum shear has a specific direction. For that, the effects of two factors (traction force and the subsurface maximum shear stress) have been studied in this section regarding their role in bearing subsurface crack initiation using the indicator of crack inclination angle. The traction force has the same bearing rolling direction, and the stress analyses showed the considerable effect of traction on both the shear stress and distribution. Thus, the crack inclination has been considered a reference for the maximum shear stress direction. The maximum shear stress under Hertzian contact has an inclination angle of ($\pm 45^\circ$) [46][71]. Accordingly, the crack angle tendency has been considered an indication for the traction role in the crack initiation due to observing the change in the crack direction close to the contact surface. Theoretically, the ideal standard coefficient of friction (μ) for the bearing contact surface is 0.05 [257]. However, surface roughness is expected to be increased during the operating conditions throughout the service. On the other hand, as the lubrication is not perfect, the friction value and hence the traction force will increase. The damaged layer of each one of the investigated samples was analyzed at a depth of 700 μm and segmented into seven subsurface layers of the same thickness (100 μm); to investigate the cracks in the bearing radial direction. [Figure 4-19](#) shows that the microcrack's inclination angles in shallower region depth of (0-100) μm tend to be approximately parallel to the contact surface. This result confirms the effect of surface traction on changing the crack initiation angle. On the other hand, cracks in the depth range of (400-600) μm have an average inclination angle of $\sim 45^\circ$, as can be seen in [Figure 4-20](#), where the effect of the traction force is significantly reduced. With increasing the contact depth, the average microcrack angles are approximately equal to the maximum shear stress angle of (45°). This finding indicates the possible role of shear stress in microcrack initiation. [Figure 4-21](#) shows the correlation of the median values of crack angles with the damaged layer depth for the investigated samples. Some microcrack angles are larger than 90° , showing the possible potential role of torque reversal throughout the wind turbine events (braking, grid-loss, generator connection/disconnection,... etc.) on crack initiation [25].

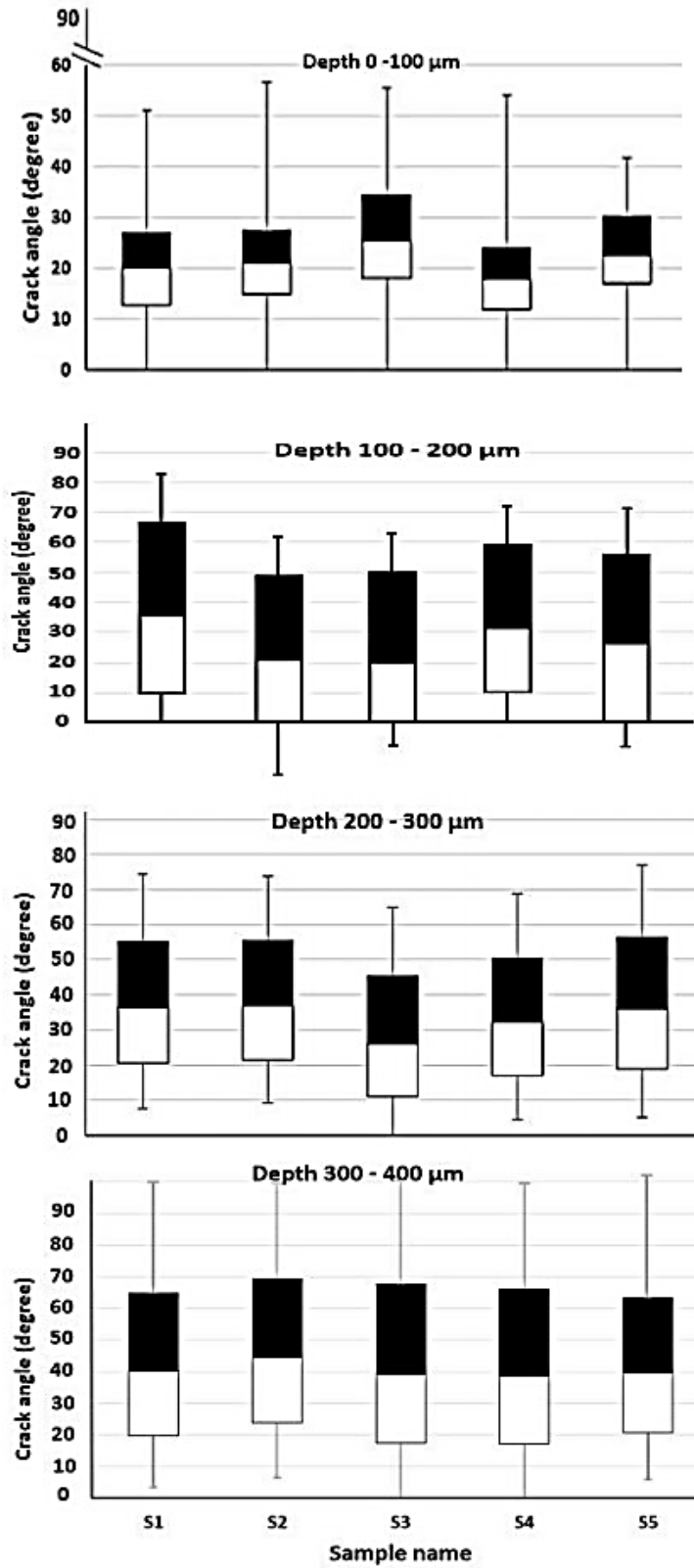


Figure 4-19 Characteristic of microcracks angles in shallow subsurface depths [247]

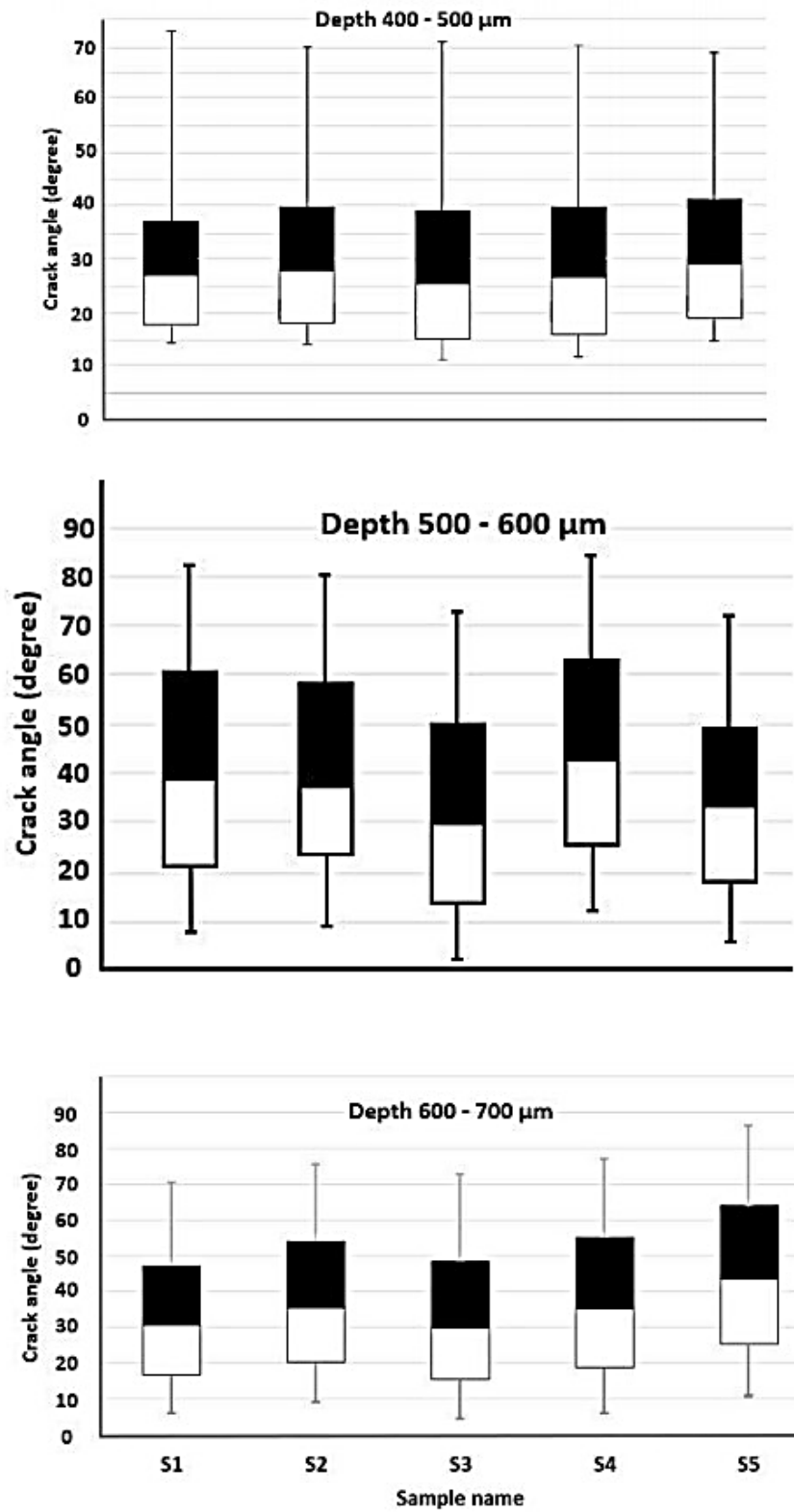


Figure 4-20: Characteristic of microcracks angles at deeper subsurface depths [247]

Figure 4-21 shows that the shear stress increases vs. depth with a high slope until reaching its maximum value, then decreases slightly. From the same figure, it can be concluded that the maximum shear stress (τ_{max}) is located in a depth range of $\sim (300\text{--}400) \mu\text{m}$, at which the cracks tend to correspond to the inclination of the maximum shear stress ($\pm 45^\circ$). On the other hand, a large number of subsurface cracks were observed in the mentioned depth, as can be seen in Figure 4-15. Based on the foregoing, it can be confirmed that there is a congruence in the results of both experimental and simulation works, and indicating to the essential role of maximum shear stress in the damage initiation.

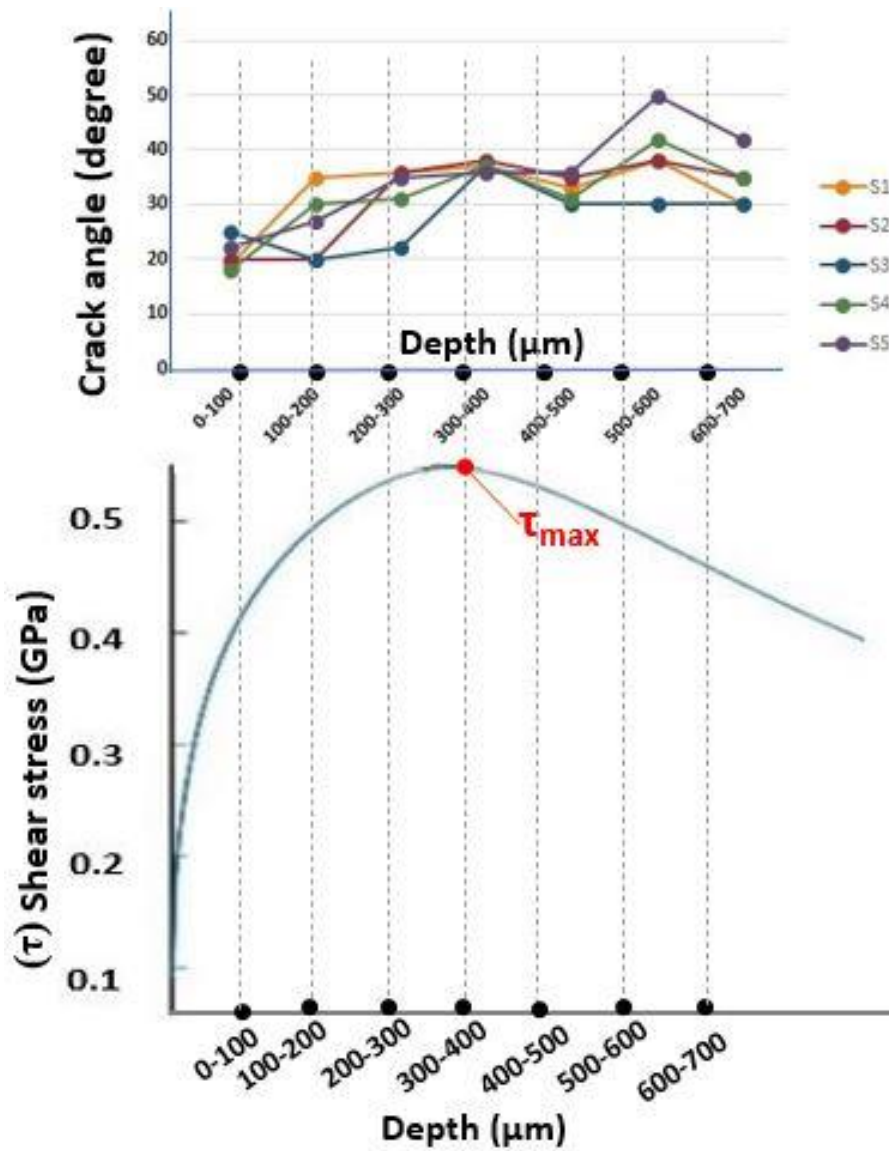


Figure 4-21: Correlation of cracks' inclination angles with depth for the investigated samples (top) and distribution of shear stress with depth (down) [247]

Two kinds of cracks can be described regarding the type of stress that causes cracks: those caused by the impact of shear stress and those caused by the principal or Von-Mises stress, creating so-called Crack Opening Displacement (COD), as can be seen in [Figure 4-22](#).

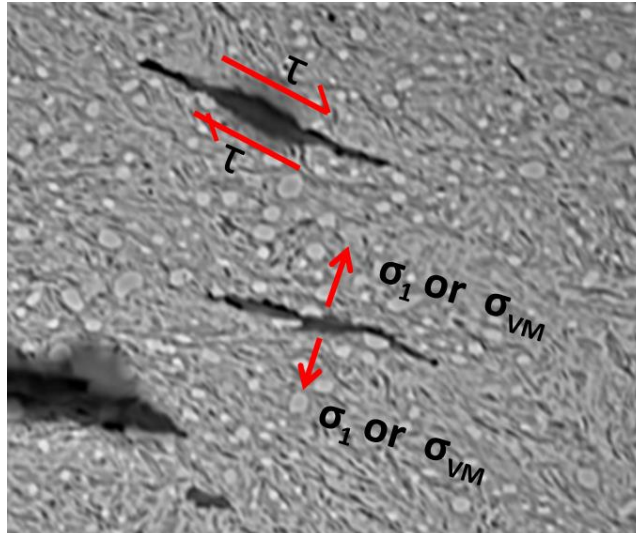


Figure 4-22: Description of cracks based on their causative stress [the researcher]

4.7 Investigation of the microstructural alterations and their triggers

Carbides and voids are the main triggers of the alterations in the microstructural objects, such as butterflies, WECs, WEAs, and DERs. For that, the investigation of both causes and effects is necessary to understand the subsurface damage of WTGB. Carbides are formed during the heat treatment process as a result of quenching, tempering, decomposition of retained austenite, and precipitation of the tempered carbides [45]. The dissolved carbon in the carbide makes it harder by \sim (30-50%) than the matrix of the bearing steel [142][143]. The metallographic investigations demonstrated that the subsurface microcracks were often not associated with non-metallic inclusions. Mostly, microcracks were observed to be initiated from the voids, which are associated with carbides. The carbides (marked in red) in [Figure 4-23\(a\)](#) are located at the embedding boundary of the inclusion with strong bonding. Microcracks (highlighted in yellow) in the same figure may be initiated due to the compressive stress of the hard carbide particle against the soft inclusion. For that, carbides are considered one of the microcracks and butterfly triggers in the

subsurface region in addition to non-metallic inclusions which have been widely reported in previous studies [84]. Carbides appeared in small size (because of the breakup of large particles) and elongated features (because of the compression stress), as seen in [Figure 4-23\(b\)](#). Voids are black spots initiated during the manufacturing and heat treatment processes, or they may be formed as gaps due to the de-bonding process of NMIs from the steel bulk. Several black spots, that locate inside and at inclusions' boundaries are oxides, but not voids as resulted from the metallographic and microstructural investigation. Cracks associated with voids may be observed to be surrounded by carbides, as seen in [Figure 4-23\(c\)](#). In contrast, voids without carbides seem to resist cracking. This is because of the hard feature of the carbide particles, which may initiate cracks around the voids. In the case of severe loading, these contiguous voids may form cracks by connecting to each other's. Voids are observed to produce butterflies in addition to NMIs. Voids near inclusions have two effects: initiating microcracks, especially if these voids are located in their tips, and de-bonding the inclusions from their matrix, as illustrated by Solano et al. [148].

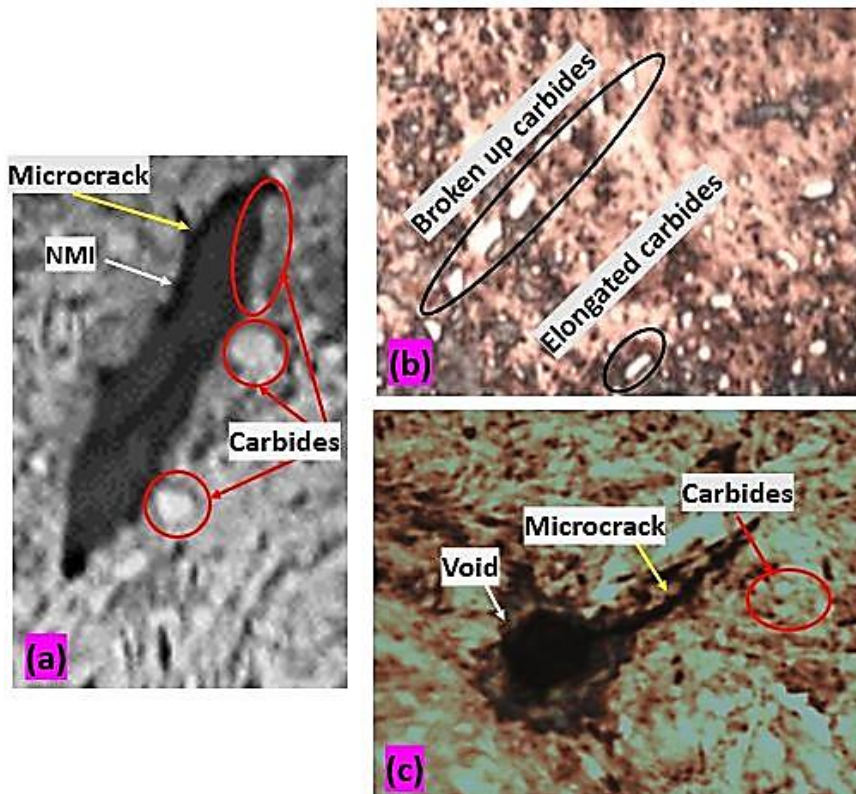


Figure 4-23: The behaviour of carbides and voids as microstructural alteration triggers [the researcher]

As illustrated in (section 3.2.4), a butterfly feature is typically a central NMI with wing/s forming a butterfly aspect in the subsurface zone (~ 1-1.5 mm beneath the contact surface), as seen in Figure 4-24(a). However, a number of butterflies were observed with dispersed nucleus, as seen in Figure 4-24(b). Mostly, the appearance of butterflies was observed in the highly localized (cyclic) shear stresses, induced during RCF. In the case of increasing the over-rolling, both the butterflies' formation frequency and the zone size in which they are generated will increase. Based on the microscopic investigations, it has been observed that the butterflies' lengths and inclinations vary with their depths (from the contact surface) in terms of the orthogonal shear stress distribution. For that, two factors may indicate the butterflies' features: the over-rolling cycles and the contact load. The pervasions of carbides and voids around the butterflies may indicate their likely initiation cause. Microscopic investigations did not show WEAs, WECs, and DERs because their formation may occur at a high level of contact pressure stress and fatigue cycles. This result supports the hypothesis that WEC, WEAs, and DERs may be formed as a result of the development of butterfly features as white networks due to the extension of multiple linking [71][84].

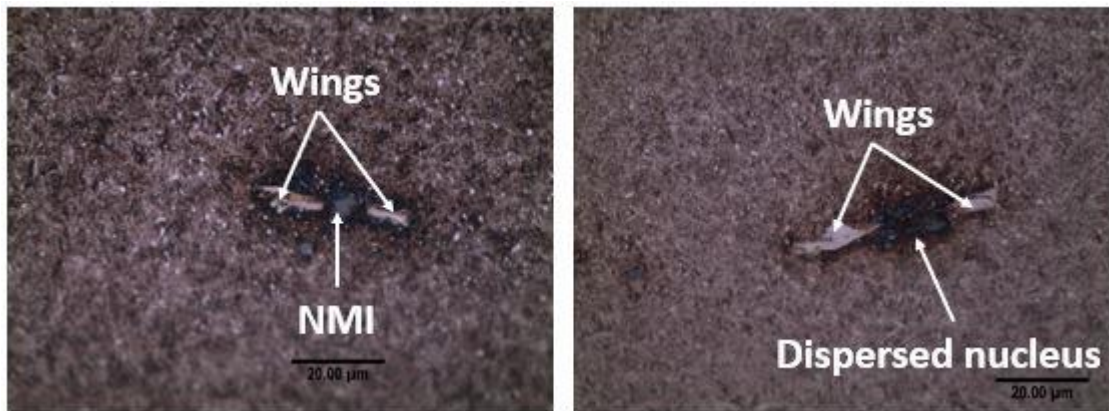


Figure 4-24: Butterfly feature (a) with a central NMI, (b) with a dispersed nucleus [the researcher]

4.8 The surface investigation related to subsurface damage

The damage initiation source has more than one opinion, the more popular one is that the damage initiates from the subsurface regions and propagates toward the surface. However, the opinion of initiating the damage from the surface and propagating to the subsurface is also considered. Which opinion is the right one is a debatable issue. Alicona surface analyzer has the ability to take images with great accuracy to show the topography of the surface before and after the damage to link the surface and subsurface damage analyses to predict the damage initiation site. [Figure 4-25](#) shows an example of the Alicona output analyses. Enlarging the surface damage initiation region shows that, the surface damage initiates at the roller contact edge. However, the damaged patches were not straight and this confirms the misalignment and for skewing of the roller contact throughout the bearing service. This surface damage pattern also confirms the stress concentration at the roller edge in spite of the modern techniques used in the roller profile design to avoid the stress concentration issue, as can be seen in [Figure 4-26](#).

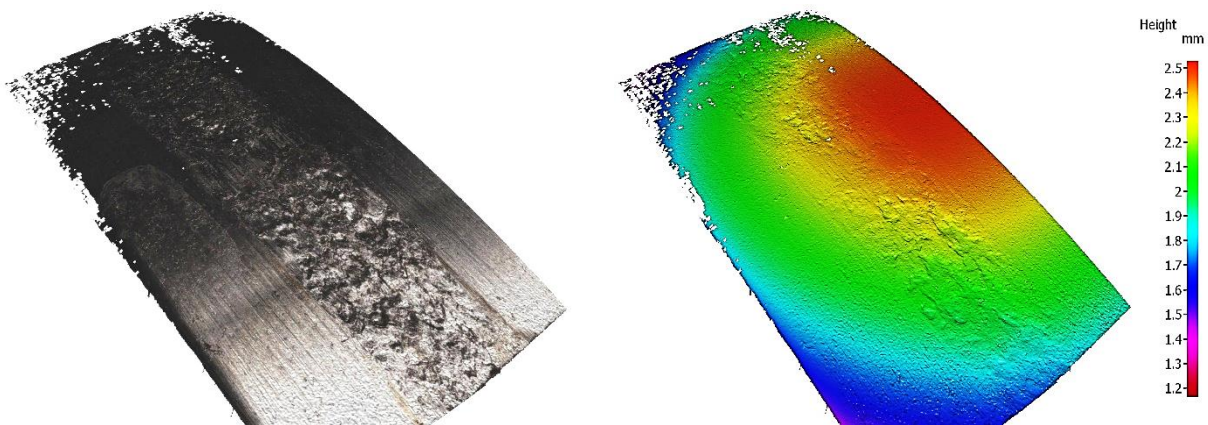


Figure 4-25: Surface damage analysing using Alicona analyser [the researcher]

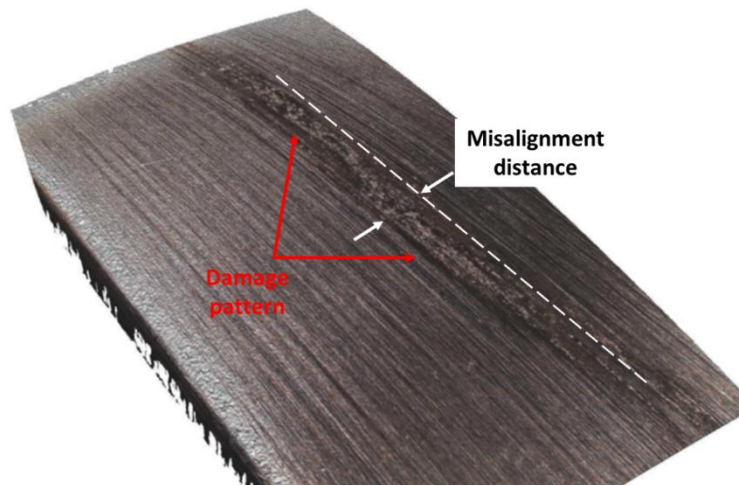


Figure 4-26: Surface damage initiation pattern [the researcher]

5

CHAPTER FIVE: SELECTING THE MOST EFFICIENT WTGB TYPE USING ANALYTICAL HIERARCHY PROCESS METHOD (AHP)

Referring to [Figure 2-7](#), it has been observed that the operating conditions of wind turbines dictated the presence of two different stress distribution patterns in the gearbox bearing: the loading and non-loading zones. In addition, the experimental and simulation results that were observed in chapter 4, as shown in [Figure 4-13](#) confirmed that the subsurface stress concentration of the inner race bearing has exceeded the standard values. Wherefore, the study of this chapter relied on selecting the optimal bearing type in terms of multi-criteria. The Analytic Hierarchy Process (AHP) is one of the most valuable methods of the Multiple Criteria Decision-Making (MCDM) approaches for selecting the optimal choice among different alternatives concerning various criteria. The comparison process was applied using the Expert Choice (EC) software tool after introducing its three structural elements: goal, criteria, and options.

5.1 Multiple Criteria Decision-Making (MCDM)

MCDM considers contradictory points of view and uses the decision-maker tools to solve complex decision problems dynamically [258]. It is a consistent family of criteria F and a set of actions, variations, or solutions A , which has eight steps, as can be seen in Figure 5-1. The Analytic Hierarchy Process (AHP) is the most common method among several decision-making methods. AHP will be used in this research to determine the most efficient bearing option among multiple types of wind turbine gearbox bearings, considering different criteria and solutions [259].

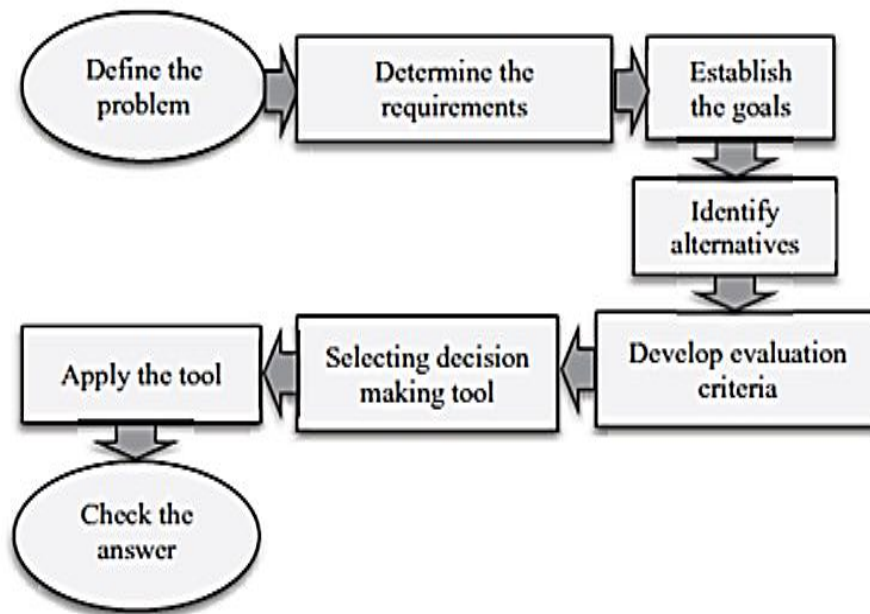


Figure 5-1: Flowchart of the general decision-making process [259]

5.1.1 Analytic Hierarchy Process (AHP)

The Analytic Hierarchy Process (AHP)—was introduced by Saaty (1977). He edited more than 30 books on this topic. More than 900 books, scientific work papers, and Ph.D. theses deal with this method. It is an effective tool, which helps the decision maker to make the best compromise decision. A series of pairwise comparison matrices for reducing complex decisions, followed by synthesis of the results. In addition, AHP captures the criteria and alternatives of the problem and indicates the degree of decision-maker constituency. As a result, the bias in the process of decision-making would be reduced. The weighting criteria of AHP are judgmental and based on the preference of the decision-maker. It can be clearly noted that in subjective problems,

the accuracy of this method can be considerably varied [259]. The AHP algorithm is an important element for investigating the consistency level. When the Consistency Index (CI) is calculated, the preferential information given by the Decision Maker (DM) will be very consistent.

5.1.2 Expert Choice (EC) software

Expert Choice (EC) software is a tool to find a compromise decision for a multi-criteria problem. Saaty and Forman created this methodology in 1983 to implement the Analytic Hierarchy Process (AHP). It has been used in different fields, such as manufacturing, agriculture, environmental management, and shipbuilding. EC solutions combine proven mathematical techniques and collaborative tools to enable the team to obtain the best decision in reaching a goal. Using AHP tools to structure the complexity and measure the competing objectives with alternatives according to the degree of importance. AHP and EC have the following steps:

- Structure a hierarchical Model;
- Pairwise comparison of the criteria and sub-criteria according to their importance in the decision concerning the main goals of the study;
- Pairwise comparison for the alternatives concerning the criteria. The alternatives assessment is one of the following tools: entering the priorities, utility curves, or rate function; and
- Performing the sensitivity analysis after synthesizing to determine the best alternative.

The starting point is the objectives; then, it moves to the main criteria and sub-criteria to select the best solution. The decomposition sequence starts from the top to the bottom of the hierarchy structure problem. Pairwise comparisons help determining the relative importance of each alternative in terms of each criterion. The value for each pairwise comparison represents the decision-maker's judgment. [Table 5-1](#) displays the importance levels on a scale from 1 to 9 [260].

The following steps describe the use of EC software: -

- Start up the EC program,
- Create a new model and describe the goal of the work,
- Choose the display mode (for example, tree mode), then input the main criteria. For each main criterion, input their sub-criteria (if available),
- Build up the comparison matrixes for (main criteria with each other, sub-criteria with each other) by activating (pairwise order from edit list),

- Input the available alternatives (variants) and build up the comparison matrixes for (each variant with criteria and sub-criteria) by activating (pairwise order from the assessment list), and
- Find the results from (the sensitivity graphic) list.

Note that: the number of all comparison matrixes = $A + B + C$

where

A: number of criteria

B: number of sub criteria groups

C: SUM of (sub criteria units + criteria units that have not sub criteria).

Table 5-1: Scale of Relative Importance [261]

Intensity of Importance	Definition	Explanation
1	importance is equal	two activities having the same contributions to the objective
3	importance is weak of one activity over another	experience and judgment are slightly favoring one activity over another
5	importance is strong or essential activity	judgment experience is strongly favor one activity over another
7	importance is demonstrated	an activity is strongly favored, and its dominance has been demonstrated in practice
9	importance is an absolute	the evidence of one activity is favoring over another has the highest order of affirmation
2,4,6,8 reciprocals of above nonzero	in-between values judgments if the activity (i) has nonzero numbers assigned to it throughout comparing with activity (j), then the later when compared with (i) has the reciprocal value.	it needs for compromising

5.2 Problem modelling

The decision problem has been hierarchically modeled as a part of the decision problem structure. Goals, criteria, and alternatives should be related to the model, as can be seen in Figure 5-2. The three levels are set up in a hierarchy, the first structure step in the AHP process method.

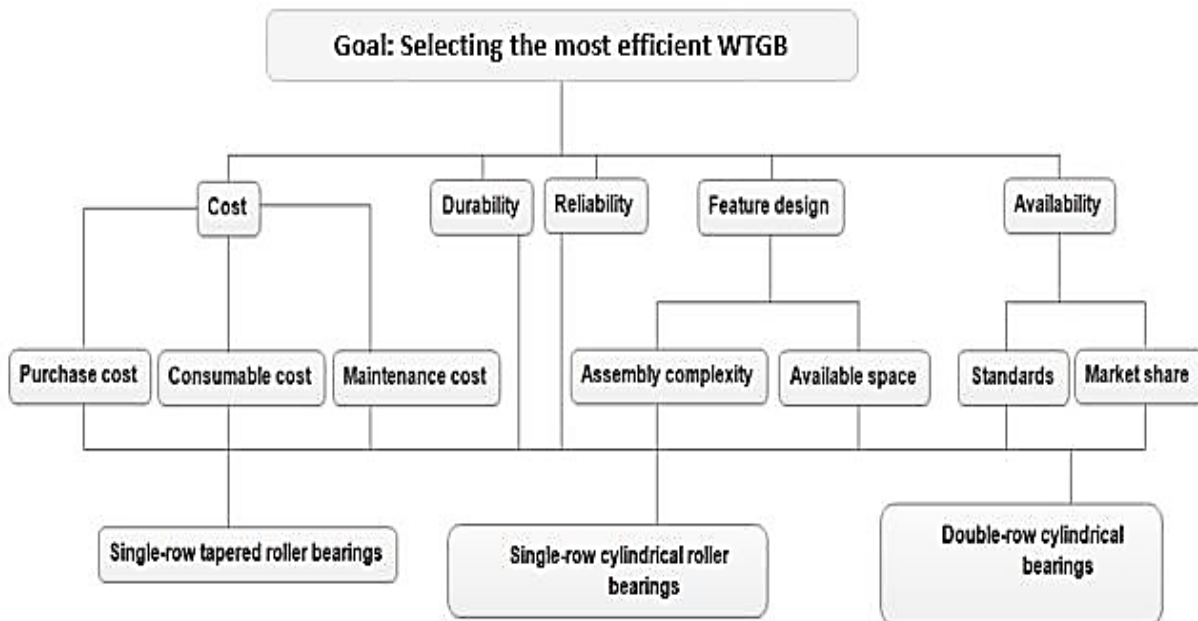


Figure 5-2: AHP structure of selecting the most efficient wind turbine gearbox bearing [262]

5.2.1 Variants (Alternatives)

The following bearing types have been introduced as variants in the applying of EC software tool: -

- 1- **Single-Row Tapered Roller Bearings (SRTTB)**: This bearing type can take high radial and axial loads in a single direction. They are designed to withstand combined loads, i.e., simultaneous-acting radial and axial loadings. The projection lines of the raceways meet to provide a proper rolling action at the location of the common point on the bearing axis so that the friction moment is low during the operation. By increasing the value of the contact angle α , the tapered roller bearing's axial load capacity increases consequently. The contact

angle is about (10° – 30°), as can be seen in [Figure 5-3](#). The optimized roller end design promotes lubricant film thickness, reducing friction, wear, and frictional heat. The bearings can run at reduced noise levels and better maintain preload.

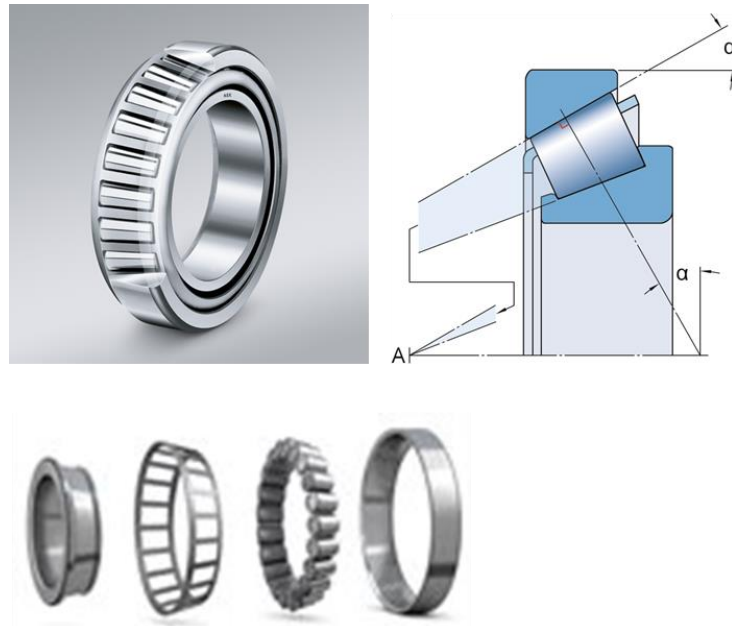


Figure 5-3: Tapered roller bearing, α : contact angle [263]

- 2- Single-Row Cylindrical Roller Bearing (SRCRB):** It has a large area of contact with the inner race. They can distribute loads across a broader surface. As a result, these bearings are suitable for high speeds, a high radial load capacity, and low friction [264]. As the load is distributed over a larger contact area, the bearing can carry a more significant load, as can be seen in [Figure 5-4\(a\)](#).
- 3- Double-Row Cylindrical Roller Bearing (DRCRB):** This type has high radial rigidity. The difference with single-row bearings is that they have two sets of inner and outer rings with two sets of rollers and cages. As their magnified strength, enhanced carrying capacity, and increased accuracy, the type is used in precision machines because of their magnified strength, as can be seen in [Figure 5-4\(b\)](#).

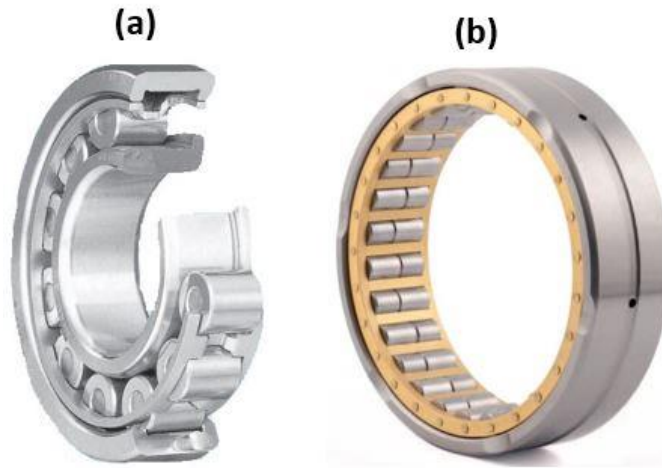


Figure 5-4: (a) Single-row cylindrical roller bearing [265] , (b) Double-row cylindrical roller bearings [266]

5.2.2 Criteria (Objectives)

Before listing the main recommended criteria to select the suitable bearing of wind turbine gearbox, it has been assumed that all the presented variants belonged to the same manufacturer under the same grade of the following criteria: cost, durability, reliability, feature of design, and existence or availability.

1- Cost: This criterion includes the initial purchase, consumables, and replacement maintenance costs of wind turbine gearbox bearing.

a) Initial purchase cost: it depends on many factors, like the manufacturing brand, bearing design, and repetition of failure. Failure Mode and Effects Analysis (FMEA) helps identifying potential failure modes by considering previous experience with similar products or the logic of common failure mechanisms. It enables the team to characterize those failures with minimum effort, reducing development costs and time. The sum of all expenses could calculate the total cost during its lifespan. As a result, the overall costs are divided into three groups: total manufacturing, capital, and Operation and Maintenance (O&M) [267].

b) Consumable cost: WTGBs have been subjected to high friction, especially at the high-speed stages, which increases the temperature. As a result, a high-quality, specific lubricant has to be used for this purpose. In addition to lubricant cost, the consumable

cost of WTGB includes the overall cost of bearing fittings. However, each type of bearing requires a specific grade of consumables at various costs.

c) Maintenance cost: Due to premature failure of WTGB within 2–5 years of operation, especially for offshore WT. Maintenance costs are mainly related to the replacement technique, which varies according to the bearing type.

2- Durability: The rating life indicates the life of the bearing calculated for 90% reliability. It is a predicted value based on a rated dynamic radial (or axial) loading. It gives the amount of time that a group of apparently identical. It can be considered a primary representation of the bearing's suitability. According to the British Standards (BS ISO 281:2007) [128], the base rating life can be calculated for radial and thrust ball and roller bearings.

3- Existence / Availability: It includes two parameters (availability of standards & market share) as follows: -

a) Availability of standards: Bearings are manufactured and tested using standards developed by various societies and associations. The most familiar standards are American National Standards Institute, International Organization for Standardization, and Antifriction Bearing Manufacturers Association. If the presented design has not matched the mentioned standards and is not available in terms of standardization criteria, it will minimize the critical value of the bearing.

b) Market share: As the required bearings are more specific, there is a significant disparity in their market share. Sometimes, there is a need to buy a customized bearing for more specific conditions. In urgent cases, it is so important to find the required suitable bearing within a short period, which directly relates to their availability in the market.

5.3 Pairwise comparison and synthesizing of analysis

The following notes should be taken into consideration to realize the matrix analysis, which has been illustrated in the [Figures 5-5 - 5-17](#): -

- 1-The comparison scale has graduated from (0-9),
- 2-The red number means that the row element is more important than the column element by the value of that number and vice versa if the number is black,
- 3-Do not consider the yellow rectangular, as it is a pointer location.
- 4-The consistency index (CI) value indicates the logical degree of the comparison process. The more logical comparison is the nearest value to (0.0). It should not exceed (1.0), i.e., the acceptable range of CI is $(0.0 < CI < 1.0)$. As a result, all pairwise comparison results for the mentioned figures seemed logical,
- 5-All comparison values were indicated according to the decision maker's requirements concerning the primary goal of the problem.

5.4 Discussion of results

The overall comparison matrixes are classified into three types as follows:

- [Figure 5-5](#) shows the comparison matrix for the main criteria concerning goals, which applies the hierarchical model structure illustrated in [Figure 5-2](#). It is reported in the cited matrix that reliability is more important than cost by 4.0 of 9.0,
- [Figures \(5-6\),\(5-7\), & \(5-8\)](#) show the comparison matrices for the sub-criteria to their main criteria.
- [Figures \(5-9\) – \(5-17\)](#) show the comparison matrices for the variants with the main and sub-criteria elements. If the main criteria have sub-criteria elements' branches, the pairwise comparison of variants should be done concerning to each sub-criteria element but not with their main criteria. For example, [Figure 5-14](#) shows that the single-row cylindrical roller bearing is 3.0 grades better than the double-row cylindrical roller bearing in terms of comparison based on the sub-criteria element (purchase cost).

- Figure 5-18 shows that the comparison process is fully complete. Each group (main criteria, sub-criteria, and variants) has a summation of 1.000.
- Figures (5-19)-(5-23) illustrate that the final results can be synthesized by applying the sensitivity graphs. It has been emphasized that the optimum compromise solution is a single-row tapered bearing. The resultant overall cost of single-row tapered and single-row cylindrical bearings has convergent values but is higher than that of double-row bearings.

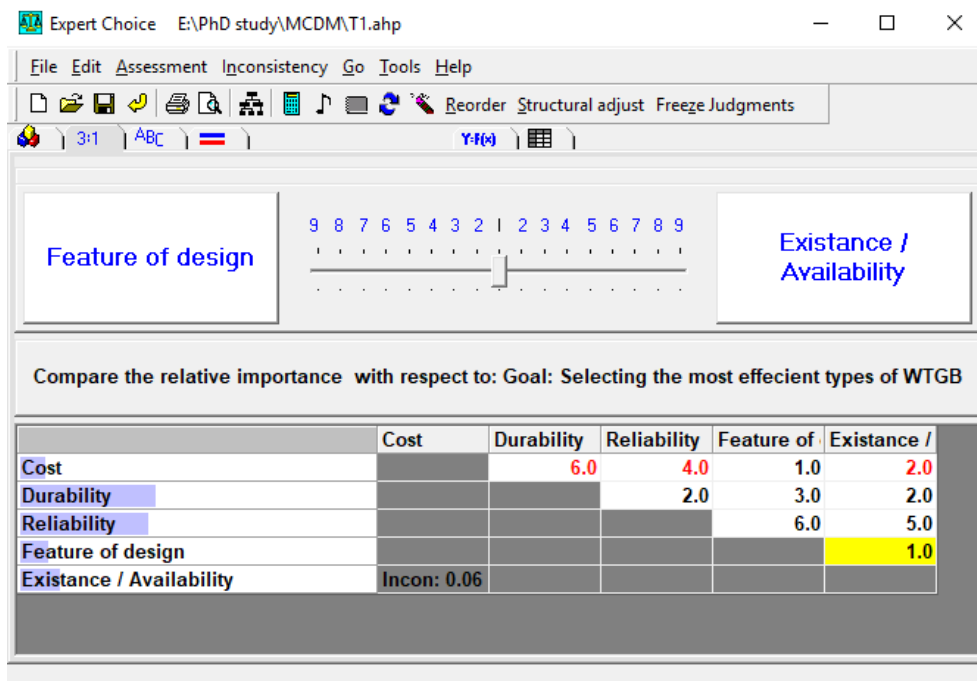


Figure 5-5: Pairwise comparison of the main criteria with respect to the goal [262]

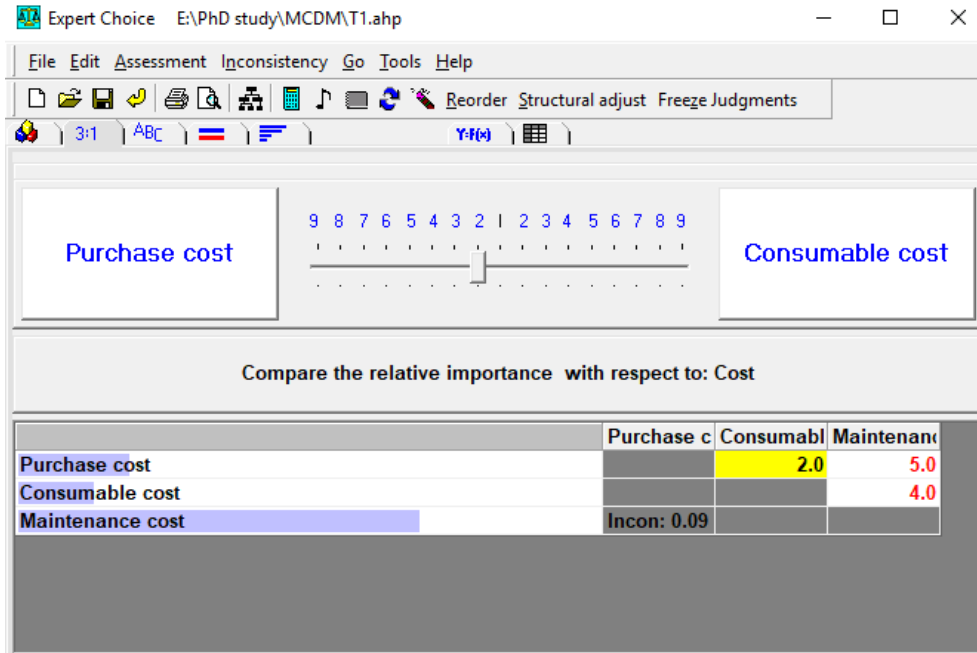


Figure 5-6: Pairwise comparison of the cost sub-criteria with respect to the goal [262]

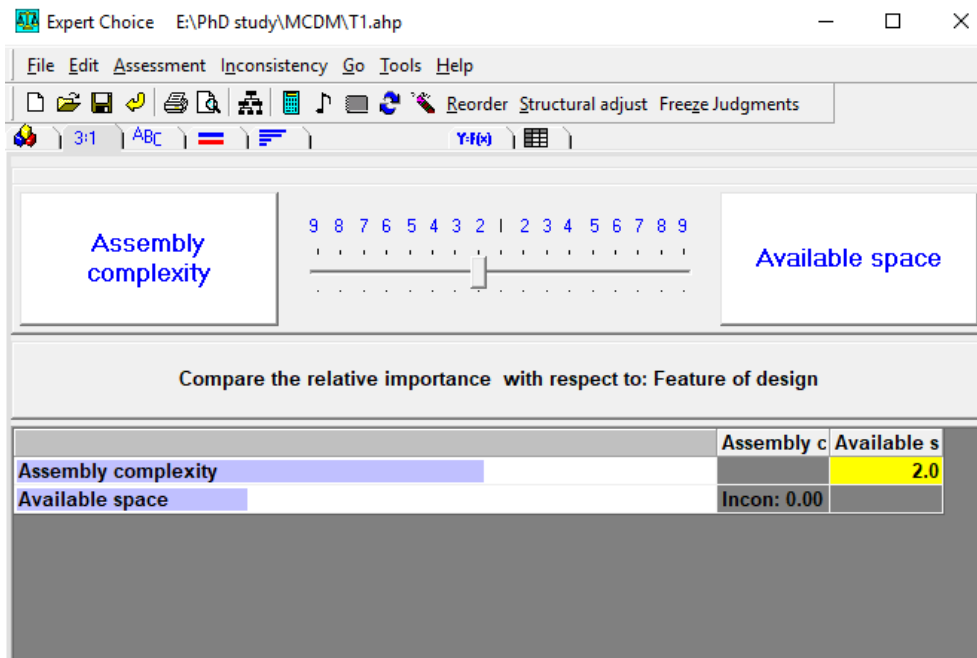


Figure 5-7: Pairwise comparison of the feature design sub-criteria with respect to the goal [262]

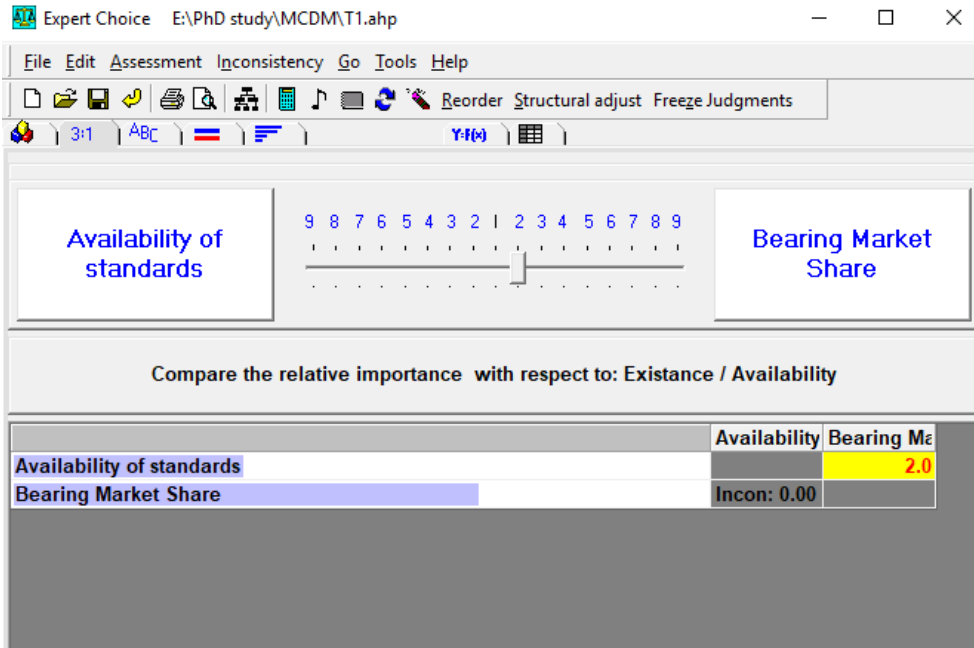


Figure 5-8: Pairwise comparison of the availability sub-criteria with respect to the goal [262]

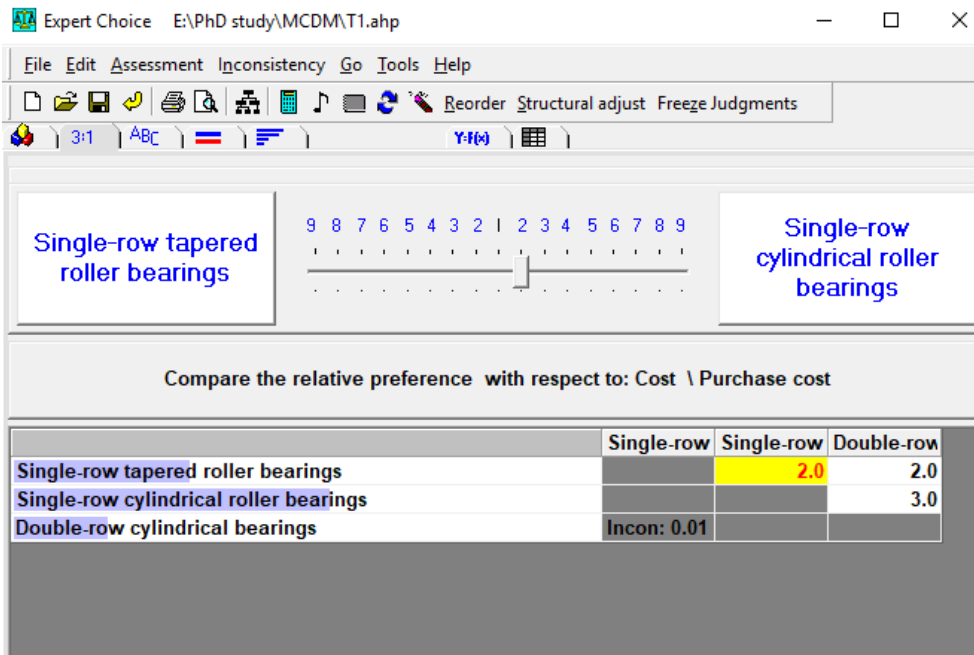


Figure 5-9: Pairwise comparison of the options with respect to the purchase cost [262]

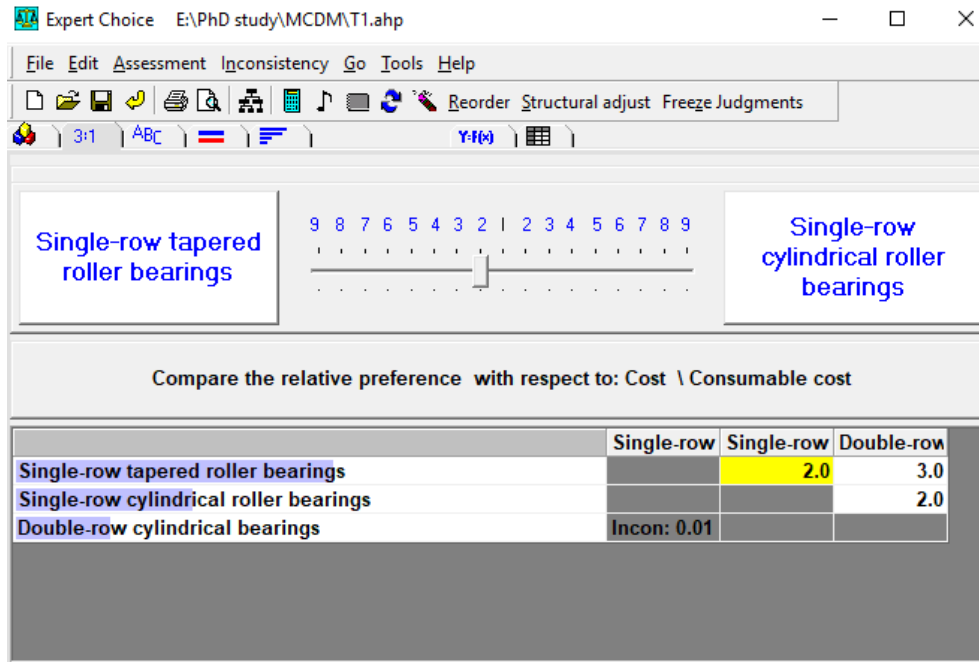


Figure 5-10: Pairwise comparison of the options with respect to consumable cost [262]

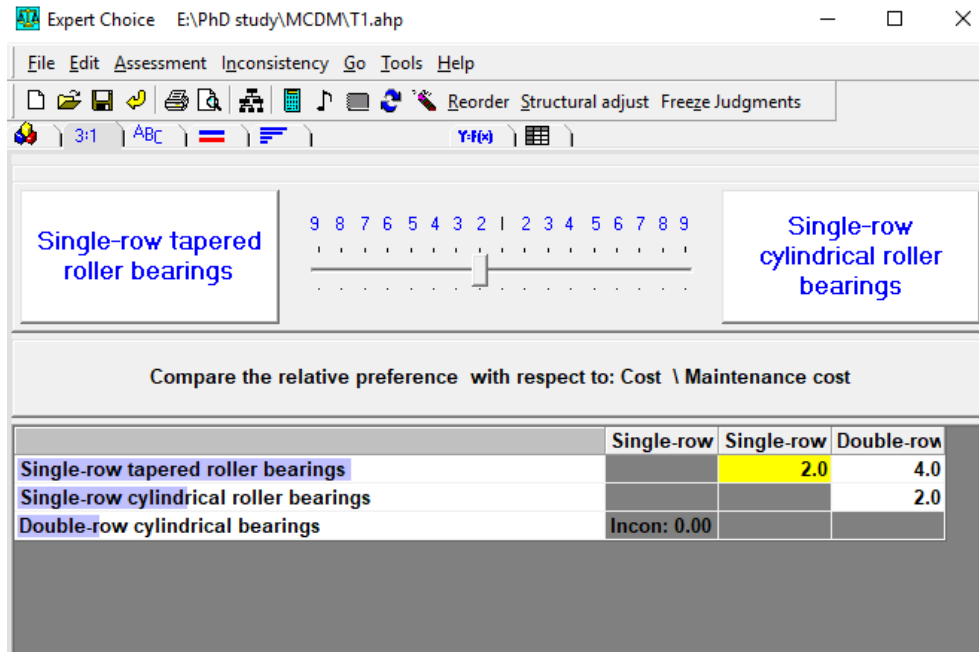


Figure 5-11: Pairwise comparison of the options with respect to maintenance cost [262]

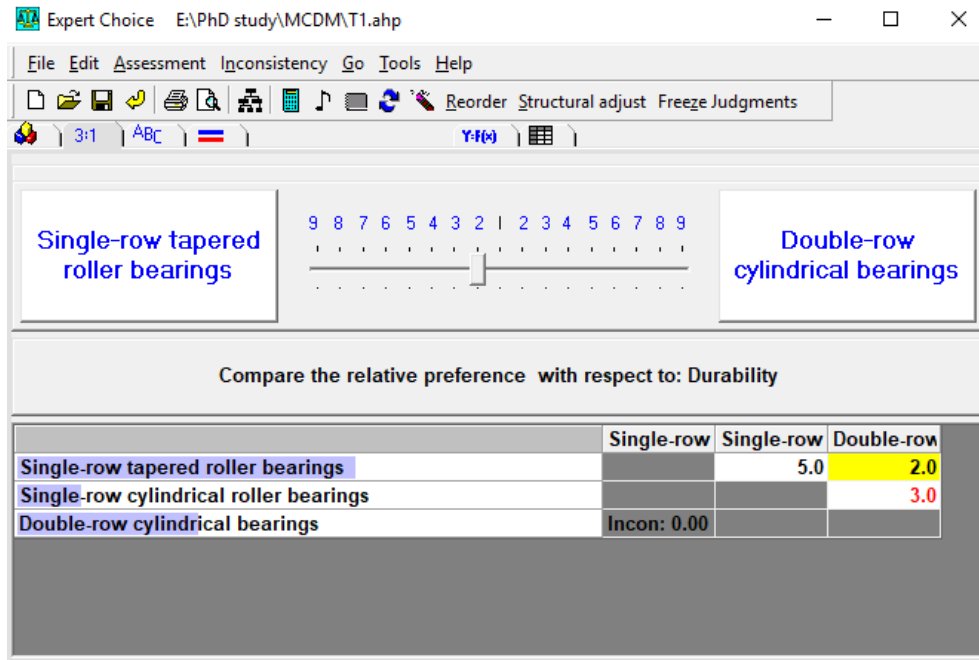


Figure 5-12: Pairwise comparison of the options with respect to the durability [262]

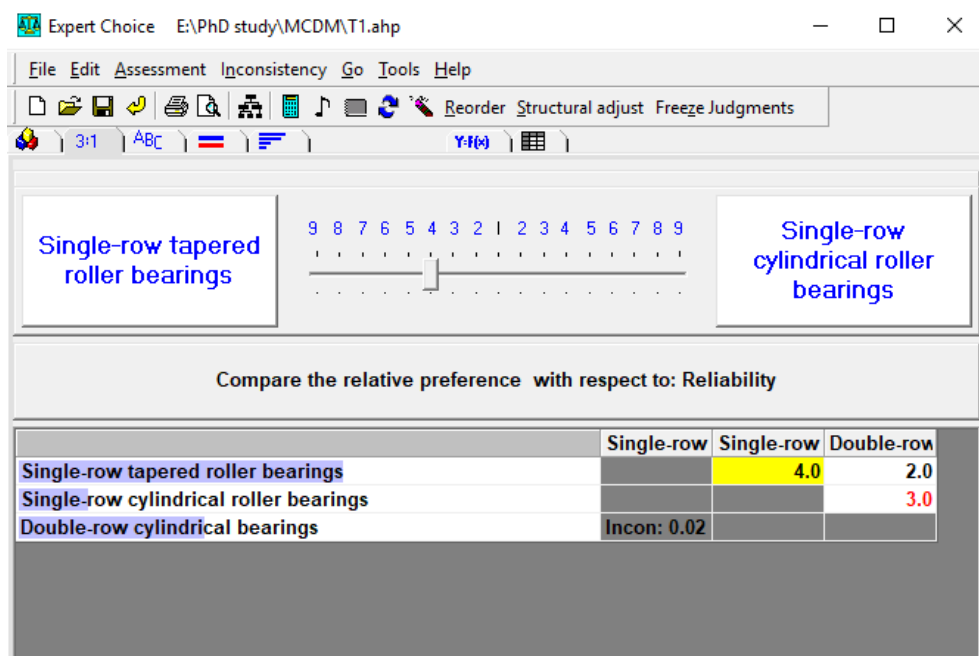


Figure 5-13: Pairwise comparison of the options with respect to the reliability [262]

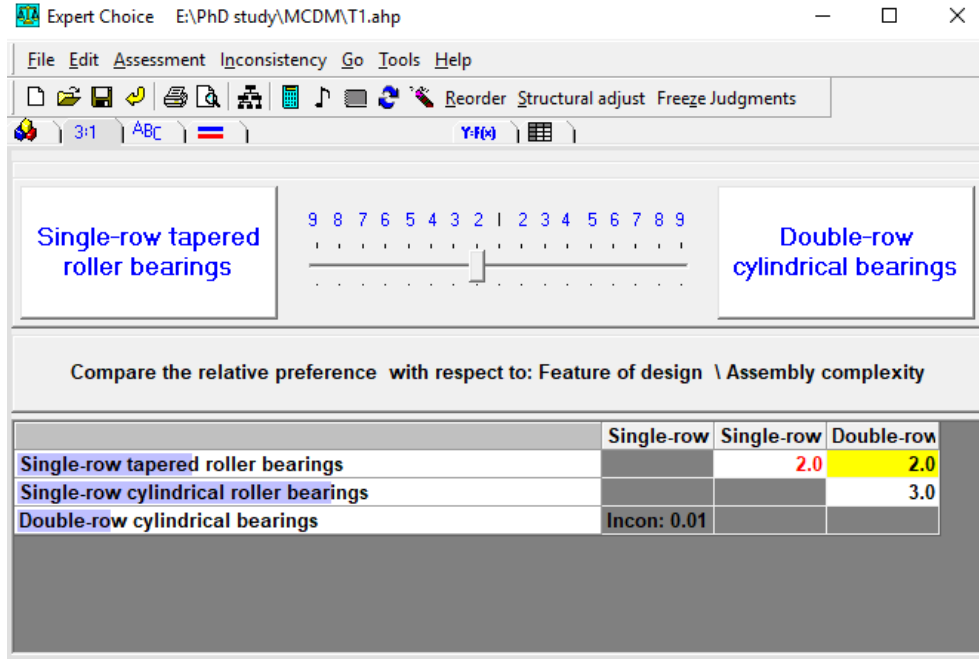


Figure 5-14: Pairwise comparison of the options with respect to assembly complexity [262]

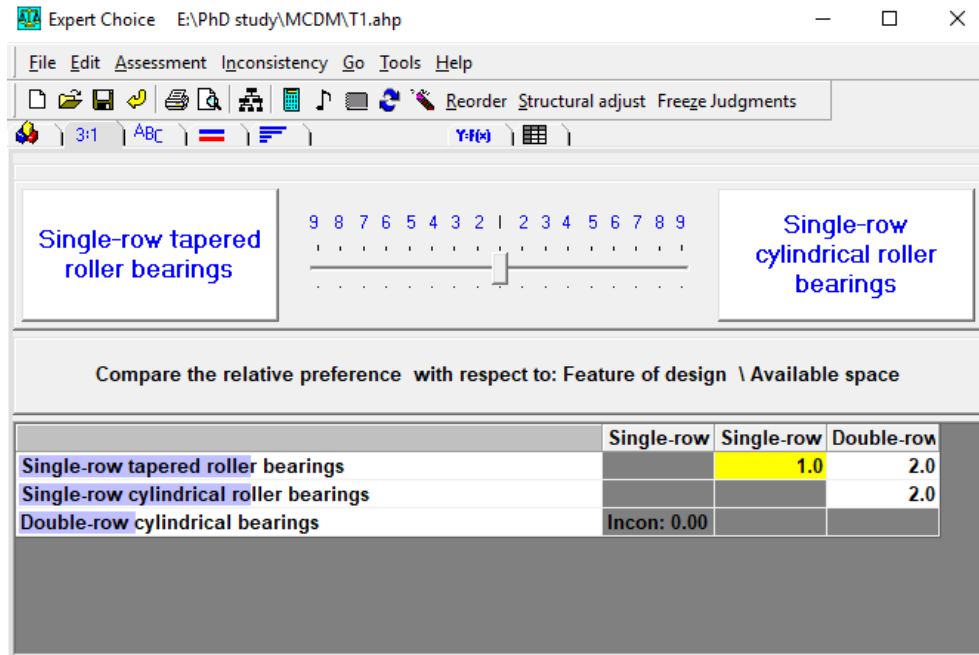


Figure 5-15: Pairwise comparison of the options with respect to the available space [262]

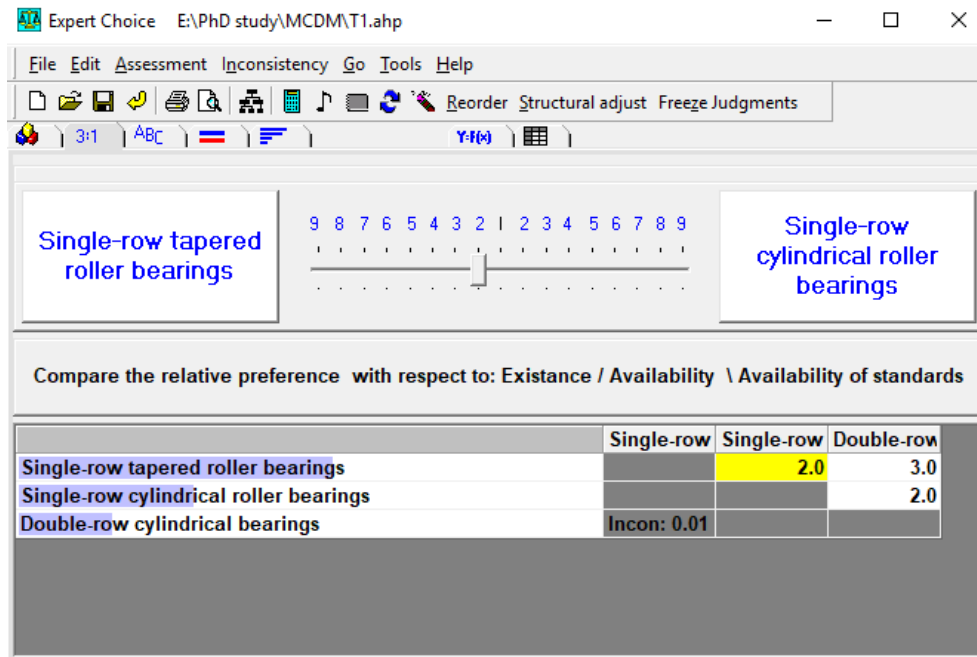


Figure 5-16: Pairwise comparison of the options with respect to availability of standards [262]

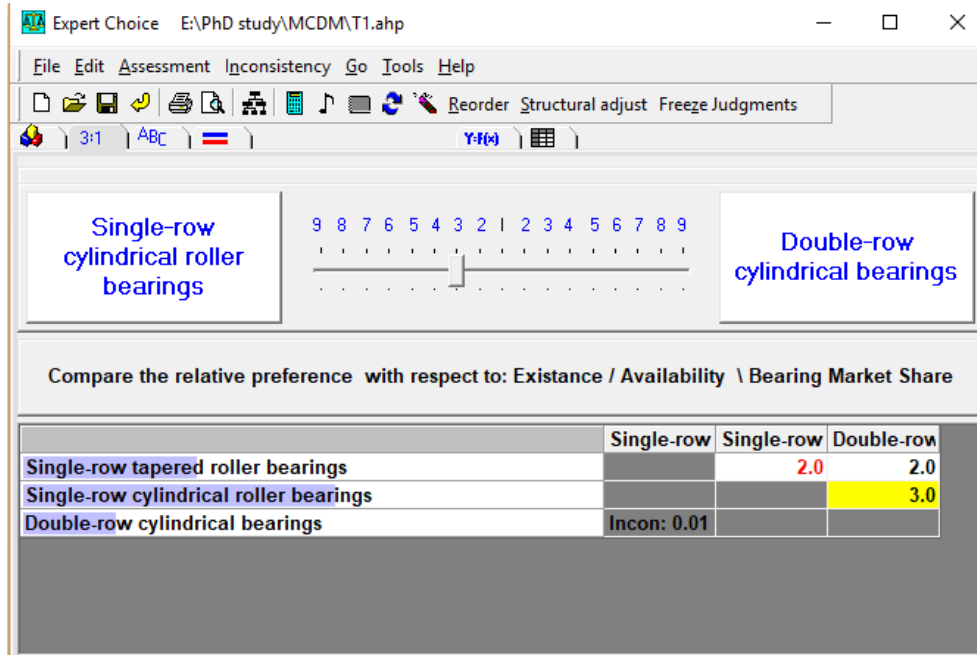


Figure 5-17: Pairwise comparison of the options with respect to bearing market share [262]

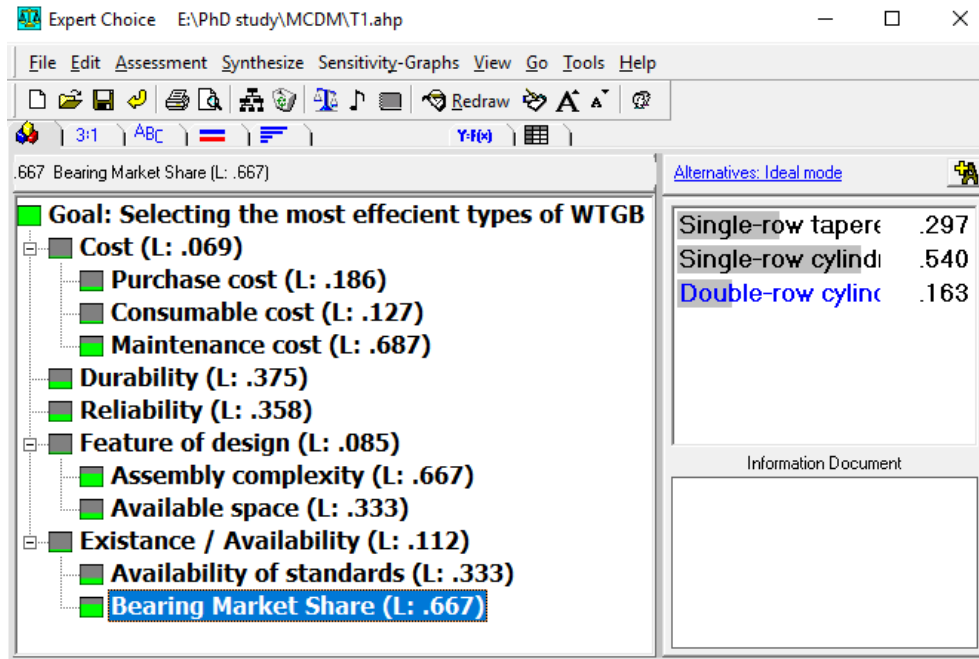


Figure 5-18: Completion of pairwise comparison [262]

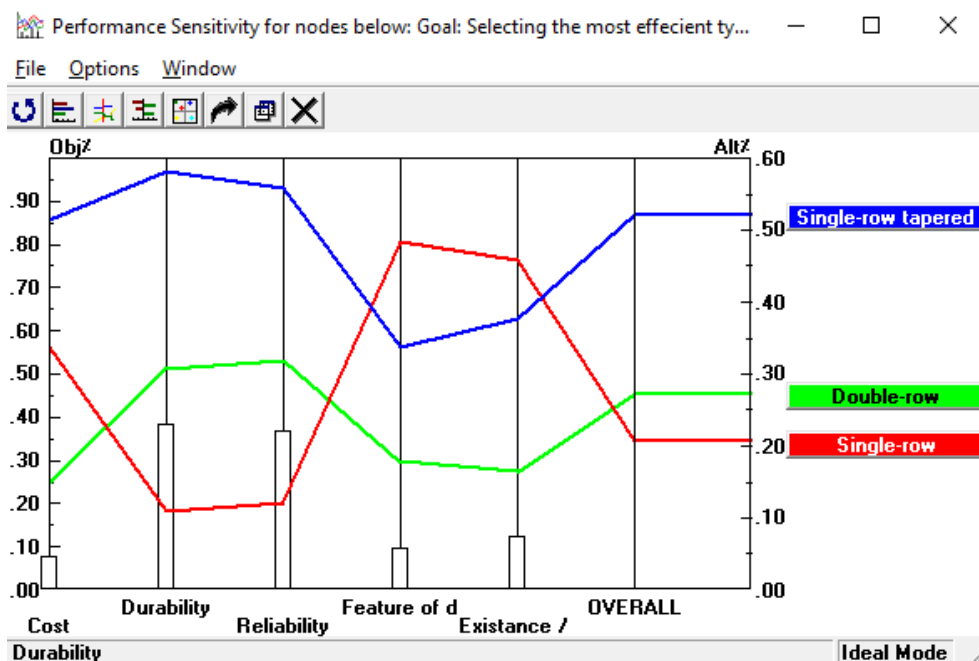


Figure 5-19: Performance sensitivity - selecting the most efficient option [262]

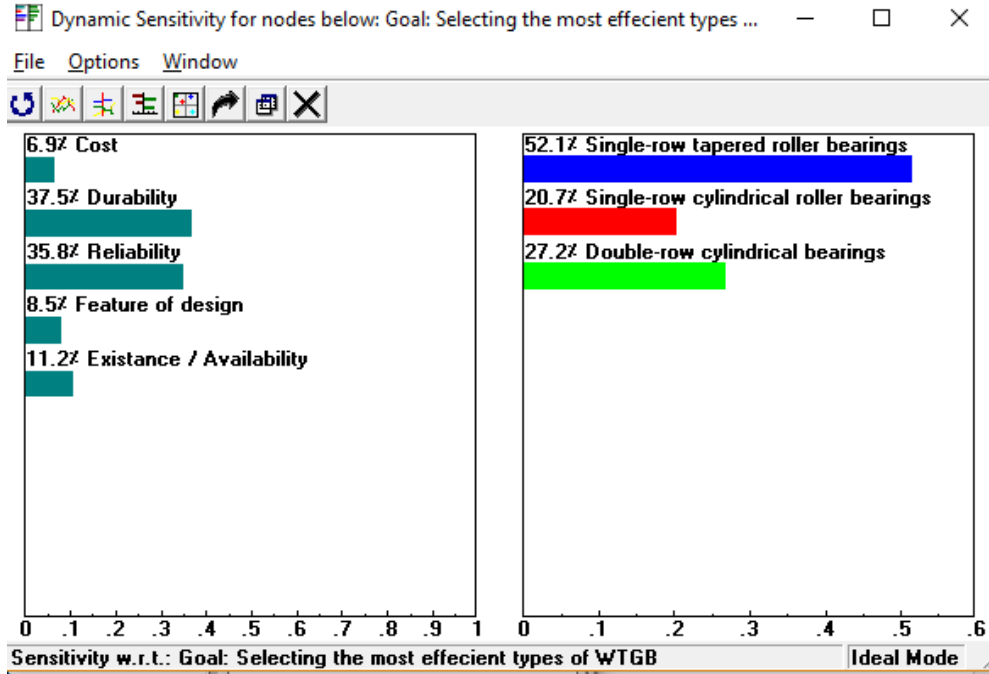


Figure 5-20: Dynamic sensitivity - selecting the most efficient option [262]

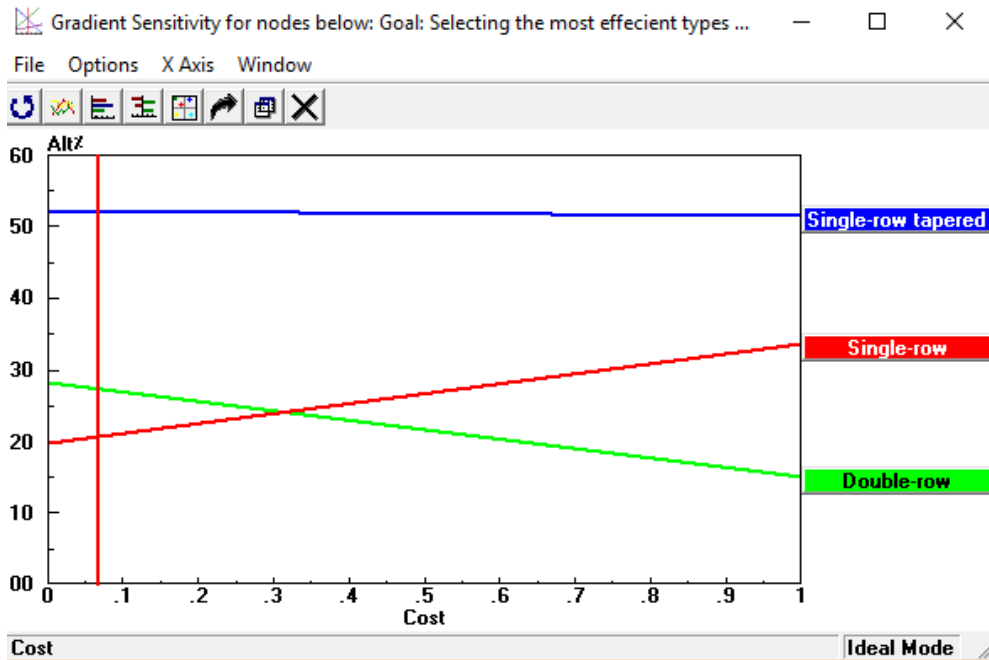


Figure 5-21: Gradient sensitivity - selecting the most efficient option [262]

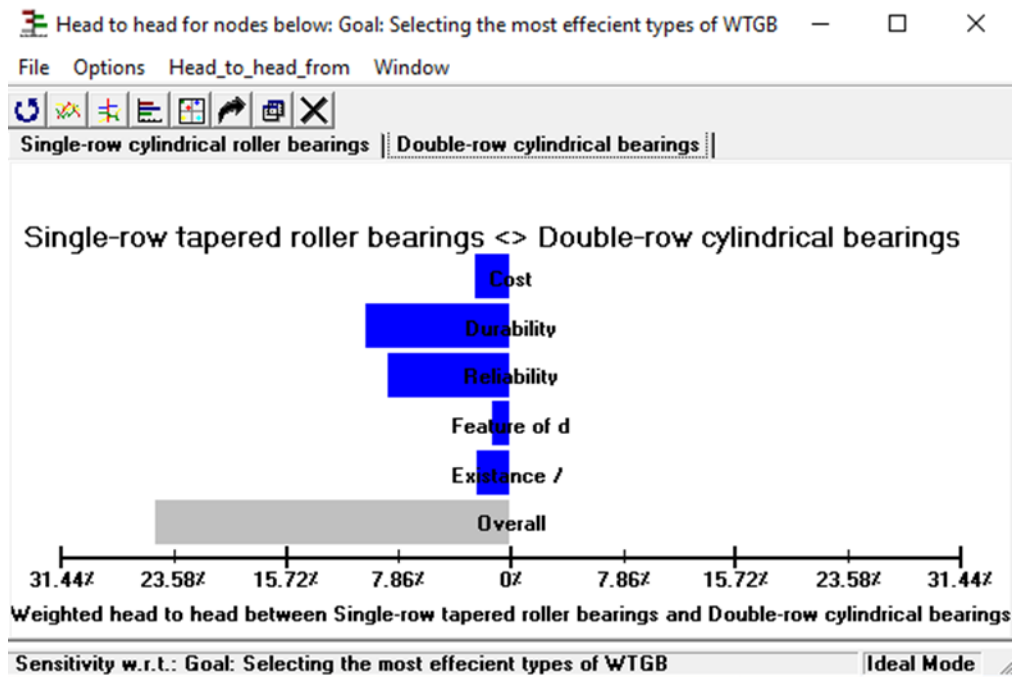


Figure 5-22: (Head-to-head) - selecting the most efficient option [262]

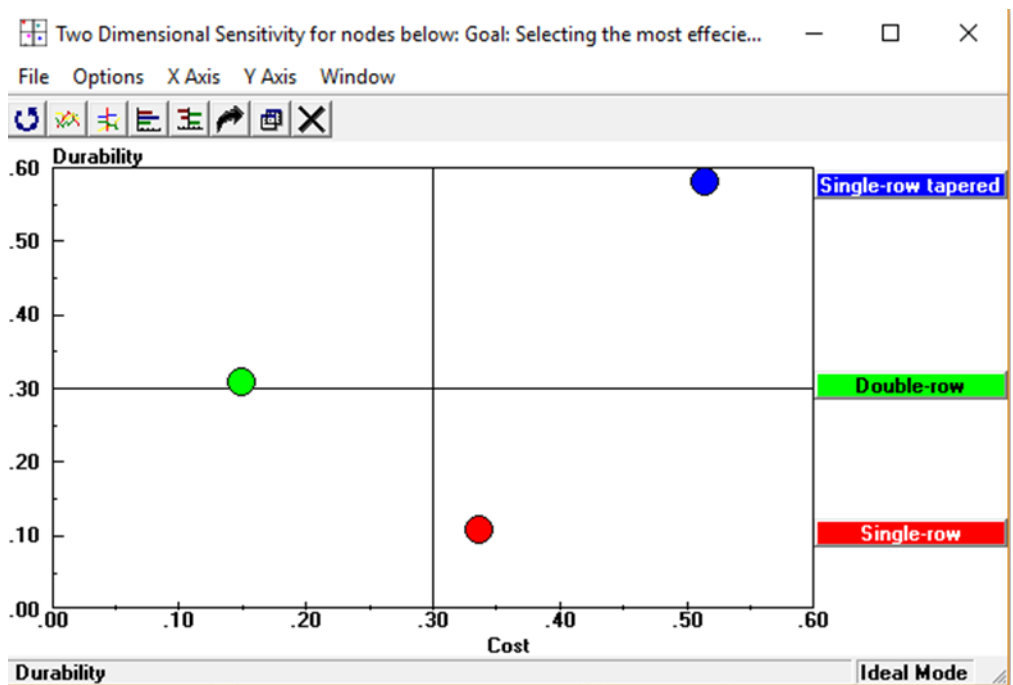


Figure 5-23: Two-dimensional sensitivity -selecting the most efficient option [262]

5.5 Chapter summary

The outputs of the previous chapters have opened the door to observe another aspect of the problem solution regarding the premature failure of WTGBs. Hence, the goal element has been formulated in terms of selecting the most efficient bearing type among the common options. Three typical bearings were evaluated for this purpose: single-row tapered, single-row cylindrical, and double-row cylindrical bearings. Cost, durability, reliability, feature design, and availability are the main criteria for conducting the pairwise comparison. Two separate paths were taken to conduct the comparison process:

- 1- Criteria / sub-criteria with each other based on the identified goal, and
- 2- The bearing types based on each element of the overall criteria / sub-criteria.

It has been concluded that the single-row tapered bearing type is the optimal choice for use in a wind turbine gearbox about 52.1% more than the other alternatives. The result is consistent with the findings of the stress analysis that demonstrated in ([section 2.8.5](#)). The preloading design of the tapered bearing type helps to resist torque variations, especially under severe loading conditions. By which the load will be distributed across the entire bearing's diameter on a nearly circular form, as illustrated before in [Figure 2-19](#).

6

CHAPTER SIX: KEY FINDINGS, CONCLUSIONS, AND RECOMMENDATIONS FOR FUTURE WORK

This chapter summarizes the key findings and the results' conclusions of this study. Some of the key findings and recommendations are supporting the previous works of other researchers. The limitations faced this study also pointed to give the other researchers better understanding and well plan for the future research in this field. Recommendations of the dissertation drawn from the contents of the theoretical and practical chapters are also illustrated.

6.1 Key findings and conclusions

1- The research background (literature review):

The expected depletion of fossil fuels and their environmental and sociopolitical impacts impose an urgent requirement to overcome the challenges of developing new sources of renewable power generation technologies, and wind turbine units are one of them. WT technology is superior

to other renewable energy technologies because it emits less CO₂ and has a higher Energy Return on Investment (EROI). Practically, WTGBs fail during the first one-fifth of their design life (L_{10}). The gearbox is an essential part of the wind turbine system, in which its bearings have the highest breakdown rate. The modified Lundberg and Palmgren (LP) method has been considered in the international standard for estimating bearing lifespan. Typically, cylindrical single-roller bearings, cylindrical double-roller bearings, and tapered roller bearings are used in wind turbine gearboxes. Two effective monitoring systems are applied in the WT system; Condition Monitoring Systems (CMS) and Supervisory Control And Data Acquisition (SCADA). The most common grades of WTGBs steel are (AISI 52100 and 100Cr6). The surface modification, the bearings' steel composition and heat treatment process significantly affect the bearing reliability and durability properties. In WTGBs, cyclic load induces rolling contact stress between the contact surfaces (rollers and rings), which then initiates microcracks and hence, spalling with pitting. The stress distribution of the RCF has been characterized as an elliptical shape according to Hertzian contact theory.

2- Wind turbine bearing failure modes and their reasons

2.1 Inclusions are unavoidable in steelmaking, where they formed in bearing steel as a combination of metals and non-metallic materials. NMIs' shapes, sizes, adherence to the matrix, and the mechanical properties of both the inclusions and the matrix should be taken on consideration in the stress analyzing around the NMIs. It has been concluded that weak NMI-matrix bonds can generate voids and free surfaces during quenching process throughout the bearing material heat treatments. Hence, inclusion damage depends on Coefficient of Thermal Expansion (CTE), elastic modulus, shape, size, and chemical composition. Hard inclusions with a low CTE, such Al₂O₃, may create larger tensile and compressive stresses than soft inclusions (such as MnS). Steel cleanliness technology can be implemented by eliminating the presence of non-metallic inclusions or making them softer; however, this process has a high cost.

2.2 As a result of the cyclic load at the bearing contact surface, the Rolling Contact Fatigue (RCF) creates contact stresses that transfer from the surface to the subsurface zone. The steel matrix has nonhomogeneous contents that include the following features: carbides, non-metallic inclusions, and voids. Accordingly, there would be a difference in the stress

distribution (stress concentration) in the subsurface zone, leading to the following scenario that may interpret the bearing failure:

- Some localized regions in the steel bulk are supersaturated with carbide particles (which are hard and brittle spherical formations) that might dissolve to form White Etching Areas (WEAs). They would compress both NMIs and voids.
- NMIs will be cracked in their tips forming “butterflies”,
- Voids (especially the contiguous ones) exposed to be stressed, hence micro-cracks will probably initiate,
- The microcracks propagate and connect with each other’s to form longer cracks and somewhat WECs networks. Both crack types extend to the surface zone causing flaking or White Structure Flaking (WSF) and then bearing failure.

2.3 Releasing and diffusion of hydrogen into bearing steel (because of water or lubrication contaminants) have been considered as one of the main drivers of WSF.

2.4 The bearing damage drivers of wind turbine gearbox are categorized as follows:

- Loading such as (impact loads, overloads, torque reversals, structural stresses, vibration, peak loads, slip, ...etc.),
- Environment such as lubricant, additives, preservatives, contamination hydrogen generation, ...etc.,
- Material such as (cleanliness, microstructural alterations by heat treatment, natural hydrogen content, residual stresses, ...etc.), and
- Others, such as (transport damage, improper mounting, quality aspects, ...etc.).

3- The analytical results of the simulation, experimental and comparative works

3.1 The simulation work:

- The operational effects of WT lead to increase bearing surface roughness and the lubrication and mounting are not perfect. Accordingly, the simulation work is applied by increasing the coefficient of friction (μ) of the bearing surface from the standard 0.05 to 0.15. However, the traction force increases, and stress concentration is changed towards the rolling surface ahead of the Rolling Direction (RD). It has been indicated that the traction force will decrease the depth of the maximum shear stress which considerably increased under the operational conditions.

- The Finite Element Analysis (FEA) simulation demonstrated that the inclusions' tips have high stress concentration, which reveals the role of NMIs in crack initiation.

3.2 The statistical and experimental work:

- Cracks may be associated or non-associated with inclusions. In this study, the non-associated patterns are about 85% of the total cracks. The associated cracks may appear in the NMI itself from the inclusion one tip, both tips, or along the side of the inclusion body.
- NMIs' sizes may not significantly affect crack initiation, as the Aspect Ratio (AR) of most damaged inclusions was observed to be in the range of (1-2).
- Carbides are white spots observed as hard particles, surrounding voids and NMI.
- Each contiguous group of voids makes it easier to initiate a new crack.
- The investigated sections had no White Etching Cracks (WECs) nor White Etching Areas (WEAs), hence, it can be concluded that their formation may be occurred after the crack initiation stage and they are a consequence of failure not a cause of it.
- There is a correlation among the traction force, the induced maximum shear stress, and the angle of the cracks closest to the contact surface. It has been concluded that the traction force would be more influential closer the bearing contact surface and has a considerable role in the damage initiation.
- The subsurface microcracks tend to have the same inclination of the maximum shear stress angle ($\pm 45^\circ$). This finding points to the potential significance of shear stress in initiating microcracks in the subsurface zone.
- Microcracks with angles $> 90^\circ$ confirm that torque reversal may cause bearing damage due to the severe operating events.
- Microcracks (with a length smaller than 15 μm) have fixed directions, which help to study the cracking initiation stage, while large cracks (with a length greater than 15 μm) tend to change their directions, by which cracking propagation can be studied.
- There is a close relationship between the direction and depth of the crack on the one hand and the type of stress causing it on the other hand.

3.3 The comparison results:

- The experimental profile of the cracks' density (number of cracks) vs. depths (distance from the contact surface) is identical to the simulation profile of Von-Mises stress distribution vs. depths. It probably confirms the considerable role of Von-Mises stress in crack initiation.
- The simulation profile of (shear stress vs. depth) indicates that the maximum shear stress (τ_{\max}) match with the following tow experimental profiles. The first one is the experimental profile of (cracks' density vs. depth), at which (τ_{\max}) locates at the same subsurface depth range. The second one is the experimental profile of (cracks' inclination vs. depth), at which the cracks tend to have the same (τ_{\max}) angle. The two results suggest that the maximum shear stress has an essential role in the initiation of subsurface microcracks.
- The experimental profile of (cracks' density vs. depths) indicated that cracks were concentrated at the shallow region, at which the cracks' inclinations tend to match the contact surface (traction force) angle. The high density of the cracks very close to the contact surface refers to the considerable role of traction relative to the Von-Misses stress effect. For that, it has been concluded that the bearing design standards of contact stress and coefficient of friction should be re-evaluated based on the practical outcomes and taking the operating events on considerations.

4- The application of the Multiple Criteria Decision–Making (MCDM) approach:

Expert Choice (EC) software is an effective Analytical Hierarchy Process (AHP) tool that expresses the Multiple Criteria Decision–Making (MCDM) approach. Three typical types of bearings can be used in wind turbine gears: single-row tapered roller bearings, single-row cylindrical roller bearings, and double-row cylindrical roller bearings. However, this technique has been utilized to select the most compromised option among different alternatives based on varying criteria and sub-criteria. The outcomes of the previous chapters indicate that the problem genesis is concentrated in the WTGBs' premature failure. Accordingly, the two prevalent criteria by which the selection process may be settled are durability (about 37.5%) and reliability (about 35.8%). The application of “EC” confirmed that single-row tapered roller bearings are the most efficient

type for the use in wind turbine gearboxes, with an outweighing percentage of 52.1% rather than single- and double-row cylindrical roller bearings. Other researchers, such as Keller and Guo [120], supported this novel result from the designing aspect and loads' distribution.

6.2 Recommendations for future work

A set of recommendations that have been formulated for future work related to addressing the problem of premature failure in wind turbine bearings, as follows:

- 1- Re-evaluating the WTGBs design standards regarding coefficient of friction and contact stress to match the effects of traction forces, severe operating conditions, and stress concentration that increases the surface roughness and stress concentration.
- 2- Unifying the assessment standards for the WTB bearing life used by bearing manufacturers to eliminate the discrepancies between these standards in addition to considering the variable loading and the extreme operating events in the L_{10} prediction method.
- 3- The quality of the wind turbine's components should be strictly monitored throughout the production, installation, operation, and maintenance processes to ensure that no broken pieces or debris are inserted into the contact regions.
- 4- Oxide inclusions reduce the RCF resistance of bearing steel and enhance premature failure. So that, it is recommended to decrease the oxygen levels in the steel throughout the steelmaking process. Moreover, the fatigue tests results should always be traced back to the steps in the steelmaking process when assessing the efficacy of quality assurance measures.
- 5- Considering the elimination of NMIs, voids, and carbides formations and the differences in Coefficients of Thermal Expansion (CTE) between the NMIs in the bearing steelmaking process.
- 6- Steel cleanliness and softening of inclusions are promising techniques that are recommended to be considered in future studies.
- 7- The oxidation coating to the bearing raceway may prevent the exposure of a new layer of metal, reduce the penetration of hydrogen, and prevent chemical reactions. As a result, it may decrease the appearance of white structure flaking on the bearing surface and prolongs its lifespan.

- 8- Overloading and underloading conditions in WT are essential factors for the premature failure of their gearbox bearings. The following two recommendations are suggested as examples of solutions that can be taken to address the problem in terms of the limitation of the transient loading: -
 - a. Using a tapered roller bearing type in the PWTG, which stays as preloaded and has minimal carrier-bearing clearances that reduce the non-torque load distribution (underloading work).
 - b. Applying a flexible coupling mechanism before and/or after the WTG to absorb the sudden loading produced by the emergency shutdown or applying the mechanical braking.
 - c. The improving of the non-rotating pin in the planetary carrier to avoid applying the contact stress at the same location of the planetary bearing inner race, which is non-rotated component.
- 9- The difference in Coefficients of Thermal Expansion (CTE) between the NMIs and the steel is the likely reason behind the detaching of the NMIs from their steel matrix, which causes cavities and voids. Accordingly, it is recommended to consider the CTE factor for the NMIs and their steel matrix in the steelmaking process.
- 10- It is highly recommended to study the following subjects in the context of researching the premature failure of WTGBs:
 - a. The steel manufacturing process to reduce or prevent the non-recommended inclusions. For example, the development of the promising technology regarding the production of soft inclusions in the steelmaking process.
 - b. The nonhomogeneous contents of the bearing steel matrix, which considerably affects the stress concentration. The subsurface objects can be simulated in terms of stress distribution.
 - c. The surface features of WTGB's to evaluate the contact stress and the coefficient of friction levels based on comparing the magnitudes of their actual loading with the standard yields.

REFERENCES

- [1] H. Yousefi, A. Abbaspour, and H. Seraj, "Worldwide Development of Wind Energy and CO2 Emission Reduction," *Environ. Energy Econ. Res.*, vol. 3, no. 1, pp. 1–9, 2019, doi: 10.22097/eeer.2019.164295.1064.
- [2] U. Singh and M. Rizwan, "SCADA System Dataset Exploration and Machine Learning Based Forecast for Wind Turbines," *Results Eng.*, p. 14, 2022, doi: <https://doi.org/10.1016/j.rineng.2022.100640>.
- [3] I. Kubiszewski, C. J. Cleveland, and P. K. Endres, "Meta-analysis of net energy return for wind power systems," *Renew. Energy*, vol. 35, no. 1, pp. 218–225, 2010, doi: 10.1016/j.renene.2009.01.012.
- [4] K. Kabbabe Poleo, W. J. Crowther, and M. Barnes, "Estimating the impact of drone-based inspection on the Levelised Cost of electricity for offshore wind farms," *Results Eng.*, vol. 9, no. October 2020, p. 11, 2021, doi: 10.1016/j.rineng.2021.100201.
- [5] J. H. I. AL-Bedhany, "Effect of Compression, Impact and Slipping on Rolling Contact Fatigue and Subsurface Microstructural Damage," The University of Sheffield, 2020.
- [6] The International Renewable Energy Agency (IRENA), "Renewable energy technologies: cost analysis series," 2012. doi: 10.1007/978-3-642-20951-2_8.
- [7] S. Sheng, "Wind Turbine Gearbox Reliability Database, Condition Monitoring, and Operation and Maintenance Research Update," in *National Renewable Energy Laboratory, U.S. Department of Energy*, 2015, p. 21, doi: 10.1080/10402004.2015.1055621.
- [8] M. H. Evans, "White structure flaking (WSF) in wind turbine gearbox bearings: Effects of 'butterflies' and white etching cracks (WECs)," *Mater. Sci. Technol.*, vol. 28, no. 1, pp. 3–22, 2012, doi: 10.1179/026708311X13135950699254.
- [9] K. Smolders, H. Long, Y. Feng, and P. Tavner, "Reliability analysis and prediction of wind turbine gearboxes," *Eur. Wind Energy Conf. Exhib. 2010, EWEC 2010*, vol. 4, no. January, pp. 2660–2682, 2010.
- [10] M. Wilkinson *et al.*, "Methodology and results of the reliawind reliability field study," *Eur. Wind Energy Conf. Exhib. 2010, EWEC 2010*, vol. 3, no. January, pp. 1984–2004, 2010.
- [11] M. H. Evans, A. D. Richardson, L. Wang, and R. J. K. Wood, "Serial sectioning investigation of butterfly and white etching crack (WEC) formation in wind turbine gearbox bearings," *Wear*, vol. 302, no. 1–2, pp. 1573–1582, 2013, doi: 10.1016/j.wear.2012.12.031.
- [12] Y. Murakami, *Metal Fatigue: Effects of Small Defects and Nonmetallic Inclusions*, First., vol. 47, no. 12. Oxford, UK: Elsevier, 2002.
- [13] D. Radaj and M. Vormwald, *Advanced methods of fatigue assessment*. Springer Heidelberg New York Dordrecht London, 2013.

- [14] S. A. Akdağ and A. Dinler, "A new method to estimate Weibull parameters for wind energy applications," *Energy Convers. Manag.*, vol. 50, no. 7, pp. 1761–1766, 2009, doi: 10.1016/j.enconman.2009.03.020.
- [15] C. Zhu and Y. Li, "Reliability Analysis of Wind Turbines," *IntechOpen*, pp. 170–185, 2018, doi: 10.5772/intechopen.74859.
- [16] J. Lee and F. Zhao, "Global Wind Report 2021," *Glob. Wind Energy Counc.*, pp. 1–80, 2021, [Online]. Available: <http://www.gwec.net/global-figures/wind-energy-global-status/>.
- [17] H. Yin, H. Shibata, T. Emi, and M. Suzuki, "'In-situ' observation of collision, agglomeration and cluster formation of alumina inclusion particles on steel melts," *ISIJ Int.*, vol. 37, no. 10, pp. 936–945, 1997, doi: 10.2355/isijinternational.37.936.
- [18] E. V. Zaretsky, "Development of high-speed rolling element bearing - A historical and technical respective," OH, United States, 1982. [Online]. Available: <https://ntrs.nasa.gov/citations/19820016621>.
- [19] G. H. Oettinger, "Energy roadmap 2050," Belgium, 2012. doi: 10.2833/10759.
- [20] European Wind Energy Association, "The European offshore wind industry key 2011 trends and statistics," Hans Bloomberg, 2012. [Online]. Available: http://www.ewea.org/fileadmin/files/library/publications/statistics/EWEA_stats_offshore_2011_02.pdf?__cf_chl_tk=iYx4Dmbvn2huVWXClY1VQd2ORmUSLkYmCUiuuicXIOk-1660831675-0-gaNycGzNA6U.
- [21] European Commission, "Communication from the Commission to the European Parliament and the Council," Brussels, 2014. doi: 10.1007/978-3-531-19201-7.
- [22] J. Ribrant and L. Bertling, "Survey of failures in wind power systems with focus on Swedish wind power plants during 1997-2005," *2007 IEEE Power Eng. Soc. Gen. Meet. PES*, pp. 1–8, 2007, doi: 10.1109/PES.2007.386112.
- [23] G. R. Fahrni and D. D. Crichton IV, "Benefits of profiling tapered roller bearings - Matching driveline component performance to the demands of higher horsepower engines of heavy duty trucks," *SAE Tech. Pap.*, no. 724, 1999, doi: 10.4271/1999-01-3767.
- [24] D. Blewett, "<https://weatherguardwind.com/how-much-does-wind-turbine-cost-worth-it/>," *Weather Guard*, 2021. <https://weatherguardwind.com/how-much-does-wind-turbine-cost-worth-it/>.
- [25] K. Stadler and J. Baum, "Premature white etching crack bearing failures in wind gearboxes," *Soc. Tribol. Lubr. Eng. Annu. Meet. Exhib. 2014*, vol. 2, no. October 2014, pp. 646–650, 2014.
- [26] K. Tamada and H. Tanaka, "Occurrence of brittle flaking on bearings used for automotive electrical instruments and auxiliary devices," *Wear*, vol. 199, no. 2, pp. 245–252, 1996, doi: 10.1016/0043-1648(96)06990-6.
- [27] M. H. Evans, A. D. Richardson, L. Wang, and R. J. K. Wood, "Effect of hydrogen on butterfly

- and white etching crack (WEC) formation under rolling contact fatigue (RCF),” *Wear*, vol. 306, no. 1–2, pp. 226–241, 2013, doi: 10.1016/j.wear.2013.03.008.
- [28] D. H. Doug Herr, “Understanding the root causes of axial cracking in wind turbine gearbox bearings,” *Wind. Eng. Dev.*, pp. 63–88, 2014, [Online]. Available: www.windpowerengineering.com.
- [29] J. Carroll, A. McDonald, and D. McMillan, “Failure rate, repair time and unscheduled O&M cost analysis of offshore wind turbines,” *Wind Energy*, vol. 19, no. 6, pp. 1107–1119, 2016, doi: 10.1002/we.1887.
- [30] A. Greco, S. Sheng, J. Keller, and A. Erdemir, “Material wear and fatigue in wind turbine Systems,” *Wear*, vol. 302, no. 1–2, pp. 1583–1591, 2013, doi: 10.1016/j.wear.2013.01.060.
- [31] J. Keller, S. Sheng, A. Cottrell, and A. Greco, “Wind Turbine Tribology Seminar Drivetrain Reliability Collaborative A Recap Workshop,” *Wind Water Power Progr.*, no. August, 2016, [Online]. Available: http://www.nrel.gov/wind/grc/meeting_drc_2016.html.
- [32] M. N. Kotzalas and G. L. Doll, “Tribological advancements for reliable wind turbine performance,” *Philos. Trans. R. Soc. A Math. Phys. Eng. Sci.*, vol. 368, no. 1929, pp. 4829–4850, 2010, doi: 10.1098/rsta.2010.0194.
- [33] H. L. and P. J. T. Yanhui Feng , Yingning Qiu , Christopher J. Crabtree, “Monitoring wind turbine gearboxes,” *Wind Energy*, pp. 1–20, 2013, doi: 10.1002/we.
- [34] U. Zafar, “LITERATURE REVIEW OF WIND TURBINES,” *researchGate*, no. November, pp. 1–32, 2018, [Online]. Available: <https://www.researchgate.net/publication/329680977>.
- [35] R. Budny, “Fixing Wind-Turbine Gearbox Problems,” 2009. [Online]. Available: <http://www.machinedesign.com/mechanical-drives/fixing-wind-turbine-gearbox-problems>.
- [36] A. Úna Brosnan, “Offshore Wind Handbook,” *Offshore Wind*, vol. 2, no. October, pp. 59–100, 2019, [Online]. Available: https://www.atkinsglobal.com/~media/Files/A/Atkins-Corporate/offshore_wind_us_brochure_2019.pdf.
- [37] J. K. Kaldellis and D. Zafirakis, “The wind energy (r)evolution: A short review of a long history,” *Renew. Energy*, vol. 36, no. 7, pp. 1887–1901, 2011, doi: 10.1016/j.renene.2011.01.002.
- [38] W. Musial, S. Butterfield, and B. McNiff, “Improving wind turbine gearbox reliability,” *Eur. Wind Energy Conf. Exhib. 2007, EWEC 2007*, vol. 3, pp. 1770–1779, 2007.
- [39] C. a Walford, “Wind turbine reliability: understanding and minimizing wind turbine operation and maintenance costs,” *Energy*, no. March, pp. SAND2006-1100, 2006, [Online]. Available: <http://prod.sandia.gov/techlib/access-control.cgi/2006/061100.pdf>.
- [40] University of Michigan, “Wind Energy Wind Resource and Potential,” *Wind Energy Factsheet, Pub. No. CSS07-09*. p. September 2020, 2020, [Online]. Available: <http://css.umich.edu/factsheets/wind-energy-factsheet>.

- [41] G. Nicholas, "Development of Novel Ultrasonic Monitoring Techniques for Improving the Reliability of Wind Turbine Gearboxes," The University of Sheffield, 2021.
- [42] Z. P. He, J. H. Zhang, W. S. Xie, Z. Y. Li, and G. C. Zhang, "Misalignment analysis of journal bearing influenced by asymmetric deflection, based on a simple stepped shaft model," *J. Zhejiang Univ. Sci. A*, vol. 13, no. 9, pp. 647–664, 2012, doi: 10.1631/jzus.A1200082.
- [43] "Wind Turbine Control Methods," *Wind Energy Design*, 2022. <https://www.ni.com/en-lb/innovations/white-papers/08/wind-turbine-control-methods.html>.
- [44] S. Yagi and N. Ninoyu, "Technical Trends in Wind Turbine Bearings," *NTN Tech. Rev.*, no. 76, pp. 113–120, 2008.
- [45] H. K. D. H. Bhadeshia, "Steels for bearings," *Prog. Mater. Sci.*, vol. 57, no. 2, pp. 268–435, 2012, doi: 10.1016/j.pmatsci.2011.06.002.
- [46] T. Bruce, "Analysis of the Premature Failure of Wind Turbine Gearbox Bearings," The University of Sheffield, 2016.
- [47] R. C. Martins, C. M. C. G. Fernandes, and J. H. O. Seabra, "Evaluation of bearing, gears and gearboxes performance with different wind turbine gear oils," *Friction*, vol. 3, no. 4, pp. 275–286, 2015, doi: 10.1007/s40544-015-0094-2.
- [48] J. L. M. Peeters, D. Vandepitte, and P. Sas, "Analysis of internal drive train dynamics in a wind turbine," *Wind Energy*, vol. 9, no. 1–2, pp. 141–161, 2006, doi: 10.1002/we.173.
- [49] IEC and 61400-1, "International Standard," 2005. [Online]. Available: <https://www.saiglobal.com/pdftemp/previews/osh/iec/iec61000/61400/iec61400-1%7Bed3.0%7Den.pdf>.
- [50] A. Jan Ukonsaari, Vattenfall, R&D and Niklas Bennstedt, "Wind turbine gearboxes maintenance effect on present and future gearboxes for wind turbines jan," Stockholm, 2016. [Online]. Available: www.energiforsk.se.
- [51] N. T. Garabedian, B. J. Gould, G. L. Doll, and D. L. Burris, "The Cause of Premature Wind Turbine Bearing Failures: Overloading or Underloading?," *Tribol. Trans.*, vol. 61, no. 5, pp. 850–860, 2018, doi: 10.1080/10402004.2018.1433345.
- [52] M. Grujicic, V. Chenna, R. Galgalikar, J. S. Snipes, S. Ramaswami, and R. Yavari, "Wind-Turbine Gear-Box Roller-Bearing Premature-Failure Caused by Grain-Boundary Hydrogen Embrittlement: A Multi-physics Computational Investigation," *J. Mater. Eng. Perform.*, vol. 23, no. 11, pp. 3984–4001, 2014, doi: 10.1007/s11665-014-1188-0.
- [53] J. Keller, "Drivetrain Reliability Collaborative Workshop and Current Events," 2016, [Online]. Available: <https://www.nrel.gov/docs/fy17osti/67443.pdf>.
- [54] H. Link, J. Keller, and Y. Guo, "Gearbox reliability collaborative phase 3 gearbox 2 test plan," (NREL)/No. NREL/TP-5000-58190 National Renew. Energy Lab., no. April, 2013, [Online]. Available: <https://www.nrel.gov/docs/fy15osti/63693.pdf>.

- [55] F. Oyague, "Gearbox Reliability Collaborative (GRC) Description and Loading," 2011. [Online]. Available: <http://www.nrel.gov/docs/fy12osti/47773.pdf>.
- [56] T. Bruce, H. Long, and R. S. Dwyer-Joyce, "Dynamic modelling of wind turbine gearbox bearing loading during transient events," *IET Renew. Power Gener.*, vol. 9, no. 7, pp. 821–830, 2015, doi: 10.1049/iet-rpg.2014.0194.
- [57] W. LaCava, Y. Xing, C. Marks, Y. Guo, and T. Moan, "Three-dimensional bearing load share behaviour in the planetary stage of a wind turbine gearbox," *IET Renew. Power Gener.*, vol. 7, no. 4, pp. 359–369, 2013, doi: 10.1049/iet-rpg.2012.0274.
- [58] H. Al-Hamadani, T. An, M. King, and H. Long, "System dynamic modelling of three different wind turbine gearbox designs under transient loading conditions," *Int. J. Precis. Eng. Manuf.*, vol. 18, no. 11, pp. 1659–1668, 2017, doi: 10.1007/s12541-017-0194-1.
- [59] T. S. and R. S. D.-J. T. Bruce, H. Long, "Formation of white etching cracks at manganese sulfide (MnS) inclusions in bearing steel due to hammering impact loading," *Wind Energy*, pp. 1–20, 2016, doi: 10.1002/we.
- [60] K. Scott, "Effects of Transient Loading on Wind Turbine Drivetrains," University of Strathclyde Engineering, 2014.
- [61] K. Stadler and A. Stubenrauch, "Premature bearing failures in industrial gearboxes Lagerfrühausfälle in Industriegetrieben," *SKF GmbH*, 2013.
- [62] F. Oyague, "Gearbox Modeling and Load Simulation of a Baseline 750-kW Wind Turbine Using State-of-the-Art Simulation Codes," *Nrel*, no. February, p. 81, 2009.
- [63] J. C. Jauregui, I. Torres, R. Garcia, and A. Leon, "Housing stiffness influence on gearbox dynamic loading for wind turbine applications," *Proc. ASME Turbo Expo*, vol. 6, no. June 2012, pp. 959–967, 2012, doi: 10.1115/GT2012-69342.
- [64] J. K. and P. G. J. Helsen, Y. Guo, "Experimental investigation of bearing slip in a wind turbine gearbox during a transient grid loss event," *Wind Energy*, pp. 1–15, 2016, doi: 10.1002/we.
- [65] P. M. Johns and R. Gohar, "Roller bearings under radial and eccentric loads," *Tribol. Int.*, vol. 14, no. 3, pp. 131–136, 1981, doi: 10.1016/0301-679X(81)90058-X.
- [66] M. B. Turi and C. S. Marks, "Bearing Selection Techniques as Applied to Mainshaft Direct and Hybrid Drives," *Timken Co.*, pp. 1–13, 2009, [Online]. Available: http://filecache.mediaroom.com/mr5str_timken/42186/download/MainShaftTechPaper.pdf.
- [67] L. Marketplace *et al.*, "Vestas V42," *Deutsche Windtechnik*, 2011. <https://en.wind-turbine-models.com/turbines/109-vestas-v42> (accessed Sep. 13, 2022).
- [68] I. El-Thalji and E. Jantunen, "A summary of fault modelling and predictive health monitoring of rolling element bearings," *Mech. Syst. Signal Process.*, vol. 60, pp. 252–272, 2015, doi: 10.1016/j.ymssp.2015.02.008.

- [69] Á. Encalada-Dávila, B. Puruncajas, C. Tutivén, and Y. Vidal, "Wind turbine main bearing fault prognosis based solely on scada data," *Sensors*, vol. 21, no. 6, pp. 1–22, 2021, doi: 10.3390/s21062228.
- [70] T. A. Harris, *Rolling bearing analysis*, Fourth. Canada: A Willey-IntersciencePublication, 2001.
- [71] M. H. Evans, "White Structure Flaking Failure in Bearings under Rolling Contact Fatigue," University of Southampton, 2013.
- [72] Y. Gong, J. L. Fei, J. Tang, Z. G. Yang, Y. M. Han, and X. Li, "Failure analysis on abnormal wear of roller bearings in gearbox for wind turbine," *Eng. Fail. Anal.*, vol. 82, no. August, pp. 26–38, 2017, doi: 10.1016/j.engfailanal.2017.08.015.
- [73] S. W. J. Tautz-Weinert, "Using SCADA Data for Wind Turbine Condition Monitoring – a Review," *Energies*, vol. 13, no. 12, pp. 1–32, 2020, doi: 10.3390/en13123132.
- [74] S. Shanbr, F. Elasha, M. Elforjani, and J. A. Teixeira, "Bearing Fault Detection within Wind Turbine Gearbox," *Proc. - 2017 Int. Conf. Sensing, Diagnostics, Progn. Control. SDPC 2017*, vol. 2017-Decem, pp. 565–570, 2017, doi: 10.1109/SDPC.2017.112.
- [75] J. Yoon and D. He, "Planetary gearbox fault diagnostic method using acoustic emission sensors," *IET Sci. Meas. Technol.*, vol. 9, no. 8, pp. 936–944, 2015, doi: 10.1049/iet-smt.2014.0375.
- [76] F. B. Oswald, E. V. Zaretsky, and J. V. Poplawski, "Interference-fit life factors for roller bearings," *Tribol. Trans.*, vol. 52, no. 4, pp. 415–426, 2009, doi: 10.1080/10402000802687890.
- [77] O. U. Kyusung Kim, Girija Parthasarathy, "USE OF SCADA DATA FOR FAILURE DETECTION IN WIND TURBINES," in *The ASME 2011, 5th international conference on Energy Sustainability*, 2011, pp. 1–9.
- [78] S. Sheng and P. Veers, "Wind turbine drivetrain condition monitoring - An overview," *Tech. Progr. MFPT Appl. Syst. Heal. Manag. Conf. 2011 Enabling Sustain. Syst.*, no. October, 2011, [Online]. Available: <https://www.nrel.gov/docs/fy12osti/50698.pdf>.
- [79] and Y. Q. W. Yang, P. J. Tavner, C. J. Crabtree, Y. Feng, "Wind turbine condition monitoring : technical and commercial challenges," *Wind Energy*, no. August 2012, pp. 1–20, 2013, doi: 10.1002/we.
- [80] K. S. Wang, V. S. Sharma, and Z. Y. Zhang, "SCADA data based condition monitoring of wind turbines," *Adv. Manuf.*, vol. 2, no. 1, pp. 61–69, 2014, doi: 10.1007/s40436-014-0067-0.
- [81] D. Scott, B. Loy, and G. H. Mills, "Metallurgical Aspects of Rolling Contact Fatigue," *Proc. Inst. Mech. Eng. Conf. Proc.*, vol. 181, no. 15, pp. 94–103, 1966, doi: 10.1243/pime_conf_1966_181_303_02.
- [82] E. V. Zaretsky, R. J. Parker, and W. J. Anderson, "Effect of component differential hardness on rolling contact fatigue and load capacity," *NASA TN D-2640, Natl. Aeronaut. Sp. Adm.*,

no. March 1965, 1965.

- [83] D. W. Reichard, R. J. Parker, and E. V Zaretsky, "Residual stress and subsurface hardness changes induced during rolling contact," *Nasa Tn D-4456*, p. 30 p., 1968.
- [84] E. Robert, B. Robert, and E. Rainer, "Investigations of bearing failures associated with white etching areas (WEAs) in wind turbine gearboxes," *Tribol. Trans.*, vol. 56, no. 6, pp. 1069–1076, 2013, doi: 10.1080/10402004.2013.823531.
- [85] A. A. Iztueta, "Microstructural Characterization and transformation Kinetics of Austempered Bearing Steels," Tecnum Univesidad De Navarra, 2015.
- [86] Y. LIU, W. WU, L. LIU, M. LIU, and Y. zhou LI, "Thermodynamics Behavior of Titanium for BOF Smelting Bearing Steel," *J. Iron Steel Res. Int.*, vol. 13, no. 6, pp. 74–78, 2006, doi: 10.1016/S1006-706X(06)60115-5.
- [87] F. J. Ebert, "Fundamentals of Design and Technology of Rolling Element Bearings," *Chinese J. Aeronaut.*, vol. 23, no. 1, pp. 123–136, 2010, doi: 10.1016/S1000-9361(09)60196-5.
- [88] A. P. Voskamp, R. Österlund, P. C. Becker, and O. Vingsbo, "Gradual changes in residual stress and microstructure during contact fatigue in ball bearings," *Met. Technol.*, vol. 7, no. 1, pp. 14–21, 1980, doi: 10.1179/030716980803286676.
- [89] A. P. Voskamp and E. J. Mittemeijer, "State of residual stress induced by cyclic rolling contact loading," *Mater. Sci. Technol.*, vol. 13, no. 5, pp. 430–438, 1997, doi: 10.1179/mst.1997.13.5.430.
- [90] A. V. Olver, "The mechanism of rolling contact fatigue: An update," *Proc. Inst. Mech. Eng. Part J J. Eng. Tribol.*, vol. 219, no. 5, pp. 313–330, 2005, doi: 10.1243/135065005X9808.
- [91] M. Perez, C. Sidoroff, A. Vincent, and C. Esnouf, "Microstructural evolution of martensitic 100Cr6 bearing steel during tempering: From thermoelectric power measurements to the prediction of dimensional changes," *Acta Mater.*, vol. 57, no. 11, pp. 3170–3181, 2009, doi: 10.1016/j.actamat.2009.03.024.
- [92] D. Jeddi and H. P. Lieurade, "Effect of retained austenite on high cycle fatigue behavior of carburized 14NiCr11 steel," *Procedia Eng.*, vol. 2, no. 1, pp. 1927–1936, 2010, doi: 10.1016/j.proeng.2010.03.207.
- [93] M. S. Devgun and P. A. Molian, "Experimental study of laser heat-treated bearing steel," *J. Mater. Process. Technol. Elsevier*, vol. 23, pp. 41–54, 1990.
- [94] D. W. Hetzner, "Refining carbide size distributions in M1 high speed steel by processing and alloying," *Mater. Charact. ELSEVIER*, vol. 46, no. 2–3, pp. 175–182, 2001, doi: 10.1016/S1044-5803(01)00121-8.
- [95] M. Wang, "Analysis of improvement of anti-contact fatigue for bearing steel by ion implantation," *Proc. - 3rd Int. Conf. Meas. Technol. Mechatronics Autom. ICMTMA 2011*, vol. 1, pp. 467–470, 2011, doi: 10.1109/ICMTMA.2011.118.

- [96] Jasdeep Singh Sahni, "Characterization and comparison of white layer by hard turning versus grinding," University of Alabama, 2004.
- [97] F. Sadeghi, "Elastohydrodynamic Lubrication Elastohydrodynamic lubrication," *Sci. , Elsevier*, 2010, [Online]. Available: <https://www.sciencedirect.com/topics/engineering/elastohydrodynamic-lubrication/pdf>.
- [98] K. Ram Mohan Rao, S. Mukherjee, P. M. Raole, and I. Manna, "Low energy isothermal plasma-immersion ion implantation of nitrogen for enhanced hardness of AISI 52100 ball bearing steel," *Surf. Coatings Technol.*, vol. 150, no. 1, pp. 80–87, 2002, doi: 10.1016/S0257-8972(01)01491-8.
- [99] S. M. Moghaddam, F. Sadeghi, K. Paulson, N. Weinzapfel, M. Correns, and M. Dinkel, "A 3D numerical and experimental investigation of microstructural alterations around non-metallic inclusions in bearing steel," *Int. J. Fatigue*, vol. 88, pp. 29–41, 2016, doi: 10.1016/j.ijfatigue.2016.02.034.
- [100] F. Sadeghi, B. Jalalahmadi, T. S. Slack, N. Rajee, and N. K. Arakere, "A review of rolling contact fatigue," *J. Tribol.*, vol. 131, no. 4, pp. 1–15, 2009, doi: 10.1115/1.3209132.
- [101] J. A. R. Bomidi and F. Sadeghi, "Three-dimensional finite element elastic-plastic model for subsurface initiated spalling in rolling contacts," *J. Tribol.*, vol. 136, no. 1, 2014, doi: 10.1115/1.4025841.
- [102] B. Jalalahmadi, F. Sadeghi, and V. Bakolas, "Material inclusion factors for lundberg-palmgren-based rcf life equations," *Tribol. Trans.*, vol. 54, no. 3, pp. 457–469, 2011, doi: 10.1080/10402004.2011.560412.
- [103] H. Fu and P. E. J. Rivera-Díaz-del-Castillo, "A unified theory for microstructural alterations in bearing steels under rolling contact fatigue," *Acta Mater.*, vol. 155, no. May, pp. 43–55, 2018, doi: 10.1016/j.actamat.2018.05.056.
- [104] A. Warhadpande, F. Sadeghi, and R. D. Evans, "Microstructural alterations in bearing steels under rolling contact fatigue part 1-Historical overview," *Tribol. Trans.*, vol. 56, no. 3, pp. 349–358, 2013, doi: 10.1080/10402004.2012.754073.
- [105] V. Šmeļova, A. Schwedt, L. Wang, W. Holweger, and J. Mayer, "Microstructural changes in White Etching Cracks (WECs) and their relationship with those in Dark Etching Region (DER) and White Etching Bands (WEBs) due to Rolling Contact Fatigue (RCF)," *Int. J. Fatigue*, vol. 100, no. March, pp. 148–158, 2017, doi: 10.1016/j.ijfatigue.2017.03.027.
- [106] P. Rycerz, A. Olver, and A. Kadiric, "Propagation of surface initiated rolling contact fatigue cracks in bearing steel," *Int. J. Fatigue*, vol. 97, pp. 29–38, 2017, doi: 10.1016/j.ijfatigue.2016.12.004.
- [107] M. H. Evans, A. D. Richardson, L. Wang, R. J. K. Wood, and W. B. Anderson, "Confirming subsurface initiation at non-metallic inclusions as one mechanism for white etching crack (WEC) formation," *Tribol. Int.*, vol. 75, pp. 87–97, 2014, doi: 10.1016/j.triboint.2014.03.012.

- [108] H. Pan, S. Dong, Y. Liang, L. Zhu, and S. Xie, "Modelling of a steel ball's grade based on image texture features," *Proc. Inst. Mech. Eng. Part B J. Eng. Manuf.*, vol. 215, no. 11, pp. 1633–1638, 2001, doi: 10.1243/0954405011519394.
- [109] Y. Y. Yang, H. S. Fang, Y. K. Zheng, Z. G. Yang, and Z. L. Jiang, "The failure models induced by white layers during impact wear," *Wear*, vol. 185, no. 1–2, pp. 17–22, 1995, doi: 10.1016/0043-1648(94)06586-1.
- [110] R. S. Sayles and E. Ioannides, "Debris damage in rolling bearings and its effects on fatigue life.," no. January 1988, 1987.
- [111] G. E. Morales-Espejel and A. Gabelli, "The progression of surface rolling contact fatigue damage of rolling bearings with artificial dents," *Tribol. Trans.*, vol. 58, no. 3, pp. 418–431, 2015, doi: 10.1080/10402004.2014.983251.
- [112] E. Kerscher, "Influence of microstructure and micro notches on the fatigue limit," *Procedia Eng.*, vol. 74, pp. 210–217, 2014, doi: 10.1016/j.proeng.2014.06.251.
- [113] F. B. Oswald, E. V. Zaretsky, and J. V. Poplawski, "Effect of Internal Clearance on Load Distribution and Life of Radially Loaded Ball and Roller Bearings," *Tribol. Trans.*, vol. 55, no. 2, pp. 245–265, 2012, doi: 10.1080/10402004.2011.639050.
- [114] J. H. Kang, B. Hosseinkhani, and P. E. J. Rivera-Díaz-del-castillo, "Rolling contact fatigue in bearings: Multiscale overview," *Mater. Sci. Technol.*, vol. 28, no. 1, pp. 44–49, 2012, doi: 10.1179/174328413X13758854832157.
- [115] J. Lai and K. Stadler, "Investigation on the mechanisms of white etching crack (WEC) formation in rolling contact fatigue and identification of a root cause for bearing premature failure," *Wear*, vol. 364–365, pp. 244–256, 2016, doi: 10.1016/j.wear.2016.08.001.
- [116] R. F. Cook and G. M. Pharr, "Direct Observation and Analysis of Indentation Cracking in Glasses and Ceramics," *J. Am. Ceram. Soc.*, vol. 73, no. 4, pp. 787–817, 1990, doi: 10.1111/j.1151-2916.1990.tb05119.x.
- [117] C. Nutakor, D. Talbot, and A. Kahraman, "An experimental characterization of the friction coefficient of a wind turbine gearbox lubricant," *Wind Energy*, vol. 22, no. 4, pp. 509–522, 2019, doi: 10.1002/we.2303.
- [118] H. Fu *et al.*, "The relationship between 100Cr6 steelmaking, inclusion microstructure and rolling contact fatigue performance," *Int. J. Fatigue*, vol. 129, 2019, doi: 10.1016/j.ijfatigue.2018.11.011.
- [119] M. R. Green, W. M. Rainforth, M. F. Frolich, and J. H. Beynon, "The effect of microstructure and composition on the rolling contact fatigue behaviour of cast bainitic steels," *Wear*, vol. 263, no. 1-6 SPEC. ISS., pp. 756–765, 2007, doi: 10.1016/j.wear.2007.01.070.
- [120] Y. Guo, J. Keller, Z. Zhang, and D. Lucas, "Planetary Load Sharing in Three-Point- Mounted Wind Turbine Gearboxes: A Design and Test Comparison," Denver West Parkway, 2017.

- [Online]. Available: <https://www.nrel.gov/docs/fy17osti/67394.pdf>.
- [121] A. Ruellan, F. Ville, X. Kleber, A. Arnaudon, and D. Girodin, "Understanding white etching cracks in rolling element bearings: The effect of hydrogen charging on the formation mechanisms," *Proc. Inst. Mech. Eng. Part J J. Eng. Tribol.*, vol. 228, no. 11, pp. 1252–1265, 2014, doi: 10.1177/1350650114522452.
- [122] K. S. Chan, "Roles of microstructure in fatigue crack initiation," *Int. J. Fatigue*, vol. 32, no. 9, pp. 1428–1447, 2010, doi: 10.1016/j.ijfatigue.2009.10.005.
- [123] L. Niu, H. Cao, Z. He, and Y. Li, "Dynamic modeling and vibration response simulation for high speed rolling ball bearings with localized surface defects in raceways," *J. Manuf. Sci. Eng.*, vol. 136, no. 4, 2014, doi: 10.1115/1.4027334.
- [124] B. G. and A. G. Jonathan Keller, "Investigation of Bearing Axial Cracking : Benchtop and Full- Scale Test Results," 2017.
- [125] S. Li, "A computational study on the influence of surface roughness lay directionality on micropitting of lubricated point contacts," *J. Tribol.*, vol. 137, no. 2, pp. 1–10, 2015, doi: 10.1115/1.4029165.
- [126] U. Zerbst, M. Madia, and H. T. Beier, "A model for fracture mechanics based prediction of the fatigue strength: Further validation and limitations," *Eng. Fract. Mech.*, vol. 130, pp. 65–74, 2014, doi: 10.1016/j.engfracmech.2013.12.005.
- [127] International Organization for Standardization, "ISO 281:2007 Rolling bearings - Dynamic load ratings and rating life," vol. 3, no. May, 2016.
- [128] ISO, "INTERNATIONAL STANDARD ISO 281/ Rolling bearings — Dynamic load ratings and rating life," *Ref. number ISO*, vol. 281, p. 2007, 2007.
- [129] M. H. Evans, J. C. Walker, C. Ma, L. Wang, and R. J. K. Wood, "A FIB/TEM study of butterfly crack formation and white etching area (WEA) microstructural changes under rolling contact fatigue in 100Cr6 bearing steel," *Mater. Sci. Eng. A*, vol. 570, pp. 127–134, 2013, doi: 10.1016/j.msea.2013.02.004.
- [130] B. C. Li, C. Jiang, X. Han, and Y. Li, "A new approach of fatigue life prediction for metallic materials under multiaxial loading," *Int. J. Fatigue*, vol. 78, pp. 1–10, 2015, doi: 10.1016/j.ijfatigue.2015.02.022.
- [131] H. Takemura, Y. Matsumoto, and Y. Murakami, "Development of a new life equation for ball and roller bearings," *SAE Tech. Pap.*, no. 724, 2000, doi: 10.4271/2000-01-2601.
- [132] T. Gram and A. Vickerfält, "Characterization of non-metallic inclusions according to morphology and composition A comparison of two different steels before and after turning," *Mater. Sci.*, p. 22, 2015, [Online]. Available: <http://www.diva-portal.org/smash/get/diva2:826891/FULLTEXT01.pdf>.
- [133] D. H. Herring, "Steel Cleanliness : Inclusions in Steel," *Heat Treat Dr.*, no. August, 2009, [Online]. Available: www.IndustrialHeating.com.

- [134] Y. Murakami, *Effects of Small Defects and Nonmetallic Inclusions*. Oxford, 2002.
- [135] T. Bruce, E. Rounding, H. Long, and R. S. Dwyer-Joyce, "Characterisation of white etching crack damage in wind turbine gearbox bearings," *Wear*, vol. 338–339, pp. 164–177, 2015, doi: 10.1016/j.wear.2015.06.008.
- [136] A. L. V. Da Costa E Silva, "The effects of non-metallic inclusions on properties relevant to the performance of steel in structural and mechanical applications," *J. Mater. Res. Technol.*, vol. 8, no. 2, pp. 2408–2422, 2019, doi: 10.1016/j.jmrt.2019.01.009.
- [137] Y. Murakami and S. Matsuoka, "Effect of hydrogen on fatigue crack growth of metals," *Eng. Fract. Mech.*, vol. 77, no. 11, pp. 1926–1940, 2010, doi: 10.1016/j.engfracmech.2010.04.012.
- [138] L. Zhang and B. G. Thomas, "State of the Art in Evaluation and Control of Steel Cleanliness," *ISIJ Int.*, vol. 43, no. 3, pp. 271–291, 2003, [Online]. Available: https://www.jstage.jst.go.jp/article/isijinternational1989/43/3/43_3_271/_pdf/-char/en.
- [139] K. Wünnenberg, "IISI study on clean steel," *Metall. Res. Technol.*, vol. 102, no. 10, pp. 687–692, 2005, [Online]. Available: <https://doi.org/10.1051/metal:2005104>.
- [140] L. Holappa and O. Wijk, *Inclusion Engineering*, 1st ed., vol. 3. Elsevier Ltd., 2014.
- [141] <https://www.totalmateria.com/page.aspx?ID=CheckArticle&site=kts&NM=196>, "Clean Steel : Part One," *Key to Metals AG*, 2007. .
- [142] A. Grabulov, U. Ziese, and H. W. Zandbergen, "TEM/SEM investigation of microstructural changes within the white etching area under rolling contact fatigue and 3-D crack reconstruction by focused ion beam," *Scr. Mater.*, vol. 57, no. 7, pp. 635–638, 2007, doi: 10.1016/j.scriptamat.2007.06.024.
- [143] J. Gegner, "Tribological Aspects of Rolling Bearing Failures," *Tribol. - Lubr. Lubr.*, 2011, doi: 10.5772/20790.
- [144] H. Singh, R. V. Pulikollu, W. Hawkins, and G. Smith, "Investigation of Microstructural Alterations in Low- and High-Speed Intermediate-Stage Wind Turbine Gearbox Bearings," *Tribol. Lett.*, vol. 65, no. 3, pp. 1–13, 2017, doi: 10.1007/s11249-017-0861-5.
- [145] P. P. Kumar and G. Balachandran, "Microinclusion Evaluation Using Various Standards," *Trans. Indian Inst. Met.*, vol. 72, no. 4, pp. 877–888, 2019, doi: 10.1007/s12666-018-1546-y.
- [146] J. Guan, L. Wang, C. Zhang, and X. Ma, "Effects of non-metallic inclusions on the crack propagation in bearing steel," *Tribol. Int.*, vol. 106, no. October 2016, pp. 123–131, 2017, doi: 10.1016/j.triboint.2016.10.030.
- [147] Y. M. & S. BERETTA, "Small Defects and Inhomogeneities in Fatigue Strength: Experiments, Models and Statistical Implications," *Extremes*, vol. 103, no. 3, pp. 239–248, 1999, doi: 10.1023/A.

- [148] W. Solano-Alvarez, E. J. Pickering, and H. K. D. H. Bhadeshia, "Degradation of nanostructured bainitic steel under rolling contact fatigue," *Mater. Sci. Eng. A*, vol. 617, pp. 156–164, 2014, doi: 10.1016/j.msea.2014.08.071.
- [149] Y. Neishi, T. Makino, N. Matsui, H. Matsumoto, M. Higashida, and H. Ambai, "Influence of the inclusion shape on the rolling contact fatigue life of carburized steels," *Metall. Mater. Trans. A Phys. Metall. Mater. Sci.*, vol. 44, no. 5, pp. 2131–2140, 2013, doi: 10.1007/s11661-012-1344-9.
- [150] F. Manieri, K. Stadler, G. E. Morales-Espejel, and A. Kadiric, "The origins of white etching cracks and their significance to rolling bearing failures," *Int. J. Fatigue*, vol. 120, no. August 2018, pp. 107–133, 2019, doi: 10.1016/j.ijfatigue.2018.10.023.
- [151] ISO 14026, "Rolling bearings - Damage and failures - Terms, characteristics and causes," 2004.
- [152] P. C. Becker, "Microstructural changes around non-metallic inclusions caused by rolling-contact fatigue of ball-bearing steels," *Met. Technol.*, vol. 8, no. 1, pp. 234–243, 1981, doi: 10.1179/030716981803275415.
- [153] Sugino K, Miyamoto K, Nagumo M, and Aoki K, "Structural Alterations of Bearing Steels Under Rolling Contact Fatigue," *Trans Iron Steel Inst Jap*, vol. 10, no. 2, pp. 98–111, 1970, doi: 10.2355/isijinternational1966.10.98.
- [154] O. Umezawa and K. Nagai, "Effects of Test Temperature on Internal Fatigue Crack Generation Associated with Nonmetallic Particles in Austenitic Steels," *Metall. Mater. Trans. A Phys. Metall. Mater. Sci.*, vol. 29, no. 12, pp. 3017–3028, 1998, doi: 10.1007/s11661-998-0209-8.
- [155] A. Grabulov, R. Petrov, and H. W. Zandbergen, "EBSD investigation of the crack initiation and TEM/FIB analyses of the microstructural changes around the cracks formed under Rolling Contact Fatigue (RCF)," *Int. J. Fatigue*, vol. 32, no. 3, pp. 576–583, 2010, doi: 10.1016/j.ijfatigue.2009.07.002.
- [156] P. Zerres and M. Vormwald, "Review of fatigue crack growth under non-proportional mixed-mode loading," *Int. J. Fatigue*, vol. 58, pp. 75–83, 2014, doi: 10.1016/j.ijfatigue.2013.04.001.
- [157] A. Melander and A. Gustavsson, "An FEM study of driving forces of short cracks at inclusions in hard steels," *Int. J. Fatigue*, vol. 18, no. 6, pp. 389–399, 1996, doi: 10.1016/0142-1123(96)00069-2.
- [158] ISO-4967, "International Standard: Steel - Determination of content of nonmetallic inclusions - Micrographic method using standard diagrams," vol. 2013, pp. 1–37, 1998.
- [159] K. Hashimoto, T. Fujimatsu, N. Tsunekage, K. Hiraoka, K. Kida, and E. C. Santos, "Study of rolling contact fatigue of bearing steels in relation to various oxide inclusions," *Mater. Des.*, vol. 32, no. 3, pp. 1605–1611, 2011, doi: 10.1016/j.matdes.2010.08.052.

- [160] U. Zerbst, M. Madia, C. Klinger, D. Bettge, and Y. Murakami, "Defects as a root cause of fatigue failure of metallic components. II: Non-metallic inclusions," *Eng. Fail. Anal.*, vol. 98, no. January, pp. 228–239, 2019, doi: 10.1016/j.engfailanal.2019.01.054.
- [161] D. Krewerth, T. Lippmann, A. Weidner, and H. Biermann, "Influence of non-metallic inclusions on fatigue life in the very high cycle fatigue regime," *Int. J. Fatigue*, vol. 84, pp. 40–52, 2016, doi: 10.1016/j.ijfatigue.2015.11.001.
- [162] C. Mapelli, "Non-metallic inclusions and clean steel," *Metall. Ital.*, vol. 100, no. 6, pp. 43–52, 2008, [Online]. Available: file:///C:/Users/tahse/Downloads/gruppofratturaogs,+Journal+manager,+462-1759-1-CE.pdf.
- [163] P. Juvonen, "Effects of non-metallic inclusions on fatigue properties of ultra-clean spring steels.," Helsinki University of Technology, 2004.
- [164] A. L. V. Da Costa E Silva, "Non-metallic inclusions in steels - Origin and control," *J. Mater. Res. Technol.*, vol. 7, no. 3, pp. 283–299, 2018, doi: 10.1016/j.jmrt.2018.04.003.
- [165] J. Courbon, G. Lormand, G. Dudragne, P. Daguier, and A. Vincent, "Influence of inclusion pairs, clusters and stringers on the lower bound of the endurance limit of bearing steels," *Tribol. Int.*, vol. 36, no. 12, pp. 921–928, 2003, doi: 10.1016/S0301-679X(03)00076-8.
- [166] T. A. Harris and M. N. Kotzalas, *Essential Concepts of Bearing Technology*, 5th ed. Taylor & Francis, 1967.
- [167] H. K. Danielsen *et al.*, "Multiscale characterization of White Etching Cracks (WEC) in a 100Cr6 bearing from a thrust bearing test rig," *Wear*, vol. 370–371, pp. 73–82, 2017, doi: 10.1016/j.wear.2016.11.016.
- [168] A. A. Kazakov, A. I. Zhitenev, and M. A. Salynova, "Extension of ASTM E2283 standard practice for the assessment of large exogenous nonmetallic inclusions in super duty steels," *CIS Iron Steel Rev.*, vol. 18, pp. 4–9, 2019, doi: 10.17580/cislr.2019.02.01.
- [169] H. Yin, H. Shibata, T. Emi, and M. Suzuki, "Characteristics of agglomeration of various inclusion particles on molten steel surface," *ISIJ Int.*, vol. 37, no. 10, pp. 946–955, 1997, doi: 10.2355/isijinternational.37.946.
- [170] S. X. Li, Y. S. Su, X. D. Shu, and J. J. Chen, "Microstructural evolution in bearing steel under rolling contact fatigue," *Wear*, vol. 380–381, pp. 146–153, 2017, doi: 10.1016/j.wear.2017.03.018.
- [171] H. Matsunaga, N. Shomura, S. Muramoto, and M. Endo, "Shear mode threshold for a small fatigue crack in a bearing steel," *Fatigue Fract. Eng. Mater. Struct.*, vol. 34, no. 1, pp. 72–82, 2011, doi: 10.1111/j.1460-2695.2010.01495.x.
- [172] W. Holweger *et al.*, "White Etching Crack Root Cause Investigations," *Tribol. Trans.*, vol. 58, no. 1, pp. 59–69, 2015, doi: 10.1080/10402004.2014.942938.
- [173] S. W. Ooi, A. Gola, R. H. Vegter, P. Yan, and K. Stadler, "Evolution of white-etching cracks

- and associated microstructural alterations during bearing tests,” *Mater. Sci. Technol. (United Kingdom)*, vol. 33, no. 14, pp. 1657–1666, 2017, doi: 10.1080/02670836.2017.1310431.
- [174] B. Gould, A. Greco, K. Stadler, and X. Xiao, “An analysis of premature cracking associated with microstructural alterations in an AISI 52100 failed wind turbine bearing using X-ray tomography,” *Mater. Des.*, vol. 117, pp. 417–429, 2017, doi: 10.1016/j.matdes.2016.12.089.
- [175] Y. Murakami, M. Naka, A. Iwamoto, and G. Chatell, “Long life bearings for automotive alternator applications,” *SAE Tech. Pap.*, no. 41 2, 1995, doi: 10.4271/950944.
- [176] N. Motion & Control, “Long-Life Bearings for Engine Accessories New ! How can we solve the problem with,” 2004.
- [177] H. Mikami and T. Kawamura, “Influence of electrical current on bearing flaking life,” *SAE Int.*, no. 724, pp. 1–8, 2007.
- [178] S. Turteltaub and A. S. J. Suiker, “Transformation-induced plasticity in ferrous alloys,” *J. Mech. Phys. Solids*, vol. 53, no. 8, pp. 1747–1788, 2005, doi: 10.1016/j.jmps.2005.03.004.
- [179] N. K. Arakere, N. Branch, G. Levesque, V. Svendsen, and N. H. Forster, “Rolling contact fatigue life and spall propagation of AISI M50, M50NiL, and AISI 52100, part II: Stress modeling,” *Tribol. Trans.*, vol. 53, no. 1, pp. 42–51, 2010, doi: 10.1080/10402000903226325.
- [180] A. P. Voskamp and E. J. Mittemeijer, “Crystallographic preferred orientation induced by cyclic rolling contact loading,” *Metall. Mater. Trans. A Phys. Metall. Mater. Sci.*, vol. 27, no. 11, pp. 3445–3465, 1996, doi: 10.1007/bf02595437.
- [181] A. Ruellan, F. Ville, X. Kleber, and B. Liatard, “Tribological analysis of White Etching Crack (WEC) failures in rolling element bearings,” 2014.
- [182] M. H. Evans, “An updated review: white etching cracks (WECs) and axial cracks in wind turbine gearbox bearings,” *Mater. Sci. Technol. (United Kingdom)*, vol. 32, no. 11, pp. 1133–1169, 2016, doi: 10.1080/02670836.2015.1133022.
- [183] A. D. Richardson, M. H. Evans, L. Wang, R. J. K. Wood, M. Ingram, and B. Meuth, “The Evolution of White Etching Cracks (WECs) in Rolling Contact Fatigue-Tested 100Cr6 Steel,” *Tribol. Lett.*, vol. 66, no. 1, pp. 1–23, 2018, doi: 10.1007/s11249-017-0946-1.
- [184] H. Harada, T. Mikami, M. Shibata, D. Sokai, A. Yamamoto, and H. Tsubakino, “Microstructural changes and crack initiation with white etching area formation under rolling/sliding contact in bearing steel,” *ISIJ Int.*, vol. 45, no. 12, pp. 1897–1902, 2005, doi: 10.2355/isijinternational.45.1897.
- [185] W. Solano-Alvarez and H. K. D. H. Bhadeshia, “White-etching matter in bearing steel. Part II: Distinguishing cause and effect in bearing steel failure,” *Metall. Mater. Trans. A Phys. Metall. Mater. Sci.*, vol. 45, no. 11, pp. 4916–4931, 2014, doi: 10.1007/s11661-014-2431-

x.

- [186] M. Alexander Stopher and P. E. J. Rivera-Diaz-del-Castillo, "Hydrogen embrittlement in bearing steels," *Mater. Sci. Technol. (United Kingdom)*, vol. 32, no. 11, pp. 1184–1193, 2016, doi: 10.1080/02670836.2016.1156810.
- [187] Y. J. Li, M. Herbig, S. Goto, and D. Raabe, "Atomic scale characterization of white etching area and its adjacent matrix in a martensitic 100Cr6 bearing steel," *Mater. Charact.*, vol. 123, pp. 349–353, 2017, doi: 10.1016/j.matchar.2016.12.002.
- [188] V. Šmelova, A. Schwedt, L. Wang, W. Holweger, and J. Mayer, "Electron microscopy investigations of microstructural alterations due to classical Rolling Contact Fatigue (RCF) in martensitic AISI 52100 bearing steel," *Int. J. Fatigue*, vol. 98, pp. 142–154, 2017, doi: 10.1016/j.ijfatigue.2017.01.035.
- [189] T. Bruce, H. Long, and R. S. Dwyer-Joyce, "Threshold Maps for Inclusion-Initiated Micro-Cracks and White Etching Areas in Bearing Steel: The Role of Impact Loading and Surface Sliding," *Tribol. Lett.*, vol. 66, no. 3, p. 0, 2018, doi: 10.1007/s11249-018-1068-0.
- [190] M. W. J. Lewis and B. Tomkins, "A fracture mechanics interpretation of rolling bearing fatigue," *Proc. Inst. Mech. Eng. Part J J. Eng. Tribol.*, vol. 226, no. 5, pp. 389–405, 2012, doi: 10.1177/1350650111435580.
- [191] B. Gould, N. G. Demas, and A. C. Greco, "The influence of steel microstructure and inclusion characteristics on the formation of premature bearing failures with microstructural alterations," *Mater. Sci. Eng. A*, vol. 751, no. February, pp. 237–245, 2019, doi: 10.1016/j.msea.2019.02.084.
- [192] V. Šmelova, A. Schwedt, L. Wang, W. Holweger, T. J. Harvey, and J. Mayer, "A study of microstructure alteration in aisi 52100 bearings due to classic rolling contact fatigue and white etching crack," *Soc. Tribol. Lubr. Eng. Annu. Meet. Exhib. 2016*, no. June, pp. 656–659, 2016.
- [193] A. Grabulov, "Fundamentals of Rolling Contact Fatigue," University of Belgrade, Serbia, 2010.
- [194] H. A. H. Al-Tameemi, "Effect of Surface Traction and Non-Metallic Inclusions on the Premature Failure of Wind Turbine Gearbox Bearings," no. December, 2018, [Online]. Available: <http://etheses.whiterose.ac.uk/19813/>.
- [195] S. M. Moghaddam, F. Sadeghi, N. Weinzapfel, and A. Liebel, "A damage mechanics approach to simulate butterfly wing formation around nonmetallic inclusions," *J. Tribol.*, vol. 137, no. 1, 2015, doi: 10.1115/1.4028628.
- [196] J. A. Martin, S. F. Borgese, and A. D. Eberhardt, "Microstructural alterations of rolling-bearing steel undergoing cyclic stressing," *J. Fluids Eng. Trans. ASME*, vol. 88, no. 3, pp. 555–565, 1966, doi: 10.1115/1.3645902.
- [197] G. Guetard, I. Toda-Caraballo, and P. E. J. Rivera-Díaz-Del-Castillo, "Damage evolution

- around primary carbides under rolling contact fatigue in VIM-VAR M50," *Int. J. Fatigue*, vol. 91, pp. 59–67, 2016, doi: 10.1016/j.ijfatigue.2016.05.026.
- [198] H. A. Al-Tameemi, H. Long, and R. S. Dwyer-Joyce, "Initiation of sub-surface micro-cracks and white etching areas from debonding at non-metallic inclusions in wind turbine gearbox bearing," *Wear*, vol. 406–407, no. January, pp. 22–32, 2018, doi: 10.1016/j.wear.2018.03.008.
- [199] W. D. PILKEY, *PETERSON'S STRESS CONCENTRATION FACTORS*, 2nd ed. New York, USA: A Wiley-Interscience Publication JOHN WILEY & SONS, INC., 1997.
- [200] H. Swahn, P. C. Becker, and O. Vingsbo, "Martensite decay during rolling contact fatigue in ball bearings," *Metall. Trans. A*, vol. 7, no. 8, pp. 1099–1110, 1976, doi: 10.1007/BF02656592.
- [201] F. G. Guzmán, M. O. Oezel, G. Jacobs, G. Burghardt, C. Broeckmann, and T. Janitzky, "Influence of slip and lubrication regime on the formation of white etching cracks on a two-disc test rig," *Lubricants*, vol. 6, no. 1, pp. 1–8, 2018, doi: 10.3390/lubricants6010008.
- [202] B. A. Szost, R. H. Vegter, and P. E. J. Rivera-Díaz-del-Castillo, "Developing bearing steels combining hydrogen resistance and improved hardness," *Mater. Des.*, vol. 43, pp. 499–506, 2013, doi: 10.1016/j.matdes.2012.07.030.
- [203] H. Lü, M. Li, T. Zhang, and W. Chu, "Hydrogen-enhanced dislocation emission, motion and nucleation of hydrogen-induced cracking for steel," *Sci. China, Ser. E Technol. Sci.*, vol. 40, no. 5, pp. 530–538, 1997, doi: 10.1007/bf02917169.
- [204] J. P. Hirth, *Effects of hydrogen on the properties of iron and steel*, VOLUME 11A., vol. 11, no. 6. METALLURGICAL TRANSACTIONS A, 1980.
- [205] E. S. Alley, "Influence of Microstructure in Rolling Contact Fatigue of Bearing Steels with inclusions," *Mech. Eng.*, vol. PhD, no. May, p. 185, 2009.
- [206] A. Oila and S. J. Bull, "Assessment of the factors influencing micropitting in rolling/sliding contacts," *Wear*, vol. 258, no. 10, pp. 1510–1524, 2005, doi: 10.1016/j.wear.2004.10.012.
- [207] A. Ramesh, S. N. Melkote, L. F. Allard, L. Riestler, and T. R. Watkins, "Analysis of white layers formed in hard turning of AISI 52100 steel," *Mater. Sci. Eng. A*, vol. 390, no. 1–2, pp. 88–97, 2005, doi: 10.1016/j.msea.2004.08.052.
- [208] ISO, "Rolling bearings — Damage and failures — Terms, characteristics and causes , BS ISO 15243:2017," Vernier, Geneva, Switzerland, 2017.
- [209] H. Ghonem and J. W. Provan, "Micromechanics theory of fatigue crack initiation and propagation," *Eng. Fract. Mech.*, vol. 13, no. 4, pp. 963–977, 1980, doi: 10.1016/0013-7944(80)90026-0.
- [210] T. H. Lin and Y. M. Ito, "Mechanics of a fatigue crack nucleation mechanism," *J. Mech. Phys. Solids*, vol. 17, no. 6, pp. 511–523, 1969, doi: 10.1016/0022-5096(69)90006-4.

- [211] Y. Nakai *et al.*, “Effects of inclusion size and orientation on rolling contact fatigue crack initiation observed by laminography using ultra-bright synchrotron radiation,” *Procedia Struct. Integr.*, vol. 2, pp. 3117–3124, 2016, doi: 10.1016/j.prostr.2016.06.389.
- [212] A. R. Aikin, “Bearing and gearbox failures : Challenge to wind turbines,” *Energy Central News*, pp. 1–24, 2021.
- [213] T. Howard, “Development of a Novel Bearing Concept for Improved Wind Turbine Gearbox Reliability,” no. January, p. 237, 2016.
- [214] S. Sheng, “Wind Turbine Micropitting Workshop : A Recap,” 2010. [Online]. Available: <http://www.osti.gov/bridge> Available.
- [215] J. Van Rensselaar, “The elephant in the wind turbine,” *Society of Tribologists and Lubrication Engineers*, vol. 66, no. 6, pp. 38–48, 2010.
- [216] G. R.L. Errichello, “Morphology of Micropitting,” *Am. Gears Manuf. Assoc.*, no. January 2011, pp. 1–20, 2017, [Online]. Available: https://www.google.com/url?sa=i&url=https%3A%2F%2Fwww.researchgate.net%2Ffigure%2FWind-turbine-HS-pinion-with-micropitting-at-edge-of-contact_fig7_284221605&psig=AOvVaw0fiJ3Rlnzpgb62hZ8Ic1oP&ust=1672033980632000&source=images&cd=vfe&ved=0CBEQjhXqFwoTClis2.
- [217] S. – the knowledge engineering Company, “Bearing damage and failure analysis Contents,” *Bear. damage Fail. Anal.*, p. 106, 2017, [Online]. Available: https://www.skf.com/binaries/pub12/Images/0901d1968064c148-Bearing-failures---14219_2-EN_tcm_12-297619.pdf.
- [218] “<https://www.ntnglobal.com/en/products/care/damage/rust.html>,” *NTN*, 2023.
- [219] S. Raadnui and S. Kleesuwan, “Electrical pitting wear debris analysis of grease-lubricated rolling element bearings,” *Wear*, vol. 271, no. 9–10, pp. 1707–1718, 2011, doi: 10.1016/j.wear.2011.01.040.
- [220] Z. Liu and L. Zhang, “A review of failure modes, condition monitoring and fault diagnosis methods for large-scale wind turbine bearings,” *Meas. J. Int. Meas. Confed.*, vol. 149, p. 107002, 2020, doi: 10.1016/j.measurement.2019.107002.
- [221] Schaeffler Group, *Rolling Bearing Damage - Recognition of damage and bearing inspection*, vol. 82. 2006.
- [222] B. and N. Bearings, “Bearing failure: Causes and cures,” *BARDEN Precis. Bear.*, p. 15, 1992, [Online]. Available: <https://bit.ly/3hN3dk1%0D>.
- [223] W. H. Detweiler, “Common Causes and Cures for Roller Bearing Overheating,” 2020. [Online]. Available: <https://bit.ly/3bGkk60>.
- [224] J. A. Ciruna and H. J. Szieleit, “The effect of hydrogen on the rolling contact fatigue life of AISI 52100 and 440C steel balls,” *Wear*, vol. 24, no. 1, pp. 107–118, 1973, doi: 10.1016/0043-1648(73)90207-X.

- [225] L. Grunberg, "The formation of hydrogen peroxide on fresh metal surfaces," *Proc. Phys. Soc. Sect. B*, vol. 66, no. 3, pp. 153–161, 1953, doi: 10.1088/0370-1301/66/3/301.
- [226] T. Imran, B. Jacobson, and A. Shariff, "Quantifying diffused hydrogen in AISI-52100 bearing steel and in silver steel under tribo-mechanical action: Pure rotating bending, sliding-rotating bending, rolling-rotating bending and uni-axial tensile loading," *Wear*, vol. 261, no. 1, pp. 86–95, 2006, doi: 10.1016/j.wear.2005.09.026.
- [227] D. Kuerten, N. Winzer, A. Kailer, W. Pfeiffer, R. Spallek, and M. Scherge, "In-situ detection of hydrogen evolution in a lubricated sliding pin on disk test under high vacuum," *Tribol. Int.*, vol. 93, pp. 324–331, 2016, doi: 10.1016/j.triboint.2015.07.028.
- [228] P. A. Bertrand, "Low-energy-electron-stimulated degradation of a multiply alkylated cyclopentane oil and implications for space bearings," *Tribol. Lett.*, vol. 40, no. 1, pp. 187–198, 2010, doi: 10.1007/s11249-010-9656-7.
- [229] P. A. Bertrand, "Chemical degradation of a multiply alkylated cyclopentane (MAC) oil during wear: Implications for spacecraft attitude control system bearings," *Tribol. Lett.*, vol. 49, no. 2, pp. 357–370, 2013, doi: 10.1007/s11249-012-0075-9.
- [230] H. Yamada, H. Uyama, and N. Mitamura, "The effects of hydrogen on microstructural change and surface originated flaking in rolling contact fatigue," *World Tribol. Congr. 2009 - Proc.*, vol. 2, p. 11, 2009, doi: 10.2474/trol.6.123.
- [231] K. Takai, H. Shoda, H. Suzuki, and M. Nagumo, "Lattice defects dominating hydrogen-related failure of metals," *Acta Mater.*, vol. 56, no. 18, pp. 5158–5167, 2008, doi: 10.1016/j.actamat.2008.06.031.
- [232] S. Fujita, S. Matsuoka, Y. Murakami, and G. Marquis, "Effect of hydrogen on Mode II fatigue crack behavior of tempered bearing steel and microstructural changes," *Int. J. Fatigue*, vol. 32, no. 6, pp. 943–951, 2010, doi: 10.1016/j.ijfatigue.2009.06.005.
- [233] J. Loos, I. Bergmann, and M. Goss, "Influence of Currents from Electrostatic Charges on WEC Formation in Rolling Bearings," *Tribol. Trans.*, vol. 59, no. 5, pp. 865–875, 2016, doi: 10.1080/10402004.2015.1118582.
- [234] M. Ščepanskis, B. Gould, and A. Greco, "Empirical Investigation of Electricity Self-Generation in a Lubricated Sliding–Rolling Contact," *Tribol. Lett.*, vol. 65, no. 3, pp. 15–20, 2017, doi: 10.1007/s11249-017-0892-y.
- [235] R. H. Vegter and J. T. Slycke, "The role of hydrogen on rolling contact fatigue response of rolling element bearings," *J. ASTM Int.*, vol. 7, no. 2, 2010, doi: 10.1520/JAI102543.
- [236] Y. Imai, T. Endo, D. Dong, and Y. Yamamoto, "Study on rolling contact fatigue in hydrogen environment at a contact pressure below basic static load capacity," *Tribol. Trans.*, vol. 53, no. 5, pp. 764–770, 2010, doi: 10.1080/10402001003790186.
- [237] M. H. Evans, L. Wang, H. Jones, and R. J. K. Wood, "White etching crack (WEC) investigation by serial sectioning, focused ion beam and 3-D crack modelling," *Tribol. Int.*, vol. 65, pp.

- 146–160, 2013, doi: 10.1016/j.triboint.2013.03.022.
- [238] N. Kino and K. Otani, “The influence of hydrogen on rolling contact fatigue life and its improvement,” *JSAE Rev.*, vol. 24, no. 3, pp. 289–294, 2003, doi: 10.1016/S0389-4304(03)00035-3.
- [239] W. H. Johnson, “II. On some remarkable changes produced in iron and steel by the action of hydrogen and acids,” in *Hydrogen and Acids on Iron and Steel*, vol. 14, no. 2, 1875, pp. 168–179.
- [240] W. Kruhöffler and J. Loos, “WEC Formation in Rolling Bearings under Mixed Friction: Influences and ‘Friction Energy Accumulation’ as Indicator,” *Tribol. Trans.*, vol. 60, no. 3, pp. 516–529, 2017, doi: 10.1080/10402004.2016.1183250.
- [241] B. Gould and A. Greco, “The Influence of Sliding and Contact Severity on the Generation of White Etching Cracks,” *Tribol. Lett.*, vol. 60, no. 2, pp. 1–13, 2015, doi: 10.1007/s11249-015-0602-6.
- [242] B. Gould and A. Greco, “Investigating the Process of White Etching Crack Initiation in Bearing Steel,” *Tribol. Lett.*, vol. 62, no. 2, 2016, doi: 10.1007/s11249-016-0673-z.
- [243] D. Kuhlmann-Wilsdorf, “The theory of dislocation-based crystal plasticity,” *Philosophical Magazine A: Physics of Condensed Matter, Structure, Defects and Mechanical Properties*, vol. 79, no. 4, Virginia, USA, pp. 955–1008, 1999.
- [244] J. Gegner and W. Nierlich, “Service Loading of Rolling Bearings in Wind Turbine Gearboxes: X-ray Diffraction Material Response Analysis of White Etching Crack Premature Failures,” *Tribol. Trans.*, vol. 61, no. 2, pp. 269–278, 2018, doi: 10.1080/10402004.2017.1314575.
- [245] J. Campbell, *Complete Casting Handbook: Metal Casting Processes, Metallurgy, Techniques and Design: Second Edition*, Second. Ledbury, Herefordshire, England: Elsevier, 2015.
- [246] N. P. Suh, “An overview of the delamination theory of wear,” *Wear*, vol. 44, no. 1, pp. 1–16, 1977, doi: 10.1016/0043-1648(77)90081-3.
- [247] T. A. Mankhi, J. H. AL-Bedhany, and S. Legutko, “Investigation of subsurface microcracks causing premature failure in wind turbine gearbox bearings,” *Results Eng.*, vol. 16, no. August, 2022, doi: 10.1016/j.rineng.2022.100667.
- [248] K. Stadler, R. H. Vegter, and D. Vaes, “White Etching Cracks - a consequence, not a root cause of bearing failure,” *SKF Evol.*, vol. 1, no. January, pp. 21–29, 2018, [Online]. Available: <http://evolution.skf.com/us/white-etching-cracks-a-consequence-not-a-root-cause-of-bearing-failure/>.
- [249] X. Zhu, “Tutorial on Hertz Contact Stress,” *Opti 521*. GitHub, Arizona, pp. 1–8, 2012, [Online]. Available: <https://wp.optics.arizona.edu/optomech/wp-content/uploads/sites/53/2016/10/OPTI-521-Tutorial-on-Hertz-contact-stress-Xiaoyin-Zhu.pdf>.
- [250] G. W. S. & A. W. Batchelor, *Engineering Tribology*, Third. Oxford, UK: Elsevier, 2005.

- [251] Y. S. Kang, R. D. Evans, and G. L. Doll, "Roller-raceway slip simulations of wind turbine gearbox bearings using dynamic bearing model," *Am. Soc. Mech. Eng. Tribol. Div. TRIB*, pp. 407–409, 2010, doi: 10.1115/IJTC2010-41191.
- [252] J. Lord and R. Larsson, "Effects of slide-roll ratio and lubricant properties on elastohydrodynamic lubrication film thickness and traction," *Proc. Inst. Mech. Eng. Part J J. Eng. Tribol.*, vol. 215, no. 3, pp. 301–308, 2001, doi: 10.1243/1350650011543556.
- [253] M. Harmon and R. Lewis, "Review of top of rail friction modifier tribology," *Tribol. - Mater. Surfaces Interfaces*, vol. 10, no. 3, pp. 150–162, 2016, doi: 10.1080/17515831.2016.1216265.
- [254] G. E. T. L.C.F. Canale, L.C.F. Canale R.A. Mesquita, *Failure Analysis of Heat Treated Steel Components*. Ohio, USA: ASM International, 2008.
- [255] C. D. Liu, M. N. Bassim, and S. S. Lawrence, "Evaluation of fatigue-crack initiation at inclusions in fully pearlitic steels," *Mater. Sci. Eng. A*, vol. 167, no. 1–2, pp. 107–113, 1993, doi: 10.1016/0921-5093(93)90343-D.
- [256] T. A. Harris and W. K. Yu, "Lundberg-palmgren fatigue theory: Considerations of failure stress and stressed volume," *J. Tribol.*, vol. 121, no. 1, pp. 85–89, 1999, doi: 10.1115/1.2833815.
- [257] S. Kabus, M. R. Hansen, and O. Mouritsen, "A new quasi-static cylindrical roller bearing model to accurately consider non-hertzian contact pressure in time domain simulations," *J. Tribol.*, vol. 134, no. 4, pp. 1–10, 2012, doi: 10.1115/1.4007219.
- [258] P. J. ŽAK, "Applying Advanced Methods in - MULTIPLE Multiple Criteria Decision Making / Aiding in Transportation & Logistics," 2011, pp. 1–56.
- [259] D. Sabaei, J. Erkoyuncu, and R. Roy, "A review of multi-criteria decision making methods for enhanced maintenance delivery," *Procedia CIRP*, vol. 37, pp. 30–35, 2015, doi: 10.1016/j.procir.2015.08.086.
- [260] P. Adamović, Č. Dunović, and M.-M. Nahod, "Expert Choice Model for Choosing Appropriate Trenchless Method for Pipe Laying," 2007, [Online]. Available: https://bib.irb.hr/datoteka/348146.Adamovic_Dunovic_Nahod_Prag_09_2007.pdf.
- [261] I. Engineering, E. Triantaphyllou, and S. H. Mann, "Using the Analytic Hierarchy Process for Decision Making in Engineering Applications : Some Challenges," *Int. J. Ind. Eng. Theory, Appl. Pract.*, vol. 2, no. 1, pp. 35–44, 1995.
- [262] T. A. Mankhi, S. Legutko, J. H. Al-Bedhany, and A. A. Muhsen, "Selecting the Most Efficient Bearing of Wind Turbine Gearbox Using (Analytical Hierarchy Process) Method AHP" *IOP Conf. Ser. Mater. Sci. Eng.*, vol. 518, no. 3, 2019, doi: 10.1088/1757-899X/518/3/032050.
- [263] SKF, "Tapered roller bearings," 2023. <https://www.skf.com/mena/products/rolling-bearings/roller-bearings/tapered-roller-bearings> (accessed Mar. 13, 2023).
- [264] SKF, "SKF cylindrical roller bearings - always in the lead Contents," Sweden, 2004. [Online].

Available:

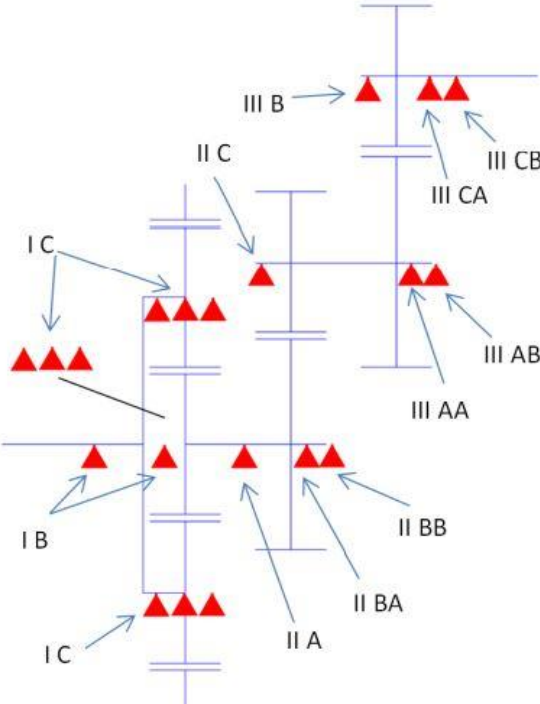
<http://www.aryanbearing.com/FileUpload/Files/Files/File/4863514115700000.pdf>.

- [265] C. R. Gillette, "NSK Rolling Bearings, Catalogue No. E1102m," *General lubrication engineering practice*. NSK Ltd, Japan, 2005, [Online]. Available: <https://www.nsk.com/common/data/ctrpPdf/bearings/e1102m.pdf>.
- [266] RKB Bearing Industrial Switzerland, "Bearing catalogue." The Alternative Power BCRKB.Rev01EN, Balerna, p. 350, 2016, [Online]. Available: <https://www.rkbtrade.com/stat/pdf/files/info-24.pdf>.
- [267] G. PUGLIA, "Life cycle cost analysis on wind turbines," CHALMERS UNIVERSITY OF TECHNOLOGY, 2013.
- [268] K. Iso, A. Yokouchi, and H. Takemura, "Research work for clarifying the mechanism of white structure flaking and extending the life of bearings," *SAE Tech. Pap.*, no. 724, 2005, doi: 10.4271/2005-01-1868.

APPENDICES

8.1 Appendix A1

Appendix A 1: Bearings' locations of a typical [50]



8.2 Appendix A2

Appendix A 2: Bearings' information of a typical [50]

Position	Designation	Dynamic load rating, C [N]	Correction factor for bearing arrangement		Adjusted dynamic load rating, [N]	Static load rating, C0 [N]	Fatigue load limit, Pu [N]	Nominal radial load [N] @ 100% output	Nominal axial load [N] @ 100% output
	u/k	u/k		(single)	u/k	u/k	u/k	u/k	u/k
I B (2x)	u/k	u/k	1,00	(single)	u/k	u/k	u/k	u/k	u/k
I C (3x3)	NU 2248-EX-M1	1830000	0,90	(triple)	1647000	2800000	295000	358039	-
II A	NCF 2980 CV	1650000	1,00	(single)	1650000	3450000	310000	89921	-
II BA	32064 X	1540000	0,95	(dual)	1463000	3100000	255000	44961	17293
II BB	32064 X	1540000	0,95	(dual)	1463000	3100000	255000	44961	100065
II C	NU 2338 ECMA	1830000	1,00	(single)	1830000	2550000	236000	179842	-
III AA	30238 J2	721000	0,95	(dual)	684950	1000000	95000	34134	12191
III AB	30238 J2	721000	0,95	(dual)	684950	1000000	95000	34134	46721
III B	NU 2228 ECML	655000	1,00	(single)	655000	830000	93000	34134	-
III CA	30230	429000	0,95	(dual)	407550	560000	57000	17067	6095
III CB	32230 J2	737000	0,95	(dual)	700150	1140000	112000	17067	54338

Position	Shaft distance, [mm]	Number of teeth - input, z1	Number of teeth - output, z2 / (z3)	Helix angle, B [°]
Planetary stage (3x planetary)	434,7 (planetary-sun)	35 (planetary)	19 (sun, output) / 89 (annulus)	6
Intermediate stage	643	85	20	10
High speed stage	434	103	23	16,5

8.3 Appendix B1

Appendix B 1: Common bearing steel compositions (wt%) [45]

Grade	C	Mn	Si	Cr	Ni	Mo	Cu	S	P	Others
AISI 1070	0.71	0.76	0.20	0.09	0.08	0.02	0.07	0.012	0.006	
En31	0.90-1.20	0.30-0.75	0.10-0.35	1.00-1.60				0.05	0.05	
AISI 52100	0.95-1.10	0.20-0.50	≤0.35	1.30-1.60	-	-	≤0.025	≤0.025	-	
SAE 52100	0.98	0.38	0.16	1.39	0.07	0.02	0.12	0.06	0.12	
SAE 52100	0.97	0.31	0.32	1.43				0.017	0.019	
"1C-1.5Cr"	0.98-1.10	0.15-0.35	0.25-0.45	1.30-1.60	≤0.25	≤0.10	≤0.35	≤0.025	≤0.025	
ShKh4	0.98-1.03	0.18-0.29	0.17-0.28	0.38-0.47						
ShKh15	1.05	0.28	0.28	1.50	0.11		0.06	0.015	0.013	
ShKh15G	0.95-1.05	0.95-1.17	0.45-0.61	1.35-1.60						
SUJ-2	1.03	0.37	0.23	1.35	0.51	-	0.15	0.023	0.018	
SUJ-2	1.04	0.39	0.25	1.47	0.07	-	0.19	0.005	0.015	
SUJ-2	1.01	0.36	0.23	1.45	0.04	0.02	0.06	0.007	0.012	O 0.0008
SUJ-2	0.98	0.37	0.18	1.42	0.07	0.03	0.12	0.003	0.016	O 0.0006
SUJ-2	0.97	0.38	0.20	1.35	0.08	0.03	0.11	0.005	0.016	O 0.0005 Al 0.009 Ti 0.0023
MMM (SKF 3M)	Mo modified 52100						0.25		≤0.015	
"1C-1.5Cr-Mo"	0.98	0.45	0.97	1.98		0.42		≤0.002	≤0.011	
"Si-Mo"	0.96-1.12	0.56-0.66	0.49-0.70			0.23-0.33				
100CrMo7-3	0.97	0.66	0.27	1.79	0.11	0.26	0.15	0.007	0.009	O 0.0005 Al 0.034
52CB	0.85	0.35	0.85	0.90		0.60				
Microalloyed	0.44	0.99	0.43					0.004	0.009	V 0.10
4320	0.21	0.62	0.20	0.49	1.73	0.20	0.16	0.018	0.010	
1070M	0.68	0.95	0.17	0.13	0.11	0.05	0.19	0.022	0.009	
S53C	0.53	0.74	0.19					0.020	0.015	O 0.008
SMn60	0.60	1.22	0.24					0.011	0.007	O 0.008
SMn65	0.66	1.19	0.24					0.009	0.006	O 0.009
SAE 1072	0.74	1.18	0.23					0.009	0.008	O 0.007
SAE 1072Cr	0.72	1.18	0.24	0.48				0.009	0.006	O 0.006
80CrMn4	0.78	0.78	0.24	0.82						
100Cr2 (W1)	0.9-1.05	0.25-0.45	0.15-0.35	0.4-0.6	≤0.30		≤0.30	≤0.025	0.03	
100Cr4 (W2)	1.0-1.1	0.25-0.45	0.15-0.35	0.90-1.15				≤0.025	0.03	
SAE 51100	0.97	0.39	0.25	1.04				0.013	0.020	
100Cr6 (W3)	0.90-1.05	0.25-0.45	0.15-0.35	1.40-1.65	≤0.30		≤0.30	≤0.025	0.03	
100CrMn6 (W4)	0.90-1.05	1.00-1.20	0.50-0.70	1.40-1.65	≤0.30		≤0.30	≤0.025	0.03	
100CrMnMo8	0.90-1.05	0.80-1.10	0.40-0.60	1.80-2.05	≤0.30	0.50-0.60	≤0.30	≤0.025	0.03	
GCrSiWV	0.98	0.49	0.75	1.50				0.004	0.012	W 1.21, V 0.29

8.4 Appendix C1

Appendix C 1:Ball bearing test conditions [268]

Test No.	Bearing type	P.C.D. diameter (mm)	Load (P/C)	Rotating speed (rpm)	Test temp. (°C)	Lubricant	Viscosity ratio κ	Lubricant condition
1~3	6202	25.5	0.39	3000~8000	120~218	Grease	0.1~0.39	Clean
4~7	6203	29.0	0.34~0.44	3000~8000	120~218	Grease	0.1~0.42	Clean, Contaminated
8~22	6206	46.5	0.15~0.71	1400~4900	50~130	VG10~HT320 oil	0.4~2.89	Clean, Contaminated
23~26	Spec. 6206	46.5	0.31	3000~6000	125	ATF oil	0.6	Contaminated
27	6303	31.5	0.18	22000	110	Grease	1.5	Clean
28	6304	35.5	0.19	15000	113	Grease	1.4	Clean
29~31	HR6304	35.5	0.25	2400	70	VG90 oil	1.6	Contaminated
32,33	Spec. B-29	60.5	0.58	2513	100	ATF oil	0.6	Contaminated
34~38	Wide 6207	53.5	0.31~0.76	1000	60~90	Grease	0.6~1.45	Clean
39,40	Double-row angular contact	43.5	0.10~0.16	8000~9200	80	Grease	0.6	Clean

8.5 Appendix C2

Appendix C 2: Roller bearing test conditions [268]

Test No.	Bearing type	P.C.D. diameter (mm)	Load (P/C)	Rotating speed (rpm)	Test Temp. (°C)	Lubricant	Viscosity ratio κ	Lubricant condition
1~9	LM11749/710	28.6	0.35~ 0.46	1500~ 3400	120~ 218	VG10~ VG68 oil	0.6~ 4.00	Clean, Contaminated
10~19	L44649/610	38.6	0.16~ 0.71	3000	51~62	VG10~ VG68 oil	0.59~ 4.00	Clean, Contaminated
20~22	Special roller and ball Brg.	15.9~ 18.0	0.19~ 0.20	1000	50~ 130	Grease	0.46~ 0.48	Clean
23,24	Spec. P34-1	49.1	0.30	4000	125	Grease	0.9	Clean
25	Spec. R34Z-21	45.9	0.28	3500	110	75W-90 oil	1.54	Contaminated
26	Spec. R45-15	53.2	0.24	3500	113	SX90 oil	1.53	Contaminated
27	Spec. DPB42	54.5	0.30	3500	60	80W-90 oil	1.68	Contaminated
28	HM88649/610	53.2	0.28	3500	70	SX90 oil	1.66	Contaminated
29	HR30304	36.4	0.34	4000	100	80W-90 oil	1.36	Contaminated
30	32205	36.4	0.26	3500	80	80W-90 oil	0.99	Contaminated
31	30306C	50.9	0.32	3000	85	SX80 oil	2.35	Contaminated
32	440KVE	515.7	0.36	570	85	Grease	3.18	Unfiltered
33	23040	258.9	0.29	10.12	85	Grease	0.1	Unfiltered
34	22211	78.7	0.16	3000	40	VG10 oil	1.08	Unfiltered
35	22211EA	78.7	0.16	3000	40	VG10 oil	0.63	Unfiltered
36	294/630ME	879.9	0.20	1.14	60	VG460 oil	0.11	Unfiltered
37	NN3019	121.0	0.32	4000	85	Grease	4.00	Clean

8.6 Appendix D1

Appendix D 1: Data results of fatigue tests for angular inclusions [12]

Cycles to failure, N_f	Inclusion size, $\sqrt{\text{area}}$ (μm)	Distance from surface, h (μm)	Nominal stress at inclusion, σ' (MPa)	Fatigue limit predicted by equations (6.1), (6.2) and (6.3), α'_w (MPa)	σ'/α'_w
Cast No 84, Hv = 581					
1.16×10^6	52.0	374	641	566 (6.3)	1.13
1.57×10^6	68.0	686	583	541 (6.3)	1.08
6.97×10^6	56.0	453	626	559 (6.3)	1.20
6.02×10^5	93.0	327	649	514 (6.3)	1.26
1.45×10^6	79.4	449	627	527 (6.3)	1.19
7.67×10^5	74.2	257	662	533 (6.3)	1.24
8.96×10^5	90.8	318	651	516 (6.3)	1.26
2.55×10^5	93.4	375	640	513 (6.3)	1.25
4.12×10^5	69.1	418	632	540 (6.3)	1.17
4.01×10^5	97.0	521	613	510 (6.3)	1.20
3.04×10^5	87.9	445	627	519 (6.3)	1.21
Cast No 119, Hv = 579					
4.92×10^6	52.7	325	650	563 (6.3)	1.15
1.63×10^6	63.8	437	629	546 (6.3)	1.15
1.66×10^6	81.3	361	643	524 (6.3)	1.23
8.31×10^5	83.8	335	648	521 (6.3)	1.24
3.66×10^5	85.6	427	631	519 (6.3)	1.21
2.13×10^6	55.4	364	642	558 (6.3)	1.15
2.98×10^6	63.3	276	659	546 (6.3)	1.21
Cast No 118, Hv = 581					
2.80×10^6	56.7	582	602	558 (6.3)	1.08
6.84×10^6	53.9	575	603	563 (6.3)	1.07
2.43×10^6	63.9	473	622	547 (6.3)	1.14
1.05×10^7	44.2	522	613	582 (6.3)	1.05
3.68×10^6	73.1	766	568	535 (6.3)	1.06
1.56×10^7	57.1	557	607	557 (6.3)	1.09
2.62×10^6	56.7	464	624	558 (6.3)	1.12
Cast No 117, Hv = 581					
8.28×10^7	33.2	402	635	610 (6.3)	1.04
4.68×10^7	51.7	424	631	567 (6.3)	1.11
2.57×10^6	54.5	382	639	562 (6.3)	1.14
1.05×10^6	26.9	367	642	632 (6.3)	1.02
4.43×10^6	72.1	803	561	536 (6.3)	1.05
1.75×10^7	46.6	521	613	576 (6.3)	1.06
Cast No 116, Hv = 574					
9.08×10^7	36.2	277	659	595 (6.3)	1.11
4.78×10^6	125.9	510	615	484 (6.3)	1.27
1.61×10^7	37.6	287	657	591 (6.3)	1.11
9.04×10^5	116.0	860	550	490 (6.3)	1.12
5.24×10^7	33.6	668	586	603 (6.3)	0.97

8.7 Appendix D2

Appendix D 2: Data results of fatigue tests for spherical inclusions [12]

Cycles to failure, N_f	Inclusion size, $\sqrt{\text{area}}$ (μm)	Distance from surface, h (μm)	Nominal stress at inclusion, σ' (MPa)	Fatigue limit predicted by equations (6.1), (6.2) and (6.3), (MPa)	σ'/σ'_w
Cast No S11, Hv = 556					
1.27×10^6	59.5	341	647	534 (6.3)	1.21
2.64×10^6	137.4	1100	506	464 (6.3)	1.09
7.88×10^6	76.7	515	614	512 (6.3)	1.20
1.60×10^8	93.1	830	556	495 (6.3)	1.12
Cast No S2, Hv = 560					
6.77×10^7	47.8	420	632	557 (6.3)	1.13
6.21×10^7	57.6	460	625	540 (6.3)	1.16
2.85×10^7	49.2	470	623	554 (6.3)	1.12
Cast No S4, Hv = 554					
3.07×10^7	40.8	390	638	567 (6.3)	1.13
2.69×10^8	112.6	1300	469	478 (6.3)	0.98
2.34×10^7	46.1	375	640	555 (6.3)	1.15
7.11×10^6	53.2	470	623	542 (6.3)	1.15
3.34×10^7	46.1	450	626	555 (6.3)	1.13
6.39×10^6	51.4	357	644	545 (6.3)	1.18
1.54×10^7	44.3	675	585	559 (6.3)	1.05
Cast No S7, Hv = 566					
3.06×10^7	55.8	1200	487	547 (6.3)	0.89
3.07×10^7	34.1	500	617	594 (6.3)	1.04
6.58×10^7	33.8	310	652	595 (6.3)	1.10
2.34×10^7	41.7	320	651	575 (6.3)	1.13
Cast No S8, Hv = 550					
5.55×10^7	54.9	680	584	536 (6.3)	1.09
2.37×10^7	58.5	655	588	630 (6.3)	1.11
2.53×10^6	72.5	440	628	512 (6.3)	1.23
8.61×10^6	40.3	56	700	564 (6.3)	1.24
2.73×10^7	46.1	390	638	552 (6.3)	1.16
4.87×10^7	26.6	415	633	605 (6.3)	1.05

8.8 Appendix E1

Appendix E 1: Values of CTE, E, ν of different types of NMI's [12]

Inclusions	Chemical composition	Average value of coeff. of thermal expansion $\alpha \times 10^{-6}/^{\circ}\text{C}$ (0 ~ 800 $^{\circ}\text{C}$)	Young's modulus E (GPa)	Poisson's ratio ν
Sulphides	MnS	18.1	(69-138)	(-0.3)
	CaS	14.7		
Calcium Aluminates	CaS · 6Al ₂ O ₃	8.8	(113)	(0.234)
	CaS · 2Al ₂ O ₃	5.0		
	CaO · Al ₂ O ₃	6.5		
	12CaO · 7Al ₂ O ₃	7.6		
	3CaO · Al ₂ O ₃	10.0		
Spinel's	MgO · Al ₂ O ₃	8.4	271	0.260
	MnO · Al ₂ O ₃	8.0		
	FeO · Al ₂ O ₃	8.6		
Alumina	Al ₂ O ₃	8.0	389	0.250
	Cr ₂ O ₃	7.9		
Nitrides	TiN	9.4	(317)	(0.192)
Oxides (Reference values)	MnO	14.1	(178)	(0.306)
	MgO	13.5	306	0.178
	CaO	13.5	183	0.21
	FeO	14.2		
Microstructure (Matrix) 1% C, 1.5% Cr steel	Austenite (γ) (850 $^{\circ}\text{C}$ → Ms)	(23.0)		
	Martensite (α') (M _f → R. T.)	(10.0)		
Average	γ → α' (850 $^{\circ}\text{C}$ → R. T.)	12.5	206	0.290

8.9 Appendix F1

Appendix F 1: Rolling Path Skewing bearings' failures [218]

No.	Conditions	Causes	Solutions
1	Rolling element contact path on raceway surface strays or skews.	<ul style="list-style-type: none"> -Deformation or tilt of bearing ring due to poor accuracy of shaft or housing, -Poor rigidity of shaft or housing, -Deflection of the shaft due to excessive clearance. 	<ul style="list-style-type: none"> -Improvement in machining accuracy of shaft and housing, -Improvement in the rigidity of shaft and housing, -Employment of adequate clearance



-Spherical roller bearing,
 -Contacts on the inner ring, outer ring, and rollers are not even,
 -The cause is poor mounting.



-The outer ring of tapered roller bearings,
 -Contact path on raceway surface strays,
 -The cause is poor mounting.



-Contact marks on rolling contact surfaces are not even

8.10 Appendix F2

Appendix F 2: Damage to retainers' bearings' failures [218]

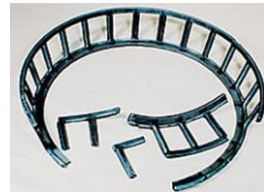
No.	Conditions	Causes	Solutions
2	<ul style="list-style-type: none"> -Breaking of retainer, -Wear of pockets or guide, -Loosening or breaking of rivet 	<ul style="list-style-type: none"> -Excessive moment load High-speed spinning or large fluctuation of speed, -Poor lubrication, -Trapping of foreign objects, -Heavy vibration, Poor mounting (cocked bearing), -Excessive heat (plastic retainer in particular). 	<ul style="list-style-type: none"> -Improvement in load conditions, -Improvement in lubrication system and lubricant, -Selection of optimum retainer, -Improvement in handling, -Study on the rigidity of shaft and housing.



-Retainer of angular contact ball bearing,
 -Breakage of machined high tension brass casting retainer L1,
 -The cause is poor lubrication.



-Retainer of spherical roller bearing,
 -Breakage of partitions between pockets of pressed steel retainer,



-Retainer of tapered roller bearing,
 -Breakage of pockets of pressed steel retainer.



-Retainer of tapered roller bearing,
 -Breakage of pockets of pressed steel retainer.

8.11 Appendix F3

Appendix F 3: Creep bearings' failures [218]

No.	Conditions	Causes	Solutions
3	-Fitting surfaces are glazed or matted, and sometimes spalled as well.	-Fitting of the inner ring is loose on the inner ring drive bearing, and that of the outer ring is loose on the outer ring drive bearing. -If the housing is made of a light alloy such as aluminum, the fit may become loose due to the difference in thermal expansion.	-Improvement in fit -Improvement in machining accuracy of shaft and housing.



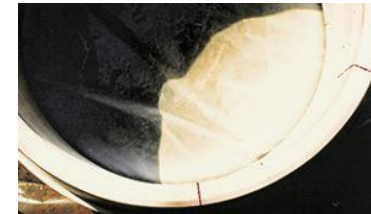
-Inner ring of the deep groove ball bearing,
-Bore wall glazed by creep.



-Inner ring of tapered roller bearing,
-Spalling due to creep at the middle of the bore wall.



-Inner ring of thrust ball bearing,
-Spalling and friction cracking due to creep on the bore wall.

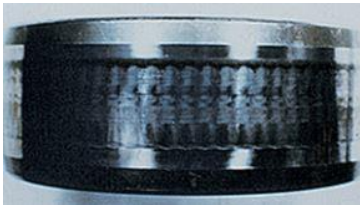


-Inner ring of tapered roller bearing,
-Spalling and friction cracking on width surface due to creep crack developed into a split reaching bore wall.

8.12 Appendix F4

Appendix F 4: Electrical pitting bearings' failures [218]

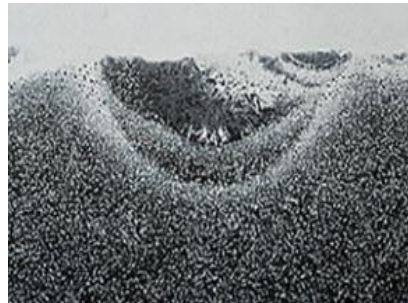
No.	Conditions	Causes	Solutions
4	-Surface is speckled visually and the speckles are clusters of tiny pits when viewed through a microscope, -Further development leads to a corrugated surface.	-Electric current passes through the bearing, and sparks are generated to fuse the raceway surface.	-Avoid flow of electric current by averting current with a slip ring or insulation bearing.



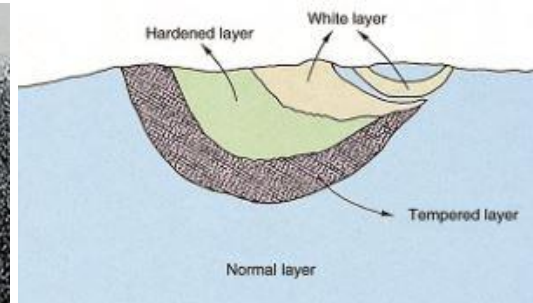
-Inner ring of cylindrical roller bearing,
-Raceway surface is corrugated by electric pitting



-Rollers of tapered roller bearings,
-Electric pitting in middle of rolling contact surfaces



-Magnified (x400) pitting of roller,
-Nital etchant develops a white layer on the cross-section.



8.13 Appendix F5

Appendix F 5: Fretting and Fretting Corrosion bearings' failures [218]

No.	Conditions	Causes	Solutions
5	<p>-Fretting surfaces wear producing red rust-colored particles that form hollows, -On the raceway surface, dents called false brinelling are formed at a spacing equal to distances corresponding to the rolling elements.</p>	<p>-If a vibrating load works on contacting elements resulting in small amplitude oscillation, lubricant is driven out from contact, and parts are worn remarkably, -The oscillation angle of the bearing is small, -Poor lubrication (no lubrication), -Fluctuating load, -Vibration during transportation, -Vibration, shaft deflection, installation error, loose fit.</p>	<p>-Inner ring and the outer ring should be packaged, separately for transportation. If not separable, bearings should be preloaded, -Use oil or high consistency grease when bearings are used for oscillation motion, -Change lubricant. -Fix shaft and housing, -Improve fit.</p>
			
<p>-Inner ring of cylindrical roller bearing, -Corrugated fretting along the full circumference of the raceway, -The cause is vibration.</p>	<p>-Inner ring of the deep groove ball bearing, -Fretting along the full circumference of the raceway, -The cause is vibration.</p>	<p>-The outer ring of cylindrical roller bearing, -Fretting rust on outside diameter surface.</p>	<p>-The outer ring of tapered roller bearing, -Fretting rust on the outside diameter surface.</p>

8.14 Appendix F6

Appendix F 6: Seizing bearings' failures [218]

No.	Conditions	Causes	Solutions
6	-Bearing generates heat and is seized up by heat disabling spinning, -Discoloration, softening, and welding of raceway surfaces, rolling contact surfaces, and rib surface.	-Dissipation of heat generated by bearing is not enough, -Poor lubrication or lubricant improper, -Clearance is excessively small, -Excessive load (or pre-load), -Roller skewing and installation error.	-Improve dissipation of heat from bearing, -Selection of suitable lubricant and determination of optimum lubricant feeding rate, -Prevention of misalignment, -Improvement in clearance and pre-load, -Improvement in operating conditions.



-Inner ring of double row tapered roller bearing,
-Seizing up discolors and softening the inner ring producing stepped wear at a spacing equal to distances between the rollers,
-The cause is poor lubrication.



-Rollers of double row tapered roller bearing,
-Rollers of the same bearing as that of the inner ring. Discoloration, spalling, and adhesion due to seizing up on rolling contact surfaces and end faces of rollers.

8.15 Appendix F7

Appendix F 7: Rust and corrosion bearings' failures [218]

No.	Conditions	Causes	Solutions
7	-Rusting or corrosion of bearing ring and rolling element surfaces, -Sometimes rusted at spacing equal to the distances between the rolling elements.	-Ingress of water or corrosive material (such as acid), -Condensation of moisture contained in the air, -Poor packaging and storing conditions, and handling with bare hands.	-Improvement in sealing effect, -Periodic inspection of lubricating oil, -Careful handling of bearing, -Measures for preventing rusting when not operating for a long period of time.



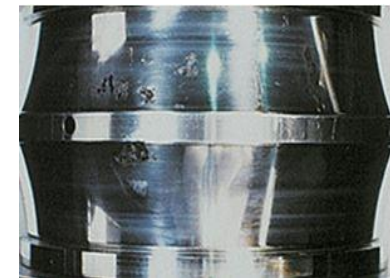
-Inner ring of tapered roller bearing,
-Rusting on raceway surface spacing equivalent to the distance between rollers. The cause is water in lubricant.



-Outer ring of tapered roller bearing,
-Rusting on raceway surface spacing equivalent to the distances between rollers. The cause is water in lubricant. Some points are corroded.



-Roller of spherical roller bearing,
-Rust as well as corrosion on rolling contact surface,
-Ingress of water.

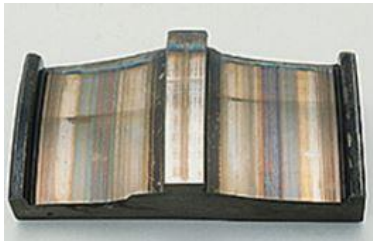


-Inner ring (split type) of self-aligning roller bearing,
-Rust and corrosion of the raceway surface,
-The cause is ingress of water.

8.16 Appendix F8

Appendix F 8: Cracking bearings' failures [218]

No.	Conditions	Causes	Solutions
8	-Splits, and cracks in bearing rings and, rolling elements.	-Excessive load, -Excessive impacts, -Overheating by creeping and rapid cooling, -Very loose fit, -Largo flaking.	-Examination and improvement of the cause of very large load, -Prevention of creep, -Correction of fit.



-Inner ring of spherical roller bearing,
-Split of raceway surface in the axial direction,
-The cause is an excessive interference fit.



-Originating point is observed at the middle of the left raceway surface.



-Outer ring of four-row cylindrical roller bearing,
-Split of raceway surface in the circumferential direction, originated from large flaking,
-The cause is large flaking.



-Outer ring of angular contact ball bearing,
-Split of raceway surface in the circumferential direction,
-The cause is the slipping of balls due to poor lubrication.

8.17 Appendix F9

Appendix F 9: Chipping bearings' failures [218]

No.	Conditions	Causes	Solutions
9	-Partial chipping of inner ring, outer ring, or rolling elements.	-Trapping of large solid, -Foreign objects impacts or excessive load, -Poor handling.	-Troubleshooting and improvements of impacts and excessive load, -Improvement in handling, -Improvement in sealing characteristics.



-Cylindrical roller bearing,
-Chipping of guide ribs of inner and outer rings,
-The cause is excessive impact load.



-Inner ring of spherical roller bearing,
-Rib chipped,
-The cause is excessive impact load.



-Inner ring of tapered roller bearing,
-Chipping of cone back face rib,
-The cause impacts due to poor mounting.



-Inner ring of double row tapered roller bearing,
-Chipping of side face,
-The cause impacts due to improper handling.

8.18 Appendix F10

Appendix F 10: Indentations bearings' failures [218]

No.	Conditions	Causes	Solutions
10	-Hollows in raceway surface produced by solid foreign objects trapped or impacts (False brinelling).	-Ingress of solid foreign objects, -Trapping of flaked particles, -Impacts due to careless handling	-Keeping out foreign objects, -Check the involved bearing and other bearings for flaking if dents are produced by metal particles, -Filtration of oil, -Improvement in handling and mounting practices.



-Inner ring (cut-off piece) of self-aligning roller bearing,
-Dents on one side of the raceway,
-The cause is the trapping of solid foreign objects.



-Rollers of spherical roller bearing,
-Dents on rolling contact surfaces,
-The cause is the trapping of solid foreign objects.



-Rollers of tapered roller bearings,
-Dents all over rolling contact surfaces. (Temper color at two ends.),
-The cause is foreign objects carried by lubricating oil.



-The inner ring of tapered roller bearing,
-Dents on the raceway surface
-The cause is the trapping of foreign objects.

8.19 Appendix F11

Appendix F 11: Speckles and discoloration bearings' failures [218]

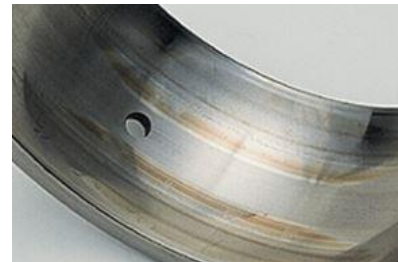
No.	Conditions	Causes	Solutions
11	<p>Speckles -Raceway surface is matted and speckled. Speckles are clusters of tiny dents.</p> <p>Discoloration -The surface color has changed.</p>	<p>-Ingress of foreign objects, -Poor lubrication, -Temper color by overheating, -Deposition of deteriorated oil on the surface.</p>	<p>Speckles -Improvement in sealing efficiency, Filtration of oil, -Improvement in the lubrication system.</p> <p>Discoloration -Oil deposition is removable by wiping with an organic solvent (oxalic acid), -If roughness is not removable by polishing with sandpaper, it is rust or corrosion. If completely removable, it is temper color due to overheating.</p>



-Inner ring of double row tapered roller bearing (RCT bearing),
-The Raceway surface is speckled,
-The cause is electric pitting.



-Ball of deep groove ball bearing,
-Speckled all over,
-The cause is foreign objects and poor lubrication.



-Outer ring of spherical roller bearing,
-Partial oil deposition on the raceway surface.



-Spherical roller bearing,
-Discoloration of inner and outer ring raceway surfaces,
-The cause is the deterioration of the lubricant.

8.20 Appendix F12

Appendix F 12: Wear bearings' failures [218]

No.	Conditions	Causes	Solutions
12	<ul style="list-style-type: none"> -The surface is worn, and dimensions are reduced compared with other portions, -The surface is mostly roughened and scored. 	<ul style="list-style-type: none"> -Ingress of solid foreign objects, -Dirt and other foreign objects in lubricant, -Poor lubrication, -Skewing of rollers. 	<ul style="list-style-type: none"> -Selection of optimum lubricant and lubrication system, -Improvement in sealing efficiency, -Filtration of lubricating oil, -Elimination of misalignment.



-The outer ring of cylindrical roller bearing,
 -Stepped wear on the raceway surface,
 -The cause is poor lubrication.



-The inner ring of cylindrical roller bearing,
 -Stepped wear on full circumference of the raceway,
 -The cause is poor lubrication.



-Outer ring of double row angular contact ball bearing (hub unit bearing),
 -Wear on one side of the raceway,
 -The cause is poor lubrication.

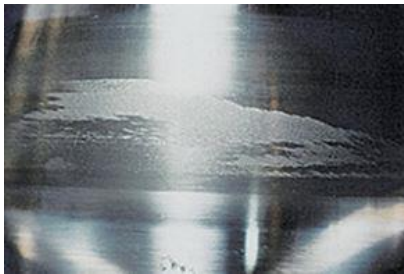


-Retainer of cylindrical roller bearing,
 -Wear of pockets of machined high tensile brass casting retainer.

8.21 Appendix F13

Appendix F 13: Smearing bearings' failures [218]

No.	Conditions	Causes	Solutions
13	-The surface is roughened, and tiny particles adhere.	-Rolling elements slip in a rolling motion and the characteristics of lubricant are too poor to prevent slippage.	-Select optimum lubricant and lubrication system capable of forming sound oil films, -Use a lubricant including extreme pressure additive, -Take precautions such as a small radial clearance and pre-load to prevent slippage.



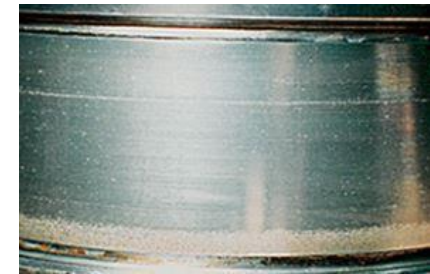
-The inner ring of cylindrical roller bearing,
-Smearing on the raceway surface,
-The cause is slippage of rollers due to foreign objects trapped within.



-Roller of the same bearing as that of the inner ring,
-Smearing on the rolling contact surface,
-The cause is slippage of rollers due to foreign objects trapped within.



-Rollers of spherical Thrust roller bearings,
-Smearing in the middle of rolling contact surfaces,
-The cause is slippage of rollers due to foreign objects trapped within.



-The inner ring of double row tapered roller bearing (RCT bearing),
-Smearing on raceway surface.

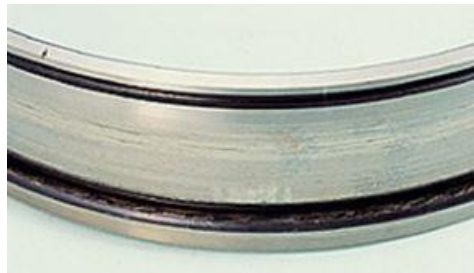
8.22 Appendix F14

Appendix F 14: Spalling bearings' failures [218]

No.	Conditions	Causes	Solutions
14	<ul style="list-style-type: none"> -Score accompanying seizing, -Mounting score in the axial direction, -Scores on the roller end face and guide rib-cycloidal scores, -Scratches in spinning direction on raceway surface and rolling contact surfaces. 	<ul style="list-style-type: none"> -Poor mounting and removing practice, -Oil film discontinuation on the contact surface due to excessive radial load, foreign object trapping, or excessive pre-load, -Slippage or poor lubrication of rolling elements. 	<ul style="list-style-type: none"> -Improvement in mounting and removing procedures, -Improvement in operation conditions, -Correction of pre-load, -Selection of adequate lubricant and lubrication system, -Improvement of sealing efficiency.



-The inner ring of the cylindrical roller bearing,
 -Spalling on rib,
 -The cause is excessive load.



-The inner ring of the cylindrical roller bearing,
 -Spalling on raceway surface and cone back face rib,
 -The cause is poor lubrication.



-Rollers of tapered roller bearing,
 -Cycloidal spalling on the end faces (Scuffing),
 -The cause is poor lubrication.



-Roller of cylindrical roller bearing,
 -Score in the axial direction on rolling contact surface caused during mounting,
 -The cause is poor mounting practice.

8.23 Appendix F15

Appendix F 15: Peeling bearings' failures [218]

No.	Conditions	Causes	Solutions
15	<ul style="list-style-type: none"> -Peeling is a cluster of very small spalls (size about 10μm), -Peeling can also include very small cracks which develop into spalls. 	<ul style="list-style-type: none"> -Likely to occur in roller bearings, -Tends to occur if the surface of the opposite part is rough or lubrication characteristics are poor, -Peeling may develop into flaking. 	<ul style="list-style-type: none"> -Control of surface roughness and dust -Selection of appropriate lubricant, -Proper break-in.



-Rollers of spherical roller bearing,
 -Peeling on rolling contact surfaces,
 -The cause is poor lubrication.



-Tapered roller bearing,
 -Development of peeling to flaking on inner ring and rollers,
 -The cause is poor lubrication.

8.24 Appendix F16

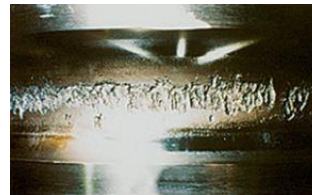
Appendix F 16: Flaking bearings' failures [218]			
No.	Conditions	Causes	Solutions
16	-The Raceway surface is flaked, -The surface after flaking is very rough.	-Rolling fatigue, -Flaking may be caused early by over-load, excessive load due to improper handling, poor shaft or housing accuracy, installation error, ingress of foreign objects, rusting, etc.	-Find the cause of the heavy load, -Examine operating conditions and adopt bearings with larger capacity as necessary. -Increase the viscosity of oil and improve the lubrication system to form an adequate lubricating oil film, -Eliminate installation errors.



-Deep groove ball bearing,
-The inner ring, outer ring, and balls are flaked,
-The cause is excessive load.



-The outer ring of the angular contact ball bearing,
-Making of raceway surface spacing equal to distances between balls,
-The cause is improper handling.



-Inner ring raceway of a deep groove ball bearing.



-Outer ring raceway of an angular contact ball bearings.



-The inner ring of the deep groove ball bearing,
-Flaking on one side of the raceway surface,
-The cause is an excessive axial load.



-The inner ring of the spherical roller bearing,
-Flaking only on one side of the raceway surface,
-The cause is an excessive axial load.



-Tapered roller bearing,
-Flaking on 1/4 circumference of inner ring raceway with outer ring and rollers discolored light brown,
-The cause is excessive pre-load.



-The outer ring of double row angular contact ball bearing,
-Flaking on 1/4 circumference of outer ring raceway,
-The cause is poor installation.



-Thrust ball bearing
Flaking on inner ring raceway (bearing ring fastened to shaft) and balls,
-The cause is poor lubrication.



-Outer ring raceway of double row tapered roller bearing (RCT bearing),
-Flaking originated from electric pitting on the raceway surface.